AD NUMBER
AD385085
CLASSIFICATION CHANGES
TO: **UNCLASSIFIED**
FROM: **CONFIDENTIAL**
LIMITATION CHANGES
TO: **Approved for public release; distribution is unlimited.**
FROM: **Distribution authorized to U.S. Gov't. agencies and their contractors; Administrative/Operational Use; 31 OCT 1967. Other requests shall be referred to Air Force Rocket Propulsion Lab., Edwards AFB, CA.**
AUTHORITY
31 Oct 1979, DoDD 5200.10 ; AFRPL ltr 5 Feb 1986

AD 385 085

AUTHORITY: AFRPL
ltr, 5 Feb 86

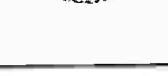

SECURITY MARKING

The classified or limited status of this report applies to each page, unless otherwise marked.
Separate page printouts MUST be marked accordingly.

THIS DOCUMENT CONTAINS INFORMATION AFFECTING THE NATIONAL DEFENSE OF THE UNITED STATES WITHIN THE MEANING OF THE ESPIONAGE LAWS, TITLE 18, U.S.C., SECTIONS 793 AND 794. THE TRANSMISSION OR THE REVELATION OF ITS CONTENTS IN ANY MANNER TO AN UNAUTHORIZED PERSON IS PROHIBITED BY LAW.

NOTICE: When government or other drawings, specifications or other data are used for any purpose other than in connection with a definitely related government procurement operation, the U. S. Government thereby incurs no responsibility, nor any obligation whatsoever; and the fact that the Government may have formulated, furnished, or in any way supplied the said drawings, specifications, or other data is not to be regarded by implication or otherwise as in any manner licensing the holder or any other person or corporation, or conveying any rights or permission to manufacture, use or sell any patented invention that may in any way be related thereto.

AFRPL-TR-67-198

Demonstration of an Advanced Transpiration-Cooled Thrust Chamber (U)

FINAL REPORT

Albert L. Blubaugh
Edward J. Zisk
Aerojet-General Corporation

TECHNICAL REPORT AFRPL-TR-67-198

31 October 1967

In addition to security requirements which must be met, this document is subject to special export controls, and each transmittal to foreign governments or foreign nationals may be made only with prior approval of AFRPL (RPPR/STINFO), Edwards, California, 93523

AIR FORCE ROCKET PROPULSION LABORATORY
Research and Technology Division
Air Force Systems Command
Edwards, California

0995

AFRPL-TR-67-198

AFRPL-TR-67-198

31 October 1967

(Unclassified)

DEMONSTRATION OF AN ADVANCED TRANSPIRATION-COOLED THRUST CHAMBER

Final Report

Albert L. Blubaugh
Edward J. Zisk

0995

FOREWORD

(U) The work described in this report was supported by the Air Force Rocket Propulsion Laboratory at Edwards, California, under Contract AF 04(611)-10922, Project Number 3058 and Task Number 305803. The AFRPL Project Officer is Mr. L. Tepe (RPRRE).

(U) This report describes all the work conducted during this program and covers the period from September 1965 to April 1967.

(U) The work was performed by the Aerojet-General Corporation, Sacramento, California. Management control of the program is supplied by Dr. C. B. McGough, Manager, Thrust Chamber Engineering, Liquid Rocket Operations. The project manager on this program is Dr. A. L. Blubaugh and the project engineer is Mr. E. J. Zisk. Thermal and hydraulic analysis was directed by Dr. R. J. LaBotz, and performance analysis was directed by Mr. D. L. Kors. The test program was conducted in the Aerojet Research Physics Laboratory under the direction of Mr. J. W. Sartori.

(U) This report contains no classified information extracted from other classified documents.

(U) This technical report has been reviewed and is approved.

L. Tepe
Project Officer, Liquid Rocket Division
Air Force Rocket Propulsion Laboratory
Edwards, California

AFRPL-TR-67-198

UNCLASSIFIED ABSTRACT

(U) An advanced transpiration-cooled thrust chamber concept developed by Aerojet-General Corporation, Liquid Rocket Operations, has been tested extensively with both N_2O_4 and ClF_3 as coolants. This concept, designated TRANSPIRE (Transpiration-Cooled Stacked Platelet Ijection Rocket Engine), utilizes stacked ultra-thin (0.001 to 0.020 in.) platelets to form a porous rocket engine combustion chamber wall. Each platelet contains precise flow control channels which meter the coolant flow to the cooled surface, and prevent the formation and growth of local hot spots.

(U) This program has demonstrated the feasibility of the TRANSPIRE concept using both N_2O_4 and ClF_3 as the transpiration coolants. Three completely transpiration cooled chambers were fabricated and tested. The N_2O_4-cooled chamber used stainless steel platelets and was tested at 100 lb and 1000 lb thrust using N_2O_4/AeroZINE 50* as propellants. The two ClF_3-cooled chamber used nickel platelets and were tested at 100 lb thrust and 1000 lb thrust using ClF_3/MHF-3 as propellants.

(U) A total of 121 tests were made with the N_2O_4-cooled chamber for a cumulative firing duration of 3076.7 seconds. Ninety-six tests were made at the 100 lb thrust level and 25 tests at the 1000 lb thrust level. The cumulative firing duration for the ClF_3-cooled chamber was 219.2 seconds with thirteen tests being made at the 100 lb thrust level and sixteen tests at the 1000 lb thrust level.

*50% UDMH + 50% N_2H_4

TABLE OF CONTENTS

		Page
I.	Introduction	1
II.	Summary	10
III.	Conclusions	15
IV.	Design and Fabrication	18
	A. Injectors	18
	B. Uncooled Chambers	28
	C. Cooled Chambers	31
	D. Thermal Instrumentation	58
V.	Testing	69
	A. Facility and Procedures	69
	B. Injector Checkout Testing	79
	C. Cooled Chamber Flow Testing	84
	D. Cooled Chamber Test Firing	86
VI.	Results	119
	A. Injector Checkout	119
	B. Cooled Chamber Flow Testing	135
	C. Injector-Chamber Compatibility	144
	D. Heat Transfer	159
	E. Cooled Chamber Performance	178
VII.	Scaling	197

APPENDICES

I. Heat Transfer Model

II. Performance Model

III. Data

LIST OF TABLES

Table	Title	Page
1	Summary of Injector Types (U)	26
2	Phase I Nominal Coolant Flow Rates (lb/sec) (U)	35
3	Phase II Nominal Coolant Flow Rates (U)	53
4	Location and Number of Thermocouples in Instrumentation Platelets (U)	63
5	Phase I Injector Checkout Test Conditions (U)	80
6	Phase II Injector Checkout Test Conditions (U)	82
7	Summary of N_2O_4-Cooled Chamber Test Conditions (100 lb Thrust) (U)	87
8	Summary of N_2O_4-Cooled Chamber Test Conditions (1000 lb Thrust) (U)	90
9	N_2O_4-Cooled Chamber Final Test Condition (U)	96
10	Summary of Phase I ClF_3-Cooled Chamber Test Conditions (100 lb Thrust) (U)	98
11	Summary of Phase I ClF_3-Cooled Chamber Test Conditions (1000 lb Thrust) (U)	98
12	Phase I ClF_3-Cooled Chamber Final Test Conditions (U)	109
13	Summary of Phase II Cooled Chamber Test Conditions (U)	111
14	Phase II ClF_3-Cooled Chamber Final Test Conditions (U)	118
15	Injector Test Performance Summary (U)	120
16	Performance Loss Summary for Uncooled Chamber Injector Tests (U)	122
17	N_2O_4/AeroZINE 50 Injector Performance (U)	123
18	ClF_3/MHF-3 Injector Performance (U)	130
19	Cooled Chamber Performance Summary (U)	179
20	N_2O_4-Cooled Chamber Performance (100 lb Thrust) (U)	180
21	N_2O_4-Cooled Chamber Performance (1000 lb Thrust) (U)	181
22	ClF_3-Cooled Chamber 32L* Performance (100 lb Thrust) (U)	186
23	ClF_3-Cooled Chamber 25L* Chamber Performance (1000 lb (1000 lb Thrust) (U)	186
24	Effect of Injector O/F on Performance (U)	195
25	Cooled Chamber Final Test Conditions (U)	198

FIGURE LIST

Figure No.	Title	Page
1	TRANSPIRE Cooling Concept	2
2	Coolant Flow Control System	5
3	Phase I Injector Design	19
4	HIPERTHIN Platelet Orientation	21
5	Injector Fabrication Sequence	22
6	Phase II Injectors	24
7	Injector Patterns (U)	25
8	Injector Water Flow Pattern Check (U)	28
9	Uncooled Chamber Assembly	30
10	Phase I Cooled Chamber Assembly	33
11	Axial Coolant Distribution (U)	36
12	Temperature Distribution in Throat Platelets, 100 psia (U)	36
13	Cooled Chamber Platelets (U)	41
14	Assembly of Nickel Platelets Prior to Machining Thrust Chamber Contour (U)	47
15	Cooled Chamber Surface	49
16	Convergent Section of Stainless Steel Chamber After Machining and Electropolish	50
17	Phase I Cooled Chambers After Final Assembly	52
18	Phase II Cooled Chamber Assembly	55
19	Instrumentation Platelet Concept	59
20	Instrumentation Platelet Assembly (U)	61
21	Location of Instrumentation Platelets in Phase I Chamber	62
22	Thermocouple Locations Relative to Phase I N_2O_4 Injector Patterns (U)	64
23	Thermocouple Locations Relative to Phase I ClF_3 Injector Patterns (U)	65
24	Locations of Thermocouples in Phase II Chamber (U)	67
25	ClF_3 Test Facility	70
26	N_2O_4/A-50 Feed System Diagram	71
27	ClF_3/MHF-3 Feed System Diagram	72

FIGURE LIST (cont.)

Figure No.	Title	Page
28	N_2O_4-Cooled Chamber on Test Stand	73
29	Research Physics Laboratory Instrumentation and Data Processing Systems	76
30	Dimensional Parameters for Vortex Injector Tests	83
31	Throat Temperature Transients During Startup (U)	92
32	Chamber Thermal Characteristics (U)	94
33	Phase I ClF_3-Cooled Chamber After 95 Sec of Testing	100
34	Transient Data From Final 100 psia ClF_3-Cooled Chamber Test (U)	101
35	ClF_3-Cooled Chamber After Final Phase I Test	105
36	Platelets From Damaged ClF_3-Cooled Chamber Showing Plugging (U)	106
37	Temperature Transients for Final Phase I ClF_3-Cooled Chamber Test (U)	107
38	Phase II Cooled Chamber After Test 1K-5B-110	112
39	Phase II Cooled Chamber Erosion	114
40	Ablative Chamber After Final 1000 psia N_2O_4 Injector Checkout Test	125
41	Thrust Vs. Chamber Pressure, Final 1000 psia N_2O_4 Injector Checkout Test (U)	126
42	Calculated Throat Area History, Final 1000 psia N_2O_4 Injector Checkout Test (U)	128
43	Performance History, Final 1000 psia N_2O_4 Injector Checkout Test (U)	129
44	ClF_3/MHF-3 Ablative Chamber After Phase I Testing	132
45	Hydraulic Characteristics of N_2O_4-Cooled Chamber (U)	136
46	Hydraulic Characteristics of Phase I ClF_3-Cooled Chamber (U)	137
47	Deviation From Laminar Flow Pressure Drop	140
48	Hydraulic Characteristics of Phase II ClF_3-Cooled Chamber (U)	142
49	Heat Marks on Interior of N_2O_4-Cooled Chamber After Testing	145
50	Injector and Interior of N_2O_4-Cooled Chamber After 100 psia Testing (U)	146

FIGURE LIST (cont.)

Figure No.	Title	Page
51	Interior of N_2O_4-Cooled Chamber After 1000 psia Testing (U)	148
52	Ablative Liner Sections After Testing (U)	149
53	Comparison of Compatibility Model with Spray Pattern on Face of 100 psia N_2O_4 Injector (U)	151
54	Compatibility Model of 49-Element Phase II Injector (U)	154
55	Ablative Liner After Testing with Vortex Injector	155
56	Phase II Cooled Chamber After Firing	157
57	Section II Steady-State Wall Temperatures, N_2O_4/A-50, 100 psia (U)	164
58	Section I and III Steady-State Wall Temperatures, N_2O_4/A-50, 100 psia (U)	166
59	Section II Steady-State Wall Temperatures, ClF_3/MHF-3, 100 psia (U)	169
60	Steady-State Wall Temperatures, Phase II (U)	175
61	Effect of N_2O_4 Coolant Flow Rate on Performance (U)	183
62	Effect of N_2O_4 Coolant Final Temperature on Performance (U)	187
63	Effect of ClF_3 Coolant Flow Rate on Performance (U)	188
64	Effect of Chamber Water Leak on Performance (U)	190
65	Performance Loss Due to Coolant (U)	194
66	Performance Degradation Due to Coolant (U)	196

NOMENCLATURE

A	=	$h_L/GC_p t$
A_t	=	Throat area
A-50	=	AeroZINE 50 (50 wt % UDMH + 50 wt % N_2H_4)
B	=	$h_L/K_m t$
CA	=	Chromel-Alumel
C*	=	Characteristic exhaust velocity
C_F	=	Thrust coefficient
C_p	=	Specific heat (coolant)
CRES	=	Corrosion REsistant Steel (Stainless Steel)
EDM	=	Electrical Discharge Machining
F	=	Thrust
G	=	Coolant weight flow rate per unit of cooled wall surface area
GN_2	=	Gaseous nitrogen
g	=	Gravitational constant
h_g	=	Gas-side film coefficient
h_L	=	Platelet-coolant film coefficient
I_{sp}	=	Specific impulse
$I_{sp,C}$	=	Specific impulse of core
k	=	Flow proportionality constant
K_m	=	Platelet (metal) conductivity
ℓ_i	=	Length of platelet primary metering groove
L	=	Distance from coolant inlet (in thermal influence zone) to chamber surface
L*	=	Chamber characteristic length
MMH	=	Mono Methyl Hydrazine
O/F	=	Mixture ratio (oxidizer flow rate divided by fuel flow rate)
$(O/F)_i$	=	Injector mixture ratio
$(O/F)_t$	=	Total mixture ratio
P_c	=	Chamber pressure
P_i	=	Platelet gas-side pressure
P_p	=	Plenum pressure

NOMENCLATURE (cont.)

P/N	=	Part number
ΔP	=	Pressure differential
r_1	=	$-A/2 + \sqrt{\frac{A^2}{4} + B}$
R	=	$(\dot{w}_{c,S})_1/(\dot{w}_{c,S})_2$
S/N	=	Serial number
T	=	Platelet temperature at X
T_C	=	Core temperature
T_c	=	Coolant temperature
$T_{c,o}$	=	Coolant inlet temperature
T_g	=	Gas temperature
T_w	=	Wall surface temperature
TC	=	Thermocouple
t	=	Platelet thickness
UDMH	=	Unsymmetrical DiMethyl Hydrazine
$\dot{w}_C$	=	Injector (core) flow rate
$\dot{w}_c$	=	Coolant flow rate
$\dot{w}_{c,i}$	=	Platelet coolant flow rate
$\dot{w}_{c,S}$	=	Coolant flow rate in a chamber Section
$\dot{w}_{c,I}, \dot{w}_{c,II}, \dot{w}_{c,III}, \dot{w}_{c,IV}$	=	Coolant flow rate in chamber sections I, II, III and IV, respectively
$\dot{w}_N$	=	Nominal (design) coolant flow rate
$\dot{w}_t$	=	Total flow rate $(\dot{w}_c + \dot{w}_C)$
X	=	Distance from coolant inlet (in thermal influence zone)
ε	=	Ratio of local area to throat area
η_{ER}	=	Energy release efficiency

NOMENCLATURE (cont.)

SUBSCRIPTS

1	=	Condition 1
2	=	Condition 2
E	=	Experimental (measured)
N	=	Nominal (calculated or design value)

I. INTRODUCTION

(U) This report presents the results of Phase I and Phase II of Contract AF 04(611)-10922 which was conducted by Aerojet-General Corporation for the Air Force Rocket Propulsion Laboratory. The work being reported was started 1 September 1965. The purpose of Phase I of this contract was to evaluate the feasibility of the TRANSPIRE (Transpiration-Cooled Stacked Platelet Injection Rocket Engine) concept for transpiration cooling of liquid rocket engines using N_2O_4 and ClF_3 as coolants. The purpose of Phase II of this contract was minimization of ClF_3 coolant requirements by improving the injector design to eliminate streaking, by using a shorter L* chamber, and by reducing wall roughness.

(U) With the TRANSPIRE concept the rocket engine chamber and nozzle is constructed by stacking together a large number of very thin metal platelets. These platelets contain channels in their surfaces which form coolant flow passages in the assembled stack. The passages bring coolant from a common supply manifold on the exterior of the stack to the heated surface. An artist's concept of a rocket engine employing the TRANSPIRE concept is shown in Figure 1. The basic method of operation of the TRANSPIRE system is shown in the detailed blowup of the stacked platelet wall. Heat from the hot combustion gases is transferred into the edge of the platelets. This heat is then conducted a short distance into the wall and is picked up by the counter flowing coolant as it passes between the platelets. After the coolant has passed through the wall it is dumped into the hot gas boundary layer where it supplies additional cooling by suppressing the boundary layer temperature and, in effect, acting as a film coolant.

(U) The use of stacked platelets to form a transpiration-film cooled rocket engine is not a new concept. The basic idea was suggested as early as 1948 by Professor M. Zucrow of Purdue University who, at that time, was acting as a consultant to a group at Ohio State University. Zucrow proposed that a chamber and nozzle be constructed using stacked washers, and that hydrogen be introduced between the washers as coolant.[1] The concept was

Figure 1. TRANSPIRE Cooling Concept

I, Introduction (cont.)

applied to a LO_2/LH_2 rocket engine being developed under government contract. Two units were constructed, one using copper washers and the other using washers of stainless steel. The stainless steel unit was tested unsuccessfully. Work on the stacked washer concept was dropped with the development of a successful regenerative cooling system for the LO_2/LH_2 engine.

(U) The stacked washer cooling system was employed by Pratt and Whitney Aircraft Corp. in 1962 for use in their cryogenic engine work. The most significant changes by Pratt and Whitney relative to the Ohio State designs were in the area of improved coolant flow control. The Pratt and Whitney design has been operated successfully at high pressures with LO_2/LH_2 propellants.

(U) The Aerojet TRANSPIRE Concept, which originated in early 1965, represents a substantial departure from earlier stacked washer cooling systems in two key areas: washer thickness and coolant flow control. Each of these areas will be discussed briefly.

(U) The platelets used in the TRANSPIRE system are 0.001 to 0.020 inches thick, which is one to two orders of magnitude thinner than the washers used in earlier systems. There are two distinct advantages inherent in the use of the thin platelets.

(U) The first advantage is that low conductivity materials can be used in place of high conductivity materials with no increase in the coolant flow requirements. This statement is best understood by noting that the platelet wall behaves much like a heat exchanger (see Figure 1). The effective platelet-to-coolant heat transfer area depends on the platelet thickness and on the depth the heat penetrates into the wall as determined by the thermal conductivity of the platelet material. The platelet thickness for a given wall material is optimized when the platelet-to-coolant heat transfer area

I, Introduction (cont.)

is sufficient to utilize the heat capacity of the coolant as fully as is practical. Thus, an optimum design can be achieved with low conductivity materials by using thinner platelets to maintain the same platelet-to-coolant heat transfer area that would be obtained with thicker platelets of higher conductivity material. Because of the high thermal resistance of the coolant film, and because of the change in conduction length with platelet thermal conductivity the overall heat transfer coefficient of the platelet-coolant system is not strongly affected by the conductivity of the platelet material.

(U) Since the thin platelets permit the use of low conductivity materials the platelet material used in a TRANSPIRE system can be selected on the basis of compatibility with the propellants. Thus, the use of N_2O_4 and ClF_3 as coolants, with their high endothermic heats of dissociation, is feasible. Moreover, high temperature, high strength platelet materials can be used to materially reduce both the coolant requirements and the system weight. High conductivity platelet materials frequently require walls that are much thicker than dictated by stress considerations in order to prevent heat penetration to the flow metering portion of the wall.

(U) The second advantage inherent in the use of thin platelets is that the coolant has a high film cooling effectiveness after it leaves the wall. The large number of low velocity coolant streams issuing from the cooled surface produces a much more stable coolant film and less mixing of the coolant film and freestream than is encountered with a smaller number of larger, higher velocity streams.

(U) The second unique feature of the Aerojet concept is its coolant flow control system. The layout of this system and its operation will be explained with the aid of Figure 2. The coolant flow control system is composed of four different elements: primary metering grooves, distribution plenum, secondary metering grooves, and thermal influence zones. The coolant enters

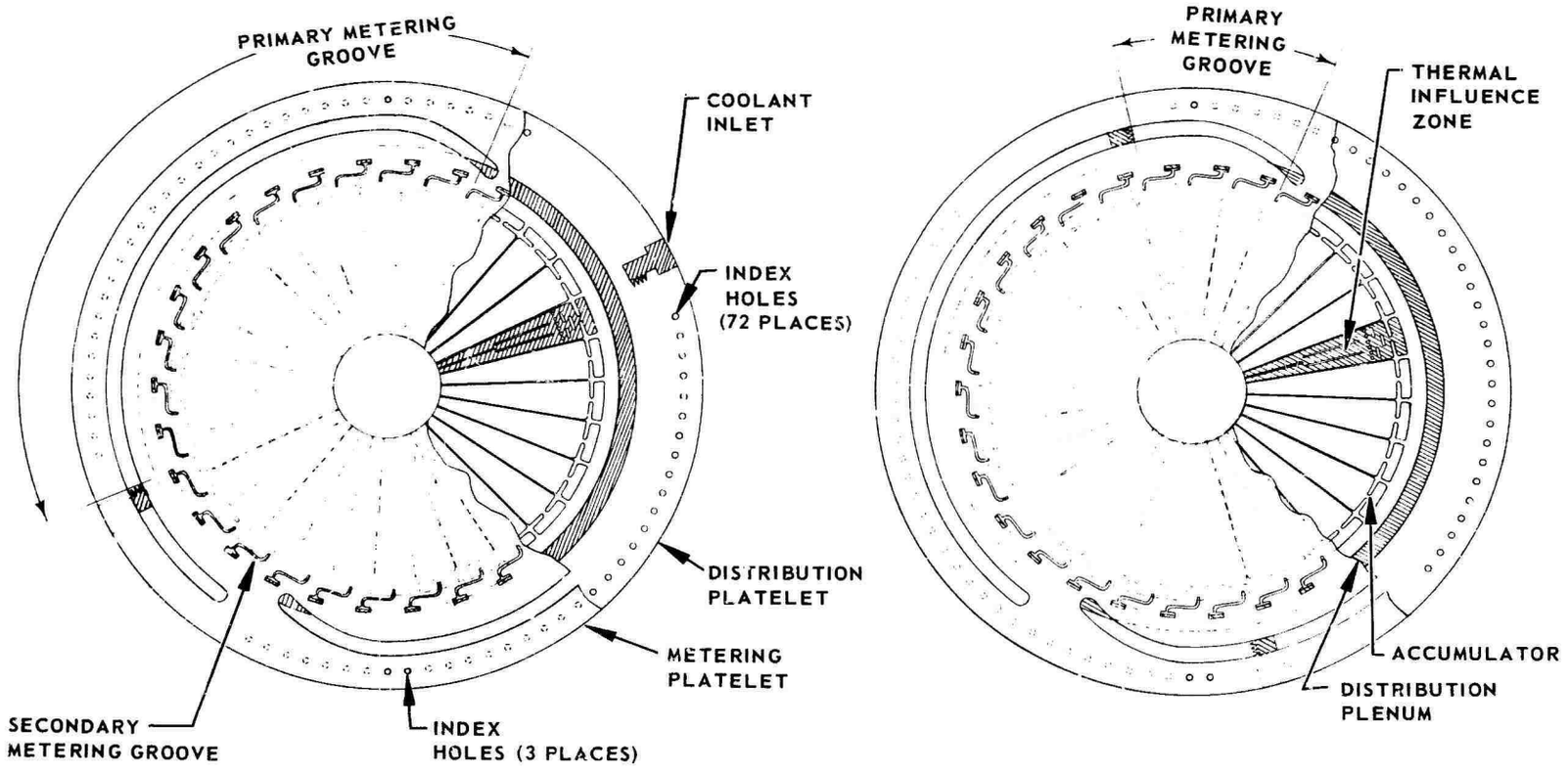

(a) PLATELETS POSITIONED (CLOCKED) TO GIVE A HIGH HYDRAULIC RESISTANCE

(b) PLATELETS POSITIONED (CLOCKED) TO GIVE A LOW HYDRAULIC RESISTANCE

Figure 2. Coolant Flow Control System

I, Introduction (cont.)

the platelets from the coolant supply manifold by way of the primary metering grooves. These grooves constitute about 90% of the hydraulic resistance in the platelet, and control the amount of coolant flowing to the platelet. From the metering grooves the coolant flows into the distribution plenum, a low pressure drop channel that serves to distribute the coolant uniformly around the platelet. On leaving the distribution plenum the coolant enters the secondary metering grooves. The secondary metering grooves provide a pressure drop on the order of 10% of that of the primary grooves. Each of these grooves empties into a separate thermal influence zone -- a region of very low pressure drop and low velocity -- where the coolant picks up the heat from the platelet.

(U) The TRANSPIRE coolant flow control system is designed to solve a problem which has plagued most conventional transpiration cooling systems - hot spot instability. With normal porous materials a hot spot tends to grow in size and severity since its hydraulic resistance increases with temperature, thus causing the coolant to bypass the overheated area. This is avoided in TRANSPIRE by the combination of the secondary metering groove and the thermal influence zone. These two regions together form a series hydraulic circuit containing a constant high resistance (secondary metering groove) and a thermally influenced low resistance (thermal influence) zone. Regardless of how the flow resistance in the thermal influence zone varies due to the local surface heat flux, the flow of coolant to the zone remains virtually unchanged. Although a hot spot may exist it continues to receive coolant and does not increase in size or intensity.

(U) It would appear that a large number of different platelets would be required to properly match the flow resistance of the individual platelets to the flow requirements and internal pressure contour. This difficulty has been overcome by a design feature which makes it possible to obtain a wide range of hydraulic resistances from a pair of platelets. This feature, called clocking, is explained with the aid of Figure 2.

I, Introduction (cont.)

(U) In the TRANSPIRE system a functional unit consists of a 0.010 to 0.020 in. thick distribution platelet and a 0.001 in. thick metering platelet. The coolant flow metering passages are the areas formed by the through-etched portion of the metering platelet when it is placed between the face of a distribution platelet and the unetched back of the previous distribution platelet in the stack. A platelet pair is shown in two orientations in Figure 2. One position (Figure 2a) produces a primary metering groove of one length. In the second position the length of the primary metering groove is a different length (Figure 2b). Thus, the hydraulic resistance of each metering-distribution platelet pair can be varied by the orientation of the platelets relative to each other (clocking).

(U) The index holes in the distribution platelet are used to determine the clocking of each distribution platelet relative to the next metering platelet in the stack. The accumulator (see Figure 2) was designed in connection with the spacing between the index holes so that the secondary metering channel can not be terminated on an unetched portion of the distribution platelet. Two of the three possible positions of the secondary metering groove relative to the accumulator are shown in Figure 2. The coolant outlet from this accumulator was designed to provide a uniform distribution of the coolant across the width of the thermal influence zone.

(U) The technical objective of the program described in this report was the demonstration of the TRANSPIRE cooling concept by means of a small scale thrust chamber test program. The program is divided into two phases. This report is the final report and covers both Phase I and Phase II.

(U) The Phase I demonstration of the cooling concept involved design, fabrication, testing, and analytical model development. The specific objectives of Phase I were:

I, Introduction (cont.)

(U) 1. Design and fabricate small thrust chambers incorporating the TRANSPIRE cooling concept

(C) 2. Test fire the chambers under the following conditions

a. Chamber pressure - 100 and 1000 psia

b. Thrust - 100 lb (@ 100 psia) and 1000 lb (@ 1000 psia)

c. Propellants - N_2O_4/AeroZINE 50* and ClF_3/MHF-3**

(U) 3. Instrument the chamber to permit acquisition of heat transfer data

(U) 4. Predict temperature profiles in the thrust chamber and predict performance loss

(U) 5. Project scaling factors to permit application of the concept to other thrust levels

(U) In order to ensure that the cooling concept is tested under a severe thermal environment a goal of the program was an injector efficiency of 94%C*.

(U) The objectives of Phase II were further demonstration of ClF_3 cooling at 1000 psia chamber pressure and 1000 lb thrust and elimination of the heat streaking problem which prevented coolant flow minimization in Phase I. The specific objectives of Phase II were:

(U) *50 wt% N_2H_4 + 50 wt% UDMH

(C) **86 wt% MMH + 14 wt% N_2H_4

I, Introduction (cont.)

(U) 1. Demonstrate transpiration cooling with ClF_3 as a coolant at 1000 lb thrust, 1000 psia chamber pressure.

(U) 2. Determine the minimum coolant flow rates required with ClF_3/MHF-3 propellants

a. Reduce chamber length

b. Mitigate the hot streaks on the chamber wall by

(1) Utilization of an injector designed for compatibility with an oxidizer transpiration cooled chamber.

(2) Elimination of wall surface roughness.

(U) As in Phase I of the program thermal instrumentation was used in the chamber to acquire heat transfer data and an injector efficiency of 94%C* was a goal of the injector design.

II. SUMMARY

A. PHASE I

(U) Two 32L* TRANSPIRE chambers were designed, fabricated, and tested in Phase I: an N_2O_4-cooled stainless steel chamber and a ClF_3-cooled nickel chamber. The two units are identical in size and very similar in design, with the main emphasis on flexibility, and not the optimization of weight and volume. Both chambers were tested at 100 lb thrust, 100 psia chamber pressure and at 1000 lb thrust, 1000 psia chamber pressure.

(C) Seven injectors were designed and fabricated for use with the Phase I cooled chambers. Three of the injectors were designated as back-up injectors, four were used for testing. Three of the four injectors used for testing met the goal of 94%C* while the fourth, the 100 lb thrust ClF_3 injector, had a C* that was 86.0% of theoretical (mean of 4 tests). Injector performance was evaluated using uncooled ablative-lined chambers that had the same inside contour as the cooled chambers.

(U) Specially constructed instrumented platelets were installed in the Phase I cooled chambers for the purpose of measuring platelet surface temperature and temperature profiles within the platelet wall. The N_2O_4-cooled chamber contained 40 thermocouples and the ClF_3-cooled chamber contained 36 thermocouples.

(U) Prior to testing, both the N_2O_4-cooled chamber and the ClF_3-cooled chamber were flow tested to verify the platelet hydraulic design. The stainless steel chamber was flowed with N_2O_4 as the calibration fluid while the nickel chamber was flowed with trichlorethylene. The calculated hydraulic characteristics agreed well with the flow test results.

II, A, Phase I (cont.)

(U) The following is a summary of the Phase I N_2O_4-cooled chamber test firing program:

100 psia Chamber Pressure, 100 lb Thrust

96 tests

2516.0 sec cumulative firing duration

Two 400 sec steady-state duration tests

Two duty cycle tests each containing eight restarts and a cumulative firing duration of 400 sec

1000 psia Chamber Pressure, 1000 lb Thrust

25 tests

560.7 sec cumulative firing duration

Two 100 sec steady-state duration tests

One duty cycle test containing three restarts and a cumulative firing duration of 80 sec

(C) The total firing time on the N_2O_4-cooled chamber was approximately 3077 sec; 139 restarts were made with the chamber. The maximum transient wall temperature was 1685°F. The maximum steady-state wall temperature was 1650°F. The chamber was in excellent condition at the conclusion of the testing and, although heat marked, showed no erosion. The hydraulic characteristics of this unit were essentially unchanged after 3077 seconds of firing time, thus indicating an absence of flow passage plugging by propellant impurities.

(U) Thirteen tests were conducted with the ClF_3-cooled chamber at 100 lb thrust. The cumulative firing duration on the chamber at the conclusion of the low thrust testing was 190 sec and the longest duration test was 78 sec. Four short duration tests were made with the ClF_3-cooled chamber at 1000 lb thrust. A leak into the chamber from a flange cooling water circuit produced $NiF_2 \cdot 4(H_2O)$ salts which plugged sections of the porous wall, resulting in severe erosion on the final Phase I test.

II, A, Phase I (cont.)

(U) Surface temperature readings as well as post-fire examination of the chambers indicated the presence of injector-induced hot streaks in both Phase I chambers. These streaks, comprising 10% to 20% of the chamber surface, in some cases resulted in temperatures up to 1000°F hotter than neighboring areas. Because of this streaking it was not possible to optimize the coolant flow rates. Compatibility models which account for the injector dynamic forces and for the reaction spray overlap patterns of the elements correlate well with the markings observed in both the ablative and cooled chambers. The ability of the chamber to operate successfully with temperature differences of this magnitude, and the fact that the streaks remained narrow and well-defined, indicates that the flow-control features of the design operated properly and precluded the hot spot instability problem inherent in other "porous" wall transpiration-cooled designs.

(U) In sections of the chamber where streaking was not severe the agreement between the predicted thermal characteristics and the experimental results was good. The TRANSPIRE system operated as designed. The performance model correlates well with the 100 psia ClF_3 and N_2O_4 data. Correlation of the Phase I 1000 psia N_2O_4 data, although possible, is not as straightforward because silica buildup on the nozzle during baseline performance evaluation with the ablative chambers produced a geometry that was different from the geometry of the cooled chamber.

(U) The results of the Phase I test program provided valuable information on the general applicability of the TRANSPIRE concept. Although the heat transfer results were masked somewhat by the injector streaking there was substantial verification of the thermal model at both the 100 psia and 1000 psia levels with N_2O_4 coolant and with stainless steel platelets and at

II, A, Phase I (cont.)

the 100 psia level with ClF_3 coolant and nickel platelets. Since the thermal model relates such basic quantities as coolant flow rate, coolant properties, platelet material and thickness, and freestream conditions to the chamber surface temperature, the application of the concept to conditions other than those tested is relatively straightforward. In scaling, the freestream conditions are scaled in the same manner as is done with any conventional cooling system. The behavior of the TRANSPIRE cooled surface would be calculated following the procedures described in Section IV.

B. PHASE II

(U) The ClF_3-cooled nickel chamber used in Phase II employed the same platelet design and chamber contour as the Phase I chambers, except that the chamber characteristic length (L*) was 25 in. instead of 32 in. The cylindrical section of the Phase II chamber was 1.75 in. shorter than that of the Phase I chambers.

(U) The instrumentation platelets used in the Phase II chamber were similar to those used in the Phase I chamber. The ClF_3-cooled Phase II chamber contained 23 thermocouples. The hydraulic characteristics of the chamber were determined from the ClF_3 flow-pressure drop data that are obtained during the oxidizer coolant lead time that preceded each test firing.

(C) Three injectors were designed for use with the Phase II cooled chamber; two injectors were fabricated. The primary consideration in the selection of the Phase II injector designs was compatibility of the injector with the oxidizer transpiration cooled chamber. The base line performance of

II, B, Phase II (cont.)

the injector used for the cooled chamber testing was obtained with 25 L* ablative-lined chamber; the C* of this injector was 93.4% of theoretical which compares favorably with the program goal of 94%C*.

(C) Twelve tests were conducted with the Phase II ClF_3-cooled chamber at 1000 lb thrust, 1000 psia pressure. The cumulative firing duration on the chamber was 21.88 seconds and the longest test duration was 8.86 seconds. The maximum steady-state wall surface temperature was 1596°F. Injector induced streaking in the convergent area of the chamber was eliminated and the heat streaks in the chamber cylindrical section were drastically reduced.

(U) One-half of the divergent section of the nozzle was eroded on the last test of the ClF_3-cooled chamber. The chamber failed because of attachment of the exhaust plume to the platelet aft retainer which produced a high local heat load, and because flashing of coolant within the chamber wall coupled with a marginal coolant lead time resulted in the platelets in the nozzle not being filled with coolant at the inception of firing. Erosion resulted when the uncooled platelets overheated. The rest of the chamber was in excellent condition.

(U) The Phase II test results demonstrated the feasibility of ClF_3 transpiration cooling at 1000 psia chamber pressure. The heat transfer data indicated that the concept operated as designed. The substantial reduction in chamber streaking indicated the importance of obtaining a smooth wall surface and of designing the injector for compatibility with the chamber. The performance model correlated well with the 1000 psia Phase II ClF_3 data.

III. CONCLUSIONS

(U) The conclusions presented in the paragraphs that follow are based on the design, fabrication and test experience that was obtained over a 20 month period with three oxidizer transpiration cooled TRANSPIRE chambers.

(U) The feasibility of transpiration cooling using the TRANSPIRE concept was demonstrated by 3295.9 seconds of test firing in 150 tests that included multiple restart duty cycles.

(U) The use of oxidizers as transpiration coolants was demonstrated with the ultra-thin TRANSPIRE platelet design. Both N_2O_4 and ClF_3 were used to cool TRANSPIRE chambers at 100 lb thrust, 100 psia and 1000 lb thrust, 1000 psia operating conditions.

(U) The TRANSPIRE concept functioned as designed. The agreement between the predicted and actual hydraulic characteristics of the chamber indicates that the flow metering aspects of the TRANSPIRE platelets functioned as designed. The successful operation of the Phase I chambers with severe injector induced heat streaks indicates that the flow control features of the TRANSPIRE concept prevented hot-spot instability.

(U) No difficulties were encountered in the fabrication of the small scale TRANSPIRE experimental chambers. There are no complicated fabrication processes that preclude applicability of the concept. Since the thermal-hydraulic design of the chamber can be adapted to any material that can be fabricated into platelets the materials of construction can be selected for compatibility with the propellants.

(U) Plugging, which was envisioned as a potential problem because of the small coolant passageways on the ultra-thin platelets, can be prevented. A cumulative firing duration of 3076.7 seconds was obtained on a single chamber

III, Conclusions (cont.)

with no change in the hydraulic characteristics of the chamber. A small filter in the coolant feed circuit was not changed or flushed during the 3076.7 seconds of testing. The key to prevention of the plugging was to start with a clean oxidizer feed system and then filter the oxidizer during fill of the run tank.

(U) The most important factor in the minimization of the coolant flow requirements is the compatibility of the injector with the oxidizer cooled chamber wall. Impingement of fuel rich zones and of injector element spray-fans on the chamber wall produces heat streaks. Adequate cooling of these zones produces overcooling in adjacent low heat flux areas. The Phase II injector was designed for compatibility with the chamber; for comparable surface temperatures the throat section of the Phase II nickel chamber was operated at half the coolant flow rate required for that section of the Phase I nickel chamber.

(U) Two other factors to be considered in the minimization of the coolant flow requirements are the surface roughness of the chamber wall and the materials of construction. Platelets that protruded into the gas stream from the surface of the wall acted as boundary layer trips and induced heat streaks or aggravated existing heat streaks. The effect of heat streaking is mitigated by the use of high conductivity materials. The Phase I nickel chamber showed less susceptibility to heat streaking than the Phase I stainless steel chamber because the nickel chamber had a smoother wall and because of the higher thermal conductivity of the nickel.

(U) The TRANSPIRE platelet is quite amenable to thermal analysis. The biggest unknown is the thermal properties of the oxidizer coolants at elevated temperatures. Both the performance and heat transfer models, developed for this program, correlate the data reasonably well.

III, Conclusions (cont.)

(U) The thermal instrumentation developed for this program was highly successful. The placement of thermocouples within the platelets permitted temperatures to be measured on the surface of the chamber wall at the desired axial and circumferential locations. Accurate determination of the temperature profile in the wall using subsurface thermocouples was not successful.

(U) Nickel material is recommended for compatibility with ClF_3 on the basis of data found in the literature and from test experience. Nickel injector bodies were used for all the ClF_3 injectors except for one which had a stainless steel body. Injector face erosion and bell mouthing of the MHF-3 fuel orifices occurred with the stainless steel body but did not occur with nickel injector bodies.

(U) Welds are particularly susceptible to attack by ClF_3 especially when subjected to mechanical deflection and thermal expansion. This fact coupled with the fact that the interhalogens react violently with water complicates the use of water coolant circuits with ClF_3 and other interhalogen propellants. The water coolant circuit leakage problem that hampered Phase I testing and ultimately led to the failure of the Phase I ClF_3-cooled chamber was precluded in Phase II by elimination of the water coolant circuits.

(C) Although 1200°F was used as the design value for the nickel chamber wall on the basis of compatibility data in the literature for fluorine, operation at higher temperatures for limited duration is feasible. The Phase II ClF_3-cooled chamber was operated for about eight seconds with surface temperatures in one location that were as high as 1596°F.

IV. DESIGN AND FABRICATION

A. INJECTORS

1. Design

(U) It was an objective of this contract to design injectors that would meet or exceed 94% of theoretical C* performance in order to provide a thermal environment that would permit a realistic evaluation of the feasibility and capabilities of the cooling concept.

(U) Seven injectors were designed for Phase I of this program. Three were designed to operate at 100 psia chamber pressure and 100 lb thrust; two of these were designated for ClF_3/MHF-3 operation and the third for N_2O_4/AeroZINE 50 operation. The remaining four injectors were designed for operation at 1000 psia chamber pressure and 1000 lb thrust; two for ClF_3/MHF-3 operation and two for N_2O_4/AeroZINE 50 operation.

(U) Figure 3 shows the general configuration of the Phase I injector designs. Each injector assembly consists of a flange, injector body, and oxidizer cap. The flange and oxidizer cap are made of 347 stainless steel and are identical for all injectors. The injector bodies are made of 347 stainless steel for the N_2O_4 injectors and, except for the S/N 1 injector, of nickel for the ClF_3 injectors. Except for the material, propellant feed manifolding, and pattern, the injector components are identical. Each of the injectors has a supplementary water coolant circuit. The supplemental coolant circuit was added as a precautionary measure to prevent oxidizer boiling during long duration runs. In the backup design the water coolant circuit was used to provide face cooling. The locations of the water coolant circuits are shown in Figure 3.

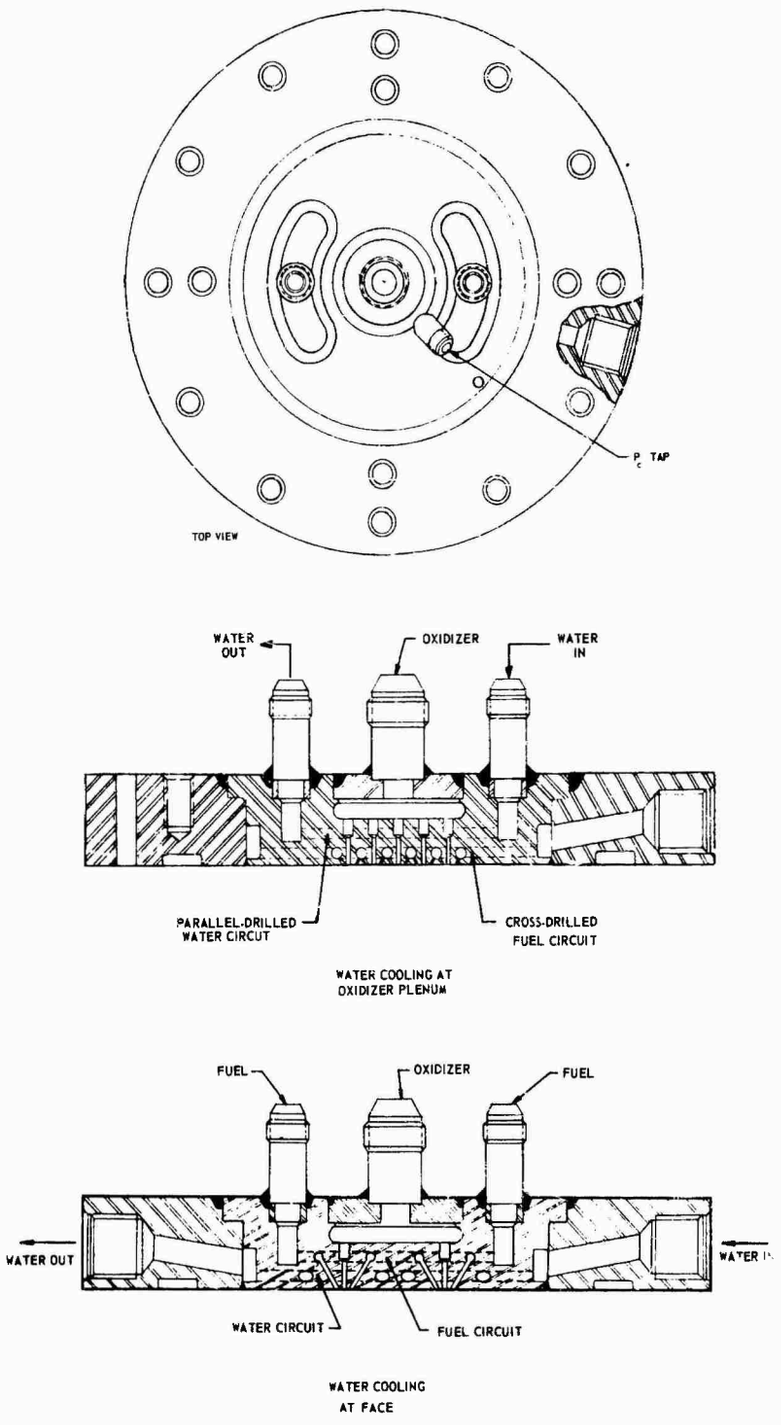

Figure 3. Phase I Injector Design

IV, A, Injectors (cont.)

(U) The triplet element was selected as the basic element for all of the Phase I injector patterns based on the experience gained on a number of Aerojet company-sponsored programs.

(U) Three injectors were designed for Phase II of this program to minimize the chamber streaking problem experienced in Phase I testing with the conventional 21 element triplet 1000 lb thrust injectors. They consisted of a HIPERTHIN injector, a vortex injector and a 49-element conventional injector. These injectors were designed to operate at 1000 psia chamber pressure and 1000 lb thrust with ClF_3/MHF-3 as propellants.

(U) The HIPERTHIN injector was selected on the basis of performance and compatibility (uniform propellant distribution across the face). The HIPERTHIN injector, like the TRANSPIRE chamber, is made from thin platelets that (unlike TRANSPIRE) are brazed together to form an integral leak-tight unit. The HIPERTHIN design used in this program employed three platelet designs: 0.006 in. thick spacer platelets, 0.0015 in. thick fuel metering platelets, and 0.0015 in. thick oxidizer metering platelets. The method of stacking the platelets to form the propellant circuits is shown in Figure 4. After assembly with two end plates, through which the oxidizer is introduced, the platelets are furnace brazed. Copper flashing on the platelets is the braze alloy. As shown in Figure 5 the brazed assembly is then machined and a flange and fuel cap are brazed to the assembly. The final operation is machining the excess structural material off the face of the injector (at the location shown in Figure 4) and electropolish to open the flow passages.

(U) The HIPERTHIN injector was designed with narrow ring of oxidizer at the outer periphery of the injector face for improved compatibility with the transpiration cooled chamber. The injector platelet material was specified as Nickel 270 for compatibility with ClF_3. The use of nickel

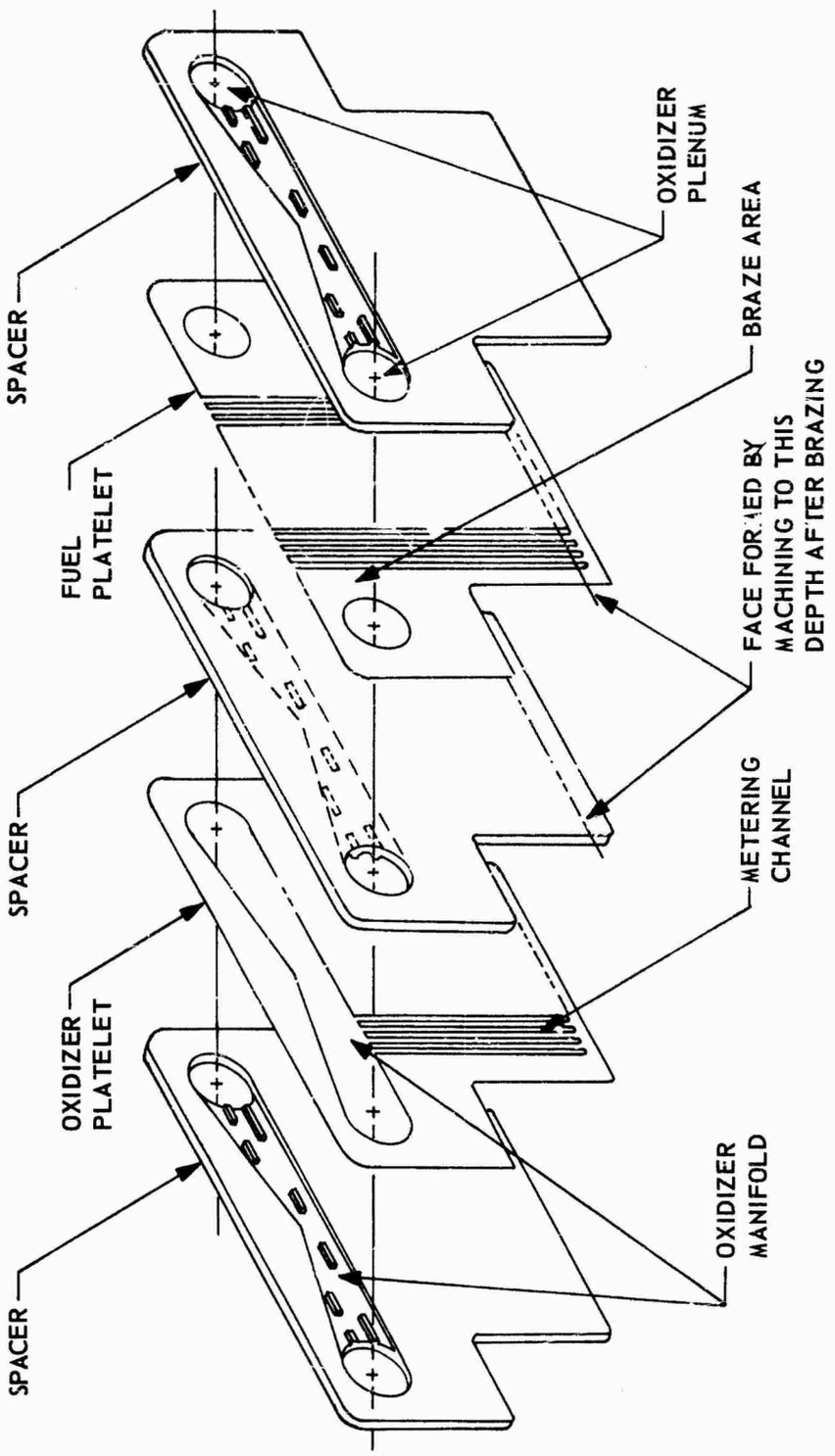

Figure 4. HIPERTHIN Platelet Orientation

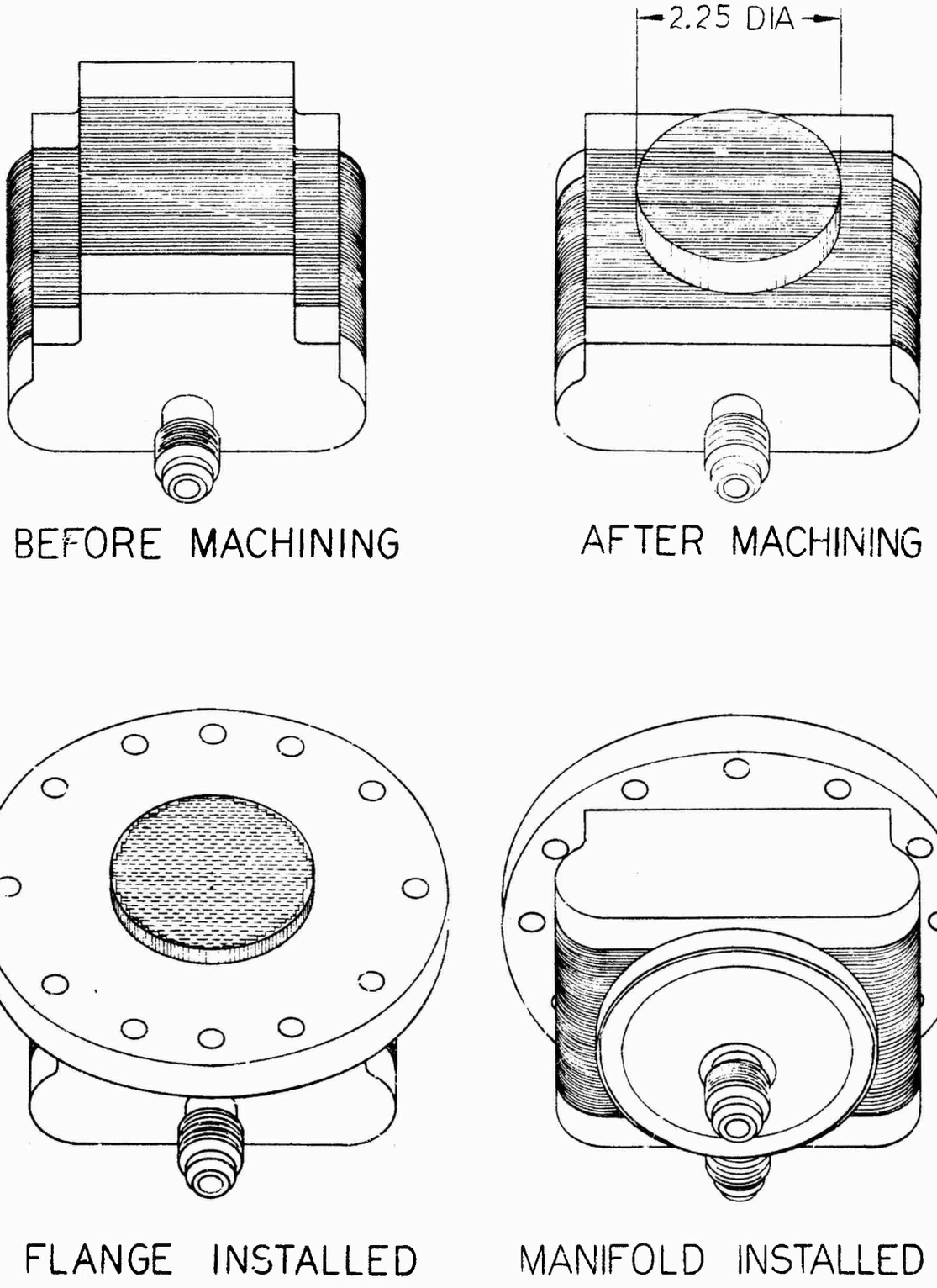

Figure 5. Injector Fabrication Sequence

IV, A, Injectors (cont.)

material presented a brazing problem since all Aerojet brazing experience has been with injectors made of CRES 347 material. A experimental braze study was conducted to resolve this problem. Small nickel samples were brazed to determine the braze cycle, braze temperature and copper plating thickness (braze alloy) that gave a good bond without blocking the propellant passages due to the flow of braze alloy.

(U) Figure 6 shows the Phase II vortex injector and 49-element injector designs. The vortex injector was designed with radial fuel orifices in the central hub of the injector and with tangential oxidizer orifices on the outer periphery of the injector for compatibility with the oxidizer transpiration cooled chamber. The injector consists of a flange, a fuel manifold assembly, a retainer assembly and a spacer. The spacer thickness can be varied to adjust the axial position of the fuel orifices relative to the oxidizer orifices for performance optimization. A water coolant circuit was added to the fuel manifold assembly to circumvent cooling problems during long duration firings.

(U) The 49-element injector is a cross-drilled injector and unlike the Phase I injectors does not have a water cooling circuit. The injector pattern consists of a central matrix of 37 (FOF) tangential fan triplets, 4 (OFO) folded triplets*, and 8 unlike doublets (see Figure 7). The injector was designed using Phase I experience to obtain good compatibility while maintaining good performance. The increased number of elements improves the mass distribution and propellant dispersion to minimize streaking in the convergent and throat areas that was experienced in Phase I testing with the 21-element triplet injector.

* The orifices of a folded triplet element are not in line, but form a triangle.

49 ELEMENT INJECTOR

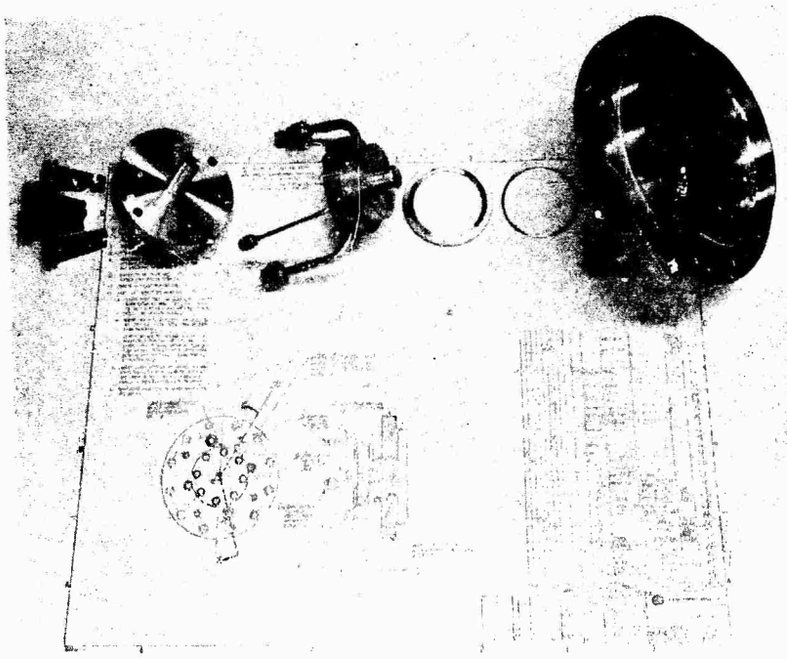

VORTEX INJECTOR ASSEMBLY

Figure 6. Phase II Injectors (u)

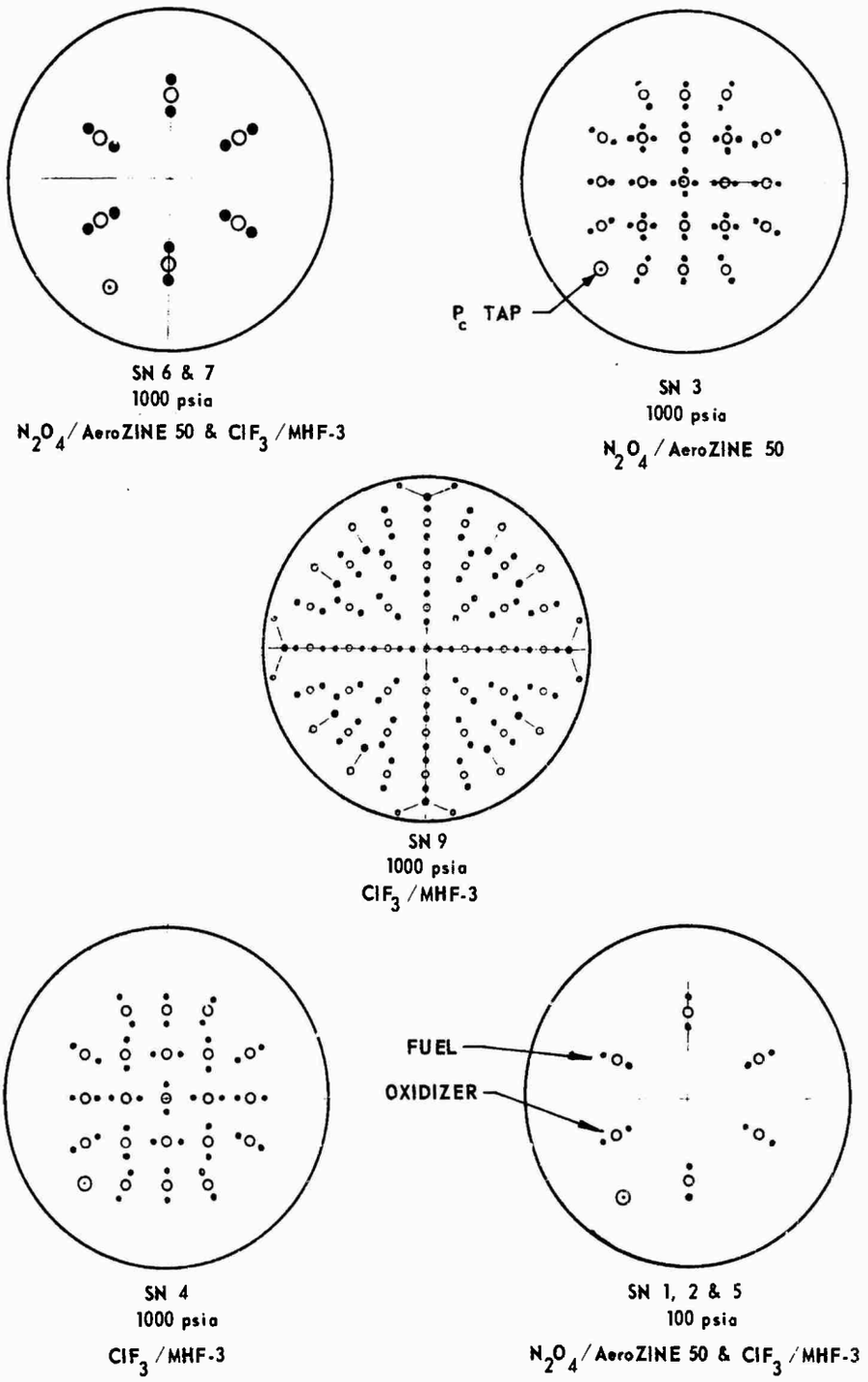

Figure 7. Injector Patterns (u)

IV, A, Injectors (cont.)

(U) The materials selected for the Phase II injectors consisted of Nickel 200 for the components exposed to the combustion products of ClF_3/MHF-3 and 304 L stainless for the remainder of the component parts.

(U) A summary of the different types of injectors designed in Phase I and Phase II is given in Table 1. The conventional injector patterns are shown in Figure 7.

(U) TABLE 1

SUMMARY OF INJECTOR TYPES (U)

P/N	S/N	Element Design	Propellant	Chamber Pressure (psia)	Location of Cooling Circuit	Injector Body Material
1122315-9	1	6 Triplets	ClF_3/MHF-3	100	At oxidizer plenum	CRES 347
1122315-9	2	6 Triplets	N_2O_4/A-50	100	At oxidizer plenum	CRES 347
1122315-19	3	16 Triplets, 5 Pentads	N_2O_4/A-50	1000	At oxidizer plenum	CRES 347
1122315-29	4	21 Triplets	ClF_3/MHF-3	1000	At oxidizer plenum	Nickel
1122315-39	6	6 Triplets	N_2O_4/A-50	1000	At face	CRES 347
1122315-49	7	6 Triplets	ClF_3/MHF-3	1000	At face	Nickel
1122315-59	5	6 Triplets	ClF_3/MHF-3	100	At oxidizer plenum	Nickel
1130922-29	8	Vortex	ClF_3/MHF-3	1000	At face	Nickel
1132431-1	9	41 Triplets 8 Doublets	ClF_3/MHF-3	1000	None	Nickel
1131610-1	10	HIPERTHIN	ClF_3/MHF-3	1000	None	Nickel

IV, A, Injectors (cont.)

2. Fabrication

(U) Seven injectors were fabricated during Phase I of this program. Two -9 injectors (See Table 1) and one each of the -19, -29, -39, -49 and -59 injectors were assembled. The -59 injector was fabricated to replace the -9 injector S/N 1 because of bell-mouthing of the injector fuel orifices coupled with poor performance during ClF_3/MHF-3 injector checkout testing. Poor injector element impingement was thought to have contributed to the low performance of the injector, therefore, no injector pattern change was made. The -59 injector was identical to the -9 injector except that the body of the injector was made of A-200 nickel instead of CRES 347. Hydroflow pictures of the 100 lb thrust -9 and the 1000 lb thrust -19 N_2O_4/AeroZINE 50 injectors are given in Figure 8. Pressure drop - flow measurements made during hydrotest indicated that all the injectors used in this program were operating as designed with no internal blockage or obstructions.

(U) Two injectors, a vortex injector and a 49-element conventional injector, were fabricated during Phase II of this program. (See Table 1.) Fabrication of a third injector, a HIPERTHIN injector, was initiated but was later terminated due to a nonrepairable intermanifold leak between the oxidizer plenum and fuel metering channels (see Figure 4). Failure to attain a good braze joint resulted because of distortion of the nickel material at high temperatures. The 1000 lb thrust 21-element triplet injector S/N 4 that was used in Phase I of the program was modified to be used as a backup injector. The modification consisted of welding and machining a lip seal ring on the injector to mate with the Phase II ablative and cooled chamber housings. No modification was made to the pattern.

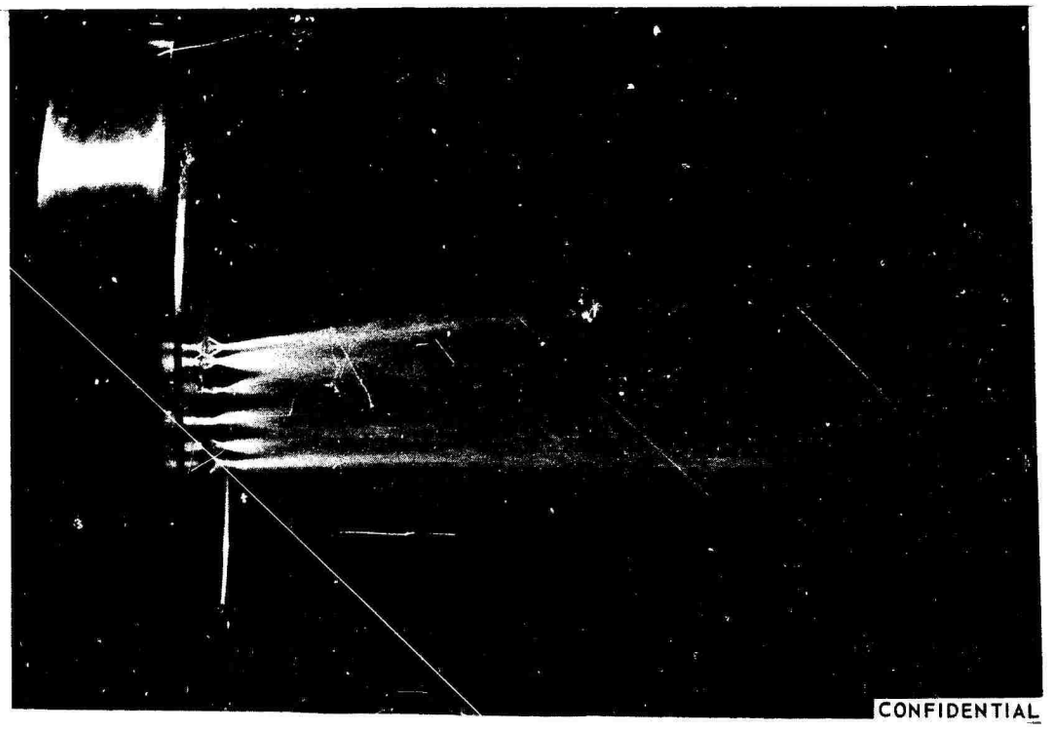

100 PSIA INJECTOR, S/N 1

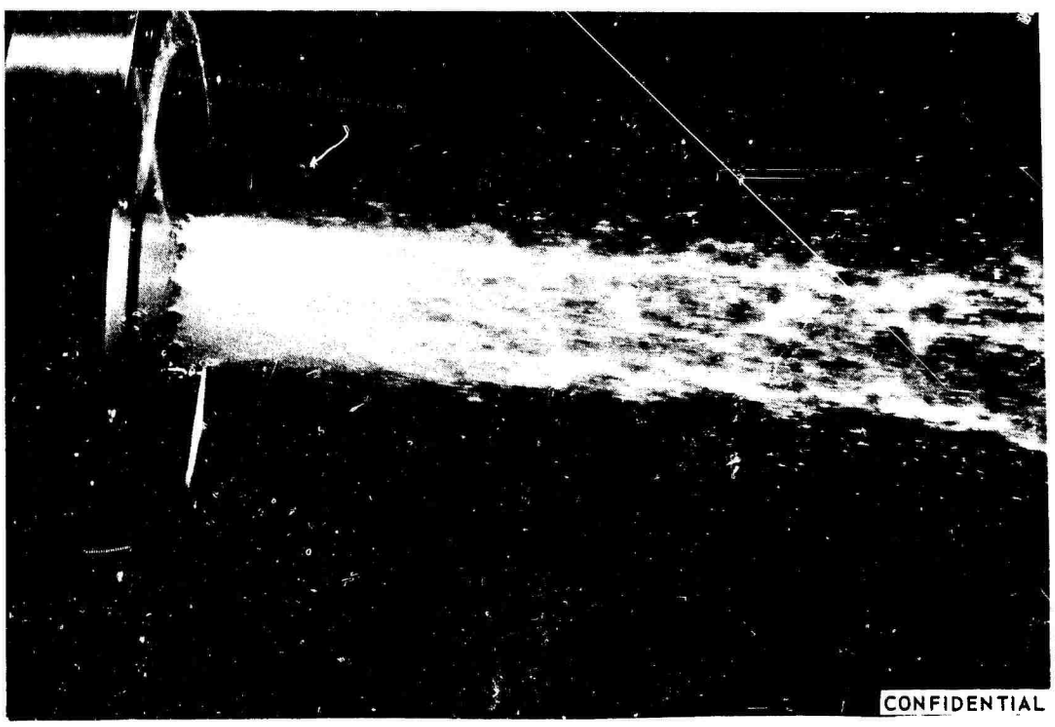

1000 PSIA INJECTOR, S/N 3

Figure 8. Injector Water Flow Pattern Check (u)

IV, Design and Fabrication (cont.)

B. UNCOOLED CHAMBERS

1. Phase I

(U) Two uncooled ablative lined combustion chambers were designed in Phase I to check injector performance and compatibility, one for use with N_2O_4/AeroZINE 50 and one for use with ClF_3/MHF-3. Both units were designed for operation at a chamber pressure of 1000 psia and 1000 lb thrust, or 100 psia chamber pressure and 100 lb thrust.

(U) The injector-chamber interface as well as the chamber inside contour of the uncooled chambers were made identical to that of the cooled chambers. This made it possible to obtain base line injector performance data that could be used to evaluate the performance of the cooled combustion chambers. The uncooled chamber design is shown in Figure 9.

(U) The ablative liner material for each of the two chambers was selected on the basis of compatibility of the liner material with the combustion gases. A carbon-filled phenyl aldehyde graphite fabric was selected for the ClF_3/MHF-3 chamber. The ablative material employed in the N_2O_4/ AeroZINE 50 chamber was a modified phenolic high char resin system reinforced with high-silica fabric.

(U) Two uncooled chambers were fabricated in Phase I along with one spare chamber ablative insert, one spare throat section, and two spare throat ablative inserts for each chamber. One chamber was built for each propellant combination. No fabrication problems were experienced. Figure 9 shows the uncooled chamber components.

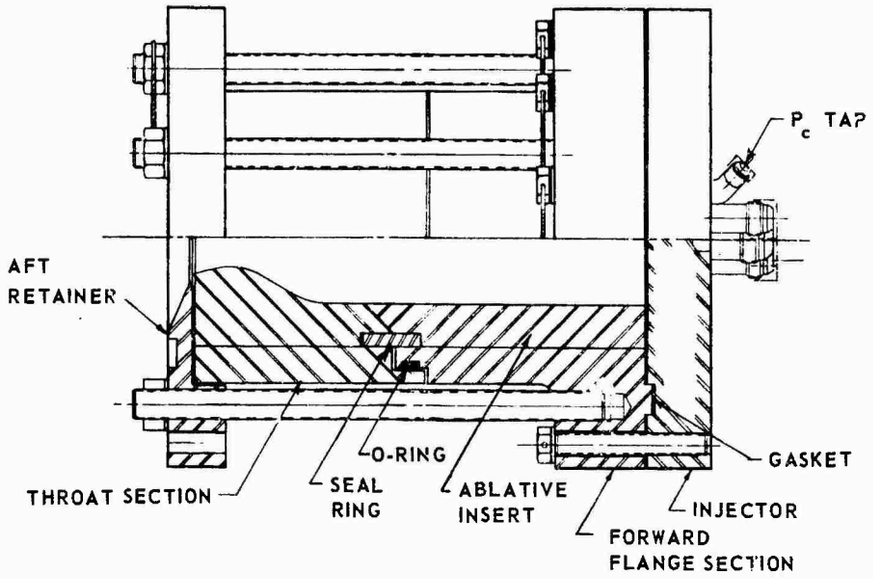

UNCOOLED CHAMBER DESIGN

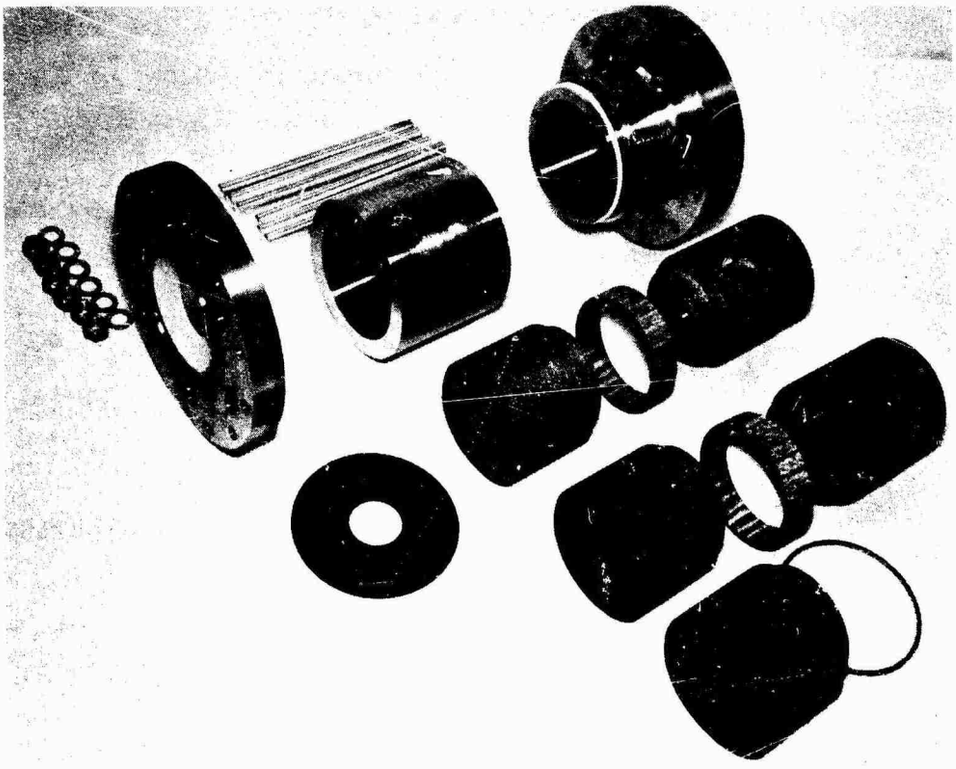

UNCOOLED CHAMBER COMPONENTS

Figure 9. Uncooled Chamber Assembly

IV, B, Uncooled Chambers (cont.)

2. Phase II

(U) The spare ClF_3 ablative liners and the uncooled chamber components that were residual from Phase I were used to fabricate the 25L* ablative lined combustion chamber that was used for checkout testing of the Phase II injectors. The Phase I uncooled chamber design was changed to reduce the overall length of the chamber assembly to obtain a 25L* chamber, to add a chamber pressure tap to the throat section of the chamber and to change the injector-chamber seal from a crush type seal to the O-ring lip type seal that was used in Phase II.

(U) One uncooled combustion chamber forward flange, two-cylindrical ablative liner inserts and two assembled throat sections from Phase I of this program were modified to conform to the design requirements for the Phase II uncooled ablative lined combustion chamber. The ablative liners that were used were designed for use with ClF_3/MHF-3 at 1000 psia chamber pressure and 1000 lb thrust.

IV, Design and Fabrication (cont.)

C. COOLED CHAMBERS

1. Phase I

(U) In Phase I of this program two transpiration cooled chambers were designed and fabricated, one with nickel platelets for use with the ClF_3/MHF-3 propellant combination and the other with 347 stainless steel for use with N_2O_4/AeroZINE 50. Both units were designed to operate at nominally 100 lb thrust with a 100 psia chamber pressure, and 1000 lb thrust with 1000 psia chamber pressure. These two units were essentially identical except for variations resulting from different coolant flow rate requirements and the substitution of nickel for stainless steel in some of the ClF_3-cooled chamber components. Because of this similarity these two units will be discussed jointly. The approach taken will be to first briefly present and describe the entire cooled chamber assembly. This will be followed by a detailed description of the design of the more important component parts.

(U) The transpiration cooled chamber shown in Figure 10 consists of an inner chamber wall composed of stacked ultra thin platelets, an outer housing to form an external manifold to the platelet stack, three seal-divider rings to divide the wall of stacked platelets into four axial hydraulic sections, and two rods to locate and index the platelets within the chamber. In addition there are four Teflon O-rings which form an inter-manifold seal between chamber sections and the external seal at the chamber housing, an aft platelet retainer to serve as a platelet loading ram and seal hub for the external housing seal, a gasket to make the chamber-injector seal, the injector, and twelve 3/8 inch diameter rods with nuts and washers to load the platelets axially through the aft platelet retainer.

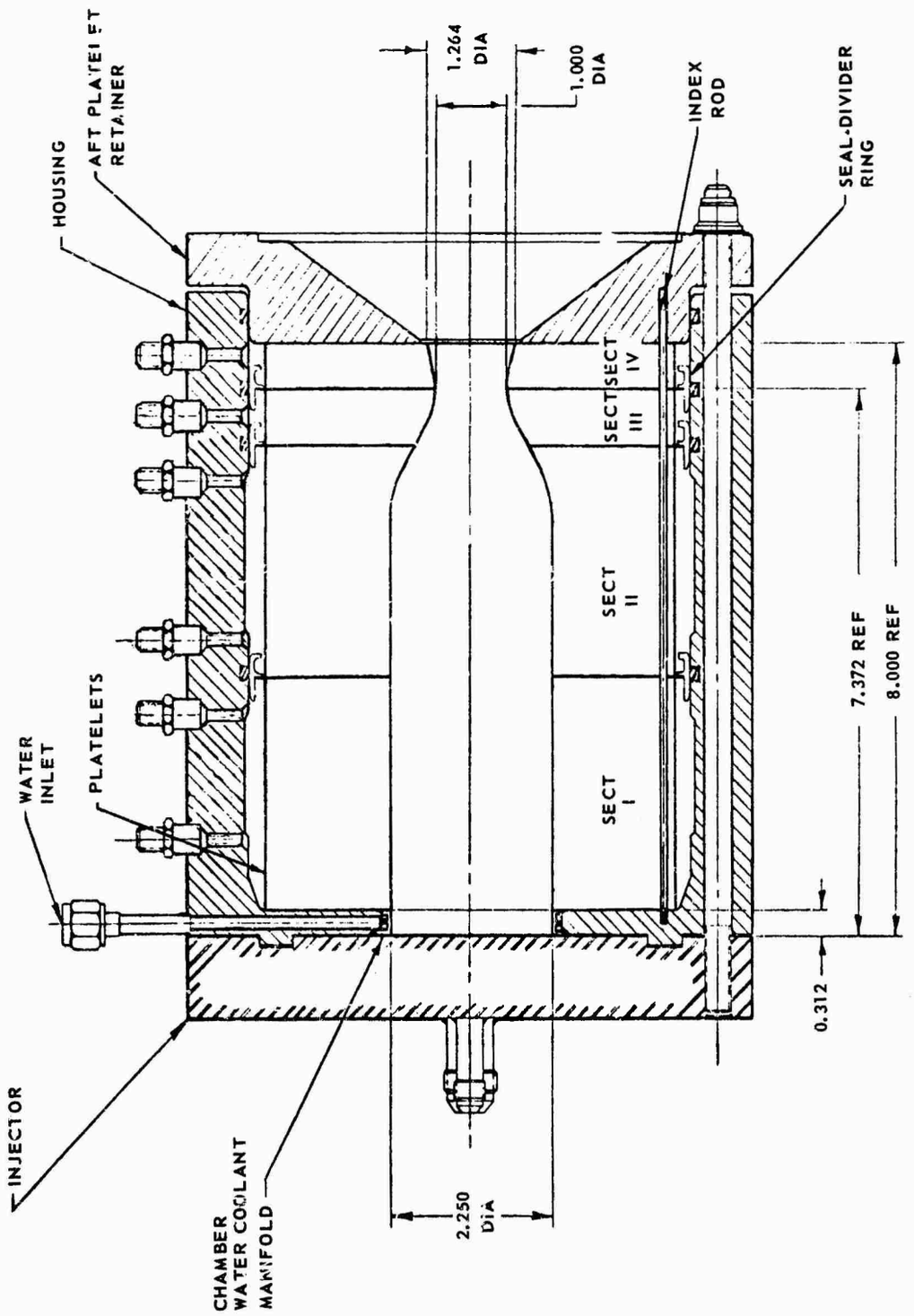

Figure 10. Phase I Cooled Chamber Assembly

IV, C, Cooled Chamber (cont.)

(U) The oxidizer coolant is fed to the chamber through four openings in the chamber outer housing. Four plenums are provided so that the coolant flow rate to each chamber section can be independently controlled. The coolant then passes through the porous chamber wall and enters the hot gas boundary layer, cooling the wall as it passes through.

(U) The cooled chamber assembly can be assembled independently of the injector to facilitate handling and test stand installation and removal.

a. Chamber Platelets

(U) In this section the design and fabrication aspects of the chamber platelets will be discussed in general terms. Specific design equations and their derivations are given in Appendix I. The platelet fabrication method and problems will be presented.

(U) The first step in the design of the platelets was the establishment of the thermal environment. Gas-side film coefficients were calculated using the results of the Aerojet Chemical Composition Computer Program (Prog. No. 166) coupled with the method of calculating film coefficients given by Bartz[2]. To account for nonuniform combustion and eddying the predicted film coefficients were multiplied by a factor which varied from 2.0 at the injector to 1.0 at the throat. No provision could be made at this time for potential circumferential heat flux variations due to the injector pattern.

(U) Film coefficients and calculated recovery temperatures were then used in conjunction with the equations given in Appendix I to design the individual platelets and establish the coolant flow

IV, C, Cooled Chambers (cont.)

requirements. Design surface temperatures on the platelets were set at 1200°F on the Ni for the ClF_3-cooled chamber and 1500°F on the stainless steel for the N_2O_4-cooled chamber. These values were selected primarily on the basis of the available propellant compatibility information.

(U) The nominal flow rates, given in Table 2, are the design flow rates obtained using the procedure described above. The hydraulic resistance of the individual platelets were set to supply these nominal values when the coolant plenum pressures were 1125 psia at P_c = 1000 psia and 116 psia at P_c = 100 psia. The axial coolant flow distribution of the ClF_3-cooled chamber at 1000 psia is shown in Figure 11. Both the nominal flow values (mass velocities) and the actual flow values that were obtained by clocking the platelet pairs are shown in the figure.

(C) TABLE 2

PHASE I NOMINAL COOLANT FLOW RATES (lb/sec) (U)

Chamber Section	N_2O_4		ClF_3	
	100 lb Thrust	1000 lb Thrust	100 lb Thrust	1000 lb Thrust
I	0.0353	0.289	0.057	0.480
II	0.0342	0.280	0.0553	0.466
III	0.0077	0.092	0.0125	0.105
IV	0.0050	0.078	0.0081	0.0682
Total	0.0822	0.739	0.1329	1.1192

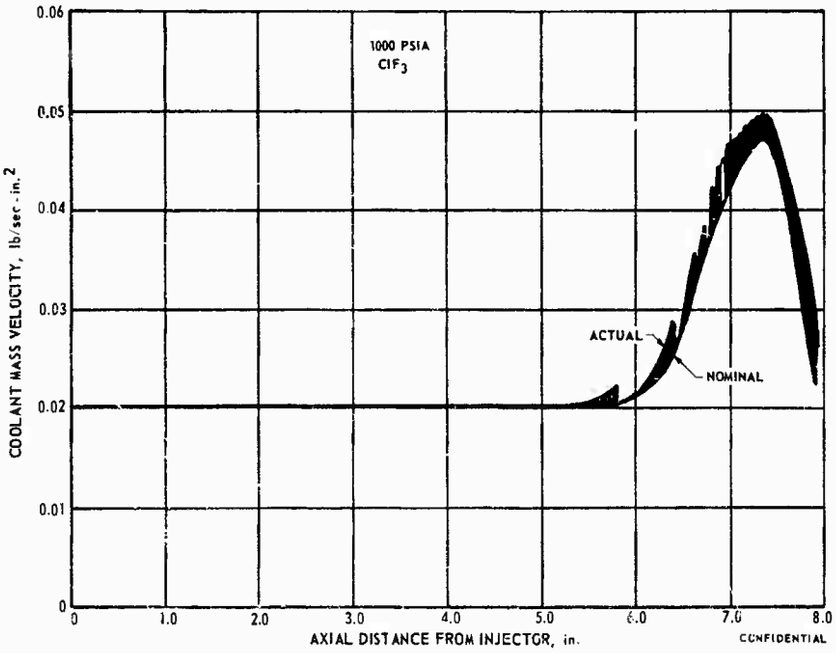

Figure 11. Axial Coolant Distribution (u)

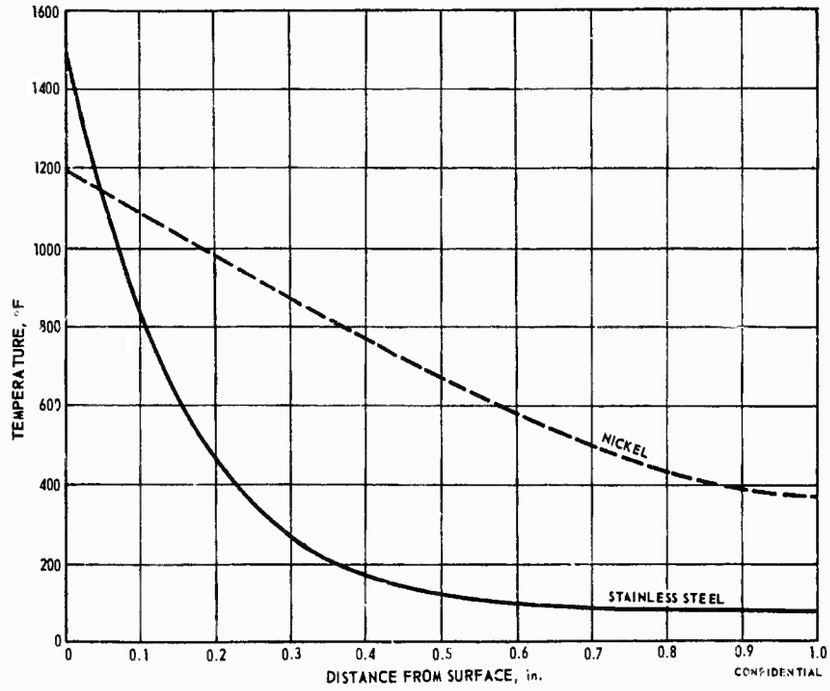

Figure 12. Temperature Distribution in Throat Platelets 100 psia (u)

IV, C, Cooled Chambers (cont.)

(U) From the injector to an area ratio of 2.5 in the convergent section of the chamber, 0.020 in. thick distribution platelets were used. From an area ratio of 2.5 in the convergent section of the chamber to the end of the nozzle (ε = 1.6), 0.010 in. thick distribution platelets were used. As discussed in Appendix I the computerized heat transfer model calculates the temperature profile in the platelet as part of the computational procedure. The temperature profiles at the 100 psia design conditions are shown in Figure 12 for the 0.010 in. thick nickel and stainless steel platelets in the throat.

(U) The use of both 0.010-in. thick and 0.020-in. thick platelets in the design was based on several considerations. First, the heat transfer analysis showed that in the low flux regions of the chamber the 0.020 in. thick platelets could operate almost as effectively as the 0.010 in. thick platelets. Using 0.020 in. thick platelets in the chamber section substantially reduced the total number of platelets required without compromising the cooling effectiveness.

(U) A second reason for the use of both 0.020-in. thick and 0.010-in. thick platelets is that having platelets of different thicknesses in adjoining sections of the nozzle allowed the effect of platelet thickness on cooling behavior to be evaluated experimentally. Since platelet thickness is a key parameter in the determination of unit costs some experimental verification of this phase of the analytical model was considered to be desirable.

(U) A final reason for the inclusion of the 0.020-in. platelets is that the instrumented platelets are also approximately 0.020 in. thick. Any uncertainty which may arise in attempting to relate the temperatures measured in the instrumented platelets to those of its neighbors would be minimized since in at least a portion of the chamber the instrumented and noninstrumented platelets would be almost identical.

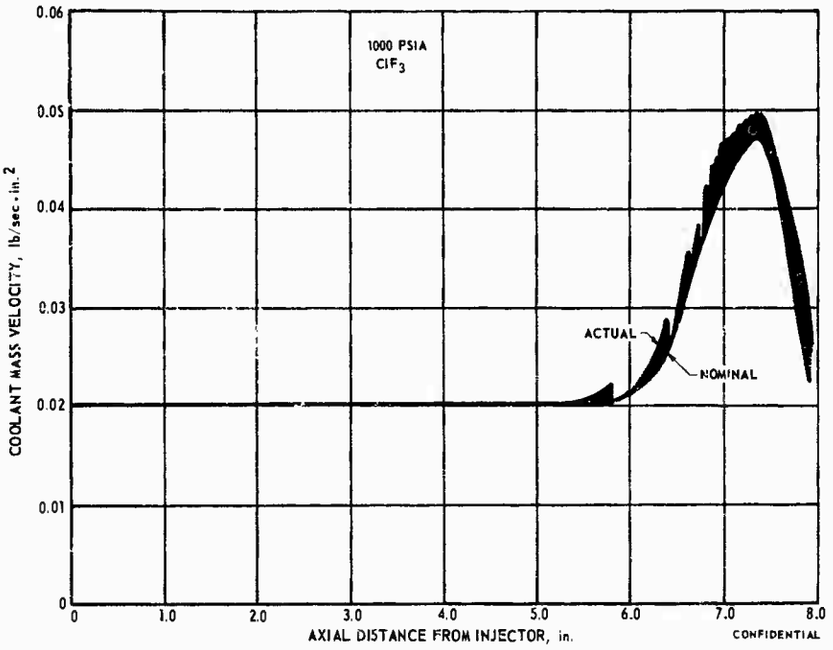

Figure 11. Axial Coolant Distribution (u)

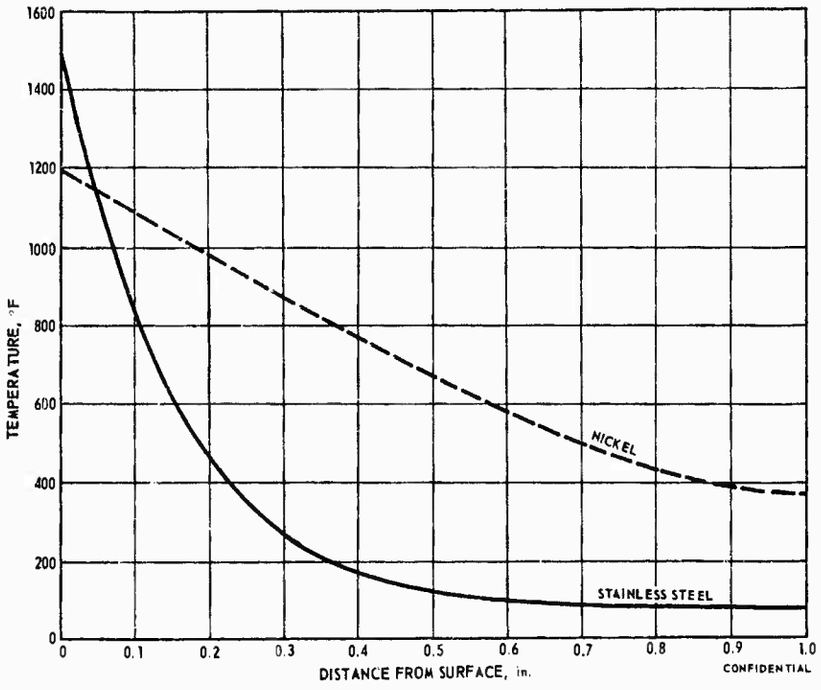

Figure 12. Temperature Distribution in Throat Platelets 100 psia (u)

IV, C, Cooled Chambers (cont.)

(U) From the injector to an area ratio of 2.5 in the convergent section of the chamber, 0.020 in. thick distribution platelets were used. From an area ratio of 2.5 in the convergent section of the chamber to the end of the nozzle (ε = 1.6), 0.010 in. thick distribution platelets were used. As discussed in Appendix I the computerized heat transfer model calculates the temperature profile in the platelet as part of the computational procedure. The temperature profiles at the 100 psia design conditions are shown in Figure 12 for the 0.010 in. thick nickel and stainless steel platelets in the throat.

(U) The use of both 0.010-in. thick and 0.020-in. thick platelets in the design was based on several considerations. First, the heat transfer analysis showed that in the low flux regions of the chamber the 0.020 in. thick platelets could operate almost as effectively as the 0.010 in. thick platelets. Using 0.020 in. thick platelets in the chamber section substantially reduced the total number of platelets required without compromising the cooling effectiveness.

(U) A second reason for the use of both 0.020-in. thick and 0.010-in. thick platelets is that having platelets of different thicknesses in adjoining sections of the nozzle allowed the effect of platelet thickness on cooling behavior to be evaluated experimentally. Since platelet thickness is a key parameter in the determination of unit costs some experimental verification of this phase of the analytical model was considered to be desirable.

(U) A final reason for the inclusion of the 0.020-in. platelets is that the instrumented platelets are also approximately 0.020 in. thick. Any uncertainty which may arise in attempting to relate the temperatures measured in the instrumented platelets to those of its neighbors would be minimized since in at least a portion of the chamber the instrumented and noninstrumented platelets would be almost identical.

IV, C, Cooled Chambers (cont.)

(U) Once the platelet thicknesses and coolant flow rates had been established the actual layout of the hydraulic network on the individual platelets was performed. The basic approach to the platelet hydraulics will be explained with reference to Figure 2 (Section I). As can be seen from this figure each platelet has four basic hydraulic elements: primary metering grooves, a distribution plenum, secondary metering grooves, and thermal influence zones. The coolant enters the platelet through the primary metering grooves. These grooves comprise roughly 90% of the hydraulic resistance on the individual platelets and their length and dimensions control the coolant flow to the platelet. The entrance to the primary metering grooves is made somewhat wider than the groove itself to give the system a built-in filter. Any dirt or particles present in the coolant which cannot pass through the primary metering grooves will lodge at the groove inlet. Since the area of the inlet is much larger than the area of the groove it can accumulate a substantial amount of dirt without producing a flow restriction.

(U) From the primary metering grooves the coolant passes into the distribution plenum. This plenum is a low resistance flow path that serves to evenly distribute the coolant around the platelet.

(U) The coolant next passes from the distribution plenum into the secondary metering groove. The secondary metering groove is a relatively high resistance flow passage which has approximately 10% of the overall pressure drop occurring in it. From the secondary metering groove the coolant enters into the thermal influence zone, which is a low flow resistance channel extending to the chamber surface. The heat transfer between the coolant and platelet occurs in the thermal influence zone.

(U) It is the combination of the secondary metering grooves and the thermal influence zone which gives the design its resistance

IV, C, Cooled Chambers (cont.)

to hot spot instability. In essence they comprise a series hydraulic circuit with a high resistance element (secondary metering groove) which is independent of local heat flux conditions, and a low resistance element (thermal influence zone) which absorbs the local surface heat flux. With this system, if the local temperature increases and the flow resistance in the thermal influence zone increases the overall resistance of the circuit remains essentially unchanged. Thus the coolant flow to the surface is uncoupled from the surface heat flux and the primary cause of hot spot instability is avoided.

(U) The platelets employing this hydraulic system were constructed using a composite design in which each hydraulic unit is composed of a thick (0.010 - 0.020 in.) distribution platelet and a thin (0.001 in.) metering platelet placed together to form a single functional unit (See Figure 2, Section I). In the platelet pair concept noncritical flow areas such as the thermal influence zone, manifolds and plenums are formed by etching the thick distribution platelet using conventional photoetching techniques. However, the critical flow areas such as the primary and secondary coolant metering channels are formed by etching passages completely through the thin metering platelet. With this design approach the depth of the critical flow control passages is no longer dependent on the etch process but is only a function of the thickness and uniformity of the original sheet stock from which the metering platelets are made. The thickness of the sheet stock can be more precisely controlled than depth of etch and can be measured before fabrication of the platelets. Since laminar flow varies as the cube of the channel depth and since the channels are 0.001 inch deep tolerances are critical. A 10% deviation in the depth of the metering channel produces a 33% deviation in the flow in that channel.

(U) There are several advantages which are gained by employing the composite platelets. By making the depth dimension independent

IV, C, Cooled Chambers (cont.)

of the etch process both manufacturing and inspection procedures are greatly simplified and hence unit costs are reduced. The second benefit is that the hydraulic resistance of the individual composite platelets is adjustable over a wide range of resistances. The platelet pairs have been designed so that the placement of the thin metering platelet on the thick distribution platelet (clocking) determines the length of the metering groove (See Figure 2, Section I). It is possible with a single design and clocking to achieve wide variation in flow rates with a constant pressure differential between manifold and chamber, or to obtain the desired flow rates with the axial decrease in chamber pressure in the throat. For the chambers used in this program the theoretical axial coolant distribution was achieved (See Figure 11) with only four metering platelet designs and three distribution platelet designs. These designs are shown in Figure 13. The small ID distribution platelet with four inlets used in the throat section is not shown. The cost savings resulting from utilization of so few platelet types was significant. In addition, it would be possible to modify the hydraulic resistance contour of the wall at any point in the test program (if preliminary test data indicate this would be desirable) by disassembling the unit, rotating distribution platelets, and reassembling.

(U) The distribution platelets vary only in the number of inlets, the thickness of the platelets, the inside diameter, and the number of indexing holes. Platelets with four inlets are used in the cylindrical portion of the chamber and platelets with two inlets are used in the convergent and throat portion of the chamber. Distribution platelets with two inlets are used with the two groove metering platelets to obtain longer primary metering grooves and, therefore, higher pressure drop. The plenum and the thermal influence zone configurations as well as the depth of etching (0.0025-in.) are the same for all distribution platelets. Some of the areas that have a controlled depth etch are crosshatched in Figure 2 (Section I).

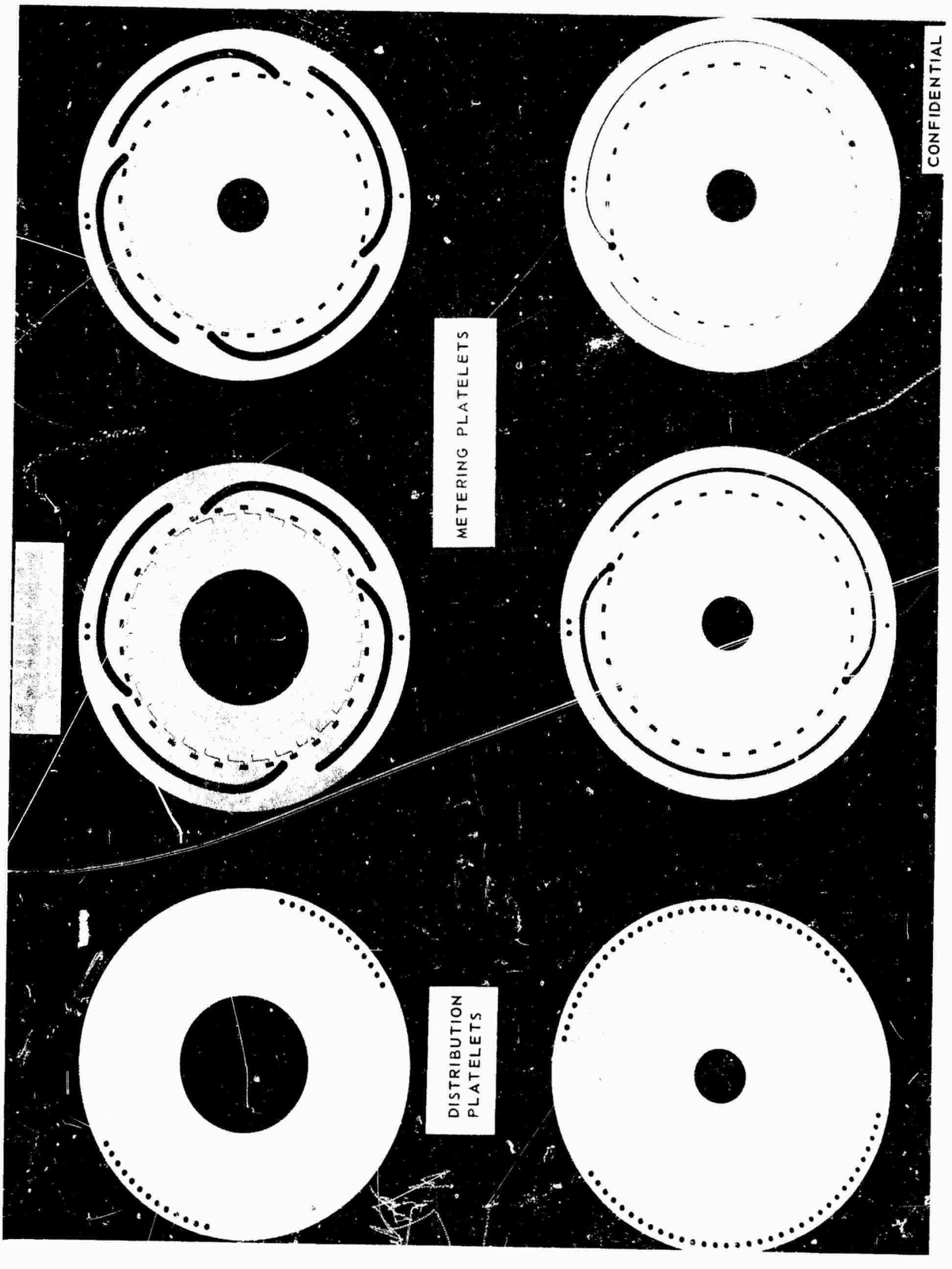

Figure 13. Coolec Chamber Platelets (u)

IV, C, Cooled Chambers (cont.)

(U) The four metering platelet configurations that are used in the cooled chamber assembly are shown in Figure 13. These metering platelets are 0.001-in. thick and the primary metering groove, the secondary metering groove, the inside diameter, and the three small holes used for assembly purposes are etched through the platelet during the photoetch fabrication process. The metering platelet configurations vary only in the number of primary grooves (two or four), the width of the metering groove, and the dimension of the inside diameter. The number and shape of the secondary metering grooves are identical for all configurations.

(U) The hydraulic resistances or platelet clockings that were used in assembling the chambers were calculated assuming a constant coolant manifold pressure on the outside of the platelets and considering the internal gas pressure profile existing along the chamber contour. Since the chamber and nozzle must operate at both 1000 psia and 100 psia it was necessary to make a design compromise. The platelet hydraulic resistances which give optimum axial coolant distribution at the one pressure level are somewhat off optimum at the other. As a result, part of the divergent portion of the nozzle was designed to be roughly 10% overcooled at the 1000 psia condition in order that it will be adequately cooled at the 100 psia condition.

(U) The platelets for the N_2O_4- and ClF_3-cooled chambers were fabricated using conventional photo etching techniques. This process uses a master enlargement of the part to be fabricated which is then photo reduced to the actual size of the part. The layout of the master enlargement or "art work" is not dependent on the material to be used, therefore the platelets for the N_2O_4- and ClF_3-cooled chambers were designed to be identical except for the material from which the platelets were made. Only one set of art work was required to fabricate the platelets for both chambers.

IV, C, Cooled Chambers (cont.)

(U) The use of identical platelets for both propellant systems was made possible by the distribution-metering platelet pair concept in which the hydraulic resistance of a pair is controlled by the orientation of the metering platelet and distribution platelets relative to each other. Thus, by changing the assembly procedure somewhat, the same platelet design was used to construct the N_2O_4-cooled chamber (stainless) and the ClF_3-cooled chamber (nickel).

(U) A $\pm$10% range of tolerance on standard stock thicknesses was allowed when ordering the material for the chamber platelets to conserve costs. This meant that precise measurements had to be made when the material was received. Thermal and hydraulic design calculations were revised and the number of platelets that made up the chamber assembly were adjusted to compensate for the deviation from the design material thickness for the chamber platelets.

b. Chamber Housing

(U) The primary function of the chamber housing was to provide a self-contained, pressure tight housing for holding the platelet stack. As such it also served as the outer wall to the four chamber coolant plenums, as a mechanical loading fixture for compressing and holding the platelet stack, and as a base for the attachment of coolant bleed valves, pressure transducers, etc.

(U) One of the restraints placed on the design was that the injectors should be easily attached to and removed from the chamber. Because of this it was not considered desirable to have the platelet stack load against the injector. Instead, a disc shaped platelet support flange 0.312 in. thick, was placed at the forward end of the chamber. Since the inside diameter

IV, C, Cooled Chambers (cont.)

of this disc was exposed to the hot combustion gases it was supplied with a water cooling circuit (See Figure 10).

(U) Four coolant bleed ports were located on the top of the housing to allow trapped air to be bled out of each of the four coolant plenums prior to testing and thus provide a "hard" coolant supply circuit. Three of the lines connecting these bleed ports to a common manifold contained check valves (Chamber Sections I, II, and III). There was no check valve in the line connecting Section IV to the manifold. The plenum pressure in this section is higher than the pressure in the other chamber sections and was used to close the check valves to the other sections when the valve isolating the bleed manifold from the dump was closed.

(U) The material selected for the chamber housing was 347 stainless steel because of its availability and compatibility with liquid ClF_3 at ambient temperature. There were no fabrication difficulties reported for either of the two chamber housings that were built. Critical dimensions on both housings were checked with no discrepancies noted.

c. Seal-Divider Ring

(U) Three seal-divider rings were designed to divide the cooled chamber into four sections, as shown in Figure 10, so that the coolant flow to each section could be independently controlled. A Teflon O-ring was used between the outside diameter of each seal-divider ring and the outer chamber housing to prevent intermanifold coolant flow.

(U) The primary reason for the separate axial hydraulic sections was to allow gross adjustment of the coolant flow distribution in case the axial heat flux distribution differed from that assumed in design of

IV, C, Cooled Chambers (cont.)

the chamber. Thus, the coolant flow rate to all parts of the chamber was not dictated by the most limiting local condition. The importance of this feature is exemplified by noting that the manifold pressure that doubles the coolant flow rate in the throat increases the coolant flow rate in the cylindrical section of the chamber by a factor of five. A secondary reason for providing for local variation in the coolant flow rates was to aid in analytical model development by permitting evaluation of the effect of film cooling carryover and evaluation of the performance degradation as a function of coolant injection point.

(U) The seal-divider ring consisted of an outer seal ring made of 304 L stainless steel fusion welded to a 0.020 in. thick disc of either 304 L stainless steel or nickel material. The 304 L stainless steel was used with N_2O_4 coolant and the nickel disc was used with the ClF_3 coolant to satisfy compatibility requirements at high temperature. A two piece construction method was used to fabricate the seal rings. A 0.020 in. thick disc was electron beam welded to a ledge in the center of a one piece ring.

d. Assembly of Cooled Chamber

(U) In this section the assembly procedure for the cooled chamber will be discussed in detail. This will include the assembly, machining and cleaning operations of the chamber platelets. A cross-section of the cooled chamber is shown in Figure 10.

(U) The assembly procedure for the N_2O_4- and the ClF_3-cooled chamber is identical except for the indexing of the platelet pairs for each chamber. The difference in platelet pair index numbers was dictated by the difference in cooling requirements for the two chambers.

IV, C, Cooled Chambers (cont.)

(U) Prior to the assembly of the chambers the thicknesses of the platelets were measured for two reasons: (1) to permit the correct number of platelets to be assembled in each section so that the divider-seal rings would be located properly with respect to the O-ring grooves in the chamber housing; (2) to verify that the metering platelets would give the correct hydraulic resistance.

(U) The assembly of the cooled chambers was initiated with the preparation of the chamber platelets for installation into the chamber housing. This included the assembling or stacking of the platelets, contour machining the inside diameter, and cleaning of the platelets. Figure 14 shows the platelets being stacked on the flange of the machining fixture to form a throat section (left) and a chamber section (right). The roughness of the inside wall of the unmachined cylindrical section is apparent in the photograph.

(U) The platelets were assembled and indexed on the machining fixture flange in the same manner as they would appear in the final chamber assembly. The platelets in the convergent and throat areas of the cooled chamber were designed with a 0.900 in. inside diameter with plans to contour machine the inside diameter. The machining of the internal surface was performed using Electrical Discharge Machining (EDM).

(U) Electrical Discharge Machining of the platelets produces a small (about 0.001 in.) burr on the platelets at the machined surface. A tack weld between platelet pairs is also produced. The burr is unsatisfactory from a heat transfer and hydraulic viewpoint and the tack weld complicates cleaning of the platelets since it makes separation of the platelets difficult. In order to eliminate this condition the chamber was electropolished on the inside diameter. The electropolishing completely removed the burr and the tack weld and left the ID of each platelet smooth. A comparison of the

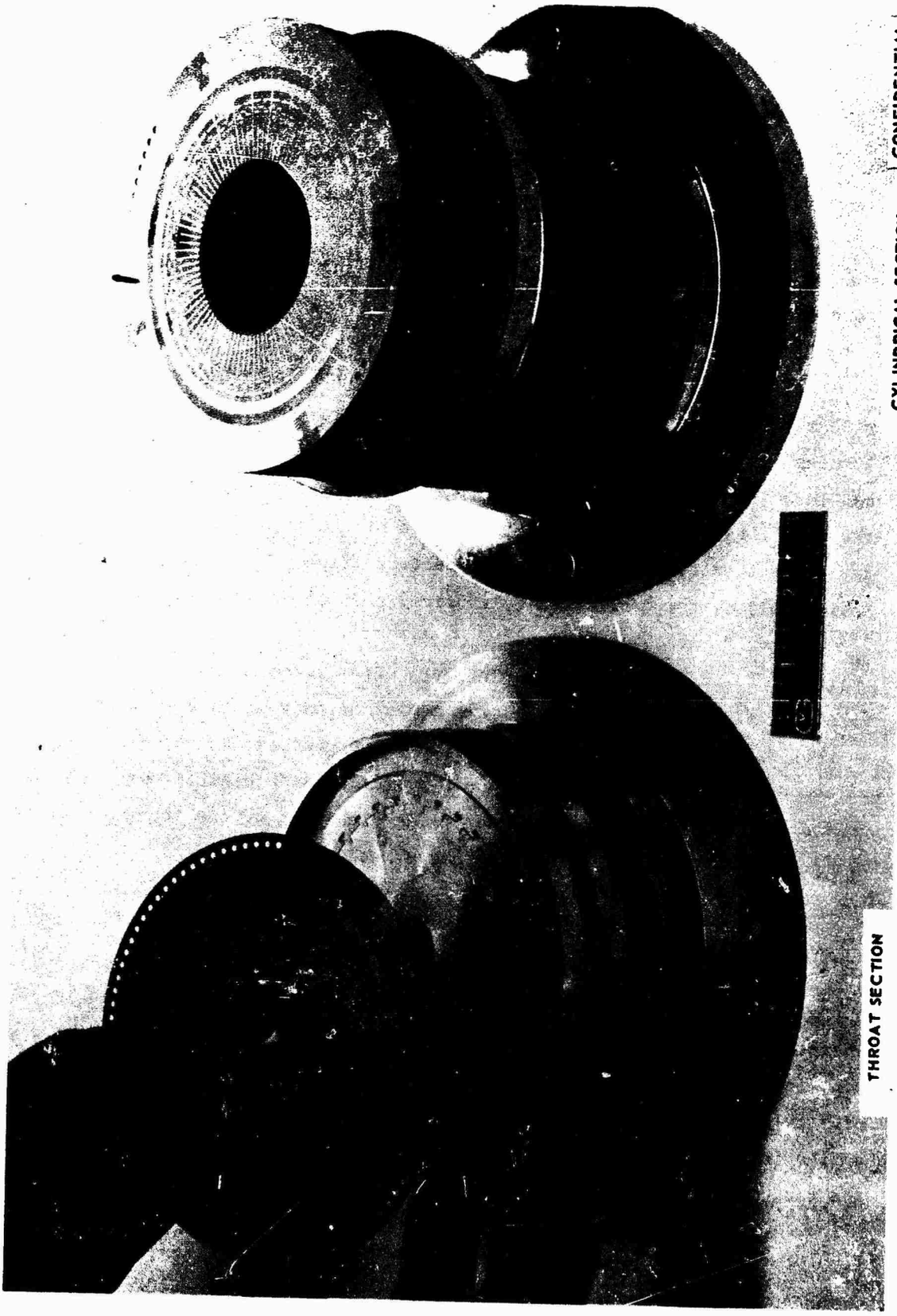

Figure 14. Assembly of Nickel Platelets Prior to Machining Thrust Chamber Contour (u)

IV, C, Cooled Chambers (cont.)

openness of the coolant passageways after EDM, but without electropolishing, and after EDM and electropolish can be seen in Figure 15. This figure shows a close-up of the surface of the chamber cylindrical sections through a mirror. The convergent section of the stainless steel chamber after EDM and electropolish is shown in Figure 16. The short dark lines on the surface of the cylindrical section are formed by alignment of the unetched ridges or "lands" that separate the thermal influence zones. The axial length of these lines is determined by the number of platelets that have the same clocking. The dark ring near the throat is the seal divider ring.

(U) Following the electropolish operation the platelets were removed from the machining fixture and the instrumentation platelet pairs were separated from the platelet sections for thermocouple installation. The complete instrumentation platelet assembly operation is discussed in Section IV,D.

(U) Assembly of the nickel platelets into the ClF_3-cooled chamber housing proved to be more difficult than was the assembly of the stainlss steel platelets into the N_2O_4-cooled chamber housing due to the distortion of the nickel platelets during handling. The nickel platelets were relatively soft and did not hold their flatness as did the stainless steel platelets. Therefore, when the nickel platelets were assembled into the housing it was necessary to use a loading ring to flatten the distorted platelets prior to and after the installation of each chamber seal ring.

(U) As can be seen in Figure 14 the cooled chamber platelets are assembled on two index rods (see also Figure 10). These rods serve two purposes. (1) They provide the index for clocking the platelet pairs to obtain the required coolant flow. (2) They were intended to align the platelets in all assembly and machining operations. However, the index holes

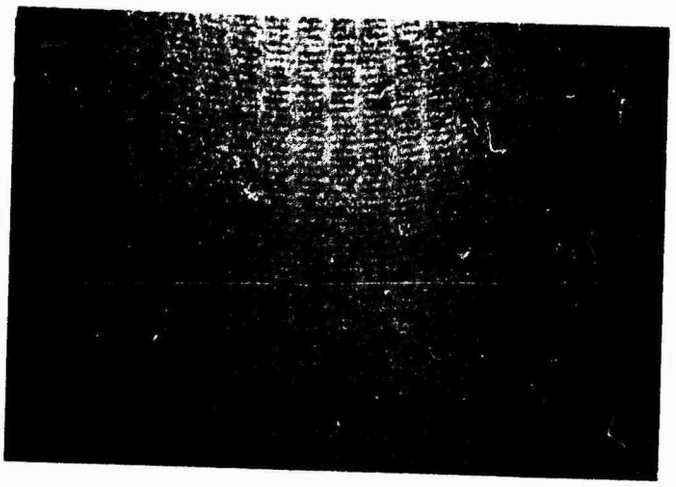

NICKEL CHAMBER AFTER MACHINING

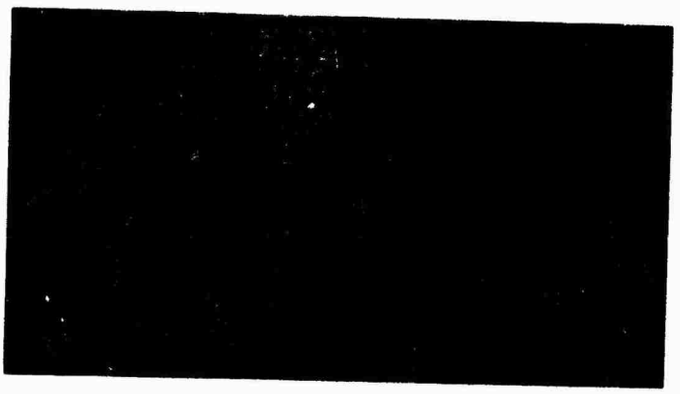

NICKEL CHAMBER AFTER MACHINING
AND ELECTRO POLISH

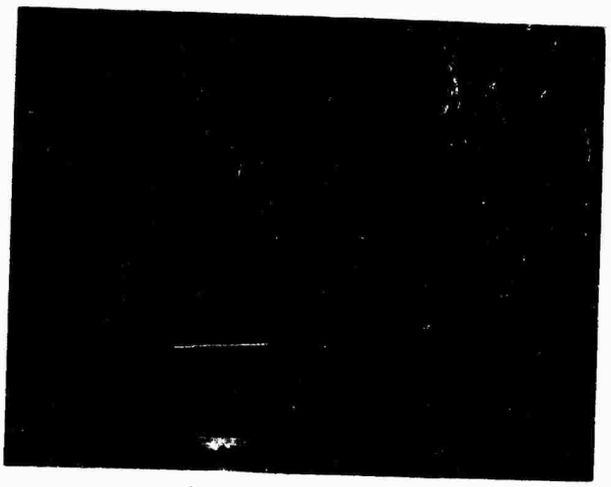

STAINLESS STEEL CHAMBER AFTER
MACHINING AND ELECTRO POLISH

Figure 15. Cooled Chamber Surface

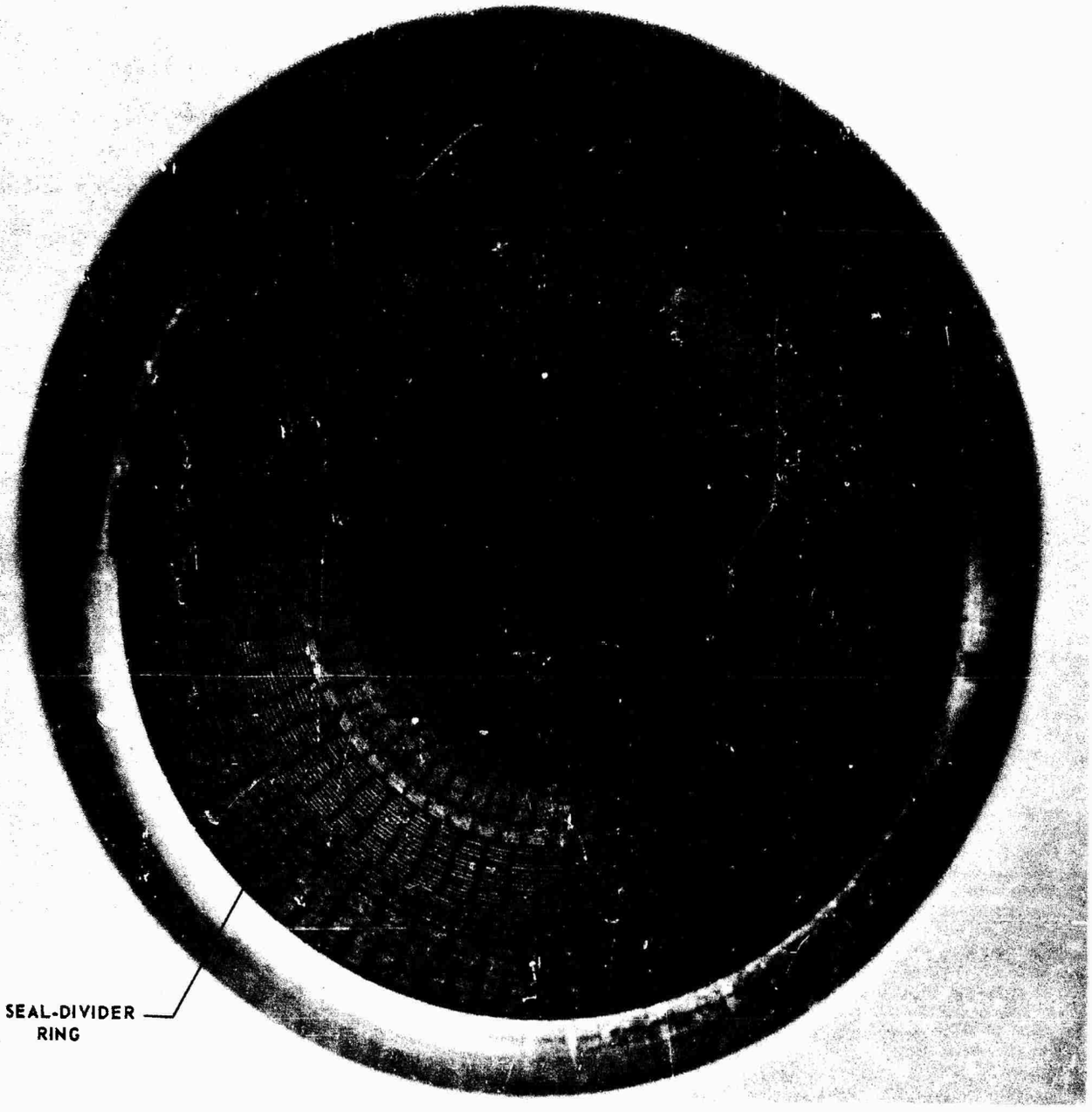

Figure 16. Convergent Section of Stainless Steel Chamber after Machining and Electropolish

IV, C, Cooled Chambers (cont.)

etched through the platelets were not all the same size. Some of these holes were smaller in ID than the OD of the index rod and had to be enlarged while others were oversized and permitted platelet movement. Thus, upon final assembly of the chamber the index rod - hole arrangement did not provide precise alignment. Many of the platelets were not concentric, and protruded as much as 0.005 in. on one side of the chamber ID.

(U) Alignment tools, machined to the contour of the chamber, were used to align the platelets. However, the instrumentation platelets are made by brazing two platelets together (see Section IV,D) and flow of braze alloy to the edge of the stainless steel instrumentation platelets produced a crown on the ID of these platelets that prevented the effective use of the aligning tools. The nickel instrumentation platelets did not have this crown and the alignment tools were used effectively in the final assembly of the ClF_3-cooled chamber. Figure 17 shows the inside of the stainless steel and nickel chambers after final assembly. Backlighting emphasizes the surface roughness that results from nonaligned platelets. The crown on the stainless steel instrumentation platelets can be seen in the figure.

(U) The final axial loading of the platelets in the cooled chamber was accomplished by tightening down the nuts on each of the 12 chamber rods. A feeler gage was used to measure the gap between the flange of the aft platelet retainer and the aft surface of the chamber housing to determine the uniformity of the platelet stack height under load. The compressed stack height was within 0.005 in. at all locations for both chambers.

2. Phase II

(U) In Phase II of this program one transpiration cooled chamber was designed and fabricated with nickel platelets for use with the ClF_3/MHF-3 propellant combination at 1000 psia chamber pressure and

STAINLESS STEEL CHAMBER

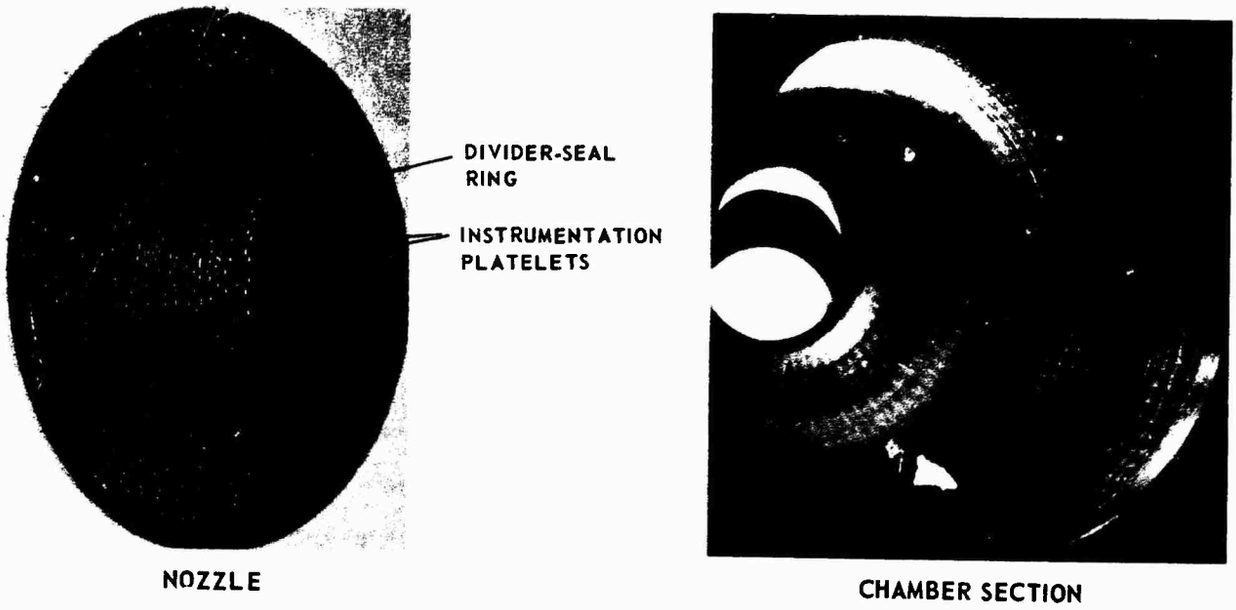

NICKEL CHAMBER

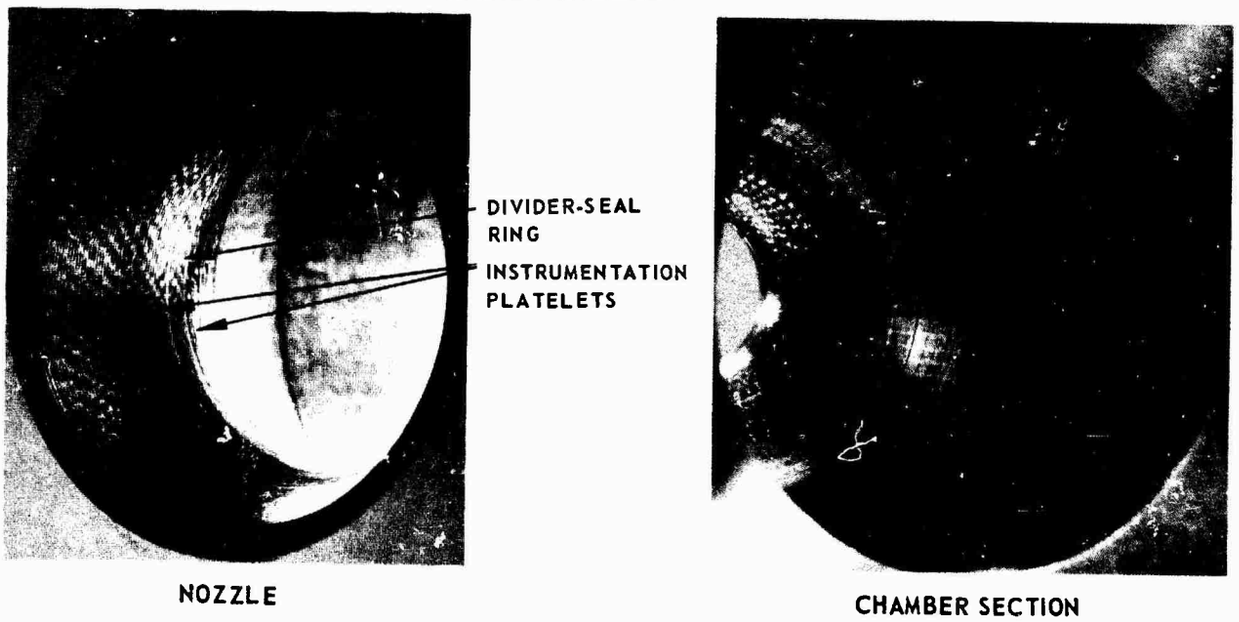

Figure 17. Phase I Cooled Chambers after Final Assembly

IV, C, Cooled Chambers (cont.)

1000 lb thrust. The Phase II cooled chamber design (Figure 18) differs from the Phase I cooled chamber design (Figure 10) in that the water coolant manifold that caused considerable problems in Phase I ClF_3 testing was eliminated, the chamber L* was changed from 31.9 to 25, the seal-divider ring at the throat was replaced by an instrumentation platelet leaving three coolant sections, the number and location of the instrumentation platelets were revised and the loading of the chamber platelets was accomplished by using the injector rather than the aft platelet retainer.

(U) The seal-divider rings are not etched and, therefore, are film-cooled by carryover from one to three upstream platelets that are clocked to have higher than nominal flow rates. However, the Phase I thermal data indicated that film cooling carryover was not especially effective. Since this raised some doubt as to whether the seal-divider ring at the throat could be film-cooled at reduced coolant flow rates, it was removed. The nominal coolant flow rates for the Phase II chamber are given in Table 3.

(C) TABLE 3

PHASE II NOMINAL COOLANT FLOW RATES (U)

Chamber Section	Coolant Flow Rate (lb/sec)
I	0.216
II	0.466
III	0.173
Total	0.855

IV, C, Cooled Chambers (cont.)

a. Chamber Platelets

(U) The platelet design that was used for the Phase I ClF_3-cooled chamber was also used for the Phase II chamber. There were sufficient platelets residual from Phase I of the program to construct the nozzle and about half of the cylindrical section of the 25L* cooled chamber. The additional nickel platelets required to complete the Phase II cooled chamber assembly were fabricated as was done in Phase I.

b. Cooled Chamber Housing

(U) The Phase II cooled chamber housing shown in Figure 18 was designed to eliminate the water coolant manifold that caused considerable problems in Phase I ClF_3 testing. This housing is a one piece welded construction unit that requires the platelets to be installed and mechanically loaded from the forward end of the housing with an injector that has a sliding type seal. Two internal O-ring seal locations were used in the housing to form three chamber coolant sections. There is only one external seal location at the injector-chamber joint.

(U) The Phase II welded housing consists of a cylindrical section made of CRES 304L material and a disc made of nickel 200 material. The nickel was used for the aft end of the housing to increase the radial dissipation of heat generated during hot firing of the cooled chamber.

(U) The coolant bleed ports were eliminated from the Phase II cooled chamber housing since they were not used in the Phase I ClF_3-cooled chamber tests.

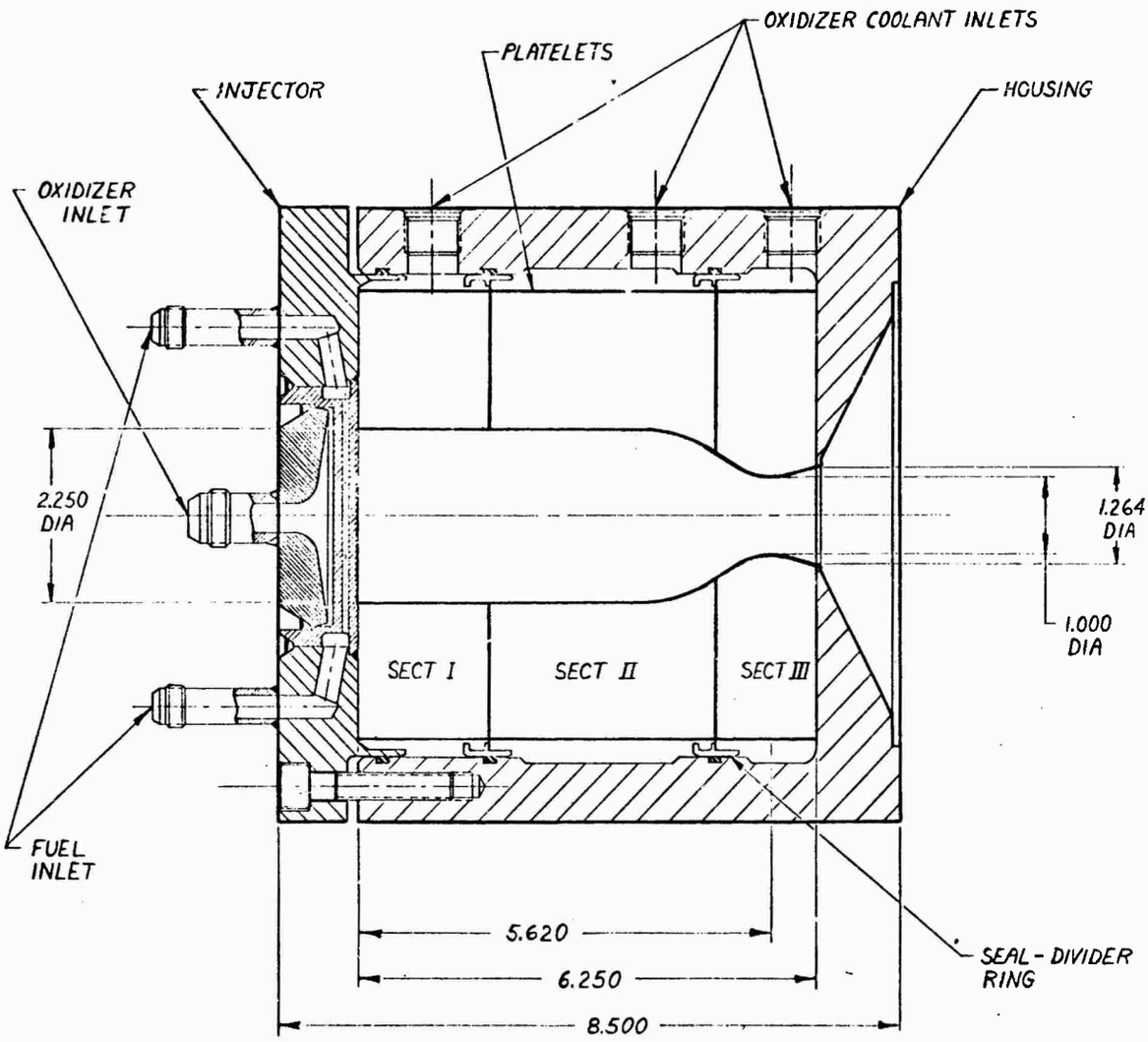

Figure 18. Phase II Cooled Chamber Assembly

IV, C, Cooled Chambers (cont.)

c. Divider Seal Rings

(U) The two divider seal rings that were used in the Phase II ClF_3-cooled chamber were residual from Phase I of the program.

d. Assembly of Cooled Chamber

(U) The assembly procedure used for the Phase I cooled chamber assembly was repeated for the Phase II cooled chamber assembly with four variations.

(1) During the assembly of the platelets in a cylindrical section and a throat section the location of the thermocouple platelets was changed and the seal-divider ring at the chamber throat was eliminated.

(2) The index rods used for the Phase II chamber were larger than those used for the Phase I chambers. An additional operation was added prior to machining the chamber inside contour to enlarge the two index rod holes in the platelets by EDM to have a tight fit with the OD of the larger diameter index rods. Precise machining of the index rod holes was done to improve alignment of the chamber platelets at the inside diameter.

(3) A tack welding operation was added prior to the assembly of the platelets into the cooled chamber housing. The metering platelets were welded to the distribution platelet at the coolant entrances near the OD of the platelets. Test results from Phase I cooled chamber testing indicated the existence of a coolant flow restriction. A visual examination of the coolant entrances of the Phase I chamber platelets showed that they were partially blocked by the 0.001 in. thick metering platelet sagging into the 0.0025 in. deep by 0.160 in. wide entrance in the distribution platelet.

IV, C, Cooled Chambers (cont.)

Tack welding the metering platelet to the blank side of the succeeding distribution platelet, at the entrance locations, was done to prevent any such flow restriction. Four resistance tack welds were made at each of the coolant entrances approximately 0.050 in. from the OD of the platelet.

(4) The tack welded platelet pairs were assembled from the divergent end of the cooled chamber toward the forward end of the chamber. The addition of the injector and the tightening of the 12 injector-chamber housing bolts to apply the axial load to the chamber platelets constitute a fully assembled Phase II chamber assembly.

IV, Design and Fabrication (cont.)

D. THERMAL INSTRUMENTATION

1. Phase I

(U) Both the N_2O_4- and ClF_3-cooled Phase I combustion chambers were instrumented with special platelets that contained surface and subsurface thermocouples. The instrumentation platelet concept (see Figure 19) utilizes two-piece construction in which two platelets are brazed together with thermocouples sandwiched between them. The base plate is unetched and contains slots for the thermocouples. The cover platelet is a special (thin) distribution platelet.

(U) Prior to fabrication of the instrumented platelets for the cooled chamber assembly the instrumentation technique was verified using a platelet pair (see Figure 19) of about one-half the ID and OD of the chamber platelets. After fabrication this sample was X-rayed to locate the thermocouple junctions, and was sectioned to determine the quality of the braze joint at the thermocouple locations. An excellent braze bond had been achieved and the braze flow around the thermocouples was uniform. A calibration check showed that the braze alloy had no adverse effect on the thermocouple operating characteristics.

(U) The design of the instrumented platelets for the cooled chamber assemblies was patterned after the design of the developmental (sample) instrumented platelet. Each of the instrumented platelets for the cooled chamber consisted of a 0.006 in. thick distribution platelet, a 0.016 in. thick base platelet and one or more sheathed 0.010 in OD thermocouples. The sheathed thermocouple contains a pair of 0.0015 in. diameter (chromel and alumel) wires inside a stainless steel 0.010 in. OD sheath. High temperature magnesium oxide electrical insulation separates the thermocouple wires from

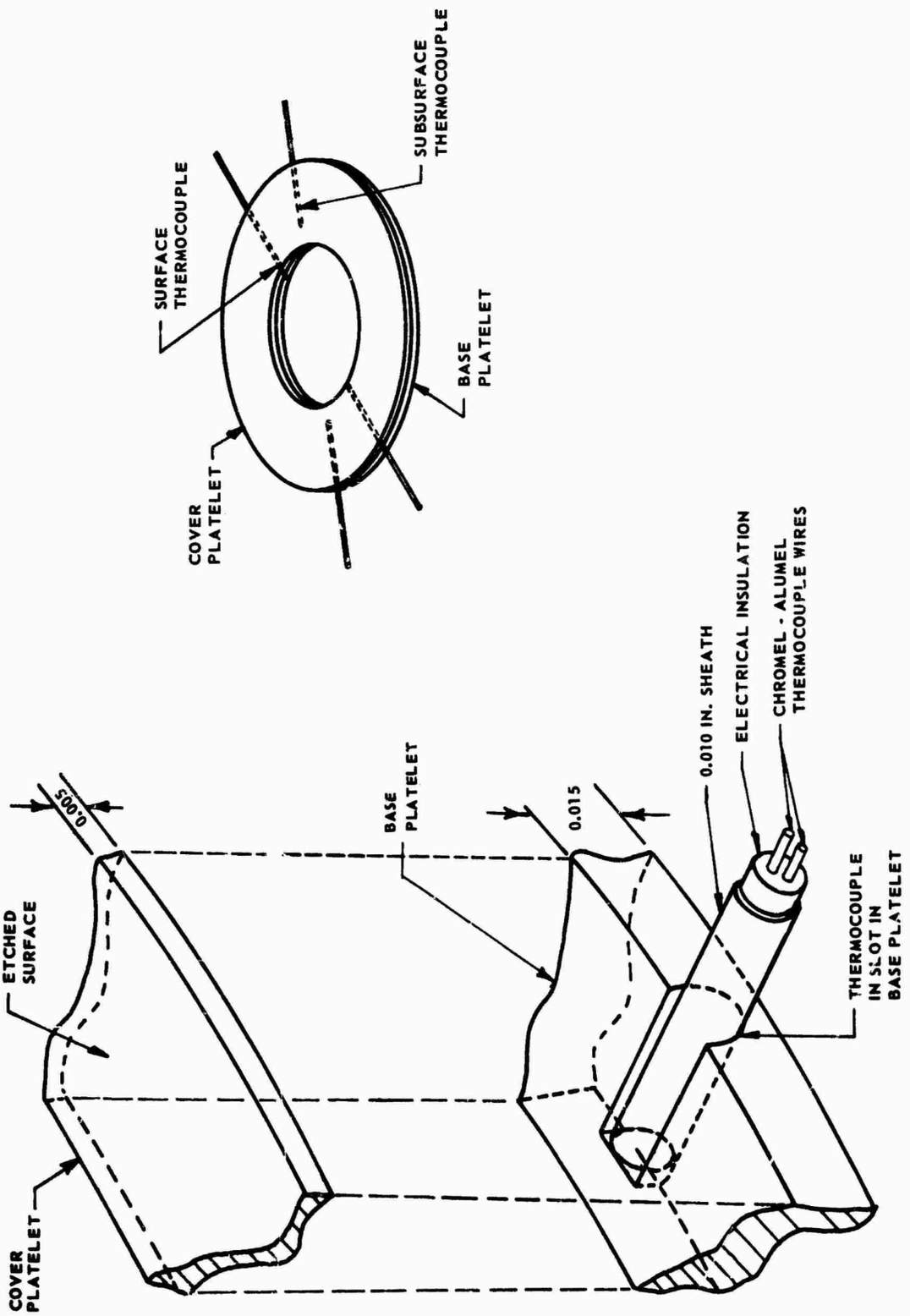

Figure 19. Instrumentation Platelet Concept

IV, D, Thermal Instrumentation (cont.)

each other and from the sheath. The thermocouples wires are fused at one end with the sheath to form a junction.

(U) The instrumentation platelet pairs are shown in Figure 20. The slots in the base (blank) platelet (Figure 20a) were made by EDM. Figure 20b shows the cover platelet and Figure 20c is a close-up view of one of the base platelets after installation of the thermocouples. Figure 20d shows a cover platelet on an instrumented base platelet. After brazing an instrumented platelet is the same as an ordinary 0.020 in. thick distribution platelet except for thickness (0.022 in.) and the thermocouples.

(U) As shown in Figure 21 the thermocouples are led through the instrumentation ports in the cooled chamber housing. The ports are sealed and the lead wires are then spliced to the thermocouple wires.

(U) Instrumentation platelet No. 6 for the N_2O_4-cooled chamber, and numbers 6 and 7 for the ClF_3-cooled chamber were not usable either because of slippage of the cover platelet relative to the base platelet during brazing or because of excess braze alloy flow into critical flow areas on the cover platelet. Figure 21 shows the location of the remaining instrumented platelets in the N_2O_4- and ClF_3-cooled Phase I chambers. The instrumented platelets were numbered from the aft end of the chamber.

(U) The thermocouples were located circumferentially within the platelets to permit measurements to be made both in line with and between streaks that were observed visually on the uncooled ablative liners used in the injector checkout tests. The axial location of each instrumentation platelet was selected to give temperatures at those locations which appeared to be most critical on the basis of the design calculations. The thermocouple locations were designed to permit measurement of the axial temperature profile

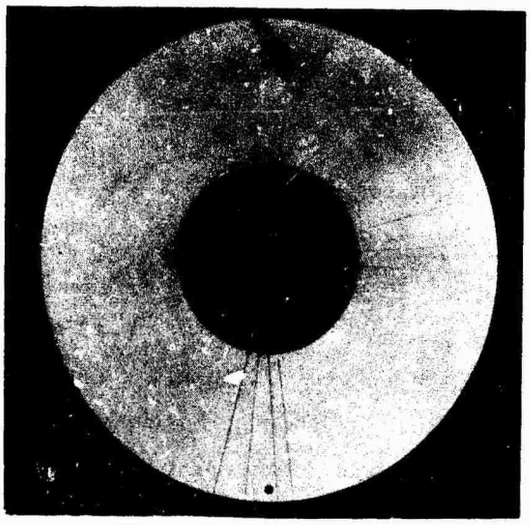

(a) BASE PLATELET AFTER MACHINING SLOTS FOR THERMO COUPLES

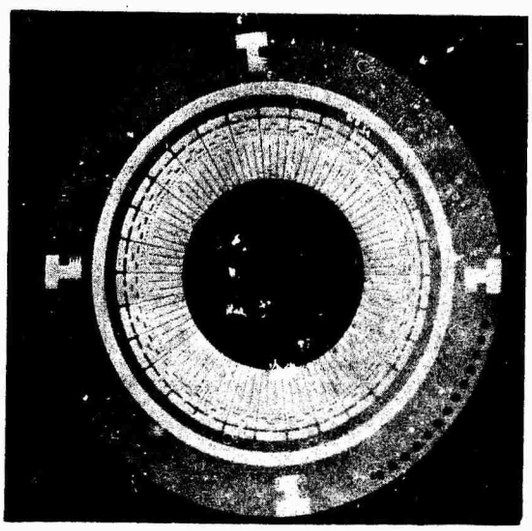

(b) COVER PLATELET

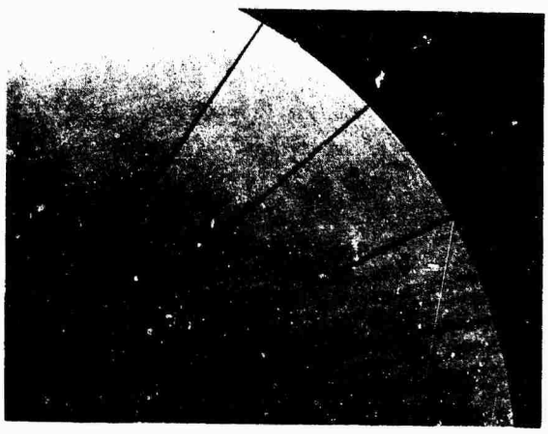

(c) THERMOCOUPLES INSTALLED IN SLOTS IN BASE PLATELET

CONFIDENTIAL

(d) COVER PLATELET ON INSTRUMENTED BASE PLATELET

Figure 20. Instrumentation Platelet Assembly (u)

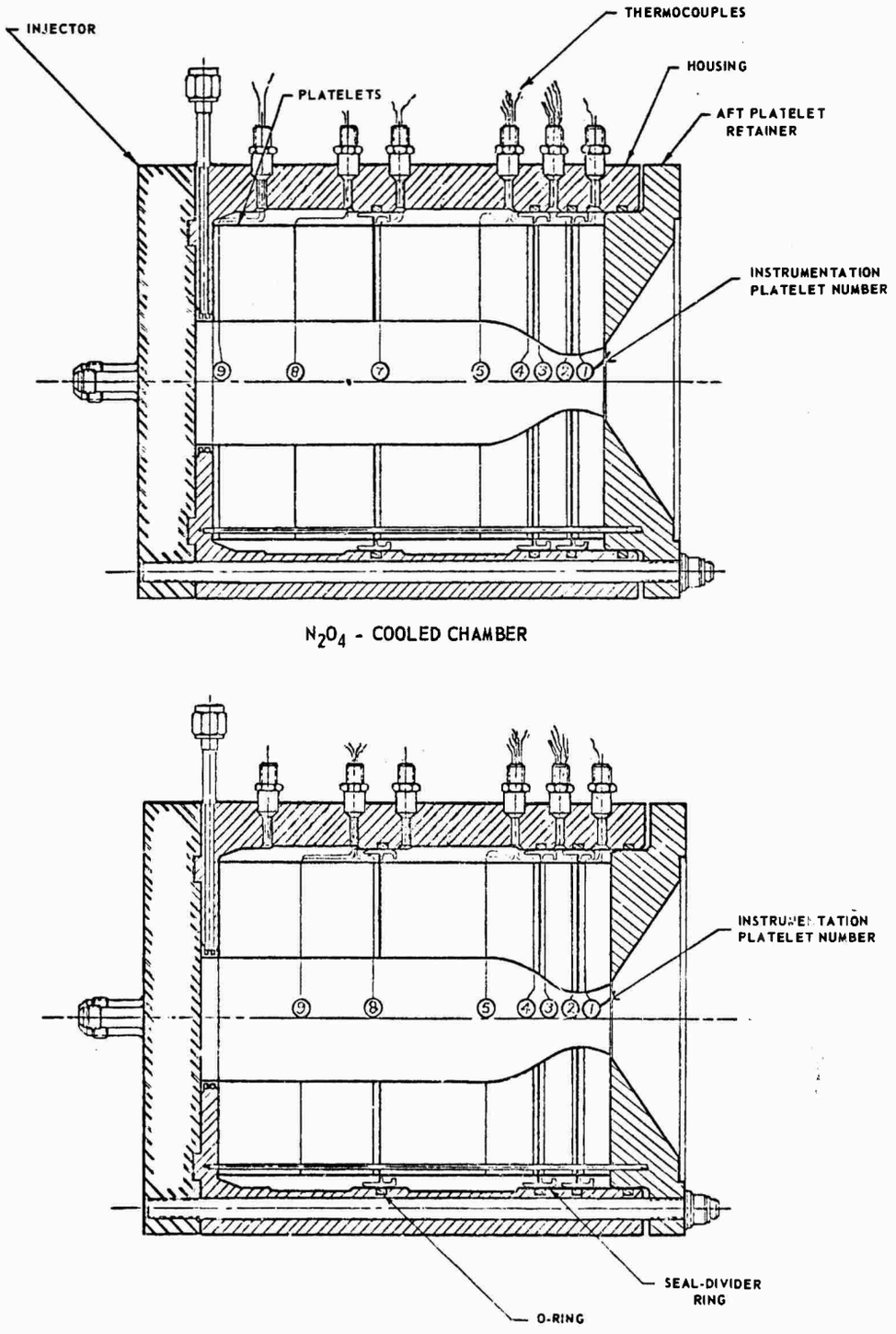

Figure 21. Location of Instrumentation Platelets in Phase I Chamber

IV, D, Thermal Instrumentation (cont.)

(two locations), of the circumferential temperature profile (platelet No. 4), and of the temperature profile in the wall (two locations).

(U) The location of the thermocouples in the platelets is given in Table 4. To help identify the individual thermocouples a two number sequence (for example 5-1) was used to designate the individual thermocouples. The first number in the sequence refers to the instrumentation platelet in which the thermocouples are located, while the second number in the sequence designates the position in a clockwise numbering system used for each platelet. The numbering of the individual thermocouples on each platelet and the location of the thermocouples relative to the injector patterns are shown in Figure 22 for the N_2O_4-cooled chamber and in Figure 23 for the ClF_3-cooled chambers.

TABLE 4

LOCATION AND NUMBER OF THERMOCOUPLES IN INSTRUMENTATION PLATELETS (U)

Instrumentation Platelet Number	Surface (ID)	0.015 in. Depth	0.030 in. Depth	0.070 in. Depth
1	2	-	-	-
2	2	2	2	2
3	2	2	-	-
4	8	-	-	-
5	2	2	2	2
6	2	2	-	-
7	2	2	-	-
8	2	-	-	-
9	2	2	-	-

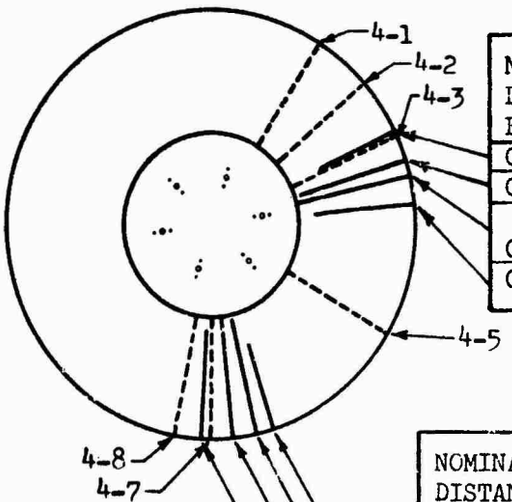

NOMINAL DISTANCE FROM ID	THERMOCOUPLES SECT I	SECT II	SECT III	SECT IV
0.070 in.	-	5-1	2-1	-
0.015	9-1	7-1,5-2	3-1,2-2	-
0.0*	9-2 8-1	7-2,5-3 4-4	3-2,2-3	1-1
0.030	-	5-4	2-4	-

* All thermocouples on platelet Number 4 are surface thermocouples.

NOMINAL DISTANCE FROM ID	THERMOCOUPLES SECT I	SECT II	SECT III	SECT IV
0.070 in.	-	5-5	2-5	-
0.015	9-3	7-3,5-6	3-3,2-6	-
0.0	9-4 8-2	7-4,4-6 5-7	3-4,2-7	1-2
0.030	-	5-8	2-8	-

100 psia INJECTOR

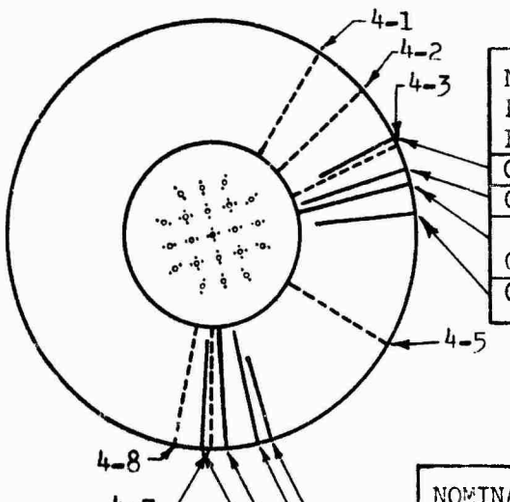

NOMINAL DISTANCE FROM ID	THERMOCOUPLES SECT I	SECT II	SECT III	SECT IV
0.070 in.	-	5-1*	2-1	-
0.015	9-1	7-1,5-2	3-1,2-2	-
0.0	9-2 8-1	7-2,5-3 4-4	3-2,2-3	1-1
0.030	-	5-4	2-4	-

* The first number in the thermocouple designation is the instrumentation platelet number.

NOMINAL DISTANCE FROM ID	THERMOCOUPLES SECT I	SECT II	SECT III	SECT IV
0.070 in.	-	5-5	2-5	-
0.015	9-3	7-3,5-6	3-3,2-6	-
0.0	9-4 8-2	7-4,4-6 5-7	3-4,2-7	1-2
0.030	-	5-8	2-8	-

1000 psia INJECTOR

Figure 22. Thermocouple Locations Relative to Phase I N_2O_4 Injector Patterns (u)

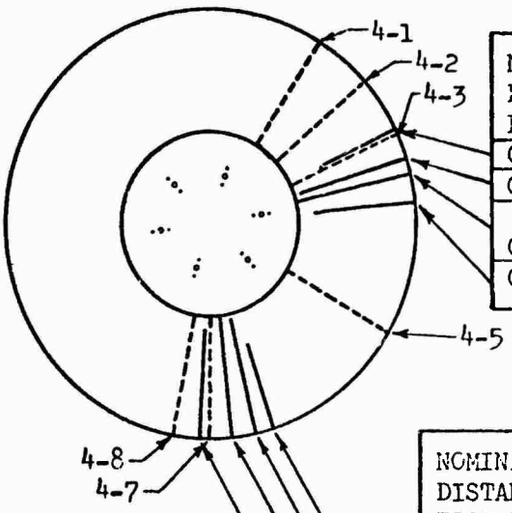

NOMINAL DISTANCE FROM ID	THERMOCOUPLES SECT I	SECT II	SECT III	SECT IV
0.070 in.	-	5-1	2-1	-
0.015	9-1	5-2	3-1,2-2	-
0.0*	9-2 8-1	5-3,4-4	3-2,2-3	1-1
0.030	-	5-4	2-4	-

* All thermocouples on platelet Number 4 are surface thermocouples.

NOMINAL DISTANCE FROM ID	THERMOCOUPLES SECT I	SECT II	SECT III	SECT IV
0.070 in.	-	5-5	2-5	-
0.015	9-3	5-6	3-3,2-6	-
0.0	9-4 8-2	4-6,5-7	3-4,2-7	1-2
0.030	-	5-8	2-8	-

100 psia INJECTOR

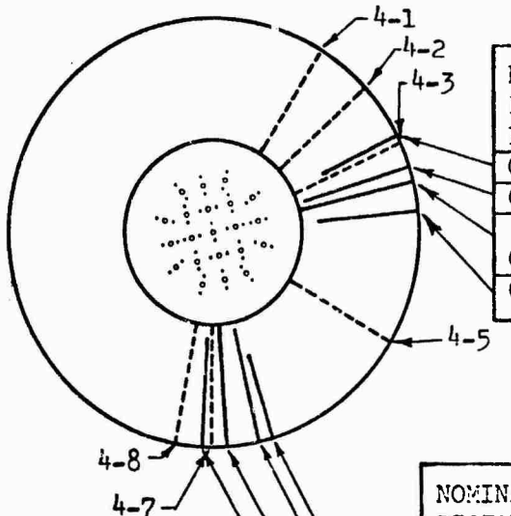

NOMINAL DISTANCE FROM ID	THERMOCOUPLES SECT I	SECT II	SECT III	SECT IV
0.070 in.	-	5-1*	2-1	-
0.015	9-1	5-2	3-1,2-2	-
0.0	9-2 8-1	5-3,4-4	3-2,2-3	1-1
0.030	-	5-4	2-4	-

* The first number in the thermocouple designation is the instrumentation platelet number.

NOMINAL DISTANCE FROM ID	THERMOCOUPLES SECT I	SECT II	SECT III	SECT IV
0.070 in.	-	5-5	2-5	-
0.015	9-3	5-6	3-3,2-6	-
0.0	9-4 8-2	4-6,5-7	3-4,2-7	1-2
0.030	-	5-8	2-8	-

1000 psia INJECTOR

Figure 23. Thermocouple Locations Relative to Phase I ClF_3 Injector Patterns (u)

IV, D, Thermal Instrumentation (cont.)

(U) It was desired to have the instrumentation platelets blend in as smoothly as possible with the inside contour of the cooled chambers. To accomplish this the instrumentation platelet pairs were assembled with the other platelets in the machining fixture for the chamber contour machining and subsequent electropolish. When the platelet stack was removed from the machining fixture the instrumentation platelet pairs were taken out of the stack, the grooves machined, thermocouples installed, and cover platelets brazed on.

(U) Prior to installation the thermocouples were X-rayed to locate the junction relative to the end of the thermocouple. After installation of each thermocouple in the base platelet the distance from the ID of the platelet to the end of the thermocouple was measured. In this way the distance from the chamber surface to each thermocouple junction was determined.

2. Phase II

(U) The instrumentation technique and method of fabrication of the instrumentation platelets used in Phase I of the program was also used in Phase II. The only differences that were made in thermal instrumentation in going from Phase I to Phase II were in the number and location of the thermocouples. A total of 25 thermocouple locations were specified for Phase II. Twenty-three of the thermocouples were operative after final assembly of the chamber. Figure 24 shows the location of the instrumentation platelets in the Phase II cooled chamber and the circumferential location of the thermocouples relative to the injector pattern. The instrumented platelets were numbered from the aft end of the chamber.

(U) The instrumentation platelets were located axially to improve the data acquisition over that of the Phase I cooled chamber testing. Instrumentation platelets numbers 2 and 5 were located approximately .250 downstream of the seal-divider rings to be out of the influence of the film

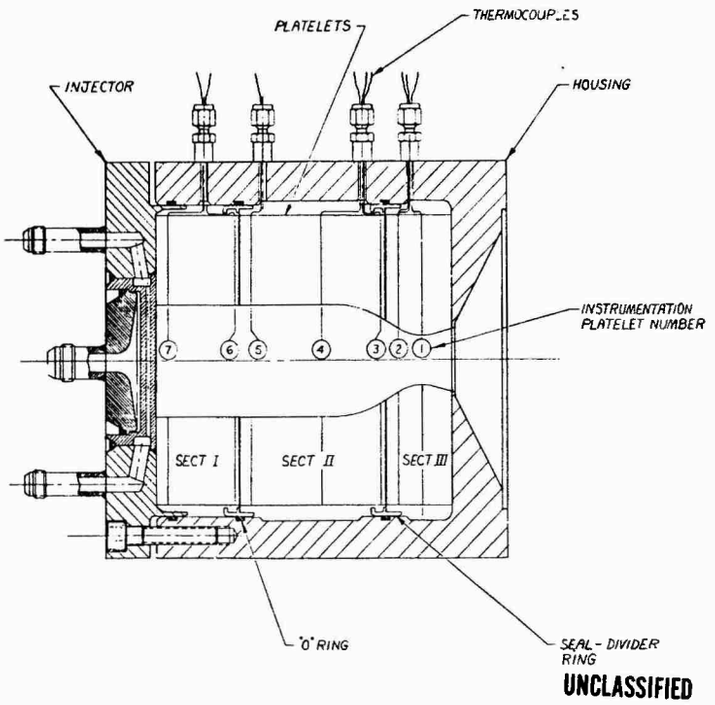

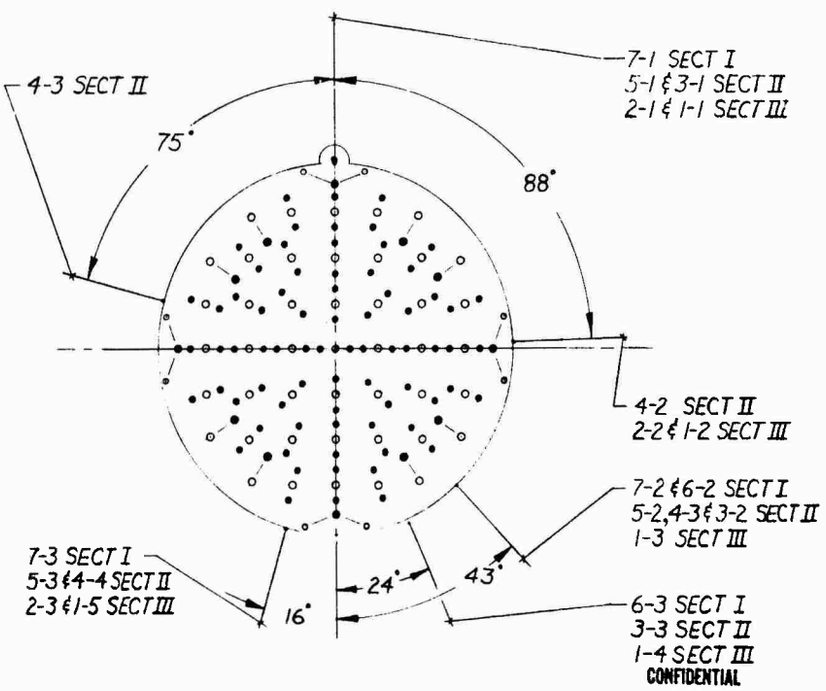

Figure 24. Locations of Thermocouples in Phase II Chamber (u)

IV, D, Thermal Instrumentation (cont.)

cooling provided for the seal-divider rings. One to three platelets proceeding the seal divider rings are clocked open to allow more coolant to flow to compensate for the uncooled thickness at the seal-divider ring.

(U) Instrumentation platelet number 1 was located at the throat to monitor the temperatures at the throat. A seal divider-ring had been located in the throat of the Phase I cooled chambers.

(U) The thermocouples were located circumferentially within the platelets to permit measurements to be made in line with and between streaks that were observed visually on the Phase II uncooled ablative liners in the injector checkout tests. These thermocouple locations were designed to permit measurement of the axial temperature profile (3 locations) and of the circumferential profile (Platelets 1, 2 and 3).

(U) The attempt during Phase I testing to measure the temperature gradient in the instrumentation platelet by means of subsurface thermocouples was unsatisfactory. The subsurface thermocouples had been placed at three different depths from the chamber surface, but were separated circumferentially as shown in Figures 22 and 23. The circumferential variation in heat flux to the wall due to injector inhomogeneity resulted in each subsurface thermocouple being in a unique thermal environment. Thus, each subsurface thermocouple provided one point in a thermal gradient peculiar to its location and not several points in a common gradient. The circumferential placement of the thermocouples was made because the location of several thermocouples along a single radius would introduce a mass of material whose thermal properties were significantly different from those of the platelet material and would therefore perturb the system being measured and thus invalidate the results. Three subsurface thermocouples were used on three platelets in critical locations since the subsurface thermocouples, not being exposed to the hot gases and higher temperatures, would be more reliable.

V. TESTING

A. FACILITIES AND TEST PROCEDURES

1. Facilities

(U) All test firings were conducted in the Research Physics Laboratory, Sacramento Plant. The ClF_3 test installation is shown in Figure 25. The N_2O_4 test stand is very similar to the ClF_3 test stand. A flow schematic of the N_2O_4 test installation is given in Figure 26 and the flow schematic of the ClF_3 test installation is given in Figure 27.

(U) Four feed circuits are used during the cooled chamber testing: the injector oxidizer circuit, the injector fuel circuit, the oxidizer coolant circuit and the water coolant circuit. These circuits are shown in Figure 28, which shows the N_2O_4-cooled chamber on the test stand prior to testing. The water circuit supplies coolant for the injector and for the manifold in the forward platelet support of the Phase I cooled chamber housing. The oxidizer coolant circuit supplies the transpiration coolant to the chamber. Flow in each circuit is started and stopped by nitrogen actuated valves. The propellant valves are equipped with automatic prefiring and postfiring nitrogen purges.

(U) No separate discussion of the feed system used for injector checkout testing has been included since the system is similar to that used in the cooled chamber testing except, of course, for the chamber coolant circuits.

(U) The test stand is mounted on a concrete test pad with the thrust chamber assembly located in the horizontal position. The propellant valves are separately operated so that the relative opening times can be readily adjusted. In order to avoid burning of fuel with the oxidizer coolant, actuation times for the injector propellant valves were set for a

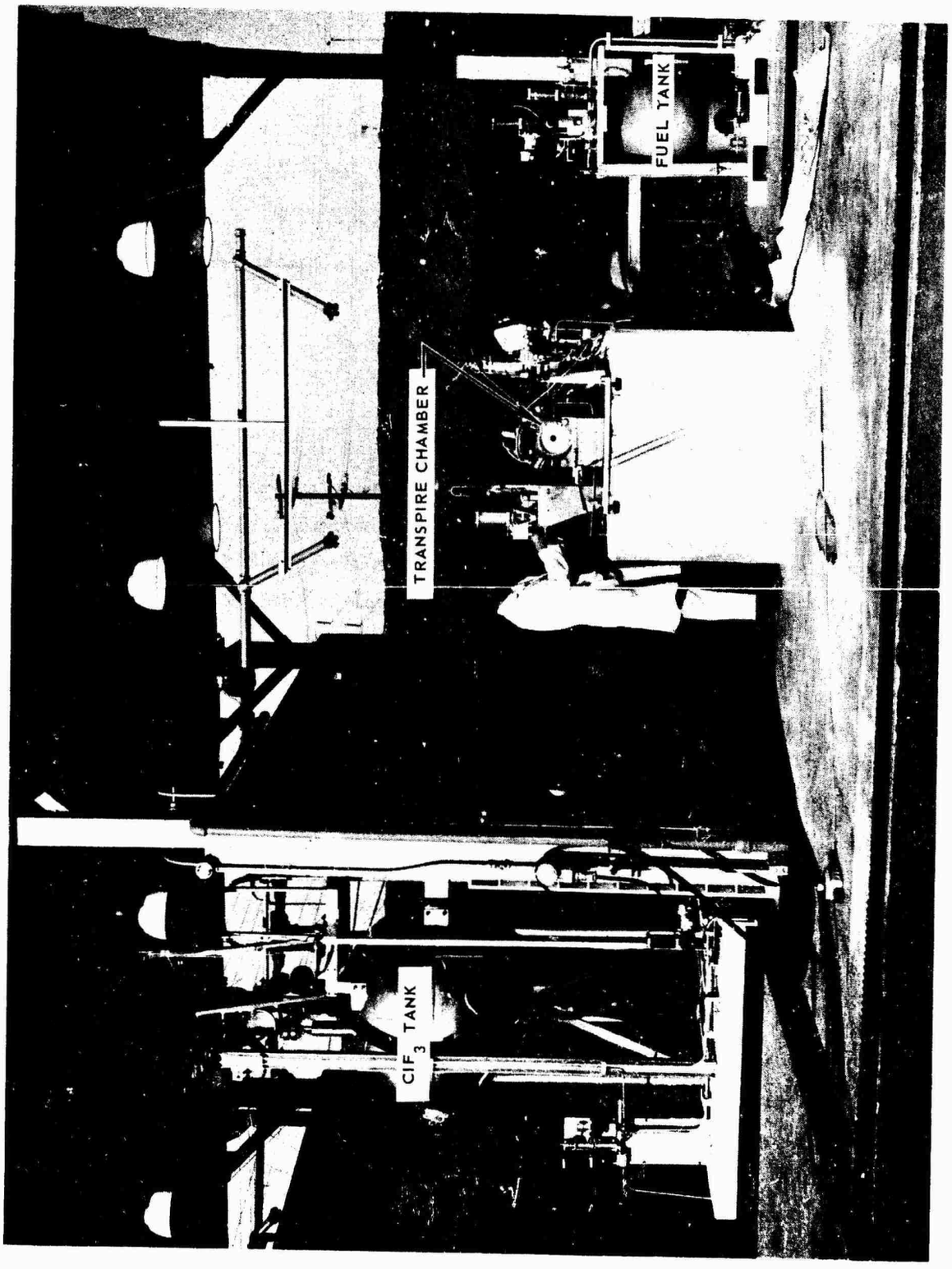

Figure 25. ClF_3 Test Facility

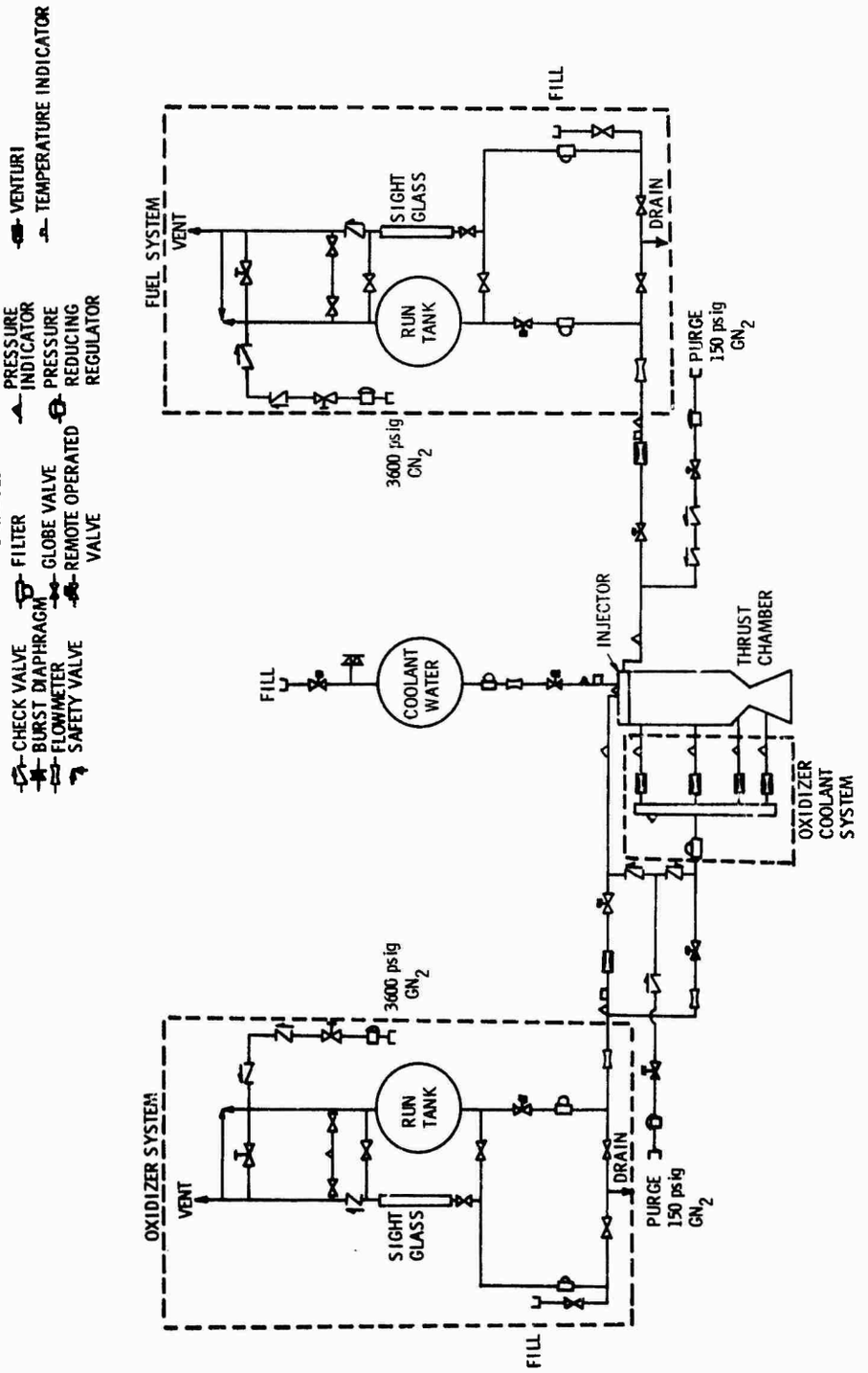

Figure 26. N_2O_4/A-50 Feed System Diagram

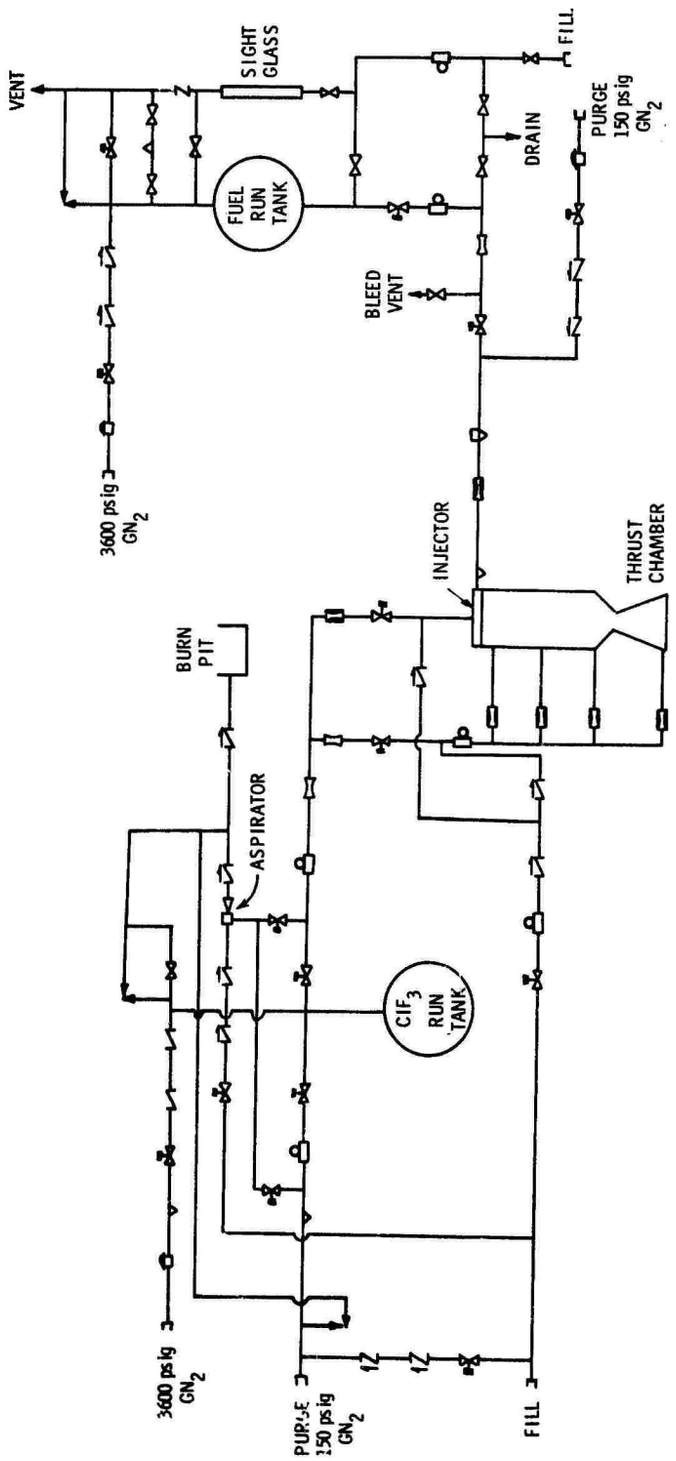

Figure 27. ClF_3/A-50 Feed System Diagram

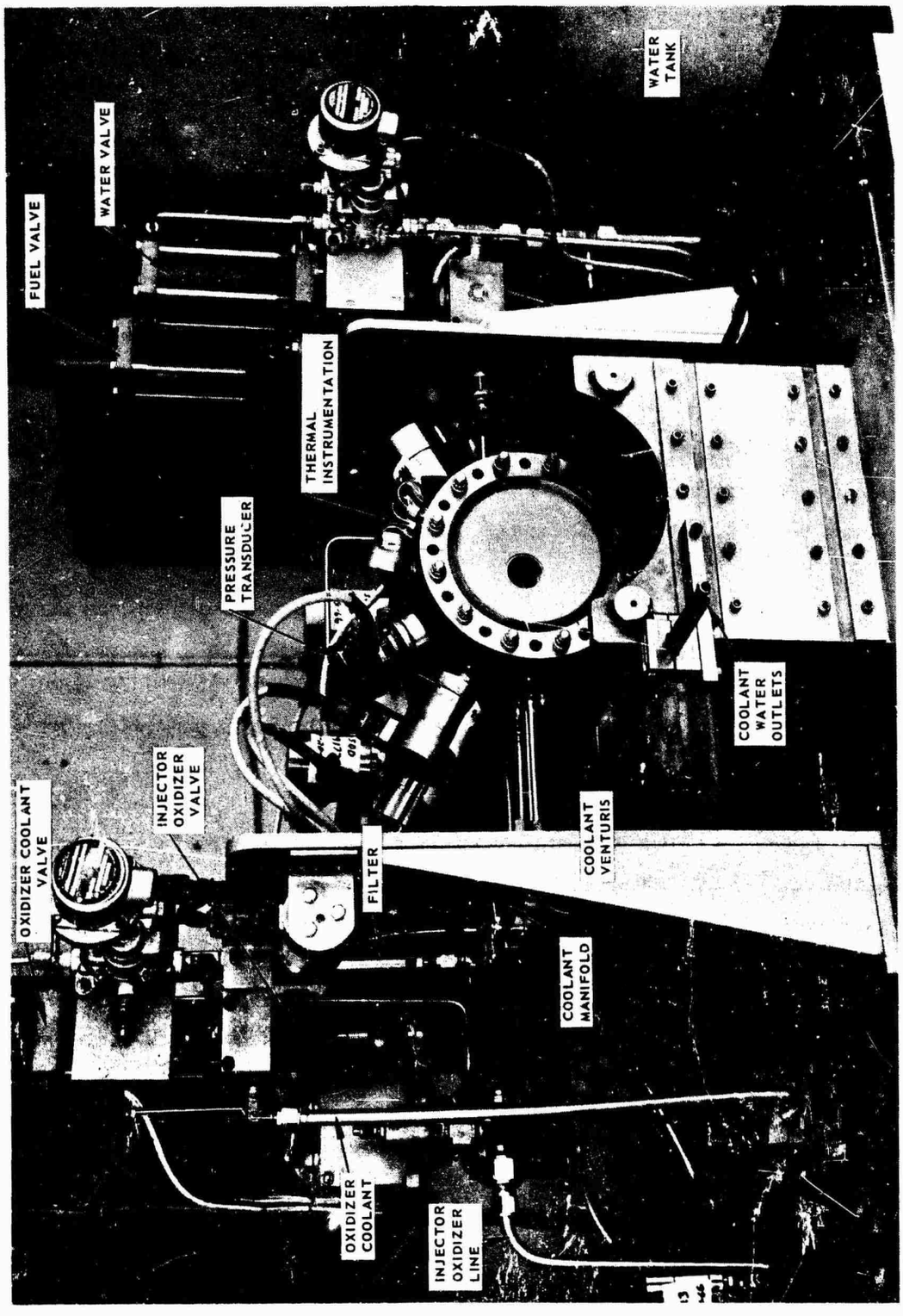

Figure 28. N_2O_4-Cooled Chamber on Test Stand

V, A, Facilities and test Procedures (cont.)

300 millisecond oxidizer lead on start and 100 millisecond oxidizer lag on shutdown. Fixed area cavitating venturis were used to control the flow of the propellants to the injector. A 40 micron absolute filter is located at the tank outlet in both propellant feed circuits.

(U) The pressurization system consists of a 650 ft^3 nitrogen tank at 3,600 psig, a 10-micron absolute filter and two 1-in. regulators which feed nitrogen gas into the top of each propellant tank through a pressurizing valve and two check valves.

(U) The water coolant system consists of a 40 gal tank, 40-micron absolute filter and a nitrogen actuated valve which feeds coolant water to the injector and chamber.

(U) The flow of coolant to the chamber sections was controlled by separate fixed area cavitating venturis. The coolant flow to each of the individual sections could be varied independently of the others simply by changing the venturi feeding that section. All the coolant was passed through a 10 micron absolute (2 micron nominal) filter.

(U) The thrust chamber test firings are controlled by an automatic sequencing unit. When the fire switch is closed the sequence unit is started which automatically energizes the fuel and oxidizer purge valves. Two seconds later the chamber coolant valve is opened. Approximately 5 sec after all chamber coolant sections are completely filled the oxidizer and fuel propellant valves are opened. (Chamber fill times were varied with coolant flow rate and are calculated from manifold, plenum and platelet volumes and the coolant volumetric flow rate.) A high temperature shutdown device was installed in the sequence unit. Prior to each test four

V, A, Facilities and Test Procedures (cont.)

thermocouples were selected to feed their electrical impulses into the shutdown device. When any one of the four temperatures exceeded the abort temperature millivolt settings, the engine was automatically shut down.

(U) The basic instrumentation that was used is as follows:

Function	Sensing Unit	Range P_c = 100 psia	Range P_c = 1000 psia
Tank Pressures	Taber Transducers	0 - 1K psig	0 - 3K psig
Chamber Pressures	Taber Transducers	0 - 200 psig	0 - 1.5K psig
Injection Pressures	Taber Transducers	0 - 200 psig	0 - 1.5K psig
Coolant Chamber Pressures	Taber Transducers	0 - 500 psig	0 - 1.5K psig
Venturi Inlet Pressures	Taber Transducers	0 - 500 psig	0 - 3K psig
Coolant Chamber Temperatures	CA Thermocouples	32°F - 2200°F	32°F - 2200°F
Thrust	Baldwin Load Cell	0 - 500 lb	0 - 2K lb
Flowrates	Potter Flowmeters Cavitating Venturis	0.3-9.0 gpm (H_2O) 0.11-2.3 gpm (H_2O)	1.0-2.7 gpm (H_2O) 0.26-18.9 gpm (H_2O)

(U) The output from the various sensing units are recorded on a direc reading 36-channel oscillograph and on an analog to digital conversion system. The instrumentation and data processing system is shown in Figure 29.

(U) The accuracy of the instrumentation using the manufacturer's quoted values and estimated values for calibration, electrical interconnections, and data reduction are as follows:

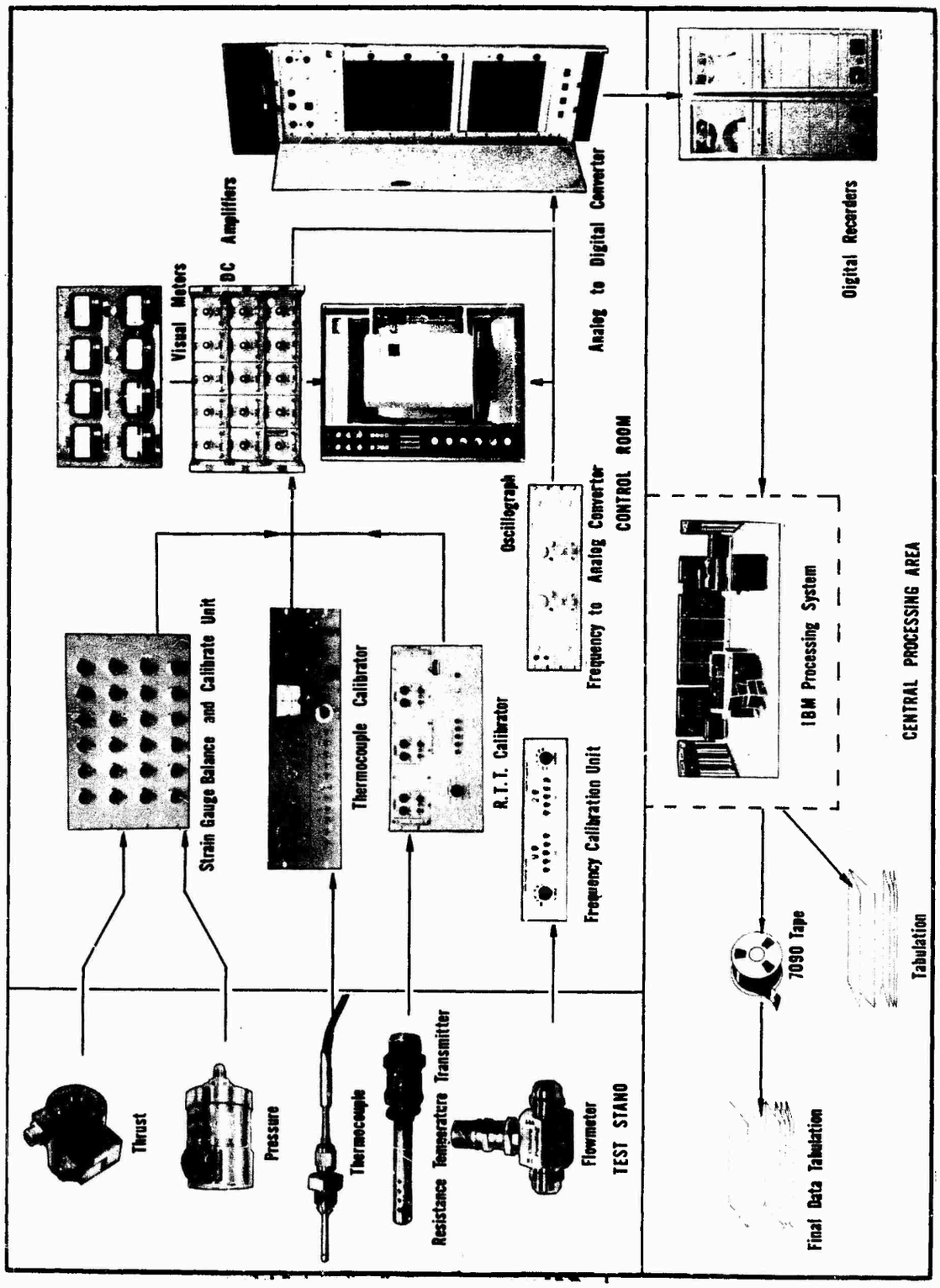

Figure 29. Research Physics Laboratory Instrumentation and Data Processing Systems

V, A, Facilities and Test Procedures (cont.)

Function	Error (% of Operating Point) Standard Deviation Error
Pressure	0.156
Temperature	
Chromel-alumel @ 1060°F	± 0.14
@ 2200°F	± 0.05
Copper-constantan @ 120°F	± 0.62
Flow (Turbine Flowmeters)	0.5
(Venturis)	0.2
Throat Areas	± 0.20
Thrust	± 0.86

2. Test Procedure

(U) Prior to each test a sequence check is made. This check consists of "dry" firing the engine to evaluate initial valve opening time, run duration, sequence of operations, and the temperature abort unit. Sequence changes or adjustments could be made at this time.

(U) The additional preparation required for ClF_3 testing is described below.

a. Cleaning (ClF_3)

(U) The ClF_3 run tank was cleaned and certified during fabrication to Aerojet Specification PM-114B. All of the associated plumbing installed in the ClF_3 feed system was cleaned as follows:

(U) All remote and manual operated valves, check valves and filters were disassembled, flushed with trichlorethylene, washed with a detergent and brush, and then flushed with water and alcohol. Liquid and

V, A, Facilities and Test Procedures (cont.)

gas lines were also cleaned in the same manner. All plumbing (valves, parts, fittings, lines) are then placed in an acid pickling solution for four hours. All parts are then rinsed with deionized water, flushed with alcohol, dried with GN_2, and size permitting, placed in a 230°F drying oven for four hours.

b. Passivation

(U) Prior to introducing ClF_3 vapors into the ClF_3 feed system the system was dried with GN_2 at 150°F for four hours. A ClF_3 cylinder containing 150 lb of ClF_3 was then connected to the fill line. ClF_3 vapors were introduced into the run tank and feed lines by remotely operating the appropriate valves. The feed system was allowed to soak with the dilute mixture of ClF_3 vapors and GN_2 for approximately 10 minutes. All of the remote operated valves were then opened separately for 2 minutes to allow the dilute mixture to pass through the valves. The operation was repeated several times with more concentrated mixtures of ClF_3 vapors until the system was completely saturated with the vapor. The feed system was then pressurized to 2300 psig (operating pressure for P_c = 1,000 psia) to allow the ClF_3 vapors to react with any crevice which was not passivated at the low pressure condition.

c. Tank Loading

(U) Upon completing the passivation the ClF_3 cylinder was disconnected, inverted and connected to the fill line. Liquid ClF_3 was then introduced into the tank, being driven by its own vapor pressure. The tank system was then allowed to soak with liquid ClF_3 for approximately 10 minutes before pressurizing the ClF_3 cylinder with GN_2 to 150 psig and transferring the remaining propellant. The cylinders were weighed before and after the fill operation to insure that all of the ClF_3 had been transferred.

V, Testing (cont.)

B. INJECTOR CHECKOUT TESTING

1. Phase I

(U) After fabrication and hydrotest the injectors were checked by test firing with ablative-lined 32L* combustion chambers. The purpose of these tests was to evaluate the performance characteristics of each injector and to identify any pattern nonuniformities. The thermocouple locations for the cooled chamber were selected on the basis of the postfire markings on the ablative chambers. A total of 22 injector checkout tests were made: twelve with ClF_3/MHF-3 (three injectors) and ten with N_2O_4/AeroZINE 50 (two injectors). The operating conditions are summarized in Table 5. The performance results are given in Section VI,A.

(U) The 100 lb and 1000 lb thrust injectors were tested over a small range of mixture ratios in anticipation of a range of operating conditions during cooled chamber testing. The testing at 900 psia nominal chamber pressure was performed to evaluate performance at reduced injector flow conditions since this mode of operation might be necessary to offset the increased pressure and thrust resulting from propellant introduced as coolant in the cooled chamber tests.

(U) Duplicate propellant flow rates were measured since each system contained a turbine type flowmeter and a fixed area cavitating venturi. Duplicate load cells were also used.

(U) Throat diameters were measured in four locations (0°, 45°, 90°, and 130°) after each test. Throat areas determined from the measured diameter (average of the four measurements) agreed to the nearest 0.001 $in.^2$ with throat areas (four cases) that were determined from a shadowgraph enlargement (10X) of the throats.

(U) TABLE 5

PHASE I INJECTOR CHECKOUT TEST CONDITIONS

Propellants	Injector P/N	Nominal Chamber Pressure (psia)	Test No.	Mixture Ratio	Duration (sec)
N_2O_4/AeroZINE 50	1122315-9 (S/N-2)	100	1K-3A-101	1.48	2
		100	102	1.50	5
		100	103	1.61	5
		100	104	1.37	3
	1122315-19 (S/N-3)	1000	105	1.67	1
		1000	106	1.68	2
		1000	107	1.78	2
		1000	108	1.55	2
		900	109	1.68	2
		900	110	1.58	2
ClF_3/MHF-3	1122315-9 (S/N-1)	100	1K-3B-101	*	2
		100	102	2.38	5
		100	103	2.21	5
		100	104	2.58	5
	1122315-29 (S/N-4)	1000	105	*	1
		1000	106	2.52	2
		1000	107	2.78	2
		900	108	2.38	2
	1122315-59 (S/N-5)	100	109	2.48	3
		100	110	2.50	5
		100	111	2.64	5
		100	112	2.24	5

*Test data invalid - propellant lines were not filled with propellant.

V, B, Injector Checkout Testing (cont.)

(U) Postfire examination of the 100 lb thrust ClF_3 injector (S/N-1) revealed that "bell mouthing" of the fuel orifices had occurred during the checkout testing. The body of this injector was stainless steel. The -59 injector (S/N-5) was fabricated with the same pattern, but a nickel body. No bell mouthing was noted with this injector at the conclusion of the injector checkout tests nor at the conclusion of the 100 lb thrust ClF_3-cooled chamber testing.

2. Phase II

(U) The baseline performance of three injectors was evaluated in Phase II using a 25L* ablative-lined combustion chamber. Two of these injectors, the Vortex S/N-8 injector and the 49-element S/N-9 injector, were new injectors. The third injector that was tested was the 21 element S/N-4 injector that had been used in Phase I. Since this injector was designated as the backup injector one test was run to characterize performance of this injector with the (25L*) Phase II chamber. Testing and measurement of the throat diameter, flow and thrust were done in the same manner as in Phase I.

(U) The injector checkout test conditions are summarized in Table 6. All tests were made with ClF_3/MHF-3 propellants at a nominal 1000 psia chamber pressure and 1000 lb thrust. The Vortex injector was designed to have good compatibility with the oxidizer transpiration cooled chamber by introducing the oxidizer tangentially at a diameter equal to the chamber I.D. and by introducing the fuel radially from a center spud. The axial and circumferential orientation of the fuel orifices with respect to the oxidizer orifices was varied to determine the effect on performance. The orientation used in each test is shown in Figure 30.

(U) TABLE 6

PHASE II INJECTOR CHECKOUT TEST CONDITIONS

Injector P/N	Type	Test No.	Mixture Ratio	Duration (sec)
1130922-29 (S/N-8)	Vortex	1K-5A-101	2.56	0.75
		102	2.59	2.00
		103	2.59	0.75
		104	2.59	0.75
1122315-29 (S/N-4)	21-element	105	2.57	0.70
1132431-1 (S/N-9)	49-element	106	2.56	0.77
		107	2.58	1.53
		108	2.16	0.75

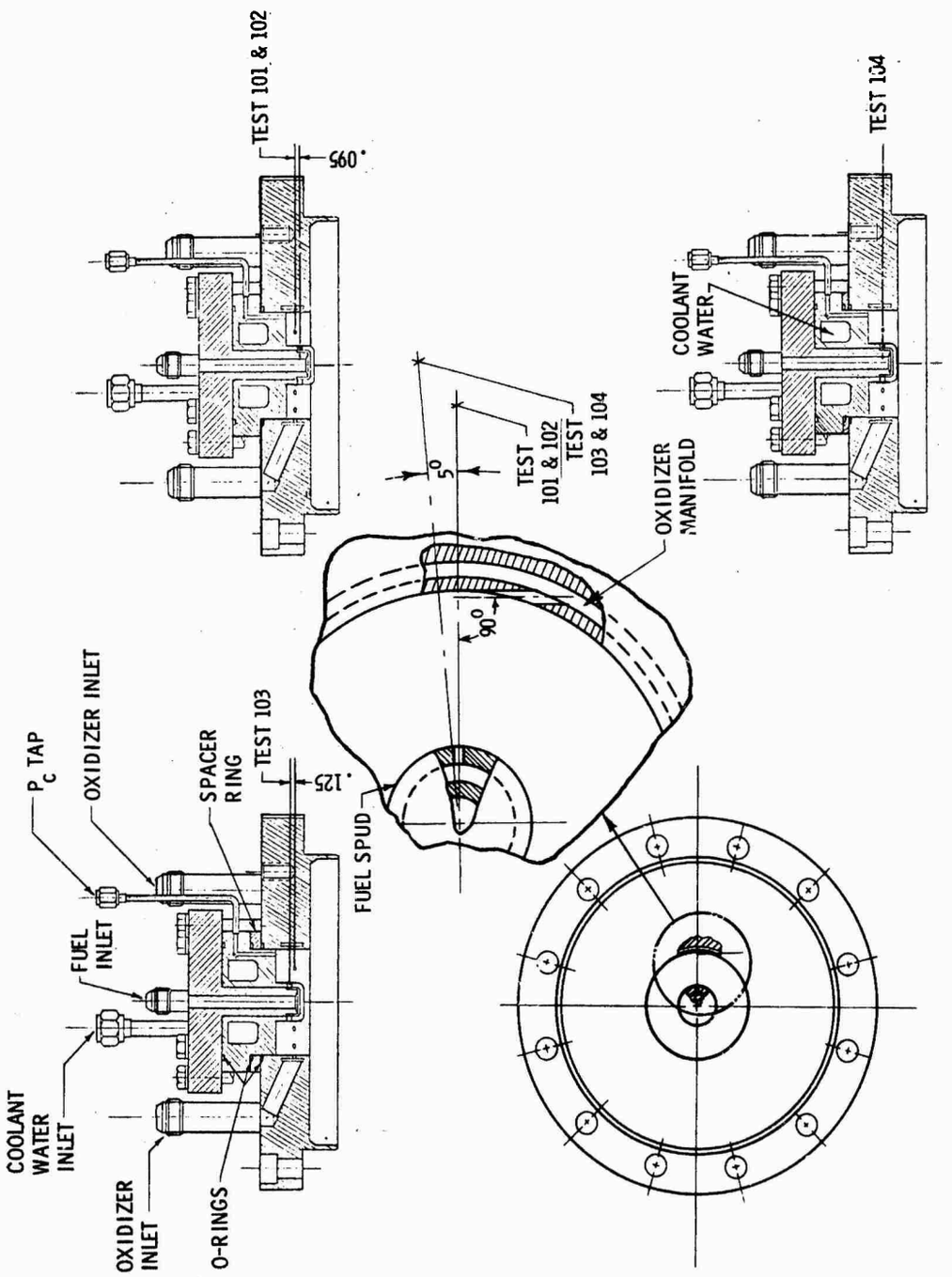

Figure 30. Dimensional Parameters for Vortex Injector Tests

V, Testing (cont.)

C. COOLED CHAMBER FLOW TESTING

1. N_2O_4 Flow Tests

(U) Prior to initiating the N_2O_4/AeroZINE 50 cooled chamber testing, the chamber coolant flow circuit was calibrated with N_2O_4. Thirteen N_2O_4 flow tests were conducted to establish the pressure drop-flow characteristics of all four chamber coolant compartments. The test setup was the same as was used for the cooled chamber test firings so that all flow conditions would be identical. Flow rates to three of the chamber coolant sections (I,II,III) were controlled with fixed area cavitating venturis. The flow rates were calculated using the manifold pressure upstream of the venturis and the venturi calibration curves. The coolant flow rate in Section IV (divergent section) was measured with a Potter micro-flowmeter. The coolant flow rate to Section IV was too small to permit utilization of a cavitating venturi. The total coolant flow rate was monitored with a turbine flowmeter. Plenum pressures in each section, venturi inlet pressure, and chamber pressure were measured with pressure transducers. The oxidizer propellant temperature was measured with a copper-constantan thermocouple.

(U) All chamber coolant sections were calibrated over a range of flow rates up to 10 times the nominal coolant flow rates for a chamber pressure level of 100 psia. All four coolant sections were flowed during the first test. In subsequent tests sections I and II were flowed together and sections III and IV were flowed separately. The coolant flow rates for Sections I, II, and III were changed by changing venturis while the coolant flow rate to section IV was changed by increasing or decreasing the oxidizer supply tank pressure. Each test was conducted by pressurizing the oxidizer feed circuit and remotely operating the chamber coolant valve. The data were recorded on the 36-channel direct-reading oscillograph.

V, C, Cooled Chamber Flow Testing (cont.)

2. ClF_3/MHF-3 Flow Tests

(U) Prior to conducting firings with the Phase I ClF_3 cooled chamber the coolant circuit was flow calibrated with trichlorethylene. Trichlorethylene was selected because of its availability, and because it would give the best combination of pressure drop and Reynolds number scaling. The chamber was not flowed on the test stand with ClF_3 because of the toxicity of ClF_3.

(U) A separate test setup which duplicated the ClF_3-coolant flow circuit was fabricated and installed in an existing feed circuit in the Engineering R&D Laboratory. All four chamber coolant compartment flow rates were controlled with cavitating venturis. The flow rates were calculated using the manifold pressure upstream of the venturis and the venturi calibration curves. The flow rate were varied during each test by increasing or decreasing tank pressure and by changing venturis. All four chamber coolant compartments were flowed simultaneously during these tests. The flow rate range covered during these tests was approximately 1/2 to 10 times the anticipated nominal coolant flow rates required for a chamber pressure level of 100 psia.

(U) Prior to conducting test firings with the Phase I nickel platelet chamber at a chamber pressure level of 1000 psia, the chamber was flowed with ClF_3 on the test stand. All chamber coolant compartments were flowed simultaneously with cavitating venturis in each flow circuit. The coolant flow rates were the same as those required for the first hot firing. All pressure and temperatures were recorded on the 36-channel direct-reading oscillograph.

(U) Because the Phase II chamber was similar to the Phase I chamber no flow tests were made with the chamber prior to test firing other than flowing with ClF_3 on the test stand at the flow rates that were used in the first cooled chamber test.

V, Testing (cont.)

D. COOLED CHAMBER TEST FIRING

1. Phase I

a. N_2O_4 Testing

(U) Testing of the N_2O_4 cooled chamber was initiated at the 100 lb thrust level. The following steps were taken to insure minimum risk of hardware damage:

(U) (1) The first tests were made with 10 times the nominal 100 lb thrust coolant flow rates.

(U) (2) The four high-temperature-abort circuits were set at 1000°F and used to monitor one surface thermocouple in each section.

(U) (3) Test series of increasing test duration were used. The first test in each series was generally of short enough duration that full chamber pressure was not achieved. Successive tests of longer duration were then made until all thermocouples indicated that steady-state had been achieved. Selected thermocouples were monitored on the oscillograph. Only 16 of the 44 thermocouples could be recorded on the digital system per test. The longer duration tests were frequently repeated to permit additional thermocouples to be monitored.

(U) The N_2O_4/AeroZINE-50 test operating conditions are summarized in Tables 7 and 8. Systematic reduction of the coolant flow was planned. On the first two 10-sec duration tests fluctuation of fuel flow and a corresponding fluctuation in chamber pressure was noted. The flow transient suggested momentary clogging of the cavitating venturi in the fuel circuit. Installation of a filter in the fuel circuit eliminated the problem.

(C) TABLE 7

SUMMARY OF N_2O_4-COOLED CHAMBER TEST CONDITIONS (100 lb THRUST) (U)

Test	Approximate Duration (sec)	Ratio of Planned Coolant Flow Rate to Nominal Value				Comments
		Sect I	Sect II	Sect III	Sect IV	
1K-3C-101	1.4	10.0	10.0	10	10	Initial test sequence selected
-102	1.9	10.0	10.0	10	10	to minimize risk to hardware.
-103	3.0	10.0	10.0	10	10	Fluctuation noted in P_c and
-104	10.0	10.0	10.0	10	10	fuel flow during 10 sec test.
-105	1.4	7.5	10.0	10	10	Coolant flows reduced in
-106	2.0	7.5	10.0	10	10	Sections I and II. Spike noted
-107	1.4	5.4	10.0	10	10	in platelet temperatures on
-108	1.4	5.4	7.2	10	10	startup.
-109	2.0	5.4	7.2	10	10	
-110	1.4	5.4	5.5	10	10	Coolant flows reduced.
-111	1.4	4.0	5.5	10	10	Fluctuation again noted in P_c
-112	1.4	4.0	4.0	10	10	and fuel flow during 10 sec
-113	10.0	4.0	4.0	10	10	test.
-114	10.0	4.0	4.0	10	10	A filter added to fuel line
-115	1.4	4.0	4.0	10	10	eliminated fluctuation in P_c
-116	1.4	4.0	4.0	10	10	and fuel flow (10 sec test).
-117	1.4	4.0	4.0	10	10	Purge sequence, coolant manifold venting and injector O/F (1.8) were varied to evaluate their thermal effects.
-118	1.4	3.2	4.0	10	10	Coolant flow reduced in Section
-119	1.4	3.2	3.0	10	10	II. Long duration tests were
-120	3.0	3.2	3.0	10	10	run to permit output of all
-121	30.0	3.2	3.0	10	10	thermocouples to be recorded
-122	30.0	3.2	3.0	10	10	under steady-state conditions.
-123	60.0	3.2	3.0	10	10	(Only 16 thermocouples could be recorded per test.)
-124	1.4	3.2	3.0	10	10	Oxidizer (injector) lead time
-125	1.4	3.2	3.0	10	10	and injector O/F (2.2) were
-126	1.4	3.2	3.0	10	10	varied to evaluate their thermal effects.
-127	1.4	3.2	3.0	10	10	Thermal effect of rate of fuel
-128	1.4	2.7	3.0	10	10	valve opening (Tests 127, 131,
-129	2.0	2.7	3.0	10	10	and 132) was evaluated. Coolant
-130	1.4	2.7	2.5	10	10	flows were reduced (Tests 128-30,
-131	1.4	2.7	2.5	10	10	133-37). Test 138 through 141
-132	3.0	2.7	2.5	10	10	were to be 3.0 sec in duration
-133	1.4	2.3	2.5	9.1	10	but were aborted by the high
-134	3.0	2.3	2.5	9.1	10	temperature trip circuit.

(C) TABLE 7 (cont.)

Test	Approximate Duration (sec)	Ratio of Planned Coolant Flow Rate to Nominal Value Sect I	Sect II	Sect III	Sect IV	Comments
1K-3C-135	1.4	2.3	2.0	8.1	10	The aborts were not caused by high temperatures, but by instrumentation components that were subsequently replaced. The final three long duration tests were run to record steady-state temperatures for all thermocouples. These and all subsequent tests were made with injector O/F of 2.2.
-136	3.0	2.3	2.0	8.1	10	
-137	1.4	2.0	1.8	7.2	10	
-138	1.2 Abort	2.0	1.8	7.2	10	
-139	1.2 Abort	2.0	1.8	7.2	10	
-140	1.2 Abort	2.0	1.8	7.2	10	
-141	2.5 Abort	2.0	1.8	7.2	10	
-142	3.0	2.0	1.8	7.2	10	
-143	10.0	2.0	1.8	7.2	10	
-144	30.0	2.0	1.8	7.2	10	
-145	60.0	2.0	1.8	7.2	10	
-146	1.4	1.8	1.6	9.1	10	Coolant flow rates were reduced.
-147	1.4	1.6	1.5	8.2	10	
-148	10.0	1.6	1.5	8.2	10	
-149	3.0	1.6	1.5	8.2	10	Two short duration (3.0 sec) instrumentation checkout tests were made and then longer duration tests were run to permit output of all thermocouples to be recorded. Test 153 was to be 60 sec in duration, but was inadvertently terminated after 10 seconds.
-150	3.0	1.6	1.5	8.2	10	
-151	10.0	1.6	1.5	8.2	10	
-152	30.0	1.6	1.5	8.2	10	
-153	10.0	1.6	1.5	8.2	10	
-154	60.0	1.6	1.5	8.2	10	
-155	1.4	1.6	1.3	6.6	10	Flow reduced in Sections II and III. Three 30 sec runs were made to record all thermocouple readings. Two tests (No. 163 and 164) were shut down by an oversensitive trip on the high temperature trip circuit.
-156	10.0	1.6	1.3	6.6	10	
-157	1.4	1.6	1.1	5.7	10	
-158	10.0	1.6	1.1	5.7	10	
-159	30.0	1.6	1.1	5.7	10	
-160	1.4	1.6	1.0	5.0	10	
-161	10.0	1.6	1.0	5.0	10	
-162	30.0	1.6	1.0	5.0	10	
-163	1.6 Abort	1.6	1.0	5.0	10	
-164	1.7 Abort	1.6	1.0	5.0	10	
-165	30.0	1.6	1.0	5.0	10	
-166	30.0	1.6	1.0	5.0	10	
-167	1.4	1.6	0.9	5.0	10	Reduction of coolant flows in Sections II and III continued. Heat marks of dark straw color apparent at end of Test 175. Heat marks are in throat and in cylindrical section within 1-1/2 inches of injector.
-168	10.0	1.6	0.9	5.0	10	
-169	1.4	1.6	0.8	5.0	10	
-170	10.0	1.6	0.8	5.0	10	
-171	30.0	1.6	0.8	5.0	10	
-172	30.0	1.6	0.8	5.0	10	
-173	1.4	1.6	0.7	5.0	10	

(C) TABLE 7 (cont.)

Test	Approximate Duration (sec)	Ratio of Planned Coolant Flow Rate to Nominal Value				Comments
		Sect I	Sect II	Sect III	Sect IV	
1K-3C-174	10.0	1.6	0.7	5.0	10	The 30 sec runs were made to
-175	1.4	1.6	0.7	4.6	10	record all thermocouple readings.
-176	3.0	1.6	0.7	4.6	10	The aborts of Tests 178, 179,
-177	30.0	1.6	0.7	4.6	10	and 180 were caused by an over-
-178	1.0 Abort	1.6	0.7	4.6	10	sensitive trip in the high
-179	2.0 Abort	1.6	0.7	4.6	10	temperature trip circuit.
-180	2.2 Abort	1.6	0.7	4.6	10	
-181	30.0	1.6	0.7	4.6	10	
-182	1.4	1.8	0.6	4.6	6	Coolant flow in Section IV
-183	2.1 Abort	1.8	0.6	4.6	6	reduced. Coolant flow in
-184	3.0	1.8	0.6	4.6	6	Section I increased to keep wall
-185	10.0	1.8	0.6	4.6	6	temperatures below 1500°F.
-186	2.0	1.8	0.6	4.6	4.6	Test 183 was shut down by an
-187	2.0	1.8	0.6	4.6	3.2	oversensitive trip in the high
-188	10.0	1.8	0.6	4.6	3.2	temperature trip circuit.
-189	30.0	1.8	0.6	4.6	3.2	
-190	30.0	1.8	0.6	4.6	3.2	
-191	10.0	1.8	0.6	4.6	3.2	Steady state duration testing.
-192	400.0	1.8	0.6	4.6	3.2	
-193	400.0	1.8	0.6	4.6	3.2	
-194	10.0	1.8	0.6	4.6	3.2	Duty cycle demonstration.
-195	400.0	1.8	0.6	4.6	3.2	
-196	400.0	1.8	0.6	4.6	3.2	

(C) TABLE 8

SUMMARY OF N_2O_4-COOLED CHAMBER TEST CONDITIONS (1000 lb THRUST) (U)

Test	Approximate Duration (sec)	Ratio of Planned Coolant Flow Rate to Nominal Value				Comments
		Sect I	Sect II	Sect III	Sect IV	
1K-3C-197	0.4	2.2	2.0	2.9	1.2	Initial test at 1000 lb thrust
-198	0.5 Abort	2.2	2.0	2.9	1.2	of short duration to minimize risk to hardware. Test 198 was shut down by trip circuit because of high temperature in throat section.
-199	0.5 Abort	2.2	2.0	3.2	1.2	Coolant flow in Section III
-200	0.5 Abort	2.2	2.0	3.2	1.2	(throat) increased. Chamber
-201	0.6	2.2	2.0	3.2	1.2	plenum bleed system was by-
-202	1.0	2.2	2.0	3.2	1.2	passing coolant from Section
-203	1.2 Abort	2.2	2.0	3.2	1.2	III to Section IV. Trip circuit
-204	2.0	2.2	2.0	3.2	1.2	prevented damage to chamber
-205	5.0	2.2	2.0	3.2	1.2	(Tests 199 and 200). Bleed
-206	0.5 Abort	2.2	2.0	3.2	1.2	system was removed after Test
-207	5.0	2.2	2.0	3.2	1.2	200. Temperatures in throat peaks near 1500.F, the trip setting, and occasionally cause an abort (Tests 203 and 206).
-208	2.0	2.2	2.0	3.2	1.2	Long duration (30-50 sec) tests
-209	8.5 Abort	2.2	2.0	3.2	1.2	planned. Thermocouples 4-1 and
-210	32.0	2.2	2.0	3.2	1.2	9-2 operating near 1500°F
-211	22.0 Abort	2.2	2.0	3.2	1.2	causing abort. Final Test (215)
-212	28.0	2.2	2.0	3.2	1.2	made with trip setting between
-213	21.7 Abort	2.2	2.0	3.2	1.2	1600 and 1750°F.
-214	23.5 Abort	2.2	2.0	3.2	1.2	
-215	50.0	2.2	2.0	3.2	1.2	
-216	100.0	2.2	2.0	3.2	1.2	Long duration and duty cycle
-217	1.6 Abort	2.2	2.0	3.2	1.2	(Test 221) demonstration tests.
-218	100.0	2.2	2.0	3.2	1.2	Abort caused by low temperature
-219	30.0	2.2	2.0	3.2	1.2	setting on trip circuit. Test
-220	30.0	2.2	2.0	3.2	1.2	219 and 220 were made with in-
-221	86.0	2.2	2.0	3.2	1.2	jector O/F of 2.0 and 2.2; respectively. All other 1000 lb thrust tests were conducted with injector O/F of 2.1.

V, D, Cooled Chamber Test Firing (cont.)

(U) A mild excursion in the readings of thermocouples in line with a radial projection through the injector elements was noted on startup. This temperature spike increased in magnitude and duration as the coolant flows were reduced. This transient was most severe in the throat (recorded on Thermocouple 2-3) and in Section I about 1.5 inches from the injector (recorded on Thermocouple 8-2). The temperature transient is illustrated in Figure 31 in which response of throat thermocouples in line with injector elements (TC 2-3) and between elements (TC 2-7) are plotted versus time for Test 1K-3C-111.

(C) Several system variables were investigated in an attempt to reduce the thermal startup transient. The peak temperature (TC 2-3) was reduced from approximately 570°F to approximately 430°F by lengthening the oxidizer lead time to the injector to 0.400 sec. By increasing the injector MR from 2.0 to 2.2 the peak temperature was reduced to approximately 310°F. Reducing the rate at which the fuel valve opened made the transient slightly more severe. Because of the behavior of the thermocouple in line with the injector elements it is hypothesized that during startup the injection velocities are too low for good atomization and raw fuel is carried to the wall where it combusts with the oxidizer coolant. As coolant flow was reduced and steady-state wall temperatures increased the transient temperatures (TC 2-3) peaked about 450°F above the steady state value.

(U) Twenty of the N_2O_4-cooled chamber tests were shut down by the high temperature trip circuit prior to the planned shutdown. The first of these aborts was caused by the response characteristics of the amplifiers in the instrumentation circuits. Replacement of these amplifiers terminated these false shutdowns. Subsequent aborts were caused either by inaccuracies in the trip setting, operation with temperatures near the trip setting, or by the thermal transient response characteristics of the cooled chamber.

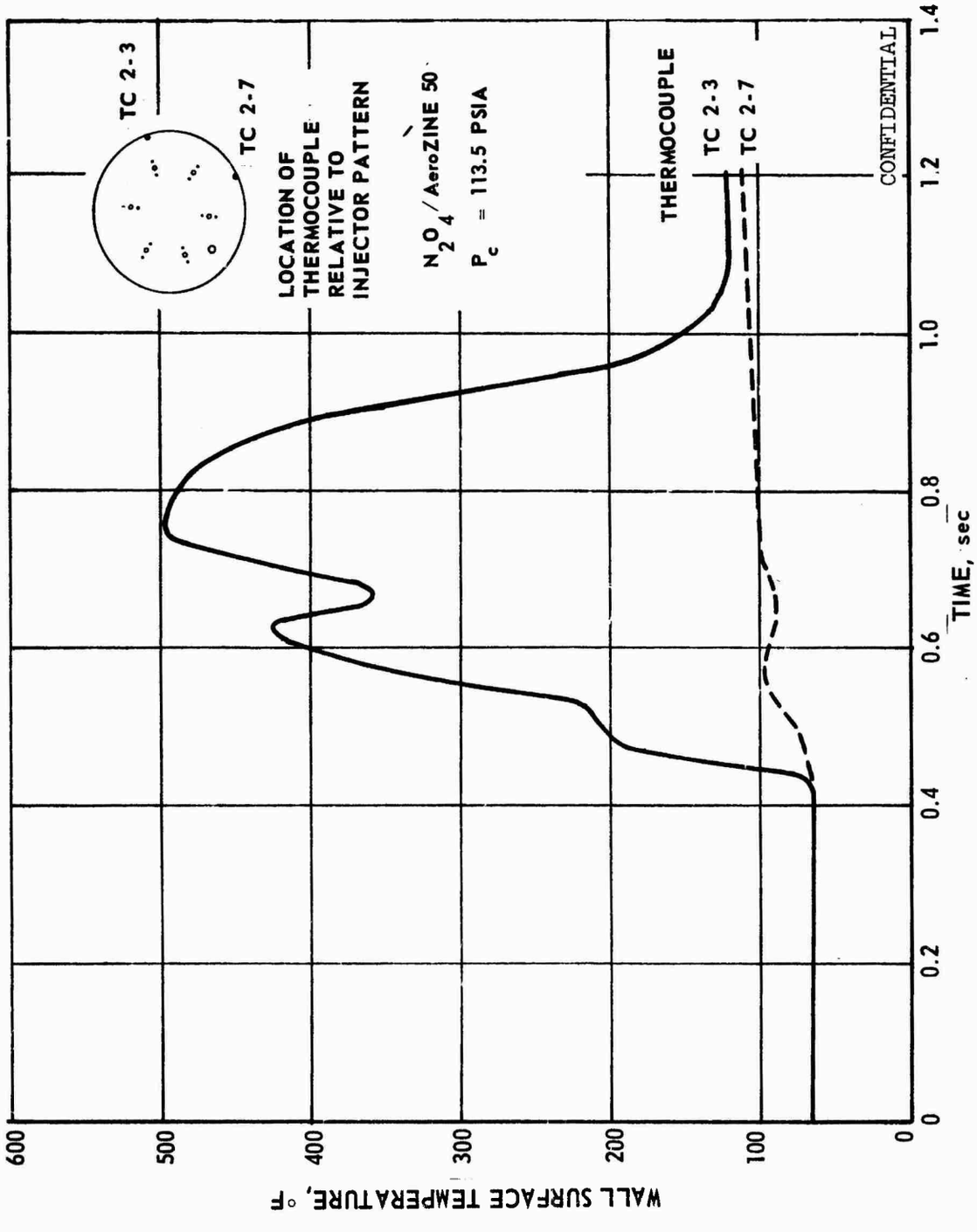

Figure 31. Throat Temperature Transients During Startup (u)

V, D, Cooled Chamber Test Firing (cont.)

(C) The chamber thermal characteristics are illustrated in Figure 32. The figure depicts the temperature transient that was recorded on thermocouple TC 9-2 (Section I), and TC 4-7 (Section II) during Test 1K-3C-215. The locations of these thermocouples are shown in Figures 21 and 23. From Figure 32 it can be seen that aborts that occurred shortly after ignition were caused by the spike in the response of thermocouple TC 4-7, and that the aborts that occurred approximately 20 sec after ignition were caused by the increase in temperature level at that time of thermocouple TC 9-2 to approximately 1600°F which is in excess of the nominal 1500°F trip setting.

(U) In many cases aborts occurred during an attempt to repeat a long duration ($\geq$30 sec) firing, for example Tests 1K-3C-163, -164, -178, -179, -180, -211, -213, -214, and -217. Since no changes had been made to either coolant flow rates or total propellant flow rates and adequate cooling had been demonstrated by the earlier test, the trip settings were increased to 1600-1750°F to permit the tests to be run.

(U) Not all of the aborts resulted from inaccuracies in the trip setting or from spikes and random variations in the peak transient temperatures. High temperatures that resulted from insufficient coolant flow through the platelets in Section III caused the aborts of Tests 1K-3C-198, -199, and -200. Inadequate coolant flow was metered to Section III in Test 1K-3C-198, and in Tests -199 and -200 a malfunction of the vent system bypassed coolant flow from Section III to Section IV. The vent system was used to vent gas from each coolant section during fill prior to each firing as is discussed in Section IV,C,2. The vent system was removed after Test 1K-3C-200 and was not used in testing the ClF_3 cooled chamber.

(U) The coolant flow rates for each section for the 1000 lb thrust operating conditions were selected on the basis of the 100 lb thrust results subject to the constraints of available venturies, venturi

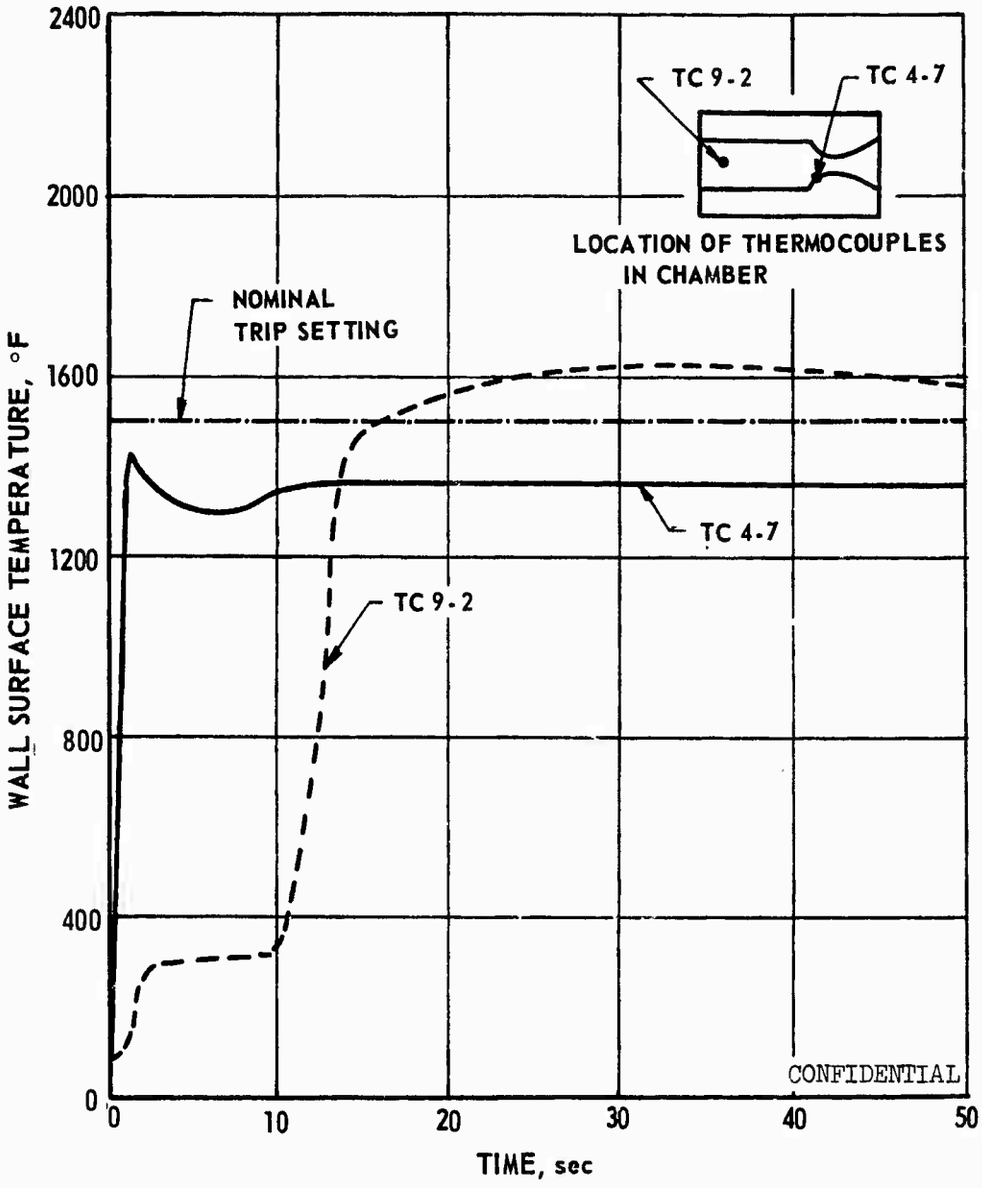

Figure 32. Chamber Thermal Characteristics (u)

V, D, Cooled Chamber Test Firing (cont.)

recovery pressures, hydraulic characteristics of the chamber, etc. Tests 1K-3C-197 and -198 indicated that the flow rate to Section III had to be increased to a value greater than that initially selected. The flow rates to all other sections were retained at the initial value.

(U) The final N_2O_4 100 lb thrust and 1000 lb thrust test conditions are summarized in Table 9.

(C) The final demonstration tests at 100 psia chamber pressure, 100 lb thrust could have been made with a lower coolant flow rate since the coolant flow in chamber Sections II, III, and IV had not been reduced to a point of producing a 1500°F maximum wall temperature in those sections. The decision to terminate the coolant optimization was influenced by the following:

(U) 1. Sufficient data had been obtained to adequately evaluate the concept. There was abundant data for evaluation of the effect of coolant flow in each section on wall temperature and performance. Flow in Section II had been reduced 16 times, for example.

(U) 2. Thermocouples were failing as a result of thermal cycling and attack of N_2O_4 and nitric acid on the alumel in the thermocouple junction. Continued testing at the low thrust condition would drastically reduce the number of surface thermocouples that would be available for the 1000 psia testing.

(C) 3. Transient wall temperatures of 1450°F were occurring in Section III. Further reduction of the flow in that section would have increased the number of aborts caused by the high temperature trip circuit or would have required a higher trip setting which compromises the protection afforded the chamber.

(C) TABLE 9

N_2O_4-COOLED CHAMBER FINAL TEST CONDITIONS (U)

	100 psia				1000 psia			
Chambers Section	$\dot{w}_c$ Coolant Flow Rate (lb/sec)	$\dot{w}_N$ Nominal Coolant Flow Rate (lb/sec)	$\frac{\dot{w}_c}{\dot{w}_N}$	Maximum Steady State Temperature (°F)	$\dot{w}_c$ Coolant Flow Rate (lb/sec)	$\dot{w}_N$ Nominal Coolant Flow Rate (lb/sec)	$\frac{\dot{w}_c}{\dot{w}_N}$	Maximum Steady State Temperature (°F)
I	0.0628	0.0353	1.78	1504	0.622	0.289	2.15	1650
II	0.0216	0.0342	0.63	1200	0.560	0.280	2.00	1575
III	0.0353	0.0077	4.59	1282	0.298	0.092	3.24	1500
IV	0.0161	0.0050	3.22	400	0.093	0.078	1.19	1050
TOTAL	0.1358	0.0822	1.65	-	1.573	0.739	2.13	-

V, D, Cooled Chamber Test Firing (cont.)

(C) In the 1000 lb testing no attempt was made to optimize the coolant flow in Section IV, i.e., to decrease the coolant flow until a 1500°F wall temperature was obtained. The main consideration prompting this decision was the number of thermocouples that lost continuity during the change over of the stand (lines, transducers, load cells, etc.) from operation at 100 lb thrust to 1000 lb thrust. This loss of thermal instrumentation would be aggravated by the additional downtime that would be required to change the flow. Both surface thermocouples in the throat (2-3 and 2-7) were inoperative. The 1500°F temperature shown for Section III in Table 9 was inferred from thermocouples 2-2 and 2-6 that are 0.015 in. below the surface. Thermocouple 1-2, the only remaining thermocouple in Section IV, failed on Test 1K-3C-216.

(U) For the most part coolant flow rates were in excess of the nominal values that were calculated as giving a 1500°F wall temperature in each section. Postfire inspection of the chamber indicated that the injector pattern was producing localized high temperature zones or streaks on the chamber wall. The coolant flow rates were dictated by these hot streaks, although 80 to 85% of the chamber surface area was overcooled, often by as much as 1000°F. The effect of injector streaking was much more severe than anticipated and is discussed in detail in Section IV,C.

b. ClF_3 Testing

(U) The ClF_3 cooled chamber was initially tested at 100 lb thrust. The 100 lb thrust and 1000 lb thrust test conditions are summarized in Tables 10 and 11. At the end of the first series of tests (Test 1K-3D-104) the water coolant manifold in the forward flange of the housing (see Figure 10, Section IV,C) was leaking. The chamber was removed from the stand and put through several flushing and drying cycles.

(C) TABLE 10

SUMMARY OF PHASE I ClF_3-COOLED CHAMBER TEST CONDITIONS (100 LB THRUST) (U)

Test	Approximate Duration (sec)	Ratio of Planned Coolant Flow Rate To Nominal Value				Comments
		Sect I	Sect II	Sect III	Sect IV	
1K-3D-101	Cold Flow	2.1	2.0	4.8	3.3	Test No. 101 was a cold flow checkout of the chamber hydraulic characteristics using ClF_3.
-102	1.5	2.1	2.0	4.8	3.3	
-103	2.1	2.1	2.0	4.8	3.3	
-104	11.0	2.1	2.0	4.8	3.3	
-105	1.8	1.4	1.4	3.8	1.8	Coolant flow in all sections reduced followed by subsequent reduction of coolant flow to Section II. The high temperature trip circuit was set for 1200°F, but produced three shutdowns although the maximum temperature recorded on oscillograph was 1120°F.
-106	2.7	1.4	1.4	3.8	1.8	
-107	2.2 Abort	1.4	1.4	3.8	1.8	
-108	11.0	1.4	1.4	3.8	1.8	
-109	2.9 Abort	1.4	1.4	3.8	1.8	
-110	21.2 Abort	1.4	1.4	3.8	1.8	
-111	10.9	1.4	1.0	3.8	1.8	
-112	27.8	1.4	1.0	3.8	1.8	
-113	15.0	1.4	0.6	3.8	1.8	Coolant flow reduced in Section II. Last test was long duration demonstration.
-114	78.0	1.4	0.6	3.8	1.8	

(C) TABLE 11

SUMMARY OF PHASE I ClF_3-COOLED CHAMBER TEST CONDITIONS (1000 LB THRUST) (U)

Test	Approximate Duration (sec)	Ratio of Planned Coolant Flow Rate To Nominal Value				Comments
		Sect I	Sect II	Sect III	Sect IV	
1K-3D-115	0.4	2.0	1.9	3.3	1.2	Chamber was eroded on last test which was planned for 50 sec duration. Abort by high temperature trip circuit came too late. Platelets plugged by $NiF_2 \cdot 4(H_2O)$ salt formed because of water leak into chamber.
-116	1.4	2.0	1.9	3.3	1.2	
-117	2.0	2.0	1.9	3.3	1.2	
-118	2.4 Abort	2.0	1.9	3.3	1.2	

V, D, Cooled Chamber Test Firing (cont.)

(U) When the chamber was examined it was found that the water leak was caused by pin-holes on the injector side of the water coolant manifold. After repair by welding the chamber was returned to the test stand. Eight additional tests were made. Figure 33 shows the ClF_3-cooled chamber on the stand at the conclusion of these tests (Tests 1K-3D-105 through 112).

(U) The water coolant manifold was again leaking after Test 1K-3D-112. The chamber was removed from the stand and cleaned as before. Repair by welding could not be made as leakage was occurring on the chamber platelet side of the flange. In order to effect a repair the stainless steel manifold was removed by dry machining, and a new nickel manifold was welded in place. Tests 1K-3D-113 (15 sec) and 1K-3D-114 (78 sec) were made after this repair.

(C) Water leaked from the manifold into Section I during Test 1K-3D-114. The water manifold was pressurized to 400 psia. Chamber pressure was 112 psia and the Section I plenum pressure was approximately 150 psia. The reaction between the ClF_3 and the water caused the pressure and temperatures in Section I to begin rising about 20 sec after ignition until the high temperature trip circuit aborted the test (see Figure 34). The temperature transient produced an 1685°F peak temperature (TC 8-2, Section I). There was no damage to the chamber.

(U) The chamber was removed and cleaned again and the water manifold was again removed by machining. Examination showed that the weld on the chamber side of the flange had been made with a single pass and was porous. The manifold was again replaced. All welds were made with a root pass and multiple filler passes. No further leakage occurred.

(U) While the chamber was being repaired the stand was set up for 1000 lb thrust testing. This changeover was made so that, if the

Figure 33. Phase I ClF_3-Cooled Chamber after 95 sec of Testing

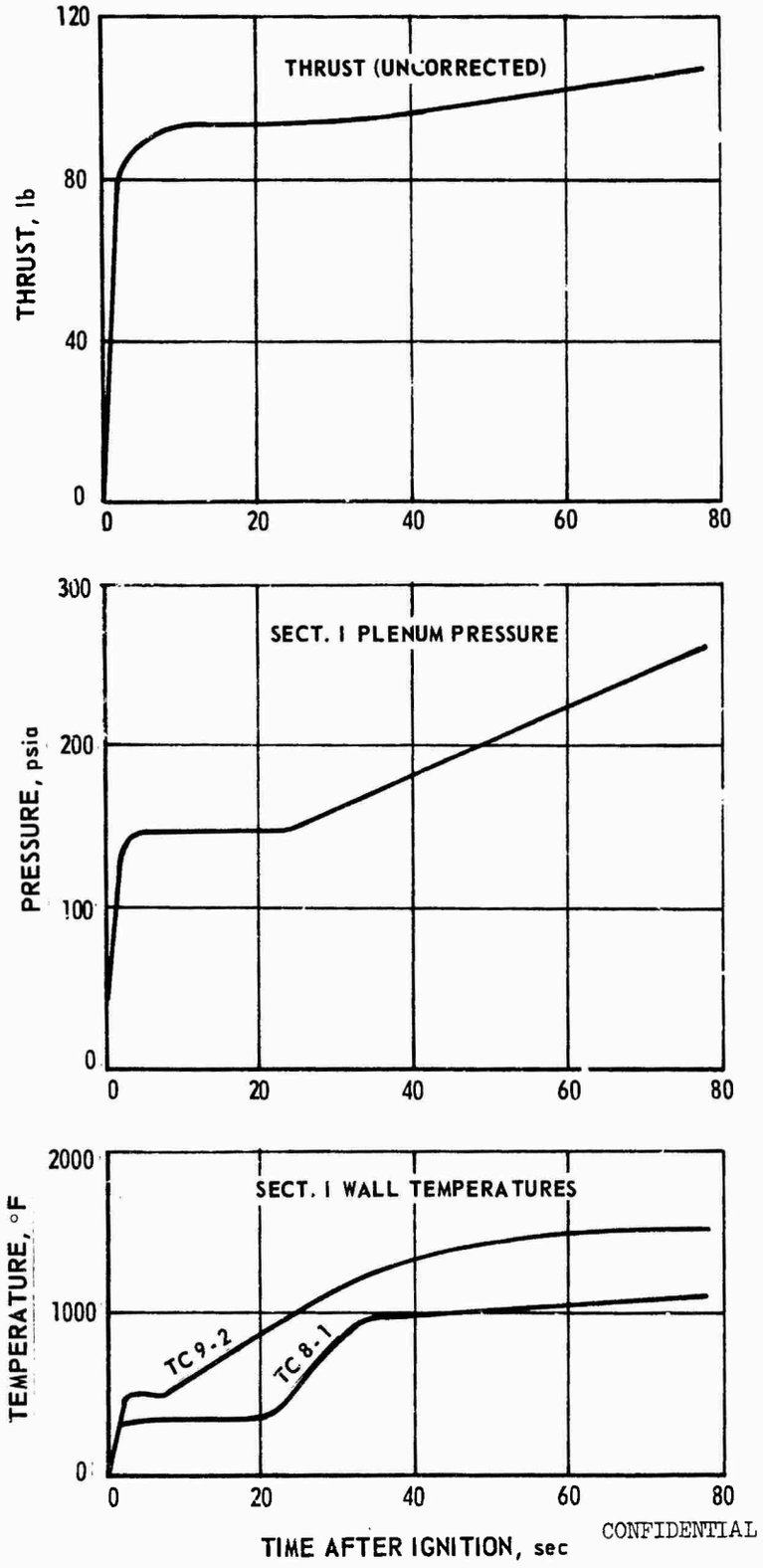

Figure 34. Transient Data from Final 100 psia ClF_3-Cooled Chamber Test (u)

V, D, Cooled Chamber Test Firing (cont.)

water coolant manifold leak persisted, data could be obtained at 1000 lb thrust conditions before the problem became so severe as to preclude testing. At this point steady-state operation at 100 lb thrust had been adequately demonstrated in the critical throat section during the 78 sec test 1K-3D-114.

(U) Prior to initiation of the testing at 1000 lb thrust a cold flow test was made on the stand using ClF_3. During the test the pressure drop across the 10 micron (absolute), (2 micron nominal) filter in the oxidizer coolant circuit increased from 40 to 800 psi. One of the bottles of ClF_3 used to fill the ClF_3 run tank evidently contained a contaminant. The filter was removed and cleaned. Passivation was accomplished by opening the run tank safety valve for a short duration to introduce ClF_3 vapors into the feed line. This process was repeated using longer valve open times and finally with the tank pressurized.

(U) Tests 1K-3D-115 (0.4 sec) and 1K-3D-116 (1.4 sec) were made. By the end of Test 1K-3D-116 the pressure drop across the filter had increased to 410 psi. This pressure drop reduced the pressure upstream of the cavitating venturis that control the coolant flow to the chamber. A larger capacity filter was added to the oxidizer coolant line upstream of the existing filter and upstream of the coolant valve.

(U) Passivation of this filter was attempted too rapidly. Upon opening the oxidizer safety valve the second time excessive ClF_3 was introduced in the line; the filter reacted explosively with the ClF_3. This reaction triggered secondary burn-through in the line and in the coolant inlet manifold. Both filters, the flowmeter and the chamber coolant valve were severely damaged. There was no damage to the chamber.

V, D, Cooled Chamber Test Firing (cont.)

(U) The feed system was refurbished and the damaged parts, including the coolant inlet manifold, were replaced. In order to eliminate future contamination of the feed system the ClF_3 run tank was drained, flushed twice with Freon 113 and dried with nitrogen gas. The tank and feed system were passivated with ClF_3 vapors mixed with GN_2. The entire system was pressurized to 2200 psia with a high concentration of ClF_3 vapors in nitrogen gas and held for two hours.

(U) Filling of the run tank was initiated by inverting the ClF_3 bottle so that liquid rather than ClF_3 vapor flowed in the fill line. As part of the fill process the ClF_3 supply bottle was pressurized with 150 psia nitrogen gas. After the GN_2 supply valve was opened to pressurize the ClF_3 bottle the filter in the fill system ignited. This was unexpected since all of the ClF_3 used in passivation had passed through the filter. Since a similar filter element was mechanically damaged by the drying nitrogen gas flow in the cleaning process it is probable that the high velocity flow of nitrogen gas in the reverse direction through the fill system filter caused mechanical damage; the passivation layer of the filter element was thereby disrupted and ignition with residual ClF_3 occurred. The damaged filter was replaced and passivated, the nitrogen pressure was reduced to 50 psia, and the propellant transfer was completed.

(U) Test 1K-3D-117 was aborted by the high temperature trip circuit 2.29 seconds after ignition.* The abort was caused by thermocouple TC 9-4 (Section I) which was oscillating between a zero and full scale reading. Postfire visual inspection of the chamber was made; the chamber was in excellent condition. There was no sign of erosion or damage in the vicinity of the erratic thermocouple. The water coolant manifold was not leaking.

*Ignition and shutdown are defined as occurring when the fuel valve is energized and de-energized.

V, D, Cooled Chamber Test Firing (cont.)

(U) Test 1K-3D-118, the final test of Phase I of this program, was to be 50 sec in duration. The test was aborted by the high temperature trip circuit (TC 2-7, Section III) 2.44 sec after ignition. Severe erosion of the chamber occurred during this test. Figure 35 shows the damage to the throat and at the forward end of the chamber.

(U) Upon disassembly of the chamber a green salt was found in the thermal influence zone of the platelets. It was located predominantly in the lower part of the horizontally mounted chamber where the water stood after Test 1K-3D-114, the last test of the 100 psia series. Platelets forward of the damaged area in the chamber section (see Figure 35) and one from the convergent section can be seen in Figure 36. The whitish appearing material opposite the cut-out section is the salt. This photograph shows both the plugged area and the absence of plugging in the primary and secondary metering grooves. Although the platelets in Figure 36 are distribution platelets, the flow paths of the metering platelet are evidenced by discoloration. No salt was found in these areas. The salt found in the thermal influence zones was analyzed by X-ray diffraction and found to be $NiF_2 \cdot 4(H_2O)$.

(U) The temperature transients recorded by several thermocouples during the final test are given in Figure 37. Thermocouple 9-4 (Section I), which was located in the damaged zone, failed during the previous test. Thermocouple 9-2 (Section I), which was located in the same instrumentation platelet as TC 9-4 but 90° circumferentially from the damaged area, gave no indication of plugging. The thermal transient indicated by thermocouple TC 8-2, which is in line with the damaged area, is similar to the transient analytically predicted for no cooling in a low heat flux (non-streaking) location. (See Section VI,D,2 for basis of selection of film coefficient multipliers of 1.5 and 0.77 used in analysis and shown in Figure 37.) Thermocouple 2-7, (Section III), located in the damaged area in the throat, was the first thermocouple to indicate the excursion. The transient recorded

CONVERGENT SECTION OF CHAMBER

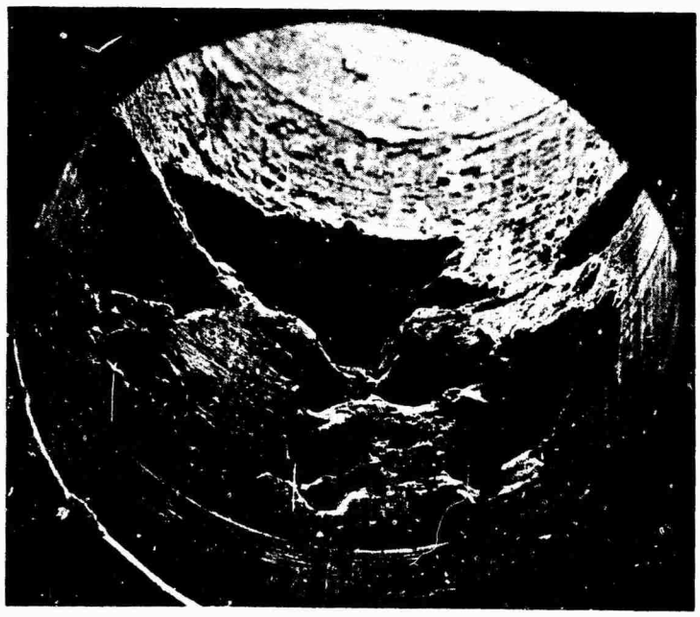

CYLINDRICAL SECTION ADJACENT TO INJECTOR

Figure 35. ClF_3-Cooled Chamber after Final Phase I Test

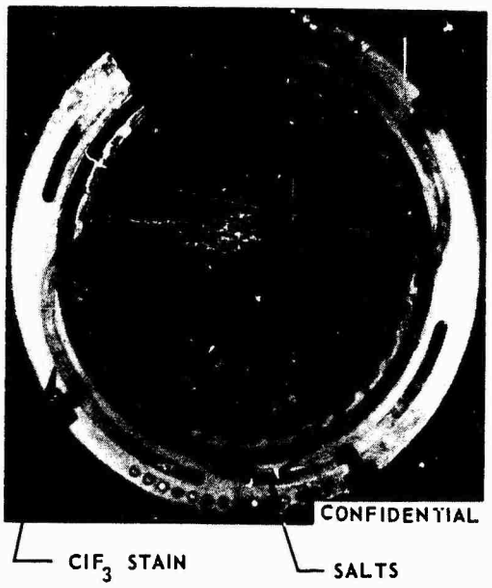

DISTRIBUTION PLATELET FROM STACK OF PLATELETS NEXT TO INJECTOR

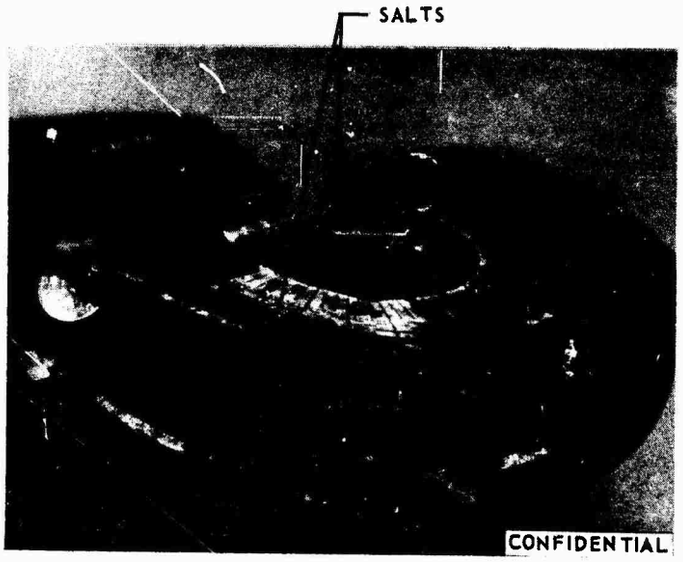

STACK OF PLATELETS SHOWING ALIGNMENT OF PLUGGED AREAS

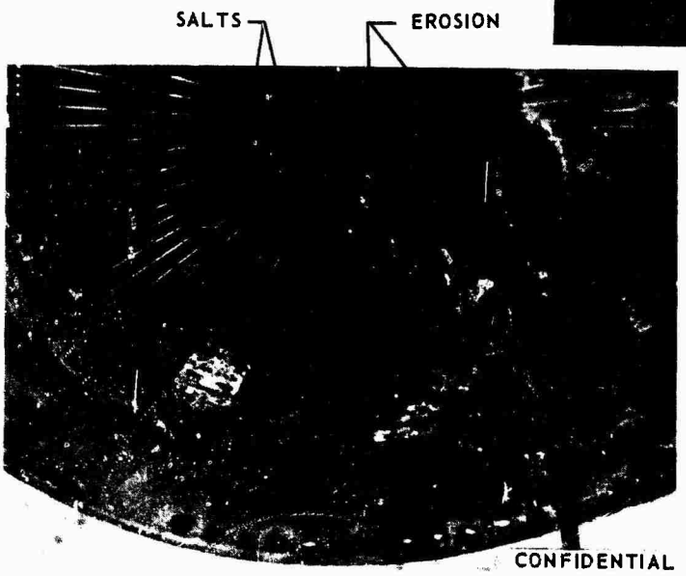

SALT DEPOSIT ON PLATELET FROM SECTION II

Figure 36. Platelets From Damaged ClF_3-Cooled Chamber Showing Plugging (u)

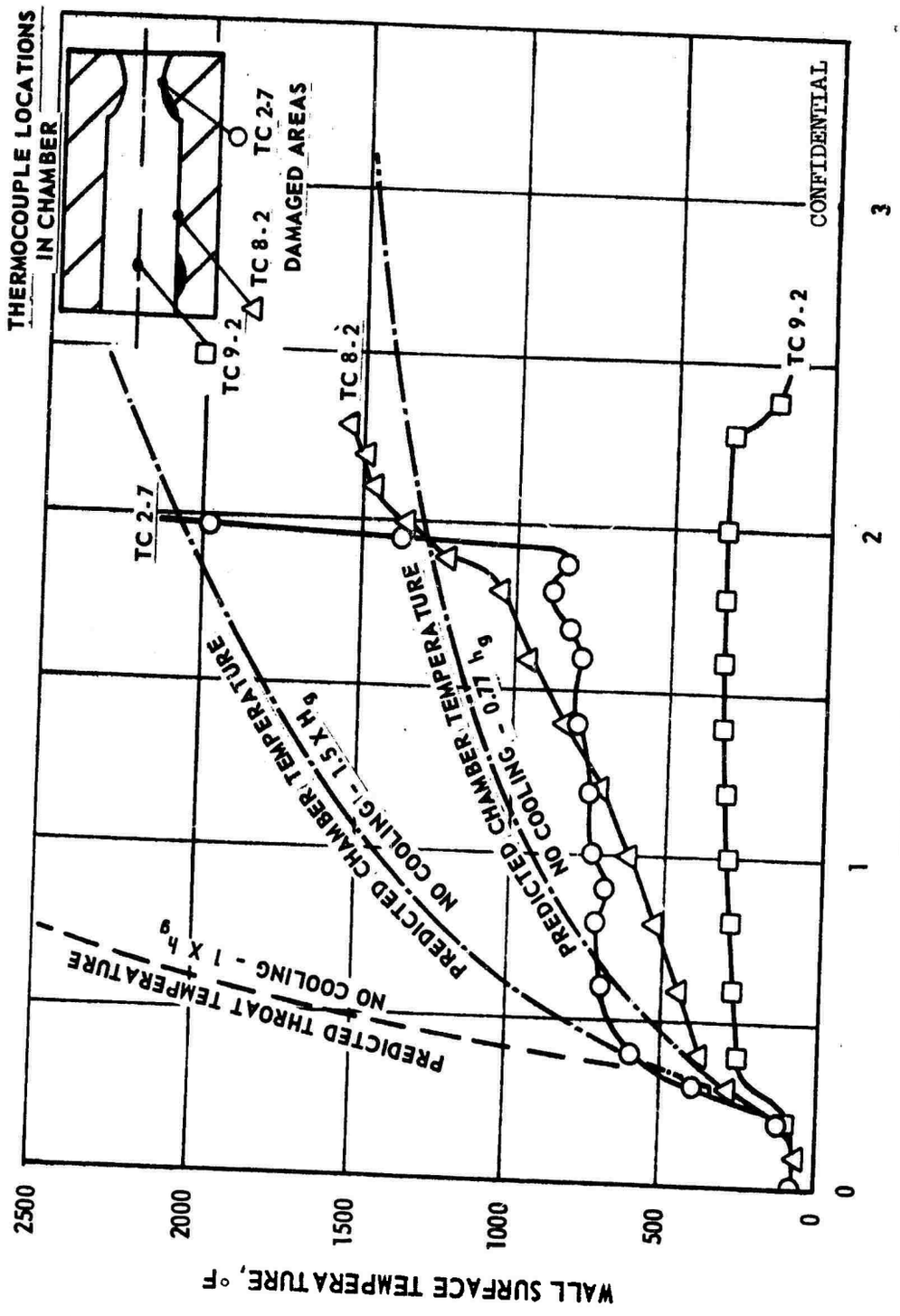

Figure 37. Temperature Transients for Final Phase I ClF_3-Cooled Chamber Test (u)

V, D, Cooled Chamber Test Firing (cont.)

on this thermocouple is not indicative of plugging: the thermocouple indicates steady state operation for 1.5 sec after the throat would be predicted to fail with no coolant flow; the excursion is at a rate of 10000°F/sec, which approaches the response time of the thermocouple and is far more rapid than would be predicted for no coolant flow. The response suggests ignition of the platelet with ClF_3 resulting from impingement of reacting metal.

(U) These data, the visual evidence of local plugging where water stood in the chamber, and the composition of the salt all indicate that the salt was formed after Test 1K-3D-114 when water stood in the chamber. Flushing failed to remove this salt which obstructed the flow of coolant into local areas. Failure of the wall apparently occurred first in the chamber section; throat region damage was initiated by reacting metal that was carried to it from the chamber region.

(U) Two very significant conclusions which could be drawn at the completion of Phase I testing with regard to the operational aspects of the TRANSPIRE concept with ClF_3 were:

(U) 1. Intricate passage geometries can be passivated successfully for ClF_3 service.

(C) 2. Passivated nickel sheet stock does not ignite with ClF_3 at temperatures up to approximately 1700°F.

(U) The final ClF_3 100 lb thrust and 1000 lb thrust test conditions are summarized in Table 12.

(C) TABLE 12

PHASE I ClF_3-COOLED CHAMBER FINAL TEST CONDITIONS (U)

	100 psia				1000 psia			
	$\dot{w}_c$	$\dot{w}_N$			$\dot{w}_c$	$\dot{w}_N$		
Chamber Section	Coolant Flow Rate (lb/sec)	Nominal Coolant Flow Rate (lb/sec)	$\frac{\dot{w}_c}{\dot{w}_N}$	Maximum Steady State Temperature (°F)	Coolant Flow Rate (lb/sec)	Nominal Coolant Flow Rate (lb/sec)	$\frac{\dot{w}_c}{\dot{w}_N}$	Maximum Steady State Temperature (°F)
I	0.077	0.057	1.35	1136	0.922	0.480	1.92	310
II	0.032	0.055	0.58	954	0.841	0.466	1.81	600
III	0.047	0.0125	3.76	655	0.341	0.105	3.25	795
IV	0.015	0.0081	1.85	1003	0.0781	0.0682	1.15	943
TOTAL	0.171	0.1329	1.29	-	2.18	1.1192	1.95	-

V, D, Cooled Chamber Test Firing (cont.)

2. Phase II

(U) The first two tests with the Phase II ClF_3-cooled chamber were run with the venturis in the injector fuel and oxidizer circuits inadvertently reversed. Operation of the cooled chamber at the highly fuel rich conditions that resulted (injector mixture ratio of 0.83), produced some heat marks near the injector where the fuel from the eight unlike doublet elements impinged on the wall. The chamber was not damaged.

(U) Ten cooled chamber tests were made with the venturis properly installed in the injector propellant feed circuits. The coolant flow rates to chamber Sections II and III were reduced twice. The total duration on the chamber was 21.88 sec, and the longest single firing duration was 8.86 sec. All tests were made at approximately 1000 lb thrust and 1000 psia chamber pressure. The cooled chamber operating conditions are summarized in Table 13.

(C) Test 1K-5B-109 was aborted by the automatic trip circuit when thermocouple TC 7-1 reached 1517°F. The trip was set at 1500°F. The trip was reset to 1650°F and Test 1K-5B-110 was made. Thermocouple TC 7-1 read approximately 1500°F during this test. Approximately seven seconds into the test thermocouple TC 7-1 failed; the erratic behavior of this thermocouple subsequently, aborted the test.

(U) The chamber pressure (P_c) tap plugged during Test 1K-5B-109. The injector was removed from the chamber after Test 1K-5B-110 to permit the pressure tap to be unplugged. Figure 38 shows the condition of chamber after this test. There were four small heat marks 90° apart on the chamber wall next to the injector at the location of the four O-F-O folded triplet elements. The other small areas of discoloration on the chamber

(C) TABLE 13

SUMMARY OF PHASE II COOLED CHAMBER TEST CONDITIONS (U)

Test No.	Duration (sec)	Flow Ratio (Coolant Flow Rate/ Nominal Flow Rate) Sect I	Sect II	Sect III	Comments
1K-5B-101	0.42	2.6	2.0	2.4	Injector fuel and oxidizer venturis reversed. Injector O/F = 0.83, TCA O/F - 1.8.
-102	0.75	2.6	2.0	2.4	
-103	0.46	2.6	2.0	2.4	Injector venturis corrected.
-104	0.75	2.6	2.0	2.4	Tests 105 and 106 were shut
-105	0.79 Abort	2.6	2.0	2.4	down by the high temperature
-106	2.43 Abort	2.6	2.0	2.4	trip circuit (TC 7-1). Trip setting was 1000°F.
-107	0.44	2.4	1.5	2.2	Tests 109 and 110 were shut
-108	1.38	2.4	1.5	2.2	down by the high temperature
-109	4.11 Abort	2.4	1.5	2.2	trip circuit (TC 7-1). Trip
-110	8.86 Abort	2.4	1.5	2.2	was set at 1500°F for Test 109. The abort of Test 110 was caused by failure of TC 7-1. The P_c tap plugged during Tests 109 and 110.
-111	0.45	2.5	1.3	1.6	Nozzle eroded on Test 112.
-112	1.04	2.5	1.3	1.6	Temperatures in throat and upstream of throat were all less than 1000°F.

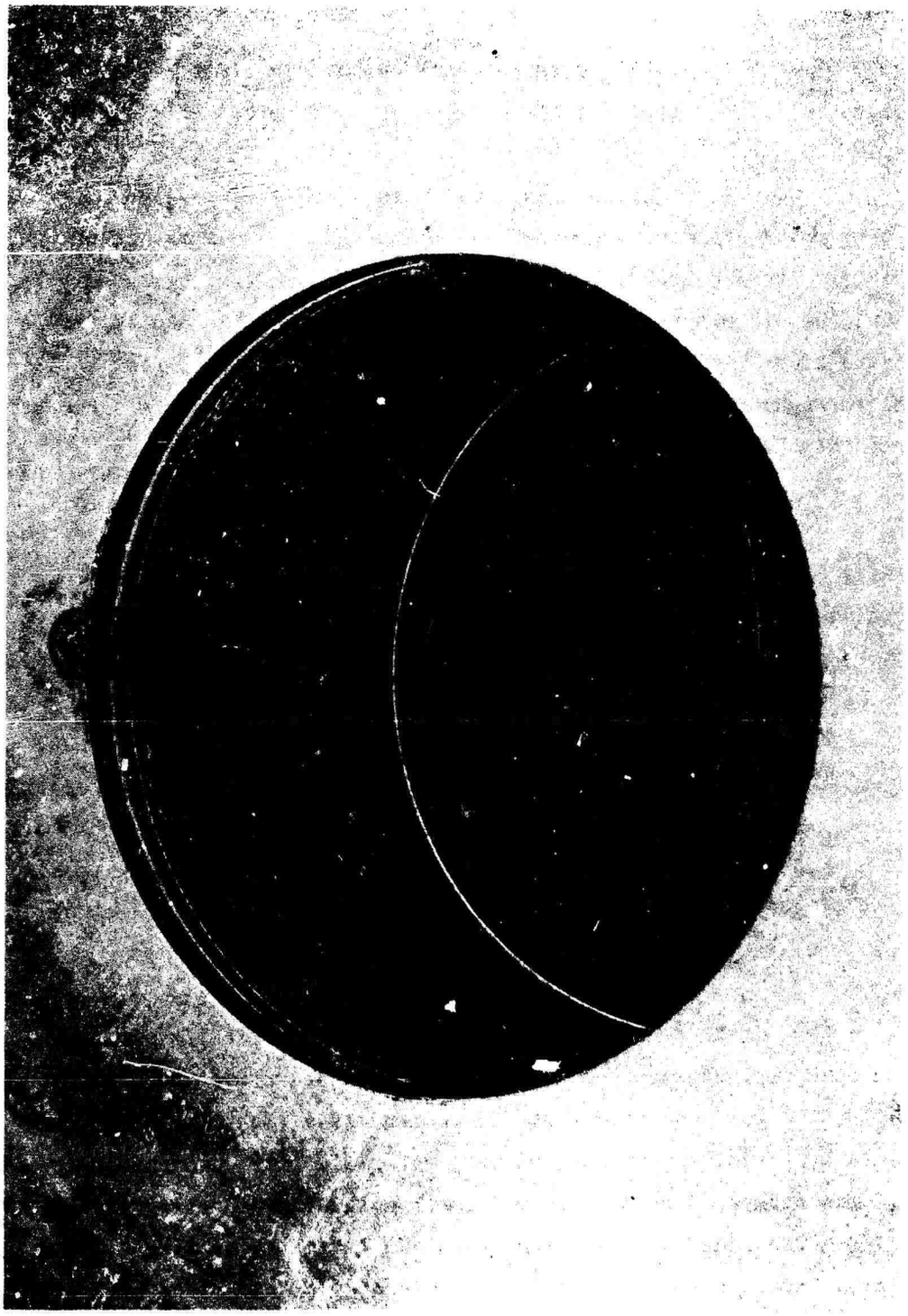

Figure 38. Phase II Cooled Chamber after Test 1K-5B-110

V, D, Cooled Chamber Test Firing (cont.)

surface, seen in Figure 38, were produced during the first two tests. Except for these conditions the rest of the chamber is in excellent condition.

(U) Testing was terminated because of erosion of the divergent section of the nozzle during Test 1K-5B-112. The damage is shown in Figure 39. Erosion occurred on about half of the surface of the divergent section, but did not include the throat. The rest of the chamber is in excellent condition. All pressures, temperatures and propellant flow rates were normal throughout the test. The failure was detected by visual inspection of the chamber after the test.

(U) The aft end of the chamber housing was removed by machining so that the damaged section could be removed for inspection without disturbing the undamaged convergent and cylindrical platelet sections. The inlets to the platelets in the damaged section were examined for plugging; the results were negative. No evidence of blockage in the primary or secondary metering grooves was found. About one-third of the damaged section was disassembled platelet-by-platelet. There was neither evidence of salting or plugging in the thermal diffusion zones nor visual evidence of coolant leakage to the outside of the chamber housing. Also the plenum pressure readings in Sections II and III were normal, indicating that there was no leakage of coolant from Section III to Section II.

(U) The time required to fill the platelets in the divergent section with coolant was re-evaluated using the start transient data from Test 1K-5B-112. It was concluded that the coolant lead time was inadequate; the platelets in the divergent section were not filled with coolant at the initiation of the firing. The erosion was the result of overheating the uncooled platelets. Two factors caused the actual fill time to be greater than that calculated before the test, namely, the presence of nitrogen purge gas in the coolant manifolding and depth of etch in the thermal diffusion zone 20% greater than nominal.

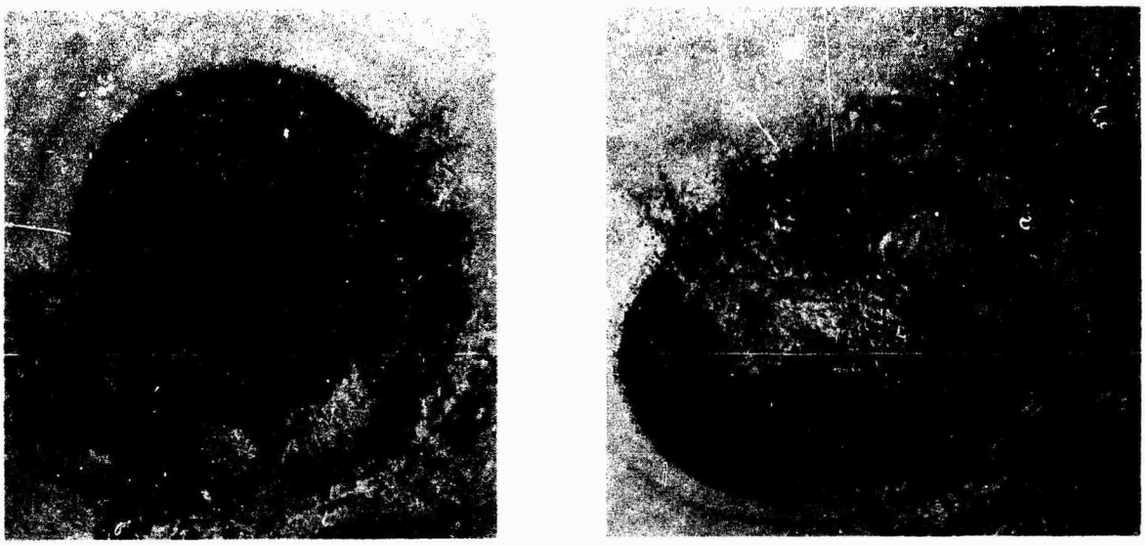

DIVERGENT SECTION OF COOLED COMBUSTION CHAMBER.
THE DARK RING IS INSTRUMENTATION PLATELET
NO. 1 LOCATED AT THE CHAMBER THROAT

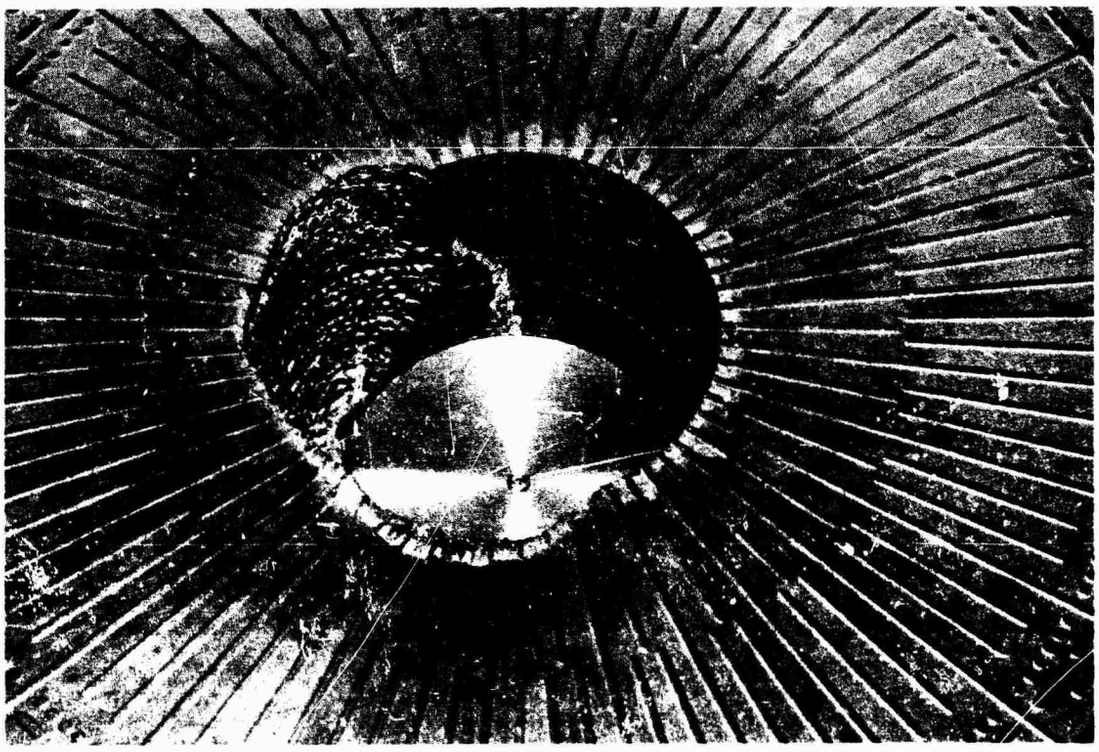

DISTRIBUTION PLATELET FROM DIVERGENT SECTION OF COOLED
COMBUSTION CHAMBER

Figure 39. Phase II Cooled Chamber Erosion

V, D, Cooled Chamber Test Firing (cont.)

(U) Nitrogen gas used in the prefire purge filled the coolant manifolding to a pressure of approximately 100 psia. This gas is trapped by the coolant and is vented through the platelets. Since Section III is comprised of low and high resistance platelets, the pressurization provided by this gas during coolant fill causes coolant to flow out of the platelets with low hydraulic resistance, thus increasing the time required to completely fill the plenum of Section III. The platelets in the divergent section have the highest hydraulic resistance, and have one inlet at the top and one inlet at the bottom of the horizontally-mounted chamber, and thus do not flow with coolant at both inlets until the trapped gas is bled off. The prefire fill time analysis assumed no gas presence in the manifold.

(U) The platelet fill time also depends on the volume of the platelet flow areas. The depths of etch of six throat section platelets, three of which were taken from the divergent section, were measured. The depths of etch in the thermal diffusion zone of these platelets ranged from 0.0024 in. to 0.0032 in. The depth of etch of the three platelets in the divergent section was 0.0027 in. or greater. The prefire fill time calculations were based on a nominal 0.0025 in. depth of etch.

(U) Another factor which prevents the platelets from being filled with coolant at ignition is flashing of the coolant. The normal boiling point of ClF_3 at atmospheric pressure is 53°F. The ClF_3 coolant enters the chamber at temperatures in excess of 53°F as the result of heat transfer from the tank and lines under pressure. During the fill time preceding ignition the back pressure is atmospheric pressure and the coolant flashes as it leaves the secondary metering grooves, that is the superheat in the liquid converts a small fraction of the coolant to vapor. Because the density of the vapor is small compared to that of the liquid a few degrees of superheat can produce a vapor volume fraction in excess of 90%. All thermocouples in the chamber indicate a drop in temperature from ambient to approximately 53°F during the fill time.

V, D, Cooled Chamber Test Firing (cont.)

(U) Flashing of the coolant in the thermal influence zone results in that area not being filled with liquid ClF_3 at ignition. During startup the increase in chamber pressure collapses the vapor; before the platelet can be cooled the volume formerly occupied by the vapor must be filled with liquid ClF_3. Since the platelets in the nozzle have the largest volume, the greatest hydraulic resistance and the highest heat fluxes they are particularly susceptible to this startup problem.

(U) Another factor that probably contributed to erosion of the nozzle of the Phase II chamber is attachment of the exhaust plume to the aft end of the chamber. The platelets terminate at a 1.6:1 area ratio. However, discoloration and erosion of the aft retainer used with the ClF_3/MHF-3 ablative lined chamber during 1000 psia testing and discoloration of the aft retainer during 1000 psia N_2O_4-cooled chamber testing, indicate that attachment of the plume to the aft end of the chamber is occurring. Experimental pressure data and Schlieren photographs, as discussed in Reference 3, suggest that the boundary layer remains attached to the rear face of an object in supersonic flow. Applied to the TRANSPIRE chambers this means that the aft end of the cooled chamber and the last platelet in the chamber are heated not only on the surface normal to flow, but on the aft surface as well. A heat flux that is 1/8 that in the throat acting over 1/4 in. of the aft surface introduces additional heat in the last platelet sufficient to exceed the heat capacity of the coolant flowing across that platelet.

(U) Summarizing the above discussion, it appears that erosion of the Phase II chamber nozzle resulted from inadequate cooling. The cooling was inadequate because of a marginal fill time coupled with flashing of some of the coolant in the platelets and because of an additional heat load due to heating the aft end by attachment of the exhaust plume.

V, D, Cooled Chamber Test Firing (cont.)

(U) The final test conditions for the Phase II chamber are summarized in Table 14. The temperature and flow conditions for both Test 1K-5B-110 and -112 are shown since Test 1K-5B-112 was not of sufficient duration for thermocouples other than those in the throat to reach their steady-state value.

CONFIDENTIAL

(C) TABLE 14

PHASE II ClF_3-COOLED CHAMBER FINAL TEST CONDITIONS (U)

	Test 1K-5B-110				Test 1K-5B-112		
Chamber Section	$\dot{w}_N$ Nominal Coolant Flow Rate (lb/sec)	$\dot{w}_c$ Coolant Flow Rate (lb/sec)	$\frac{\dot{w}_c}{\dot{w}_N}$	Maximum Steady State Temperature °F	$\dot{w}_c$ Coolant Flow Rate (lb/sec)	$\frac{\dot{w}_c}{\dot{w}_N}$	Maximum Steady State Temperature °F
I	0.216	0.519	2.4	1550	0.545	2.52	1500(1)
II	0.466	0.702	1.5	961	0.587	1.26	(2)
III	0.173	0.377	2.2	656	0.275	1.59	925
TOTALS	0.855	1.598	1.87		1.407	1.65	

(1) The thermocouple, TC 7-1, that recorded the highest temperature in Section I during Test 1K-5B-110 failed during that test. Since the coolant flow rate is virtually unchanged from Test -110 the temperature is inferred from the data from that test.

(2) Steady state was not achieved. Thermocouple TC 3-2 that read 961°F on Test 1K-5B-110 had reached 880°F at shutdown on Test 1K-5B-112.

VI. RESULTS

A. INJECTOR CHECKOUT

(U) The injectors used in the cooled chamber tests were initially fired with uncooled chambers to obtain baseline injector performance values. A summary of these performance values for the injectors used for cooled chamber testing is tabulated on Table 15. The testing and test conditions are described in Section V,B.

(C) In order to insure that the thermal environment was hot enough to adequately test the cooling concept a goal of the program was an injector combustion efficiency of 94% C*. As can be seen in Table 15, both N_2O_4/AeroZINE 50 injectors (S/N -2 and -3) met this goal; the performance of the 1000 lb thrust ClF_3/MHF-3 injectors used for cooled chamber testing (S/N-4 and 09) was within 1% of the desired C* goal. Only the 100 lb thrust ClF_3/MHF-3 injector (S/N -5) deviated in performance substantially from the desired goal.

(U) The N_2O_4/AeroZINE 50 and ClF_3/MHF-3 injectors were tested with ablative lined combustion chambers (see Section IV,B). The internal contour of these uncooled chambers was identical to the transpiration-cooled configurations.

(U) Except for Injector S/N -5, the theoretical C* values for the injectors were high, as indicated by Table 15. However, C* values calculated from test data are valuable only for comparing consistency on a particular configuration and not as a real measure of injector performance. This is because measured P_c is not representative of combustion P_c, and the large effect of boundary layer buildup in the throat for small nozzles is not accounted for. Also, C* cannot be used with independently calculated C_f values for calculating specific impulse without introducing considerable error due to chamber/nozzle interactions.[4]

(C) TABLE 15

INJECTOR TEST PERFORMANCE SUMMARY (U)

Propellant	Chamber L*	Injector Type	Injector S/N	Nominal Thrust (lb)	No. of Tests	Mean % Theoretical C*	Mean % Theoretical I_{sp}	Injector Energy Release Efficiency η_{ER}
N_2O_4/A-50	32	6 Element	2	100	4	95.6	95.6	98.4
	32	21 Element	3	1000	6	99.4	94.0	95.5
ClF_3/MHF-3	32	6 Element	5	100	4	86.6	81.4	84.2
	32	21 Element	4	1000	4	93.2	85.6	88.2
ClF_3/MHF-3	25	21 Element	4	1000	1	94.2	87.2	89.8
	25	49 Element	9	1000	3	93.6	85.9	88.4

VI, A, Injector Checkout (cont.)

(U) A more valid measure of injector performance is through the use of the parameter defined as energy release efficiency, (η_{ER}), also shown in Table 15. This parameter is derived by utilization of the Interaction Theory Loss Analysis performance model developed by Aerojet, and reported in Ref. (4). This method consists of calculating all significant I_{sp} losses except the energy release loss, and subtracting these losses from the ideal one-dimensional shifting equilibrium I_{sp} to define a maximum I_{sp} availability. The difference between this maximum I_{sp} availability and the test I_{sp} is defined as the energy release loss. One minus the ratio of the energy release loss to the theoretical I_{sp} is the energy release efficiency, η_{ER}. This energy release efficiency is then corrected to a 1:1 nozzle area ratio to establish the combustion efficiency without chamber/nozzle interaction. Table 16 lists the significant losses for both the N_2O_4/AeroZINE 50 and ClF_3/MHF-3 injector checkout tests.

(C) The energy release efficiencies (η_{ER}), of 98.4% and 95.5% for the N_2O_4/AeroZINE-50 100 lb thrust and 1000 lb thrust tests, respectively, are considered very good for a combustion chamber of this small size. For a small chamber, η_{ER} is expected to be lower than for a larger size engine because of element proximity to the wall. The small chamber has a greater percentage of elements in proximity to the chamber wall, resulting in less interaction with propellants from other elements. The low η_{ER} values for the ClF_3/MHF-3 tests appear to be somewhat characteristic of this propellant combination.

(U) A summary of performance parameters for the N_2O_4/AeroZINE 50 test series, 1K-3-101 through 110, is shown in Table 17. As the first step in the analysis the data were evaluated just prior to shutdown using the postfire nozzle throat area in the calculations. Exit areas were measured at the conclusion of all testing, and an estimate of the area for each test was made.

(C) TABLE 16

PERFORMANCE LOSS SUMMARY FOR UNCOOLED CHAMBER INJECTOR TESTS (U)

Propellants	N_2O_4/A-50[2] (O/F=1.6)		ClF_3/MHF-3 (O/F=2.4)		ClF_3/MHF-3 (O/F=2.6)	
Injector	6-Element S/N-2	21-Element S/N-3	6-Element S/N-5	21-Element S/N-4	Vortex S/N-8	49-Element S/N-9
Nominal Thrust Level (lb_f)	100	1000	100	1000	1000	1000
Area Ratio of Nozzle	1.6	1.6	1.6	1.6	1.6	1.6
Chamber L* (in.)	32 L*	32 L*	32 L*	32 L*	25 L*	25 L*
Nozzle Losses (sec)						
Friction	1.7	1.5	1.7	1.5	1.5	1.5
Geometry	4.7	4.5	4.0	4.2	4.2	4.2
Kinetic	0.5	0.0	0.4	0.0	0.0	0.0
Chamber/Injector Losses (sec)						
Heat Transfer	0.0	0.0	1.0	0.8	0.7	0.7
Σ Calculated Losses (sec)	6.9	6.0	7.1	6.5	6.4	6.4
I_{sp} Theoretical (sec)	249.5	253.3	248.5	253.0	252.0	253.0
I_{sp} Maximum Availability (sec)	242.6	247.3	241.4	246.5	245.6	246.6
I_{sp} Actual[1] (sec)	238.6	235.9	202.0	216.5	170.0	217.2
Energy Release Loss (sec)	4.0	11.4	39.4	30.0	75.6	29.4
Energy Release Efficiency (η_{ER})%	98.4%	95.5%	84.2%	88.2%	70.0	88.4
% Theoretical I_{sp}	95.6%	94.0%	81.4%	85.6	67.4	85.9

(1) Based on calibrated venturi flow data
(2) A-50 abbreviation used for AeroZINE 50

(C) TABLE 17

N_2O_4/AeroZINE 50 INJECTOR PERFORMANCE (U)

Test No.	P_c, psia		O/F		% I_{sp} (theo)		% C* (theo)		Inj S/N
	1*	2	1	2	1	2	1	2	
1K-3A-101	--	101	--	1.48	--	93.3	--	95.0	2
102	--	103.5	--	1.50	--	96.5	--	96.0	2
103	104.5	104.4	1.72	1.62	96.4	95.7	99.9	95.8	2
104	105	105.7	1.48	1.37	96.5	95.7	99.8	95.5	2
1K-3A-105	992	986	1.66	1.66	93.5	92.2	102.5	101.0	3
106	974	870	1.67	1.67	93.6	96.5	101.5	100.0	3
107	1028	909	1.76	1.76	92.8	95.7	102.2	99.0	3
108	896	815	1.55	1.55	92.7	97.8	99.5	99.0	3
109	923	835	1.68	1.67	92.4	95.6	101.6	100.0	3
110	823	750	1.58	1.58	92.1	98.0	100.0	98.5	3

*1 Initial steady-state data, throat area based on prefire measurements

2 Final steady-state data, throat area based on postfire measurements

VI, A, Injector Checkout (cont.)

The results of this analysis, based on the test data just prior to shutdown and postfire measurements, yielded percent theoretical I_{sp} and C* performance values that were unrealistically high for some of the high P_c tests, as shown in Table 17.

(U) To determine the reason for the apparent performance discrepancy, the ablation effects on the throat and exit areas were examined. It was noted that for the high P_c tests, with N_2O_4/AeroZINE 50, a nozzle extension was formed by the silica during the test, as shown in Figure 40. The silica emanated from the ablative liner material during firing. It was not known whether the silica had solidified during or after the test. Formation before termination of the test would affect performance due to an exit area increase. Tests 109 and 110 were analyzed by the following method to determine the effect of throat ablation and of the silica extension.

(U) First, a plot of thrust versus P_c was made, as shown in Figure 41. From this plot it was assumed that neither the throat area nor the exit area changed (no ablation) until F versus P_c began to deviate from a linear relationship. This assumption is apparent for a constant mixture ratio from the relation:

$$F = C_F A_t P_c$$

$$(C_F = \text{constant})$$

The practical point selected for the beginning of throat area change was at the maximum P_c point in the "loop" shown in Figure 41. Performance was calculated at this point using the prefire throat and exit area values. Performance at this point was 6% lower in % theoretical I_{sp} than the

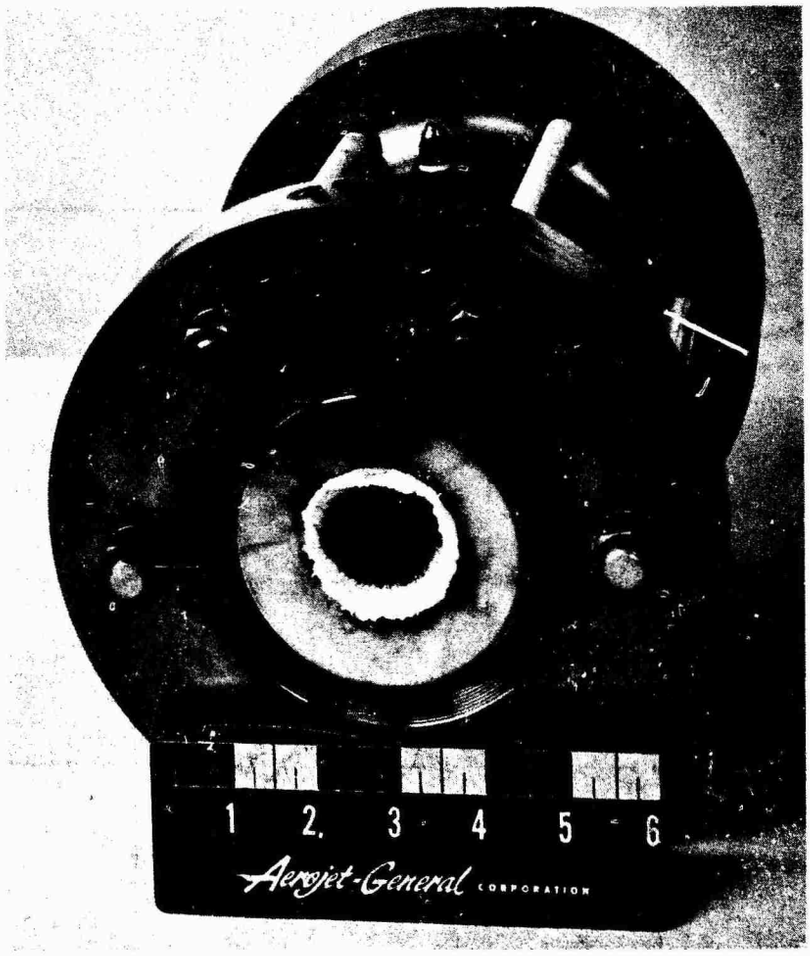

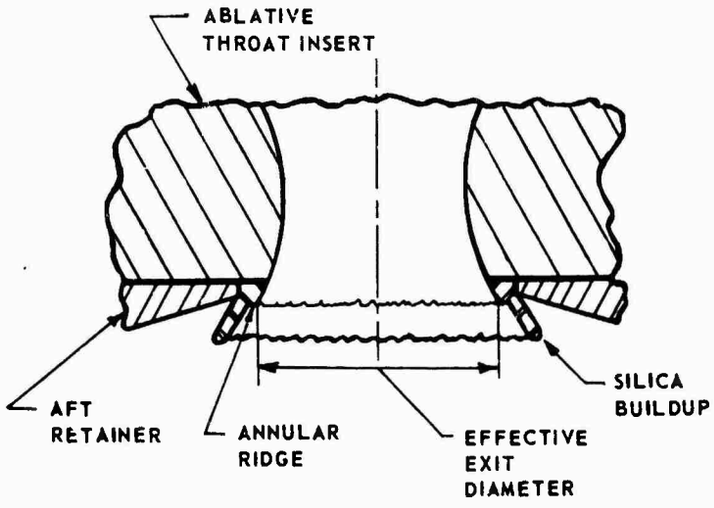

Figure 40. Ablative Chamber after Final 1000 psia N_2O_4 Injector Checkout Test

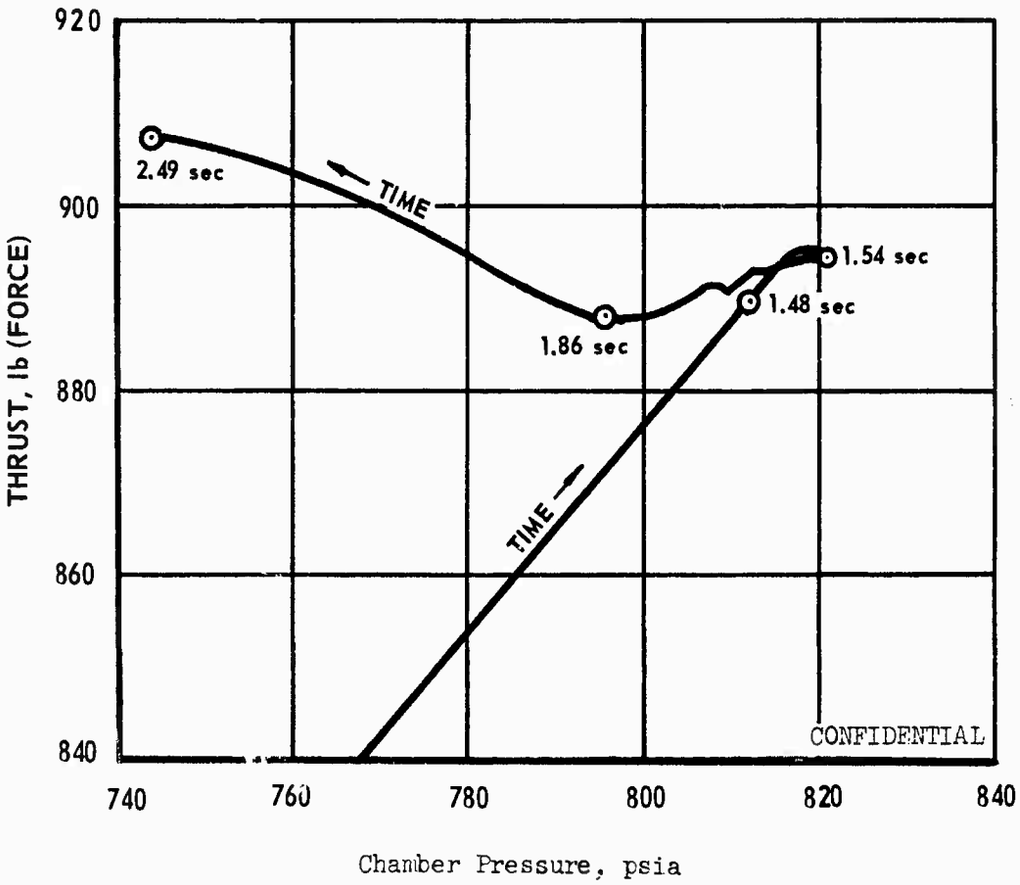

Figure 41. Thrust vs Chamber Pressure, Final 1000 psia N_2O_4 Injector Checkout Test (u)

VI, A, Injector Checkout (cont.)

performance calculated from the data taken prior to shutdown and from postfire throat and exit area evaluations. Since the mixture ratio and flow rate remained constant, the performance should not vary after initial heat-up, unless the silica build-up was acting as a nozzle extension.

(U) It was desirable to confirm the throat area (A_t) during the test, as it was questionable whether postfire A_t represented actual A_t during the test due to thermal expansion effects. C* was calculated at the maximum P_c point (see Figure 41) and the throat area ablation rate was determined for the remainder of the test by holding C* constant and calculating A_t from:

$$A_t = \frac{\dot{w}_t \, C^*}{P_c g} \qquad (1)$$

The throat area ablation rate thus determined is shown in Figure 42. As indicated, the final calculated throat area is within 0.008 $in.^2$ of the postfire measured value. For test No. 1K-3C-109, it was within 0.003 $in.^2$ of the postfire measured value. Using the ablation rate above for the A_t, performance was plotted as shown in Figure 43. It is obvious from the figure, curve No. 2, that including the A_t ablation alone does not correct the apparent performance change. Therefore, the exit area change associated with the crystalline silica buildup previously mentioned was examined. It was found that if the exit area increase due to the silica buildup was considered in conjunction with the A_t ablation rate, the apparent performance increase with time disappears, and % I_{sp} is maintained nearly constant throughout the steady-state tests, as shown by curve No. 3 in Figure 43.

(U) The final exit area for this evaluation was assumed to be that indicated by Figure 40. As shown in the figure, an annular ridge is formed on the inside surface of the silica, where support for the molten silica was

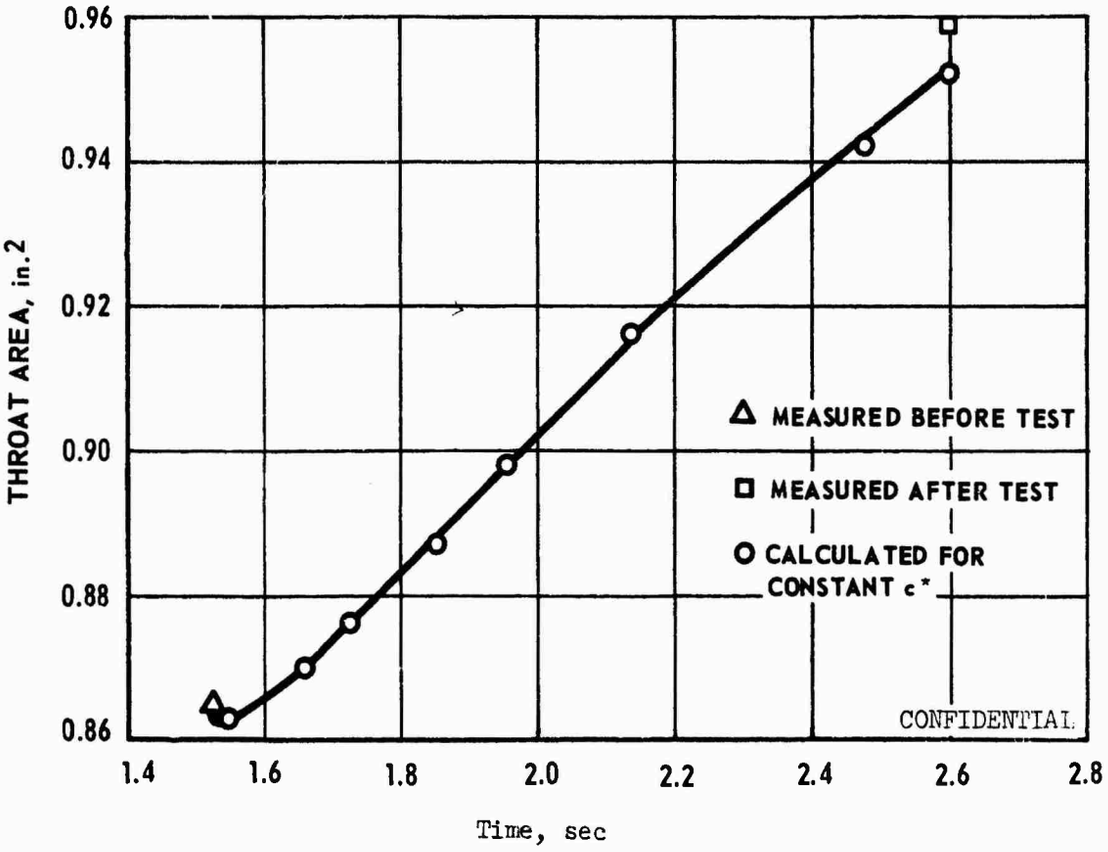

Figure 42. Calculated Throat Area History, Final 1000 psia N_2O_4 Injector Checkout Test (u)

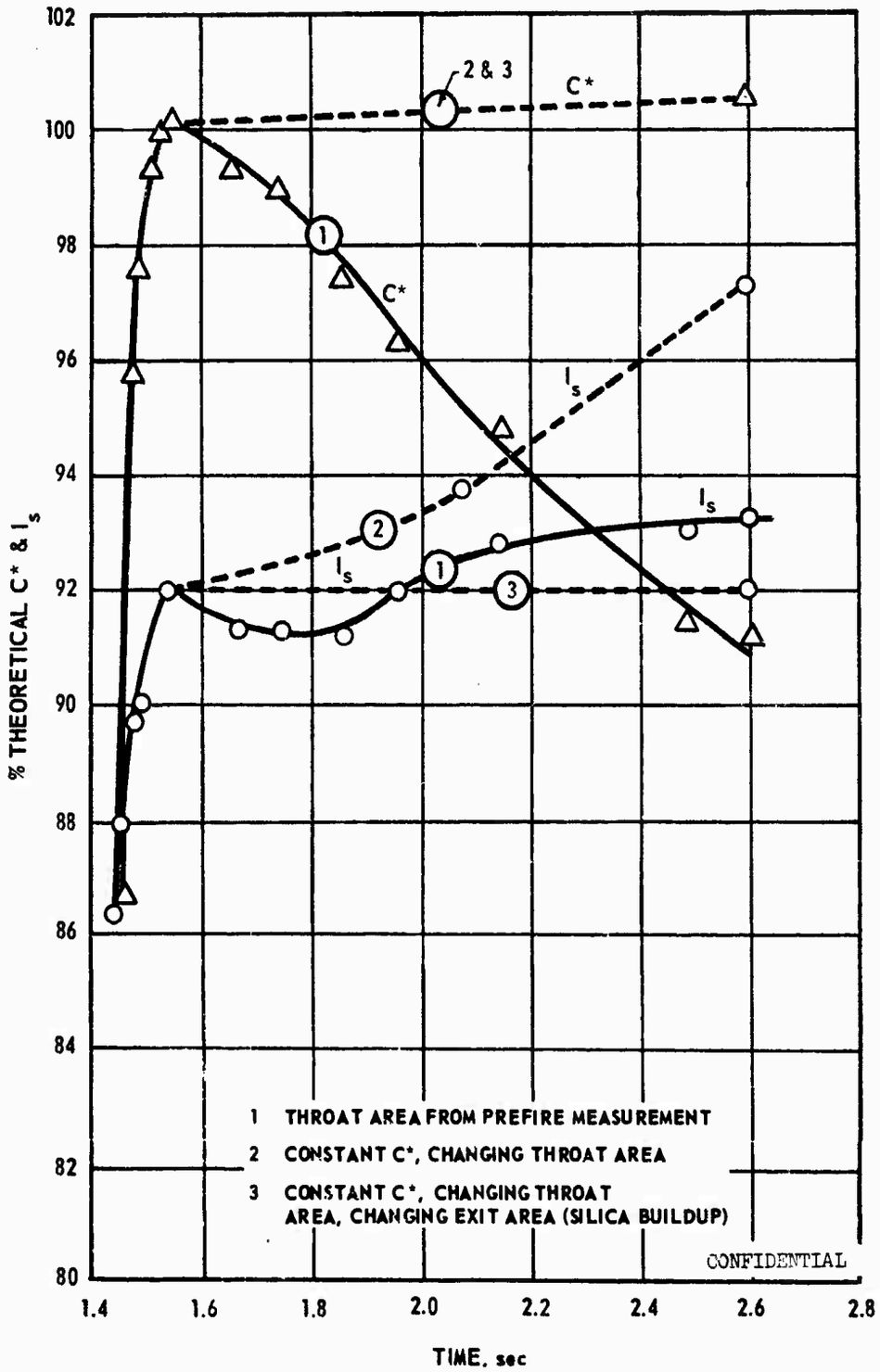

Figure 43. Performance History, Final 1000 psia N_2O_4 Injector Checkout Test (u)

(C) TABLE 18

ClF_3/MHF-3 INJECTOR PERFORMANCE (U)

Test No.	Chamber L* (in.)	Injector Type	Injector S/N	Vacuum Thrust (lbf)	Mixture Ratio O/F	Vacuum I_{sp}, % theo.	C* % Theo.
1K-3B-101	32	6 Elem	1	71.1	(1)	(1)	(1)
102	32	6 Elem	1	95.8	2.38	81.3	83.8
103	32	6 Elem	1	97.4	2.21	83.0	84.0
104	32	6 Elem	1	95.4	2.58	80.5	82.3
105	32	21 Elem	4	953.4	2.55	85.0	90.0(2)
106	32	21 Elem	4	976.4	2.52	86.0	93.1
107	32	21 Elem	4	974.4	2.775	85.4	93.3
108	32	21 Elem	4	890.4	2.39	86.1	96.4(3)
109	32	6 Elem	5	97.9	2.48	81.0	82.5
110	32	6 Elem	5	99.5	2.50	82.3	83.7
111	32	6 Elem	5	94.9	2.64	79.6	81.4
112	32	6 Elem	5	98.9	2.24	83.3	85.1
1K-5A-101	25	Vortex	8	739.4	2.56	63.8	69.1
102	25	Vortex	8	688.9	2.59	63.2	71.4
103	25	Vortex	8	774.4	2.59	67.3	77.5
104	25	Vortex	8	770.4	2.59	70.0	81.8
105	25	21 Elem	4	1018.4	2.57	87.2	94.2
106	25	49 Elem	9	968.4(4)	2.56(4)	83.7(4)	93.9(4)
107	25	49 Elem	9	998.4	2.57	85.9	93.0
108	25	49 Elem	9	1043.3	2.20	85.9	93.8

(1) Steady state was not reached.
(2) Large change in throat area makes C* value suspect.
(3) Test results difficult to interpret because of loss of coating in throat - see text.
(4) No millisadic data, results based on oscillograph data.

VI, A, Injector Checkout (cont.)

provided by the steel retainer ring. It was assumed that thrust was supported to the aft end of this annular ridge; beyond that point the silica was probably molten and was not capable of supporting any thrust. From the above evaluation, it was established that the most representative data point for performance evaluation of the high P_c tests was early in the test at maximum P_c, after initial heatup, and using prefire nozzle areas for the calculations. The results of perfcrmance thus calculated are summarized in Table 17 in the columns designated by the number 1.

(U) The ablative lined chambers used for ClF_3/MHF-3 injector checkout tests did not produce a nozzle extension buildup as was noted for the N_2O_4/AeroZINE 50 uncooled chamber. However, a resinous deposit formed in the throat during the Phase I 1000 lb thrust tests. Throat areas were smaller at the end of each of the first three 1000 lb thrust tests than at the beginning. This trend was offset by the loss of segments of the coating on the last Phase I 1000 lb thrust test (1K-3B-108); the throat area at the end of this test was larger than at the beginning of the test. Figure 44 shows the ClF_3/MHF-3 ablative chamber after Test 1K-3B-108. The coating and areas where segments of the coating have broken off can be seen.

(U) The throat section of the ablative lined 25 L* combustion chamber that was used for Phase II ClF_3/MHF-3 injector checkout testing had a ZTA graphite insert. There was no deposition of resinous material on this throat and virtually no change in throat diameter after testing.

(U) The performance calculations based on data taken near the end of each test and on throat areas calculated from throat diameter measurements made after each test are shown in Table 18. The first test at 100 lb thrust (1K-3B-101) did not achieve steady state. The first and last 1000 lb thrust Phase I test results are difficult to interpret because of change in the throat area that occurred during the tests.

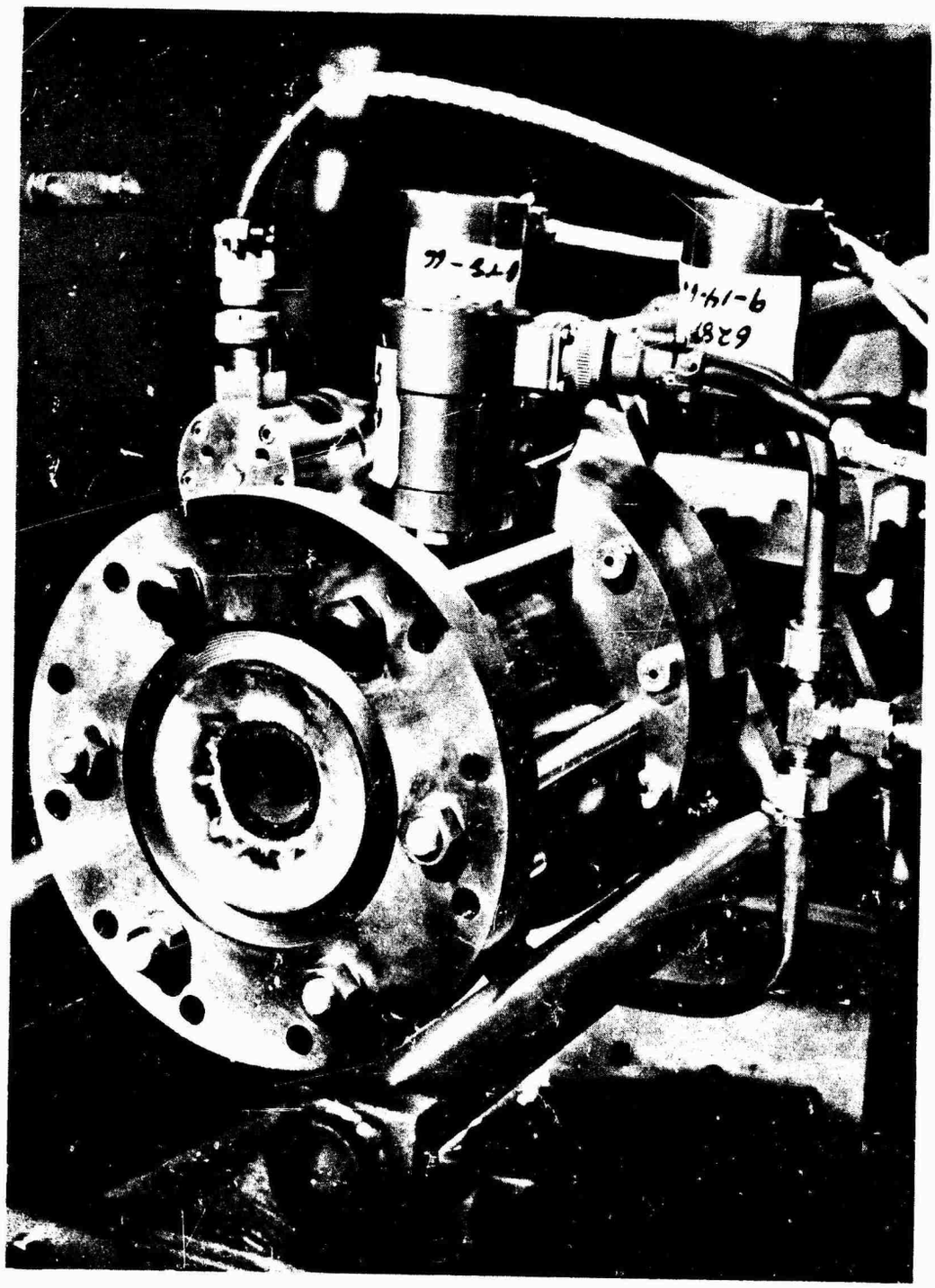

Figure 44. ClF_3/MHF-3 Ablative Chamber after Phase I Testing

VI, A, Injector Checkout (cont.)

(U) Four tests were made with the vortex injector. The second test was a longer duration repeat of the first test. For the third and fourth test the axial and circumferential position of the fuel orifices (center spud) relative to the oxidizer orifices was changed as discussed in Section V,B,2 (Figure 30). Since performance did not improve substantially with these changes no further tests were made to optimize the injector dimensional parameters.

(U) Since the Phase I 1000 lb thrust ClF_3/MHF-3 injector (S/N-4) was used as backup injector in Phase II a single test firing was made with this injector and the 25 L* ablative lined chamber. The apparent 1.6% specific impulse increase accompanying the reduction in chamber length cannot be accounted for. There is no significance in the 1.6% since this is typical of the deviation in performance from test to test. However, it is significant that performance did not decrease with the shorter L* chamber. No discrepancy could be found in the data; however, droplet vaporization analysis indicated that a 7% decrease in performance would be expected at the lower L* (Test 1K-5A-105). One explanation for this anomalous behavior is to suspect this test result since it was obtained with a single test. However, the fact that a reduction in chamber L* did not decrease performance coupled with the fact that an improved injector design (49-element injector has more elements and better spray overlap) did not improve performance suggests that there is either an additional loss not being considered (for example, overexpansion due to attachment of the exhaust plume to the aft end of the chamber) or that the theoretical I_{sp} is not as high at these pressure levels as predicted.

(U) The 49-element 1000 lb thrust injector (S/N-9) was selected as the prime injector for cooled chamber testing on the basis of performance and compatibility with the oxidizer transpiration cooled chamber. Performance of this injctor with the 25 L* chamber was comparable to that obtained with the 21-element injector and the 32 L* chamber; erosion of the ablative liner

VI, A, Injector Checkout (cont.)

near the injector was much less. Good performance with the 49-element injector was expected because of the low thrust per element. Further improvement in performance with this pattern has been predicted for larger impingement angles on the basis of more efficient propellant atomization.

VI, Results (cont.)

B. COOLED CHAMBER FLOW TESTING

1. Phase I

(U) Coolant flow-pressure drop measurements were made for both the N_2O_4-cooled chamber and the ClF_3-cooled Phase I chamber in flow tests and during firings. The purpose of obtaining these data was to determine if the stacked platelet assemblies were actually providing the coolant flow control they were designed to give and also to see if there was any evidence of plugging occurring during the testing.

(U) The flow testing of the two chambers was done prior to the test firings. The N_2O_4-cooled chamber was flowed with N_2O_4 on the test stand while the ClF_3-cooled chamber was flowed with trichlorethylene in the Engineering R&D Laboratory because of the health hazard posed by the ClF_3 (see Sections V,C).

(C) The results of the flow tests and test firings are given in Figures 45 (N_2O_4-cooled chamber) and 46 (ClF_3-cooled chamber). These figures give the data for each of the four coolant sections in both chambers. The metering platelets used in Sections I, II, and III of the N_2O_4-cooled chamber measured 0.0011 $\pm$ 0.0001 in. in thickness; six samples of the Section IV metering platelets all measured 0.0010 in. In order to show the effect of the metering platelet thickness (the depth of the primary metering groove) on the chamber hydraulic characteristics, pressure drop - flow predictions were made for both 0.0011 in. channels (measured thickness) and 0.0010 in. channels (nominal thickness) for Sections I, II, and III of the N_2O_4-cooled chamber.

(C) The general character of the results for all eight sections is remarkably similar. The flow test data are in excellent agreement with the theoretically predicted behavior. The data follow the curves predicted for

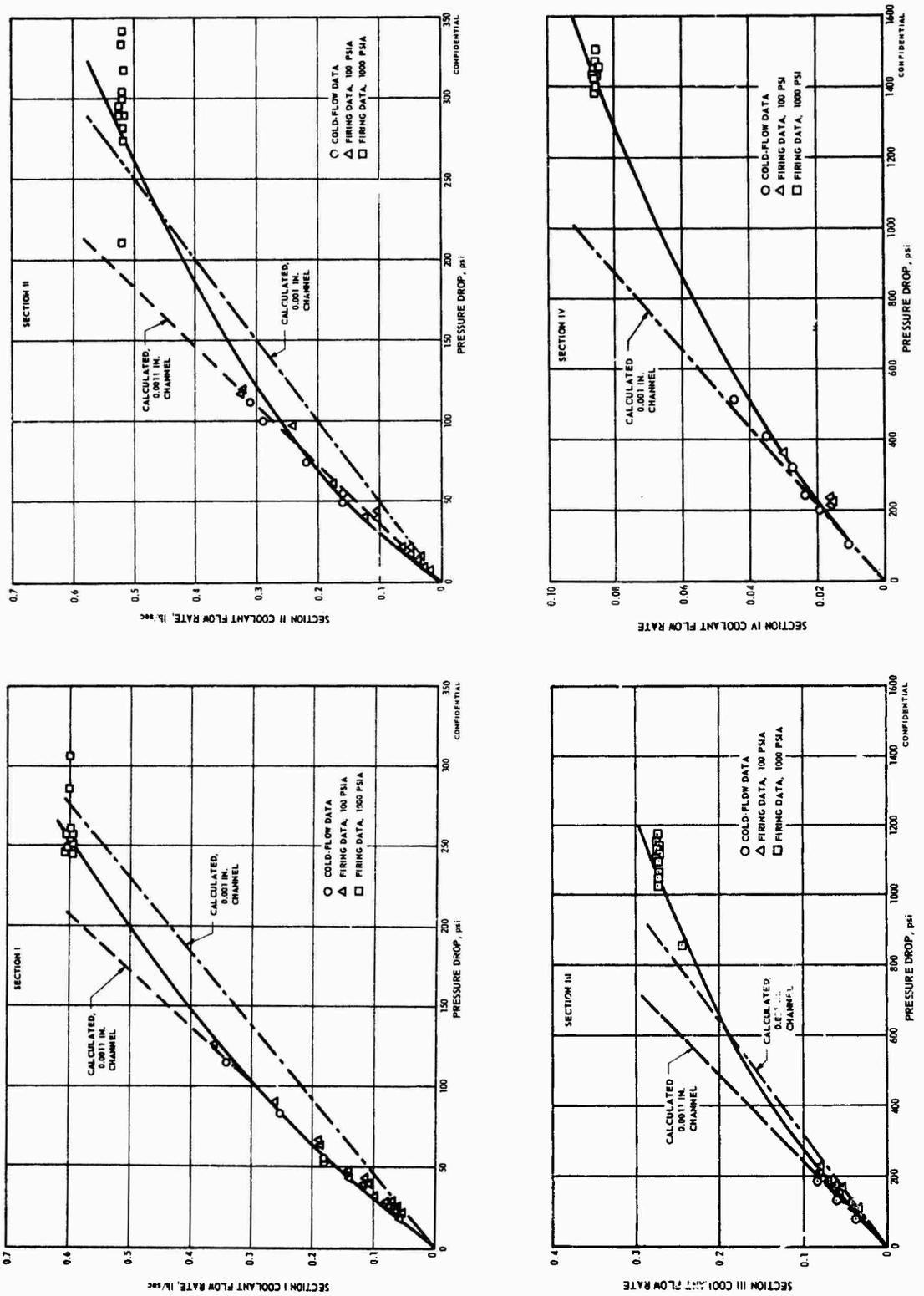

Figure 45. Hydraulic Characteristics of N_2O_4-Cooled Chamber (u)

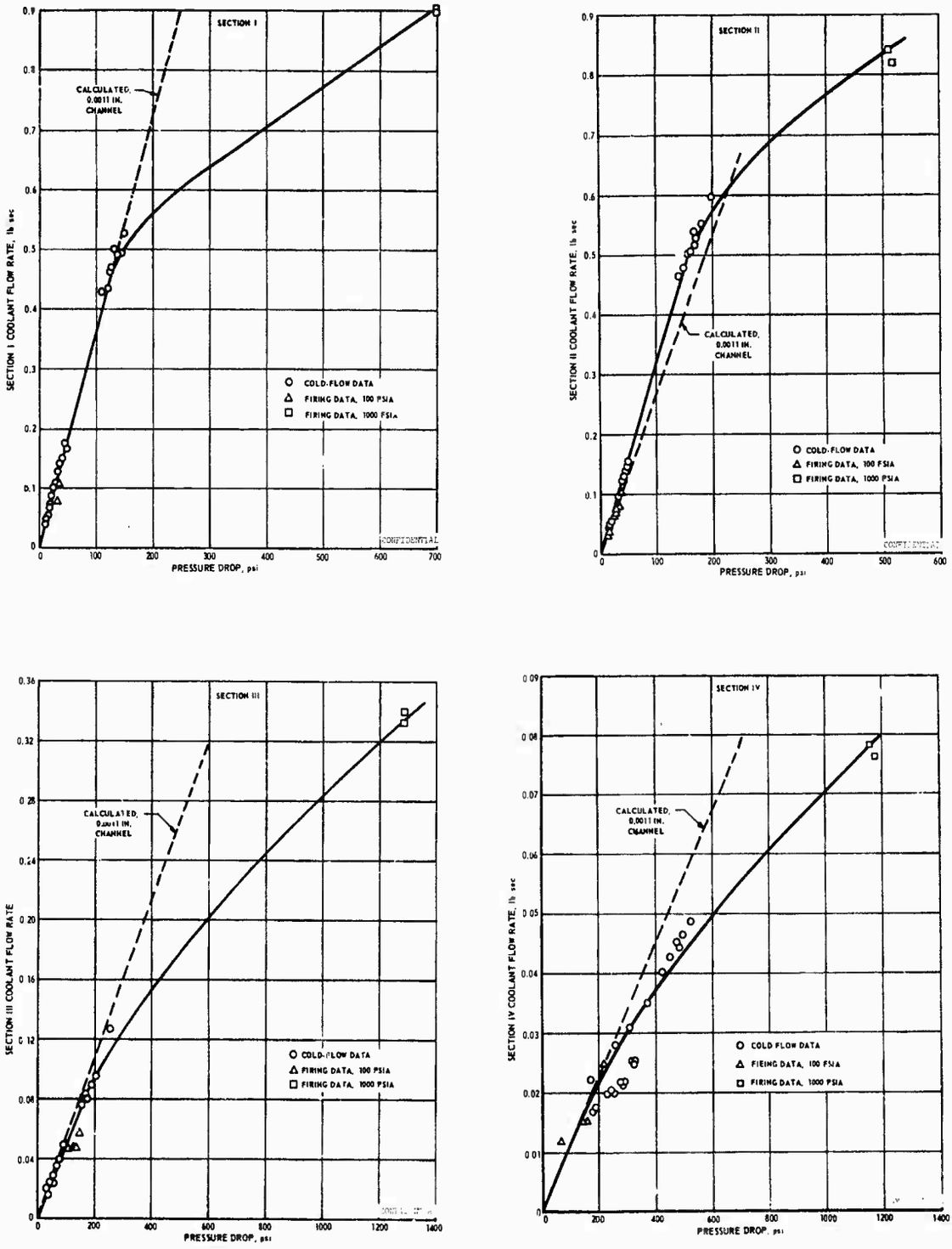

Figure 46. Hydraulic Characteristics of Phase I ClF_3-Cooled Chamber (u)

VI, B, Cooled Chamber Flow Testing (cont.)

the measured thickness of the metering platelets. The 100 psia firing data points are also in good agreement with the predicted curves, but with pressure drops slightly (0-10%) higher than the flow test results. The 1000 psia firing data show substantial departures from the anticipated behavior, with the measured pressure drops being much higher than would be predicted using laminar flow relationships. Except for Section III in each of the chambers the primary metering groove Reynolds numbers at both the 100 psia level and the 1000 psia level are below 2000. The Reynolds number in the N_2O_4-cooled chamber Section III is 2200 at the 1000 psia flow conditions while that of the corresponding ClF_3-cooled chamber section is 2750.

(U) The hydraulic design of the platelets was carefully reviewed in an attempt to explain the deviation of the 1000 psia du.ing data from the predicted pressure drop. The pressure drop in the distribution plenum, two-phase pressure drop in the thermal influence zone, and entrance and exit losses do not account for the deviation. The pressure drop in each section during the coolant lead time preceeding ignition was virtually identical to the pressure drop during firing, which ruled out the possibility of housing distortion or platelet compression due to hydraulic forces in the plenums and pressure forces in the chamber. The match in pressure drop during coolant flow preceeding ignition to the pressure drop during firing ruled out any thermal effects, such as heat penetration to the metering grooves.

(U) Platelets from the ClF_3 chamber were examined for a possible indication of flow restriction since ClF_3 flow paths are evidenced by a slight discoloration of the nickel surface. Flow paths corresponding to the primary and secondary metering groove can be clearly seen on the distribution platelet and they indicate no abnormal behavior. However, from the discoloration of the metering platelet it was obvious that flow in the inlet region had occurred on both sides of the metering platelet. Examination of a stack of

VI, B, Cooled Chamber Flow Testing (cont.)

platelets revealed that the 0.001 in. metering platelets were sagging into the 0.0025 in. x 0.140 in. distribution platelet inlet, and in some instances a slight curl on the edge of the metering platelet was practically blocking the inlet. Thus, the inlet to the platelets is apparently the source of the additional pressure drop.

(C) The effect of the inlet flow restriction is shown in Figure 47. This figure shows a plot of percent departure from laminar flow behavior as a function of Reynolds number for six of the eight platelet sections. The two platelet sections not shown on this figure are Sections I and II of the ClF_3-cooled chamber. Since they contained the salt deposits in 1000 psia tests their behavior should not be considered simultaneously with that of the clean sections. It is quite apparent from the curve of Figure 47 that the departure from laminar pressure drop at 1000 psia is a direct function of metering groove Reynolds number. Both the laminar and turbulent flow points fall on the same straight line. This indicates that the transition from laminar to turbulent flow behavior is gradual and that no sudden change occurs near a Reynolds number of 1500 to 2000. This behavior would result from the existence of a restriction in the coolant flow circuit.

(U) Although the inlet flow restriction has no serious consequences it will be precluded in future designs. For example, small unetched areas in the inlet, similar to those in the thermal influence zone, could be used to support the metering platelet.

2. Phase II

(U) In order to preclude the flow restriction at the platelet coolant inlet that occurred with the Phase I chambers each metering platelet in the Phase II chamber was tack-welded at the inlet locations to the unetched

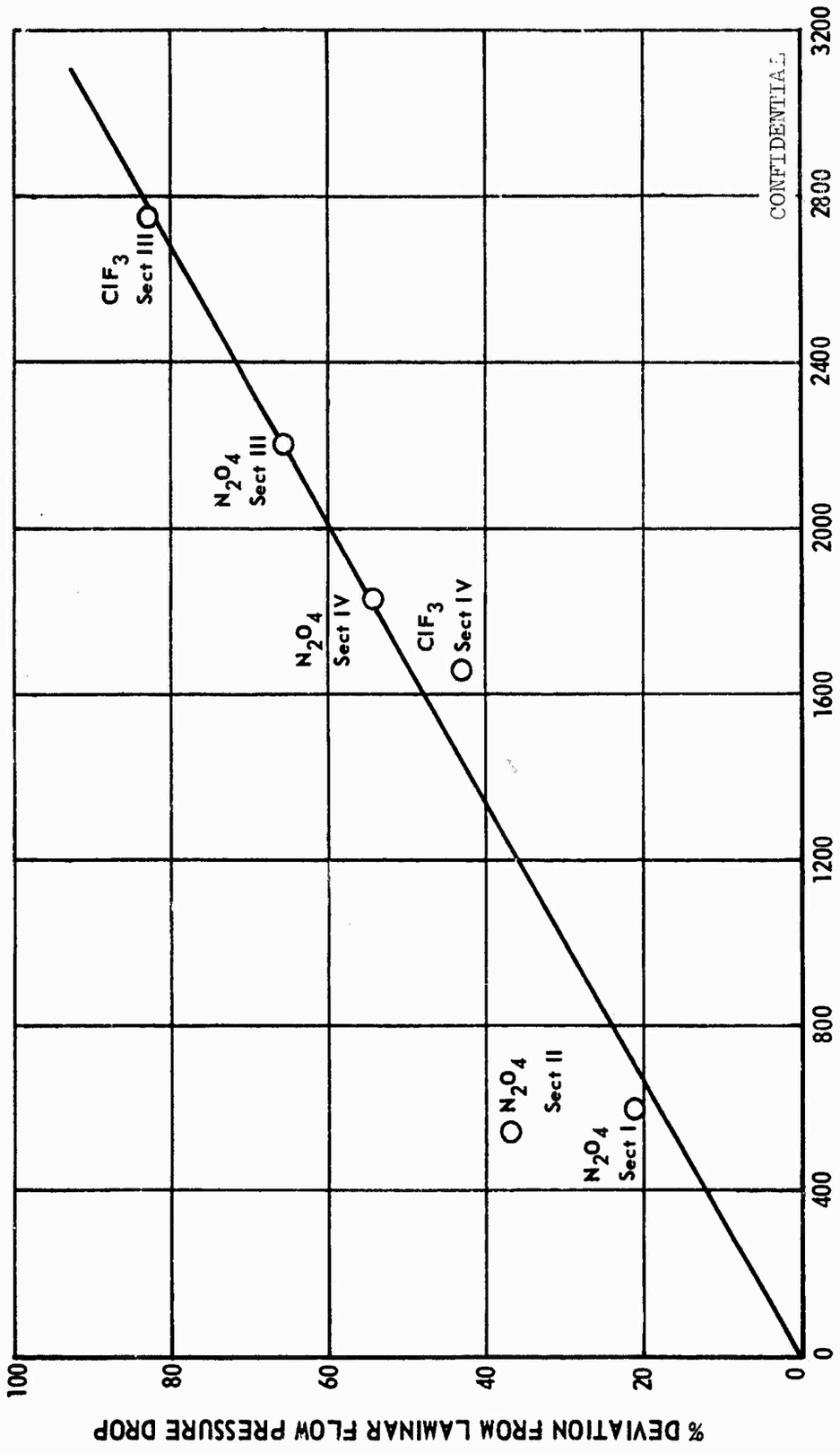

Figure 47. Deviation from Laminar Flow Pressure Drop (u)

VI, B, Cooled Chamber Flow Testing (cont.)

back of the distribution platelet next to it in the stacked assembly. The purpose of the weld was to prevent the metering platelet from sagging into the etched inlet area on the face of the distribution platelets.

(U) Since the TRANSPIRE hydraulic characteristics had been adequately verified in Phase I and since the Phase I and Phase II chambers were hydraulically similar no flow calibration tests were made with the Phase II cooled chamber. A single flow test with ClF_3 was made on the test stand prior to the first cooled chamber test. The pressure drops obtained in this test agreed with pressure drops predicted for the chamber with 0.0010 to 0.0011 in. deep metering grooves.

(U) The hydraulic characteristics of the Phase II ClF_3-cooled chamber are shown in Figure 48. The hydraulic characteristics were determined from the pressure drop - flow data obtained during the coolant lead time prior to each firing and have been corrected to 70°F for comparison with the predictions. The back pressure on the coolant circuit is atmospheric pressure.

(U) The deviation from laminar flow that characterized the Phase I cooled chamber flow test results at high coolant flow rates did not occur with the Phase II chamber. The source of the turbulent pressure drop, blockage of the inlet to the distribution platelet by the metering platelet, was apparently properly identified and the corrective action, tack welding the metering platelets to the back of the distribution platelets, was successful.

(U) In the Phase II cooled chamber assembly the injector was used to load the stack of platelets. After test 1K-5B-110 the injector was removed from the cooled chamber assembly to permit the P_c tap to be unplugged. The hydraulic characteristics that were obtained upon reassembly

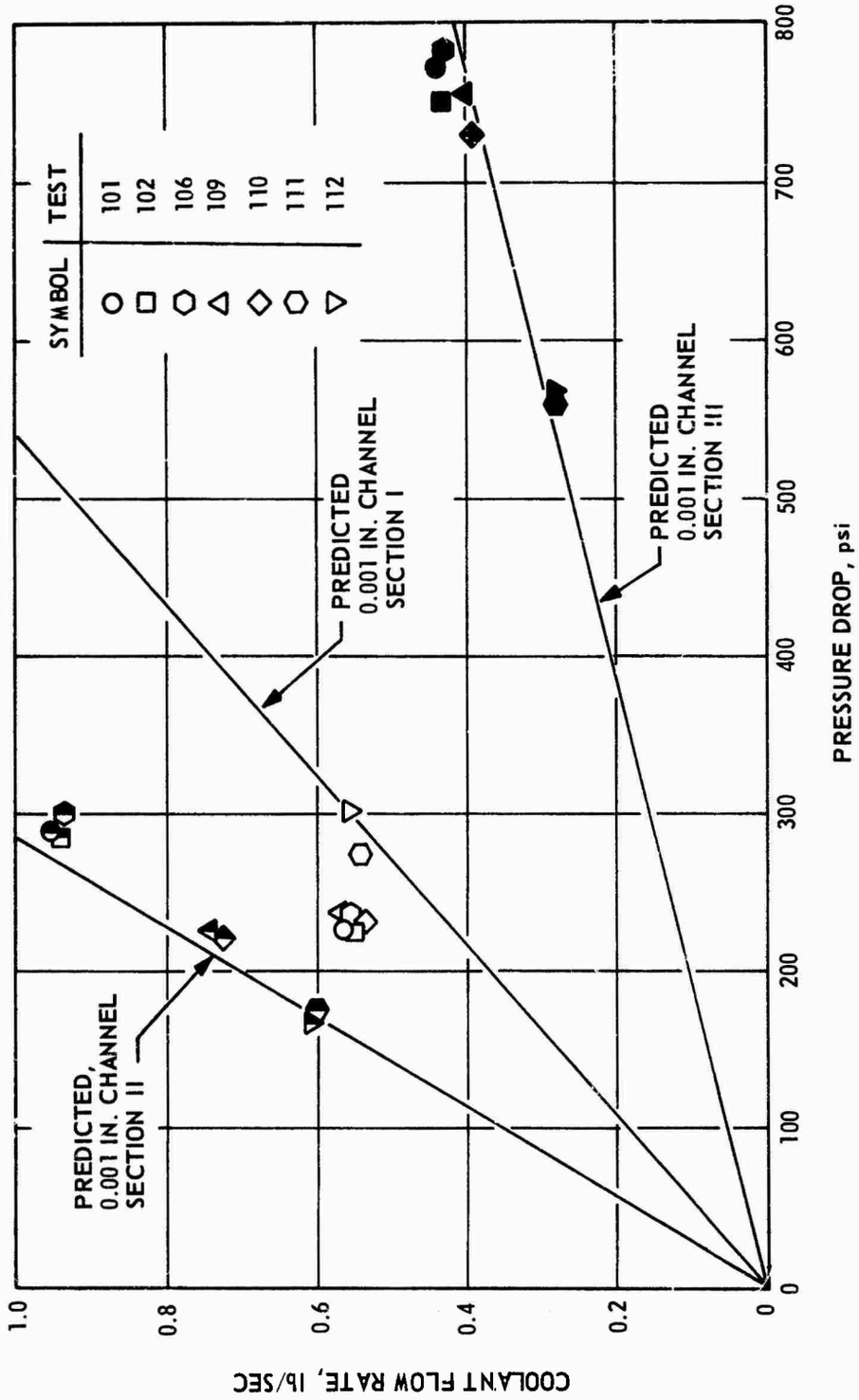

Figure 48. Hydraulic Characteristics of Phase II ClF_3-Cooled Chamber (u)

VI, B, Cooled Chamber Flow Testing (cont.)

of the unit differed from those that were obtained before removal of the injector. The most pronounced effect was in chamber Section I, which is adjacent to the injector. Apparently the platelet stack was not fully compressed on initial assembly. The flow-pressure drop data for chamber Section I before and after injector replacement fell within the spread predicted for the chamber on the basis of an uncertainty of 0.0001 in. in the effective depth of the flow metering grooves.

VI, Results (cont.)

C. INJECTOR-CHAMBER COMPATIBILITY

1. Phase I

(C) Complete optimization of the coolant flow rates to the four sections of the Phase I N_2O_4- and ClF_3-cooled chambers was not possible because of severe chamber streaking by both the 100 psia (100 lb thrust) and 1000 psia (1000 lb thrust) injectors. The chamber streaks, or localized hot zones, occurred on the chamber wall adjacent to the injector and in the convergent and throat area of the chamber. Figure 49 shows the N_2O_4-cooled chamber at the conclusion of testing. The dark areas in the chamber are heat streaks where high wall temperatures (1200 to 1650°F) have darkened the stainless steel. There was no erosion.

(U) The heat mark patterns are significant when related to the injector pattern. As shown in Figure 50, the six heat marks in the vicinity of the injector, or Section I of the cooled chamber, occurred radially outward of the impingement point of the fan from each pair of the six injector elements. This same heat pattern can be seen on the face of the 100 psia injector shown in the same Figure. The heat marks in the convergent and throat areas of the chamber occur between those in the cylindrical section and, as can be seen in Figure 50, are in line with the elements of the injector. Fuel rich combustion gases are, quite likely, impinging on the oxidizer cooled chamber wall and combusting. Because of the localized heating due to the 100 psia injector pattern the coolant flow could not be fully optimized. Based on visual observation and measured temperatures approximately 80% of the N_2O_4-cooled chamber was substantially overcooled. Temperature difference between the hot streak zones and the overcooled zones was in the range of 600 to 1000°F.

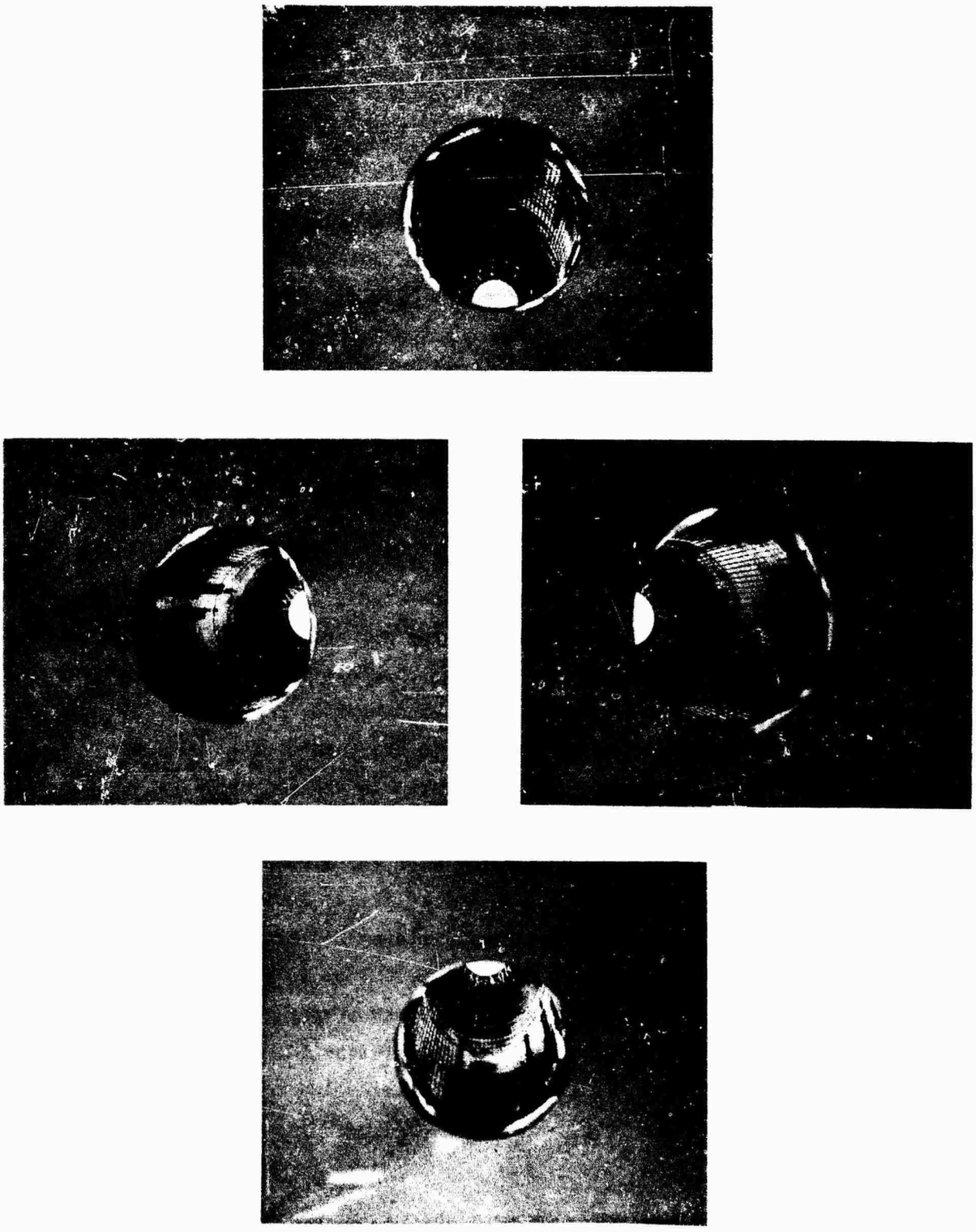

Figure 49. Heat Marks on Interior of N_2O_4-Cooled Chamber after Testing

Figure 50. Injector and Interior of N_2O_4-Cooled Chamber after 100 psia Testing (u)

VI, C, Injector-Chamber Compatibility (cont.)

(U) The heat marks in the chamber at the conclusion of the 1000 psia, 1000 lb thrust testing (Figure 49) were even more severe and more highly localized than for the 100 psia, 100 lb thrust operation. Despite the high steady-state wall temperatures recorded during the 1000 psia N_2O_4 tests the majority of the chamber surface area was overcooled. The more severe streaking at 1000 psia made the coolant utilization even less efficient than at 100 psia. The hot streaks in the vicinity of the injector initially occurred radially outward of the impingement point of the fan from each pair of peripheral elements (12 locations), and then spread out at a trip or irregularity in the chamber surface as shown in Figure 51. Other examples of trips can be seen in Figure 51 at the 7:00 o'clock position at the end of Section I (about the midpoint of the cylindrical section) and in Figure 50 in the convergent area of the chamber.

(U) A definite correlation exists between the heat patterns on the walls of the cooled combustion chamber and the walls of the ablative lined chambers used for the injector checkout tests. The heat patterns on the walls of the uncooled chamber as related to the injector elements of the 1000 psia N_2O_4 injector are shown in Figure 52a. The dark areas on the ablative liner next to the injector face are fuel rich zones located radially outward from each of the injector elements. The four largest areas are in line with the radial projection from the four pentad elements. The white areas are hot zones where silica material has flowed to the surface and solidified.

(U) The hot zones for the 100 psia injectors existed between the injector elements. Silica from these areas flowed down into the chamber throat as shown in Figure 52b.

(U) The condition of the ClF_3/MHF-3 ablative chamber section relative to the 1000 psia -29 injector pattern is shown in Figure 52c. The predominate ablation pattern lies on a radial projection from an inner triplet

Figure 51. Interior of N_2O_4-Cooled Chamber after 1000 psia Testing (u)

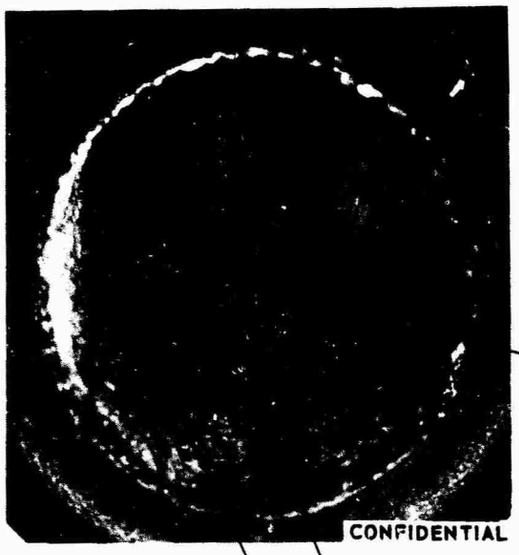

(a) 1000 PSIA N_2O_4/A-50
INJECTOR AND ABLATIVE CHAMBER SECTION AFTER TESTING

WHITE SILICA
(HOT AREAS)

(b) NOZZLE OF ABLATIVE THROAT SECTION AFTER FOUR 100 PSIA N_2O_4/A-50 TESTS

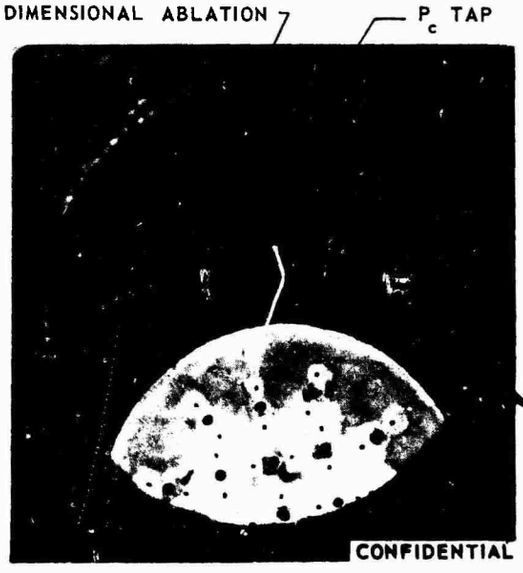

(c) 1000 PSIA ClF_3/MHF-3
INJECTOR AND ABLATIVE CHAMBER SECTION AFTER TESTING

HAIR LINE CRACKS

Figure 52. Ablative Liner Sections after Testing (u)

VI, C, Injector-Chamber Compatibility (cont.)

element and between two outermost triplet elements. Two smaller ablation patterns can be seen between the predominate ones on a radial projection from the impinging fans of two triplet elements. These ablation patterns define the critical hot zones at the chamber wall. Even though four predominate erosion patterns occurred in the chamber wall within two inches of the injector face no throat erosion existed.

(U) Simple analytical models have been developed which describe the chemical composition and radial motion of the combustion products as they move downstream from the injector. These models correlate well with the heat marks observed in the N_2O_4-cooled chamber and in the ablative chamber sections after 100 and 1000 psia testing. The models for the 100 psia N_2O_4/AeroZINE 50 injector are shown in Figure 53.

(U) The chemical model is developed by defining the shape, size, and mixture ratio distribution of a spray envelope that is characteristic of a particular element, its energy release efficiency and the flow rate in that element. As can be seen in Figure 53 the triplet element is characterized by an ellipse. The mixture ratio distribution is shown as an oxidizer-rich zone and two fuel-rich zones. The overlap of these envelopes when superimposed on the injector pattern indicates areas that are oxidizer or fuel-rich in composition or where inter-element combustion will occur.

(U) The dynamic model defines for each injector element a stream tube the size of which is dependent on the type of element, its mixture ratio, flow rate and energy release efficiency. It is then assumed that as the combustion products move downstream the stream tubes will move relative to each other and the chamber walls so that a zero radial pressure gradient condition exists. In the dynamic model the stream tubes are represented by circles centered about each element. These circles are then adjusted to the "relaxed position", in which minimum overlap results and which is considered to represent

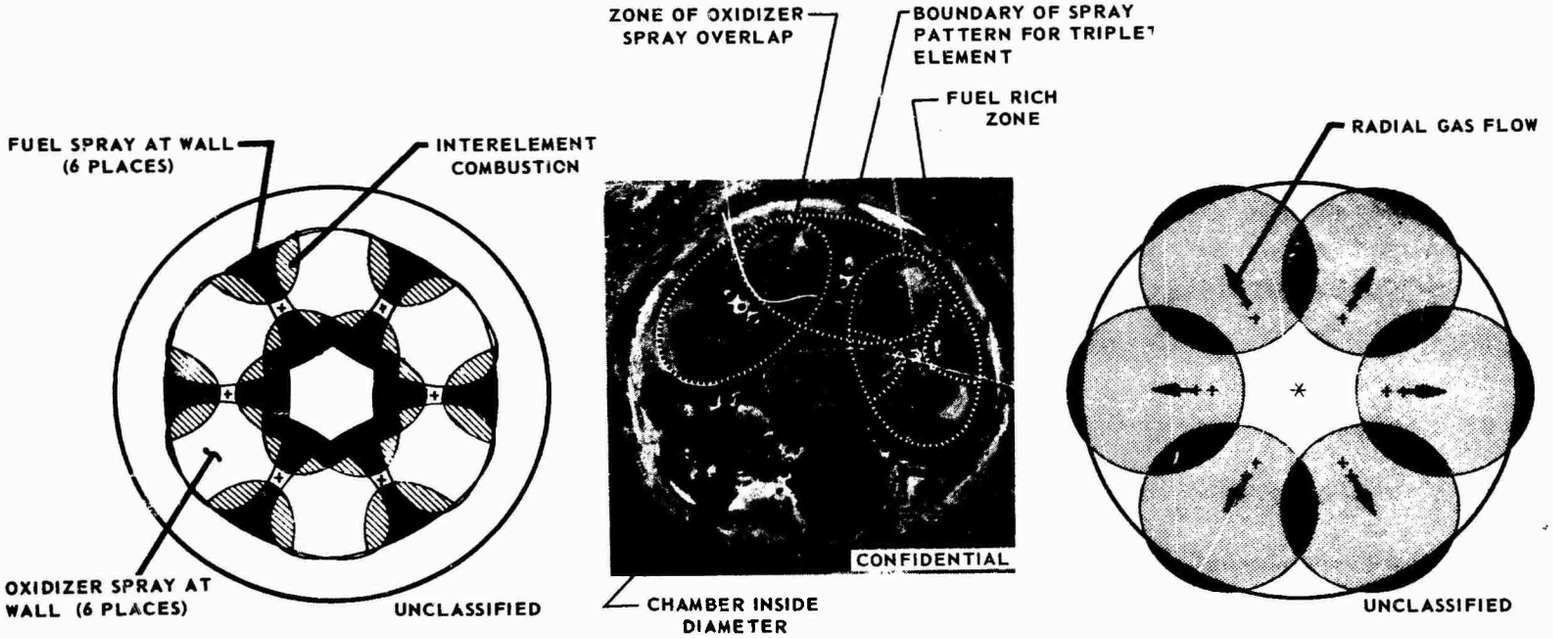

CHEMICAL MODEL OF 100 PSIA N_2O_4/A-50 S/N 2 INJECTOR

100 PSIA N_2O_4/A-50 S/N 2 INJECTOR AFTER TESTING

DYNAMIC MODEL OF 100 PSIA N_2O_4/A-50 S/N 2 INJECTOR

Figure 53. Comparison of Compatibility Model with Spray Pattern on Face of 100 psia N_2O_4 Injector (u)

VI, C, Injector-Chamber Compatibility (cont.)

the zero radial pressure gradient condition. A vector is drawn from the original position of the stream tube to its center in the relaxed position. The length of the vectors and their direction indicates the location and severity of cross-winds.

(U) As shown in Figure 53, the chemical model of the 100 psia N_2O_4/AeroZINE 50 injector predicts that six hot zones will exist between elements where the fans of the elements intersect. These hot zones correspond to the six heat marks in the cylindrical section of the cooled chamber, shown in Figure 50. The dynamic model indicates that the fuel-rich zones, which the chemical model shows to be centered on each element, will migrate toward the wall as the combustion gas flows away from the injector. The six heat zones in the convergent section of the N_2O_4-cooled chamber probably result from combustion of this fuel-rich gas with the oxidizer transpiration coolant.

2. Phase II

(U) One of the main objectives of Phase II was the optimization of coolant flow by reduction of the injector induced heat streaking at the wall of the chamber. The injector design selected as the most promising to accomplish this objective was the HIPERTHIN injector. This injector design features pattern uniformity because of the multiple number of orifices, peripheral control of fuel injection to provide an oxidizer rich boundary at the chamber wall and potentially good performance as demonstrated on other programs. A vortex injector with the oxidizer injected tangentially at the chamber I.D. was also considered a promising candidate for excellent compatibility with the oxidizer transpiration cooled chamber. Uncertainty as to performance potential made the vortex design second choice. As discussed in Section IV,A,2,b fabrication problems precluded the use of the HIPERTHIN injector and poor performance (see Section V,A) made the vortex injector unacceptable.

VI, C, Injector-Chamber Compatibility (cont.)

(U) The 49-element injector that was used for the Phase II cooled chamber testing was designed on the basis of Phase I experience. The compatibility model of the injector is shown in Figure 54. A large number of elements was used for three reasons. Primarily, a large number of elements permitted the elements on the periphery near the chamber wall to be placed in close proximity to each other to preclude the spray fan or the resultant spray from two intersecting spray fans from hitting the wall. Secondly, a large number of elements was used to obtain a fairly uniform mass distribution across the face of the injector and thus minimize radial gas flow toward the wall. Finally, performance predictions indicated that good performance could be maintained by reducing the thrust per element despite the reduction in chamber L* (32 in. for the Phase I chamber to 25 in. for the Phase II chamber). The inclusion of eight unlike doublets at the outer periphery of the pattern provided an oxidizer rich zone at the wall for improved injector-chamber compatibility.

(U) The condition of the ablative liner (cylindrical section) after four vortex injector checkout tests is shown in Figure 55. Figure 52c, which shows a similar liner section after four checkout tests with the 21-element S/N-4 injector, provides a comparison. The oxidizer was introduced tangentially in the vortex injector at the chamber wall. The low performance of the vortex injector (see Section VI,A) means that much of the oxidizer remained on the wall and did not enter the combustion process. Thus, Figure 55 shows the compatibility of hot ClF_3 with FM 5064 material. The vortex injector would have had excellent compatibility with the ClF_3-cooled chamber. From the results exemplified in Figures 44, 52, and 55, the following interpretation can be made concerning ClF_3 injector characterization using carbon-filled phenylaldehyde graphite fabric liners: the presence of a grey deposit or a grey surface indicates a fuel rich zone; a black surface or dimensional ablation exposing unreacted carbon cloth indicates an oxidizer rich zone; smooth dimensional ablation including the carbon cloth results from a hot streak.

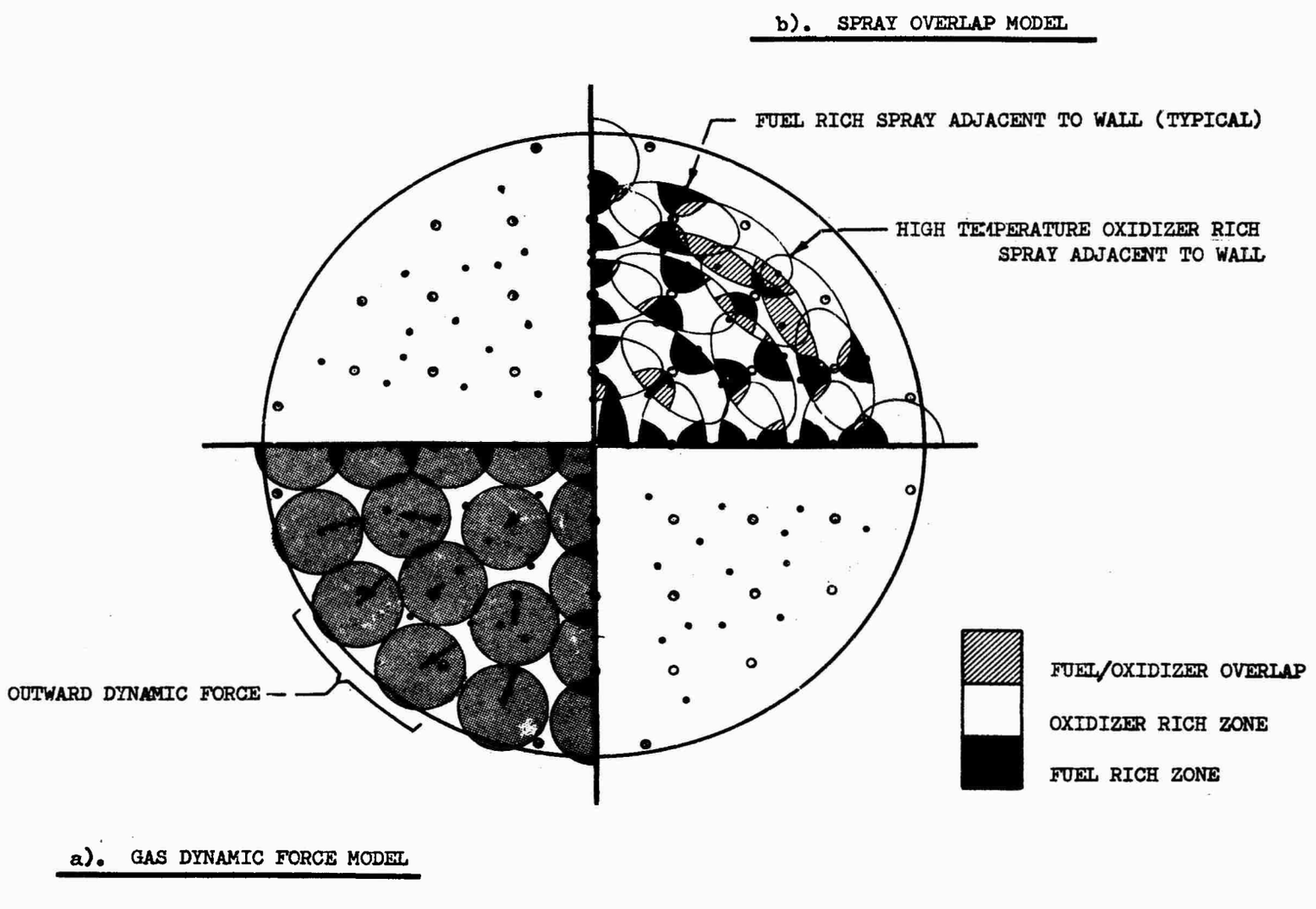

Figure 54. Compatibility Model of 49-Element Phase II Injector (u)

Figure 55. Ablative Liner After Tesving with Vortex Injector

VI, C, Injector-Chamber Compatibility (cont.)

(U) At the conclusion of the injector checkout tests that were made to determine the baseline performance of the 49-element injector the ablative liner used in the testing was examined for streaking. Minor dimensional ablation occurred adjacent to the four folded triplet elements. The number of localized erosion areas was greatly reduced over that obtained with the 21-element 1000 lb thrust injector. The deposition of resinous material in the throat that characterized Phase I 1000 lb thrust testing did not occur.

(U) Improved compatibility that was predicted for the 49-element injector and indicated by the checkout tests with ablative liners was evidenced in the cooled chamber test results. The condition of the ClF_3-cooled Phase II chamber after Test 1K-5B-110 (8.9 sec duration) is shown in Figure 56. The heat mark at the top of the pictures is one of four 90° apart and is produced by the folded triplet element. The heat mark on the back of the platelet in line with the heat mark on the chamber surface (top of pictures) is at the location of the P_c tap. This mark corresponds to a recess in the face of the injector where the excess weld material around the P_c tap was machined away after welding. There were eight other small heat marks, some of which can be seen in Figure 56. These marks occurred during tests 1K-5B-101 and -102 which were conducted with the injector fuel and oxidizer venturis inadvertently reversed. The eight marks were caused by high fuel and low oxidizer flow in the eight unlike doublets which resulted in fuel impingement on the oxidizer cooled wall. These eight streak marks tended to clean up with subsequent testing. The remaining chamber surface showed no evidence of injector streaking; the condition of the chamber after this test was excellent.

(U) The thermal data that were obtained from the thermocouples on the chamber surface also indicated that the 49-element 1000 lb thrust injector produced less circumferential and axial variation in the heat flux to the wall than was produced by the 21-element Phase I 1000 lb thrust injector. From these data and the Phase I experience with both N_2O_4-cooled

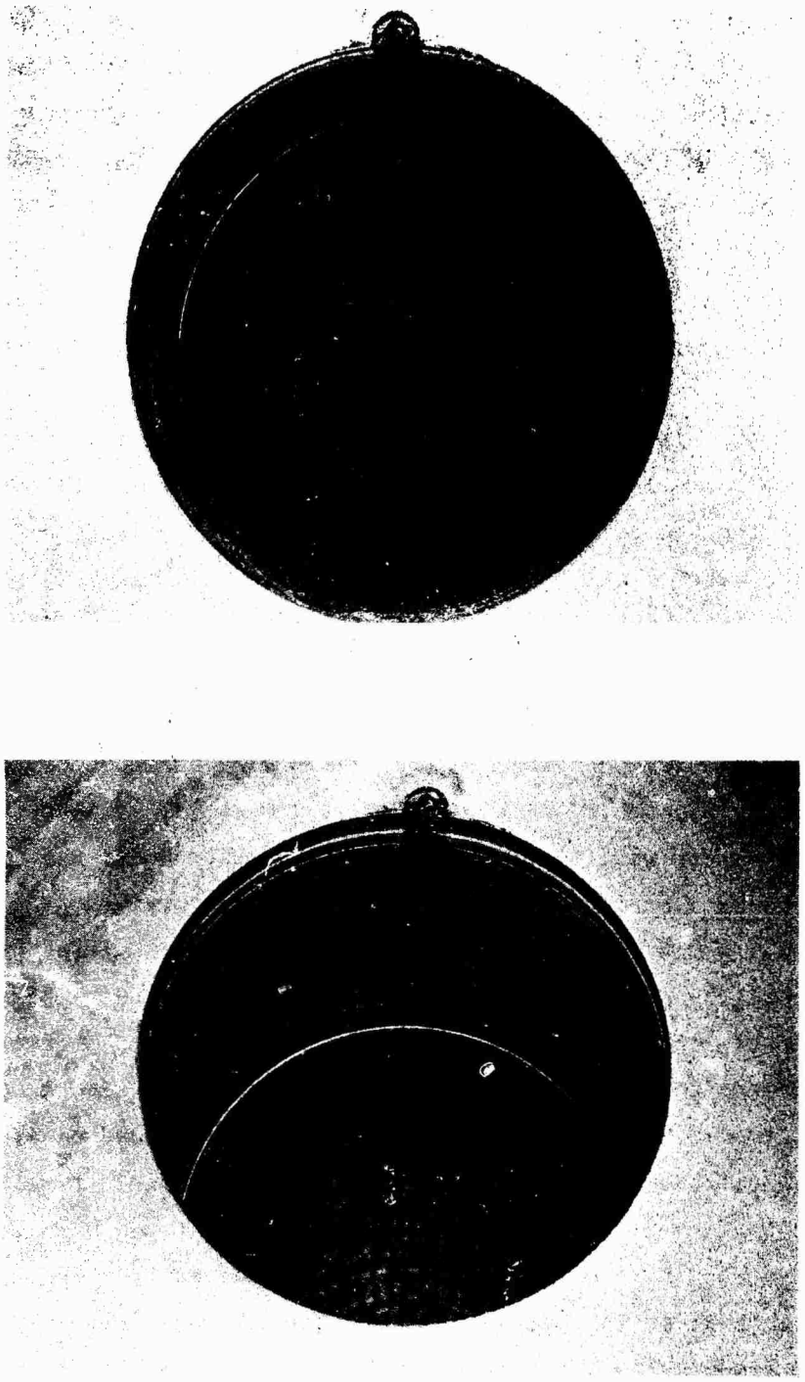

Figure 56. Phase II Cooled Chamber after Firing

VI, C, Injector-Chamber Compatibility (cont.)

stainless steel chambers it was concluded that coolant flow optimization requires that the injector be designed for compatibility with the oxidizer transpiration cooled chamber, that wall roughness increases heat transfer to the wall and disrupts the boundary layer which starts heat streaks at trips or aggravates existing heat streaks, and that high conductivity material for the chamber mitigates the effect of streaking.

VI, Results (cont.)

D. HEAT TRANSFER

1. Introduction

(U) The heat transfer data obtained during this test program consisted of coolant flow rates and surface and subsurface wall temperatures. These data were analyzed to determine how well the TRANSPIRE cooling system worked and also to evaluate the accuracy of the analytical design model. Since, to a large extent, these goals are interdependent both the evaluation of the cooling effectiveness and the analytical design model will be presented simultaneously in this section.

(U) The analytical design approach used in this program is outlined in Section IV,C,1,a, while the specific equations and their derivations are presented in Appendix I. All the thermal design equations have been programmed for an IBM 1130 computer. In addition to performing the hot gas - to platelet - to coolant heat transfer calculations and iterations, this program can also calculate the film cooling carry-over effect received from the two platelets immediately upstream of the platelet under consideration. This option has proved helpful in the interpretation of some test results.

(U) Most of the data analysis was restricted to the interpretation of surface temperature readings. This was done for several reasons. First, the cooling effectiveness of the wall can be evaluated in terms of only two quantities, coolant flow rate and wall surface temperature. These two values alone express the overall cooling effectiveness of the system. Second, subsurface temperatures can be related to surface temperatures only by way of the thermal model; hence they cannot be considered as primary data as far as system cooling effectiveness is concerned. The value of the subsurface temperatures arises in the evaluation of the thermal model. The platelet temperature profiles that the subsurface temperature data should provide give considerable insight into the thermal processes occurring in the wall. Finally, the injector

VI, D, Heat Transfer (cont.)

streaking encountered in this test program rendered much of the subsurface data extremely difficult to interpret by making valid platelet temperature profiles virtually unachievable. As pointed out in Section IV,D, the surface and subsurface thermocouples on any platelet were all positioned at different circumferential locations. The large circumferential variations in heat flux which resulted from the injector streaking placed each thermocouple in a different thermal environment and this made meaningful determination of the platelet temperature profile impossible.

(U) In Section II of the chamber not all the platelets have the same clocking (hydraulic resistance) as was the case in Section I. The clocking is changed 17 times in Section III and 30 times in Section IV. Because of the number of parallel flow circuits, each with a different hydraulic resistance, the flow rate of each platelet pair will not necessarily be proportional to total flow rate of the section. For example, test firing at 100 psia chamber pressure with a 115 psia Section III plenum pressure produces a pressure drop of approximately 20 psid across the platelets at the high contraction ratio end of that section, and a pressure drop of approximately 60 psid across the platelets in the throat. If the plenum pressure is increased to approximately 155 psia the coolant flow in the section is doubled. However, the pressure drop at the high contraction ratio end of Section III is now 60 psid, which results in three times the flow in that area; in the throat the pressure differential is now 98 psid which results in a 48% increase in the flow there. Thus, operation at the off-design pressure differential conditions produces a coolant maldistribution within the section.

(U) During flow testing of the cooled chambers the back pressure (chamber pressure) is uniform. In the test firings the back pressure varies with the chamber pressure profile. Thus, the flow rate or the plenum pressure, and the flow distribution within Sections III and IV differ in going from flow testing to firing.

VI, D, Heat Transfer (cont.)

(U) The following equations were used to relate plenum pressures and individual platelet flows at one operating condition to another. The coolant in the metering channels is essentially isothermal and incompressible, and the flow is laminar. From equation 30 of Appendix I, the coolant flow rate for an assembled platelet pair is

where:
$$\dot{w}_{c,i} = k \left[\frac{(P_p - P_i)}{\ell_i}\right] \qquad (2)$$

k = flow proportionality constant
ℓ_i = length of a platelet metering groove
P_i = platelet gas-side pressure
P_p = plenum pressure
$\dot{w}_{c,i}$ = platelet coolant flow rate

The total flow rate in a section then is:

$$\dot{w}_{c,S} = k\sum \frac{(P_p - P_i)}{\ell_i} = k\left[P_p \sum \frac{1}{\ell_i} - \sum \frac{P_i}{\ell_i}\right] \qquad (3)$$

Let $(\dot{w}_{c,S})_1$ be the flow rate in a section when $(P_p)_1$ is the plenum pressure and $(\dot{w}_{c,s})_2$ the flow rate of the coolant in that section when the plenum pressure is $(P_p)_2$. If $R = (\dot{w}_{c,S})_1/(\dot{w}_{c,S})_2$, then

$$(P_p)_2 = (P_p)_1 \left(\frac{1}{R}\right) - \left(\frac{1}{R}\right) \frac{\sum \left(\frac{P_i}{\ell_i}\right)_1}{\sum \frac{1}{\ell_i}} + \frac{\sum \left(\frac{P_i}{\ell_i}\right)_2}{\sum \frac{1}{\ell_i}} \qquad (4)$$

VI, D, Heat Transfer (cont.)

The terms $\left(\frac{P_i}{\ell_i}\right)$ were identified for conditions 1 and 2 since $\sum\left(\frac{P_i}{\ell_i}\right)_1 \neq \sum\left(\frac{P_i}{\ell_i}\right)_2$ when one condition is a flow test and the other is a firing.

(U) Equation (4) was developed in terms of a flow ratio, R, since the flow to each section is generally controlled by a fixed area cavitating venturi and, therefore, is known. Besides being useful in calculating plenum pressures for a new flow rate from prior test results and in calculating test firing plenum pressures from the flow test results, equation (4) was used to calculate the flow maldistribution in a section for off-nominal operation. If R is the ratio of a measured section flow rate to the nominal flow rate, then the plenum pressure at nominal conditions, $(P_p)_N$, in terms of the measured plenum pressure, $(P_p)_E$, is

$$(P_p)_N = \frac{(P_p)_E}{R} - \frac{1}{R}\left[\frac{\sum\left(\frac{P_i}{\ell_i}\right)_E}{\sum\frac{1}{\ell_i}} - \frac{\sum\left(\frac{P_i}{\ell_i}\right)_N}{\sum\frac{1}{\ell_i}}\right] \qquad (4)$$

From equation (2) the ratio of the actual platelet flow rate to the nominal platelet flow rate is

$$\frac{(\dot{w}_{c,i})_{actual}}{\dot{w}_{c,i})_N} = \frac{(P_p)_E - (P_i)_E}{(P_p)_N - (P_i)_N} \qquad (5)$$

VI, D, Heat Transfer (cont.)

In applying this equation the plenum pressures were taken from the test data while the local gas pressures (P_i) were obtained from the measured chamber pressure and analytically calculated pressure profiles.

(U) Nominal (design) flow rates are tabulated in Table 2 (Section IV,C,1,a), for the four sections of the N_2O_4-cooled chamber and for the four sections of the ClF_3-cooled chamber.

(U) The gas side heat transfer coefficients used in the data analysis were calculated by a form of the simplified Bartz[2] equation. The freestream gas temperature was taken to be the combustion temperature of the propellants corrected by a combustion efficiency term.

2. Phase I

a. 100 psia N_2O_4- Cooled Chamber Tests

(U) A curve summarizing the surface temperatures for chamber Section II of the 100 psia, N_2O_4-cooled chamber, is given in Figure 57. The test data shown on this figure are thermocouple readings at the end of each test, and generally represent the steady-state values. The abscissa of this plot (Figure 57) is the ratio of the actual total sectional flow rate to the design flow rate. Since Chamber Section II has essentially a constant area ratio and, hence, a constant back pressure within the chamber, the local (platelet) flow rate ratio (as calculated by equation 5) is the same as the section flow rate ratio. The thermocouples shown in Figure 57 are numbered 4-5, 4-7, 5-3, and 5-7. None of these aforementioned thermocouples are in line, although thermocouples 4-7 and 5-7 are within five degrees of each other. Analytically predicted temperatures obtained by utilizing the actual test

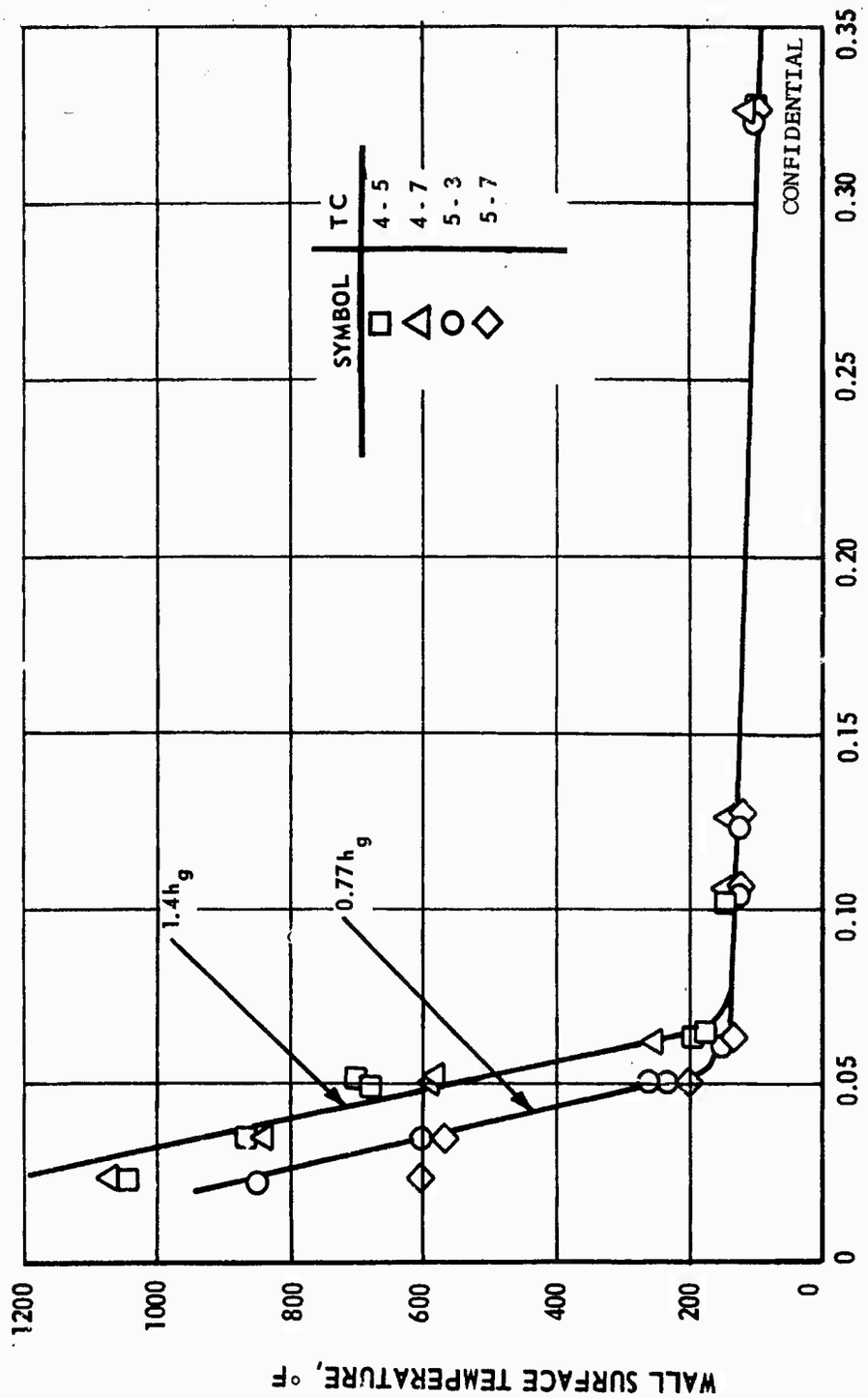

Figure 57. Section II Steady-Stage Wall Temperatures, N_2O_4/A-50, 100 psia (u)

VI, D, Heat Transfer (cont.)

conditions insofar as possible, are shown by the solid line in Figure 57. These calculations consider film cooling carry-over from the two previous platelets and also take into account the fact that instrumented platelets are thicker (0.0235 in. vs 0.0178 for its neighbors). The hot gas heat transfer coefficient h_g was varied to find the limits that would enclose the data. The data are included in an envelope generated by the use of a heat transfer coefficient in the range 0.000362 Btu/in.^{2}sec-°F to 0.000658 Btu/in.^{2}sec-°F. When compared with the heat transfer coefficient calculated by means of the Bartz equation, the lower and upper bounds of the data are defined by the curves resulting from a multiplying factor of 0.77 and 1.4. The agreement between the slope of the data in Figure 57 and that resulting from the analytical model is excellent.

(U) The data from Sections I and III are shown in Figure 58. These data were not amenable to analysis. The data from Section III will be used to exemplify the problem.

(C) The coolant flow rates on the instrumentation platelets were calculated using equation (5) and the measured plenum pressures and measured section flow rates. For example, the coolant flow ratio (actual to nominal) on thermocouple platelet No. 2 is 2.3, and on platelet No. 3 is 11.0 when the overall Section III flow ratio is 4.6. These flow ratios were used with the measured surface temperatures and the heat transfer model, as had been done with the Section II data, to evaluate the multiplier on the gas-side heat transfer coefficient that would correlate the data. For the 1240°F wall temperature that was measured at the overall flow ratio of 4.6, this multiplier is 5.0. The boundary layer temperature is predicted to be approximately 2600°F.

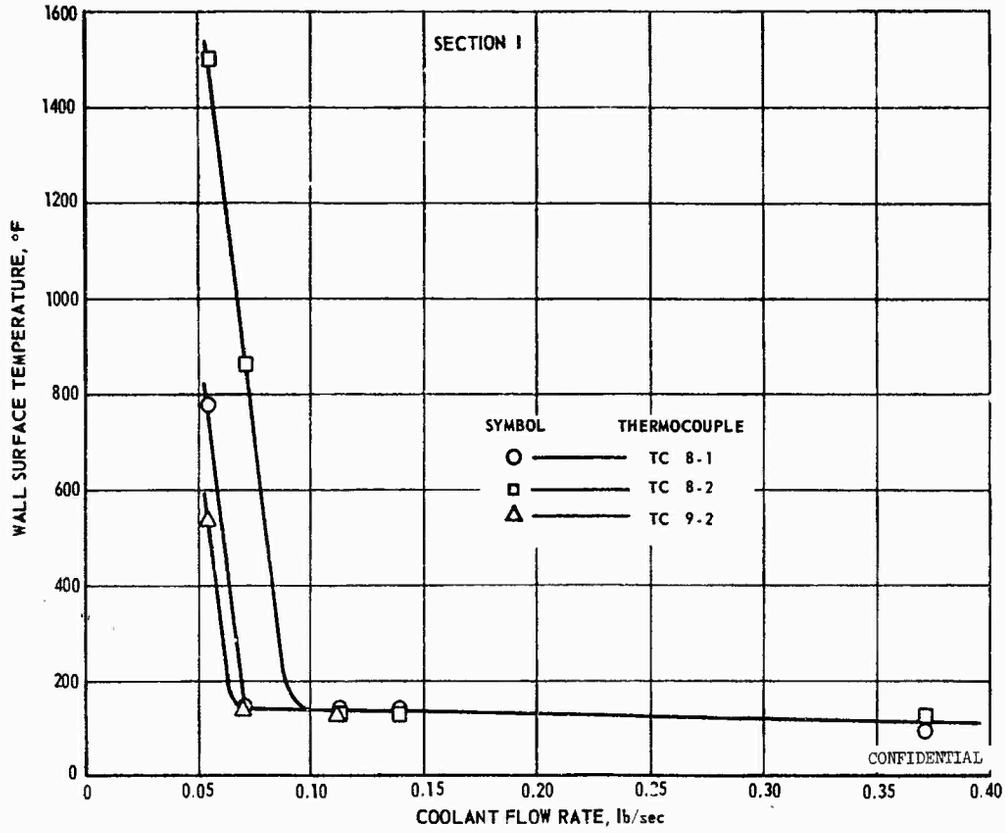

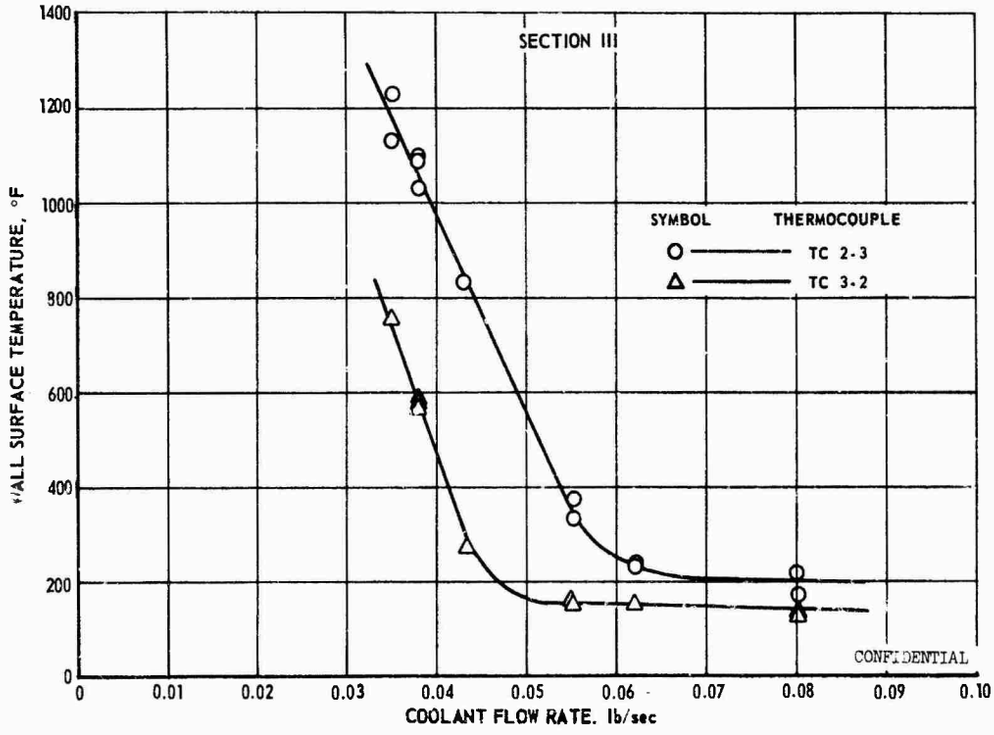

Figure 58. Section I and III Steady-State Wall Temperatures, N_2O_4/A-50, 100 psia

VI, D, Heat Transfer (cont.)

(U) It is obvious that any physical disturbance that would produce a heat transfer coefficient that is five times the best estimate value would also disrupt the film cooling. Thus, the film cooling representation in the heat transfer model cannot possibly simulate the actual conditions in the throat and, therefore, the model cannot be applied.

(C) The heat flux to the throat instrumentation platelet at the location of thermocouple 2.3 is 8.25 Btu/in.^{2}sec. This heat flux is two times that predicted using the stagnation temperature in the throat as the driving temperature and a film coefficient calculated using the correlation of Bartz. It is fairly obvious that a heat flux this high can only result from boundary layer turbulence and/or boundary layer combustion.

(U) There are two reasons why the heat transfer is inordinately high in the convergent section of the nozzle. The wall of the nozzle was relatively rough with instrumentation platelet No. 3 protruding an estimated 0.005 in. above its neighbors, which is considerably greater than the thickness of the boundary layer laminar sublayer at this point. The disruption of the boundary layer and the resulting increase in local surface film coefficient could be very significant. In addition, it is entirely possible that some combustion could be taking place in the boundary layer since the observed injector streaking patterns indicate fuel rich zones can persist all the way to the throat (see Section VI,C). A rough wall and injector induced heat streaks were also observed in Section I of the chambers.

b. 1000 psia N_2O_4- Cooled Chamber Tests

(U) The 1000 psia, N_2O_4- cooled chamber tests were made with only one set of flo ratios and, therefore, graphs similar to those

VI, D, Heat Transfer (cont.)

for the 100 psia data could not be drawn. An analysis was performed at two thermocouple locations, TC 4-7 (Section II) and TC 2-2 (Section III, 15 mils below the surface) to correspond as nearly as possible with those used in the analysis of the 100 psia data. TC 3-2 and TC 2-3, used in the analysis of the 100 psia data, were inoperative during these runs. There is excellent correlation between the Section II data and the model (1167°F measured on TC 4-7 versus 1200°F predicted with model) when a film coefficient multiplying factor of 1.4 is used. Again, however, a very large throat section film coefficient multiplying factor is required to make the model fit the Section III test data.

(U) The 1000 psia results are in substantial agreement with those of the 100 psia data. The analytical model agrees well with the test results in Chamber Section II, but apparently is inadequate in describing effects near the throat for the reasons cited earlier.

c. 100 psia ClF_3- Cooled Chamber Tests

(U) Thermal steady-state was achieved in eight of the 100 psia ClF_3-cooled tests. The coolant flow rate to chamber Section II was the only one that was varied enough times during testing to permit construction of a plot of wall temperature versus section flow ratio. The data for this section are shown in Figure 59. Analytical results for heat transfer coefficients with multipliers of 0.77 and 1.4 are also shown in the figure as was done in Figure 57 for the 100 psia N_2O_4 test results.

(U) A heat transfer coefficient multiplier of 2.0 is needed to correlate the Section III data at flow rate ratio of 3.8 (thermocouple TC 2-3). Unfortunately, there were no additional steady-state points to define a temperature versus flow ratio curve. The film coefficient multiplier needed to correlate the data, although large, does not preclude application of the heat transfer model.

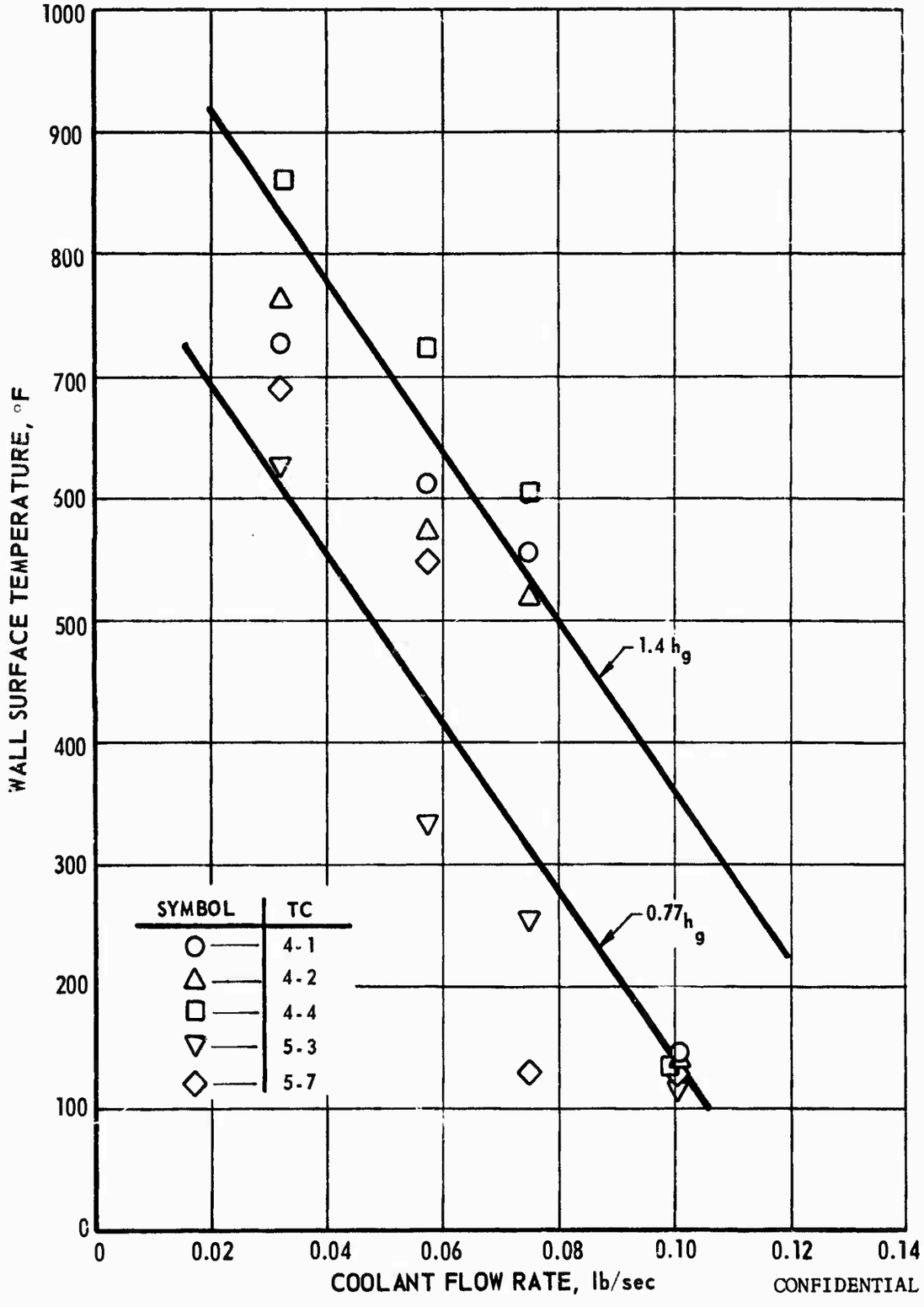

Figure 59. Section II Steady-State Wall Temperatures, ClF_3/MHF-3, 100 psia (u)

VI, D, Heat Transfer (cont.)

d. 1000 psia ClF_3-Cooled Chamber Tests

(U) The test data for the 1000 psia ClF_3-cooled firings consist of four tests of limited durations. The durations of these tests in the order they were run were: 0.44, 1.35, 2.29, and 2.44 seconds. Except for thermocouples TC 9-4 and 8-2 (Section I) all thermocouples appear to have reached their steady state values in even these short tests. The reason TC 9-4 and TC 8-2 did not stabilize will be explained.

(C) In test 116, thermocouples TC 9-4 and TC 8-2 (Section I) were registering 1500°F and 1300°F, respectively, at shutdown and were still rising rapidly at this time. Each of these thermocouples, as well as TC 4-6, (Section II), were located in the lower part of the horizontally mounted chamber where failure occurred on the fourth test. Since in all likelihood TC 9-4 and TC 8-2 were running uncooled due to the salt formation in the platelets, they never would stabilize. The higher temperatures read by TC 4-6 are probably due to the absence of film cooling from the nonflowing upstream region.

(C) The bulk of the data for the unobstructed regions of chamber Section I, fall near 300°F while the bulk of the data in Section II fall between 500°F and 600°F. This occurs despite the fact that the coolant flow rate and heat flux should be essentially the same in each section. The reason for this occurrence is probably the plugging of coolant channels in the lower part of chamber Section I. As a result a maldistribution of coolant flow occurs, with the coolant which was intended for the lower portion of the platelets now circumvented through the upper portion and overcooling it. It is postulated that, if this plugging did not occur, the bulk of Section I and Section II data would lie between 500°F and 600°F.

VI, D, Heat Transfer (cont.)

(U) No analytically predicted temperatures are given for Sections I and II due to the fact the model predicts a two-phase mixture coming out of the wall. This implies, of course, that liquid coolant is entering the boundary layer. Under these conditions the analytical model is no longer applicable. It can be stated however, that the wall should be at, or slightly above, the coolant saturation temperature, which would place the predicted value in the middle of the test data.

(C) The predicted surface temperature for the throat is 810°F: the data lie between 530°F and 960°F. Again, the thermocouple with the highest temperature is the thermocouple at the bottom of the chamber, TC 2-7. This higher temperature may be the result of a lack of film cooling carry-over from the plugged channels in the chamber section.

(U) Although the data obtained in the 1000 psia ClF_3-cooled tests are not extensive, they do provide some valuable information. The predicted temperatures are well within the range of experimental values, indicating the analytical model is credible. In addition, the temperature response of TC 9-4 (Section I) coupled with that of the throat thermocouples strongly suggests that the throat was adequately cooled and that the throat erosion which did occur was the result of the impingement of erosion products coming from near TC 9-4.

e. General Discussion of Phase I Results

(U) The data from Section II of the 100 psia and 1000 psia N_2O_4-cooled chamber tests and the data from Section II of the 100 psia ClF_3-cooled chamber tests correlate with the predictions made with the analytical heat transfer model when a gas-side film coefficient multiplier of 0.77 to 1.4 is used. This excellent correlation over a wide range of

VI, D, Heat Transfer (cont.)

flow rates indicates that the heat transfer model works reasonably well and, therefore, it can be used to scale to different thrust levels and chamber pressures.

(U) Section II of the N_2O_4- and ClF_3-cooled chambers at 100 psia and Section IV of the N_2O_4-cooled chamber at 1000 psia operated with wall temperatures that were below the design value with coolant flow rates that were approximately equal to, or less than the nominal value (see Tables 9 and 12). It is, therefore, concluded that except for the heat streaking problem the TRANSPIRE concept operated as designed.

(U) The chamber wall in Sections I and III of the N_2O_4-cooled chamber was not smooth. As discussed in Section VI,C these surface irregularities apparently acted as boundary layer trips, as heat marks could be seen to initiate from them (see Figures 50 and 51). These visual observations, when coupled with the abnormally high heat fluxes that were calculated from the Section I and III data at 100 psia and 1000 psia, indicate that surface roughness aggravated the injector streaking problem. On the other hand, the wall of the ClF_3-cooled chamber was much smoother than that of the N_2O_4-cooled chamber (see Figure 17, Section IV,C,4). The thermocouple data from Sections I and III at 100 psia and 1000 psia, could be correlated with the heat transfer model. The heat fluxes to the wall were at least half those observed in the N_2O_4 testing. It is concluded from this comparison that minimization of the coolant flow rate requires a smooth chamber contour.

(C) As can be seen in Figures 57 and 58, temperature differences of as much as 500 to 1000°F occurred between thermocouple locations

VI, D, Heat Transfer (cont.)

in the chamber sections. The high temperature readings occurred on thermocouples that were located in the heat streak patterns. Even in Section II, which was relatively free of visual indication of heat streaks, evidenced heat streaks in the thermal data since the multiplier on the gas-side film coefficient that correlated the data varied from 0.77 to 1.4 depending on location in the chamber. It is obvious, then, that optimization of the coolant flow requirements cannot be accomplished until the injector induced heat streaks are eliminated.

(C) The ClF_3-cooled chamber was not operated at 1000 psia for long enough durations to give conclusive thermal data. However, on the final test the throat operated at steady-state conditions for 1.5 seconds. The temperature of the wall was approximately 790°F. This gives a qualitative indication that operation of a ClF_3 transpiration-cooled chamber at 1000 psia chamber pressure and 1000 lb thrust is feasible.

(U) Reduction of the thermal data for Section III was complicated by the use of instrumented platelets that were approximately twice the thickness of the nominal 0.010 in. thick platelets. New instrumentation techniques are required that will permit instrumentation of 0.010 in. thick platelets. The use of the 0.023 in. thick instrumentation platelets in Section II, which contained platelets that were nominally 0.020 in. thick, proved to be quite satisfactory. The instrument technique of placing thermocouples in the platelets gave good readings of the surface temperatures. The response time of the thermocouples was excellent.

(U) Platelets of a nominal 0.010 in. thickness were used in Section III and platelets of a nominal 0.020 in. thickness were used in Section II. The effect of platelet thickness was to have been determined

VI, D, Heat Transfer (cont.)

by comparing temperatures from the aft end of Section II (Instrumentation Platelet No. 4) to temperatures from the forward end of Section III (Instrumentation Platelet No. 3). The location of the two instrumentation platelets relative to each other is shown in Figure 21 (Section IV,D) for the N_2O_4- and ClF_3-cooled chambers. Flow maldistribution in Section III at the off-nominal conditions precluded evaluation of the effect of platelet thickness. As discussed earlier a flow ratio (actual to nominal) of 4.6 in Section III produces a flow ratio of 11.0 at instrumentation platelet No. 3. Thus, instrumentation platelet No. 3 and No. 4 were never operated at the same flow conditions.

3. Phase II

(U) Heat transfer data and analytical results similar to that obtained in Phase I are shown in Figure 60 for the Phase II chamber. The data are not shown for Section I of the Phase II cooled chamber since no variation was made in the coolant flow rate.

(U) The pressure drop across the platelets in Section II is the difference between the plenum pressure (PTCC-2) for Section II and the chamber pressure (P_c). The flow, therefore, on the instrumentation platelets in this section can be calculated from this pressure difference and the hydraulic resistance of the platelets. The only unknowns are the heat transfer coefficient and the amount of film cooling carryover. Analysis of the data was made assuming no film cooling carryover, carryover from one and carryover from two upstream platelets. Different values for the heat transfer coefficient were assumed for each film carryover condition. Data from a specific thermocouple location could be correlated by a single heat transfer coefficient at all flow conditions only when no film cooling carryover was used in the model. The heat transfer coefficients that are determined in

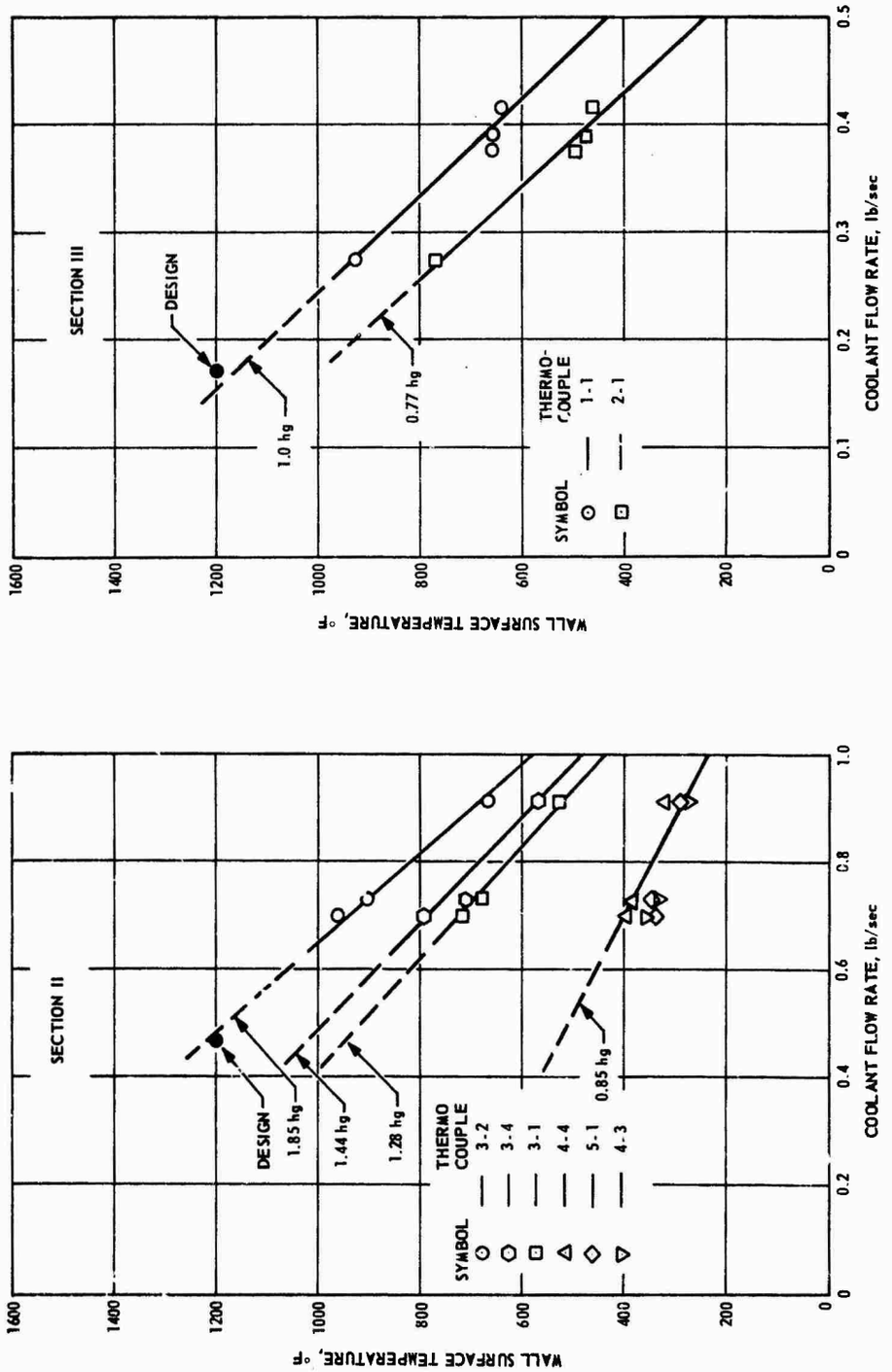

Figure 60. Steady-State Wall Temperatures, Phase II (u)

VI, D, Heat Transfer (cont.)

this manner are unique and are in excellent agreement with the Phase I results. The difference in heat transfer coefficients that correlate the data from the various thermocouples (see Figure 60) is a measure of the circumferential and axial variation heat flux to the wall.

(U) The correlation of the temperature data from chamber Section III, the nozzle section, is more complicated since the gas pressure at the axial position of each instrumentation platelet along the chamber contour is not known. Thus, the precise value of the flow on the platelet is not known. The model was used to correlate the data using back pressure, film cooling carryover and gas-side heat transfer coefficients as variables, assuming that there is no change with coolant flow rate in the heat transfer coefficient or the ratio of the local gas pressure to chamber pressure. Only one combination of pressure ratio and heat transfer coefficient matched the data from each thermocouple at all test conditions. The heat transfer coefficients determined in this manner are consistent with the Phase I results and the Phase II results for Section II (see Figure 60). Film cooling carryover from one upstream platelet correlated the data.

(U) The data for instrumentation platelet No. 1 (throat) correlated with the model for a back pressure that was 78% of chamber pressure. The theoretical pressure profile predicts a pressure in the throat that is about 57% of chamber pressure. Instrumentation platelet No. 2 is located in the convergent section of the nozzle at area ratio -1.2. The gas pressure at this area ratio theoretically is 89.5% of chamber pressure. The data from this instrumentation platelet correlated with flow rates that were obtained assuming 100% P_c as the back pressure. Thus, the data from thermocouples 1-1 and 2-1 (see Section IV,D,2 for location of these thermocouples) were correlated with flow rates that were lower than would be predicted on the basis of the

VI, D, Heat Transfer (cont.)

theoretical pressure gradient in the nozzle. It is not known whether this results because of a bias in the model that is caused by the assumptions and simplifications inherent in the model or whether the particular geometry or blowing effect of the transpiration cooling causes the pressure gradient in the nozzle to differ slightly from the theoretical profile.

(U) As can be seen in Figure 60 the analytical results that correlate the data have been extrapolated to the design conditions. The obvious inference is that the maximum wall temperatures in Sections II and III would be approximately 1200°F, the design value, at the design flow rate. Thus, using the model to extrapolate the data indicates that the TRANSPIRE chamber operated as designed.

VI, Results (cont.)

E. COOLED CHAMBER PERFORMANCE

(U) The test data obtained during the cooled chamber testing were evaluated to determine what performance loss was incurred due to the transpiration cooling system. A tabulated summary of this cooled chamber performance data including a comparison with the uncooled data is shown in Table 19.

1. N_2O_4/AeroZINE 50 Cooled Chamber Performance

(U) The coolant I_{sp} loss listed in Table 19 includes the influence of a change in overall mixture ratio. From Figure 61 it is apparent that the theoretical performance is decreased at the cooled test overall mixture ratio (O/F). These overall O/F's were in excess of stoichiometric. It is probable that less performance loss could have been demonstrated if the core (injector) had been optimized in O/F for peak system performance. (Peak system performance with transpiration cooling or film cooling does not necessarily occur at the optimum O/F for uncooled or regeneratively cooled chambers.)

(U) The N_2O_4-cooled chamber tests were run with an injector mixture ratio of approximately 2. The injector checkout tests, which were used as a performance datum for cooled test evaluation, were run at an O/F of about 1.6. Therefore, the zero coolant case I_{sp} used for comparison herein corresponds to the injector test I_{sp} minus the change in theoretical I_{sp} between O/F of 1.6 and 2.0. This was considered permissible since mixture ratio sensitive losses, such as mixture ratio distribution and nozzle kinetic losses, were found to be negligible. Tables 20 and 21 are a performance summary of the longer duration N_2O_4-cooled tests.

CONFIDENTIAL

(C) TABLE 19

COOLED CHAMBER PERFORMANCE SUMMARY

PROPELLANTS	N_2O_4/A-50					ClF_3/MHF-3				
THRUST LEVEL (LBF)	100			1000		100		1000		
CHAMBER L* (in.)	32			32		32		25		
COOLANT FLOW (% of Total Flow)	0	28	50	0	28	0	26	0	30	33
THRUST CHAMBER MIXTURE RATIO	2.0	3.3	5.0	2.0	3.3	2.4	3.7	2.6	4.1	4.4
TEST I_{sp} VACUUM (Sec.)	233.0	195.0	147.5	235.5	185.5	202.6	189.0	215.5	175.5	167.0
COOLANT LOSS, ΔI_{sp} (Sec.) (Referenced to Uncooled I_{sp})	0	38.0	85.5	0	50.0	0	13.6	0	40.0	48.5
COOLANT LOSS, ΔI_{sp} (Percent) (Referenced to Uncooled I_{sp})	0	16.2	36.7	0	21.3	0	6.7	0	18.5	22.5

(C) TABLE 20

N_2O_4-COOLED CHAMBER PERFORMANCE (100 LB THRUST) (U)

Test No.	Injector Mixture Ratio $(O/F)_i$	Theo. I_{sp} @ $(O/F)_i$ (sec)	Total Mixture Ratio $(O/F)_t$	Theo. I_{sp} @ $(O/F)_t$ (sec)	I_{sp} Test, Vac (sec)	% Theo. I_{sp} @ $(O/F)_t$	Flow Ratio $\dot{w}_c/\dot{w}_t$
1K-3C-							
104	1.99	245.6	6.970	180.0	116.8	64.8%	0.624
106	1.98	245.7	6.262	184.0	113.1	61.5	0.588
109	1.98	245.7	5.354	192.0	133.6	69.6	0.530
110	1.98	245.7	4.951	196.7	132.4	67.3	0.498
111	1.95	246.0	4.606	201.7	134.8	66.8	0.473
113	2.00	245.5	4.388	205.3	161.0	78.4	0.442
121	2.00	245.5	4.098	210.5	173.5	82.4	0.410
122	1.96	245.9	4.042	211.4	173.3	81.9	0.411
123	1.98	245.7	4.049	211.3	174.1	82.3	0.409
129	2.11	244.1	4.235	208.0	169.4	81.4	0.405
143	2.18	243.3	3.765	216.5	181.2	83.6	0.330
144	2.18	243.3	3.740	217.0	182.4	84.0	0.329
145	2.18	243.3	3.758	216.6	184.3	85.0	0.329
146	2.09	--	3.589	--	--	--	--
148	2.16	243.5	3.580	220.0	186.6	84.8	0.309
151	2.13	243.9	3.526	220.7	189.2	85.7	0.306
152	2.14	243.8	3.543	221.0	189.7	85.8	0.306
154	2.18	243.3	3.615	219.5	201.6	91.8	0.309
159	2.13	243.9	3.322	224.8	201.2	89.5	0.275
162	2.14	243.8	3.291	225.2	199.3	88.4	0.266
165	2.17	243.4	3.336	224.5	204.6	91.1	0.267
166	2.15	243.6	3.305	225.0	195.6	86.9	0.266
168	2.13	243.9	3.230	226.2	195.4	86.3	0.259
171	2.16	243.5	3.253	225.5	205.6	91.1	0.257
172	2.16	243.5	3.267	225.4	197.9	87.7	0.258
174	2.09	244.3	3.123	228.3	199.0	87.1	0.249
177	2.16	243.5	3.220	226.7	199.3	87.9	0.248
181	2.14	243.8	3.184	227.3	196.8	86.5	0.248
185	2.13	243.9	3.309	225.0	193.4	85.9	0.271
189	2.18	243.3	3.208	227.0	205.2	90.3	0.243
190	2.13	243.9	3.151	227.6	193.6	85.0	0.244
192	2.19	243.4	3.223	226.2	191.5	84.6	0.244
193	2.17	243.4	3.195	227.0	194.7	85.7	0.243

(C) TABLE 21

N_2O_4-COOLED CHAMBER PERFORMANCE (1000 LB) THRUST (U)

Test No.	Injector Mixture Ratio $(O/F)_i$	Theo. I_{sp} @ $(O/F)_i$ (sec)	Total Mixture Ratio $(O/F)_t$	Theo. I_{sp} @ $(O/F)_t$ (sec)	I_{sp} Test, Vac (sec)	% Theo. I_{sp} $(O/F)_t$	Flow Ratio $\dot{w}_c/\dot{w}_t$
1K-3C							
198	1.95	252.5	3.07	231.0	177.4	76.8	0.276
205	2.00	252.0	3.23	227.5	184.0	80.9	0.291
207	2.06	251.0	3.26	227.0	177.7	78.3	0.282
210	2.06	251.0	3.26	227.0	184.1	82.1	0.282
211	2.07	251.0	3.27	226.7	182.9	80.6	0.281
212	2.07	251.0	3.27	226.7	183.3	80.8	0.282
213	2.08	250.7	3.29	226.2	182.8	80.8	0.282
214	2.06	251.0	3.27	226.7	184.1	81.2	0.282
215	2.08	250.7	3.29	226.2	185.3	81.9	0.283
216	2.06	251.0	3.27	226.7	186.4	82.2	0.282
218	2.07	251.0	3.28	226.5	184.4	81.4	0.283
219	2.21	248.5	3.50	221.7	179.1	80.7	0.286
220	2.02	251.5	3.19	228.3	183.9	80.5	0.281

VI, E. Cooled Chamber Performance (cont.)

(U) Since the same injector and the same internal chamber-nozzle contour was used for both the uncooled chamber tests and the cooled chamber tests, the losses from the uncooled tests were applied as a constant percentage of theoretical I_{sp} for the cooled tests. Thus, the area between the uncooled test losses and the cooled test curve in Figure 61 was attributed to the coolant loss.

(U) Figure 61 also includes two curves corresponding to performance prediction models. The lower curve on each plot assumes that there is no energy exchange between the coolant and core and, therefore, only the core contributes to I_{sp}, i.e.:

$$I_{sp} = \left(\frac{\dot{w}_C}{\dot{w}_t}\right) I_{sp,C} \qquad (6)$$

Where:

$\dot{w}_C$ = Injector (core) flow rate

$\dot{w}_t$ = Total (injector plus coolant) flow rate

$I_{sp,C}$ = I_{sp} of core at injector mixture ratio.

(U) The other performance model curve assumes that energy is exchanged from the core to the coolant until the coolant and core are in thermal equilibrium. The I_{sp} of each component is then calculated as described in Appendix II, and the summation is a prediction of performance. The assumption was made that combustion between the core and coolant was negligible due to the small chemical reaction potential between the two streams with the

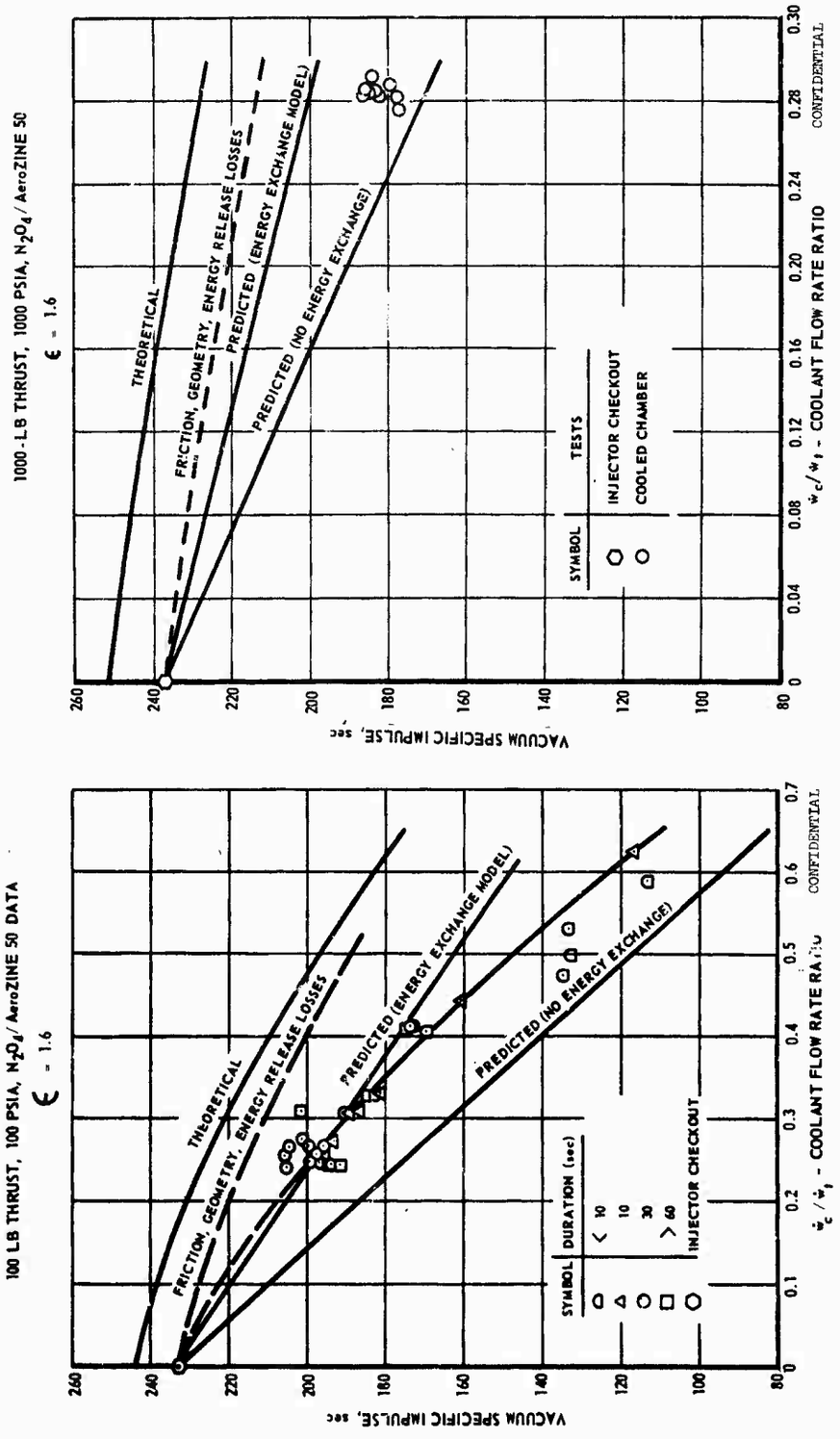

Figure 61. Effect of N_2O_4 Coolant Flow Rate on Performance (u)

VI, E, Cooled Chamber Performance (cont.)

core operating near stoichiometric mixture ratio during the N_2O_4-cooled tests (2.0 test vs 2.2 stoichiometric). With the assumption of no combustion between the core and the coolant, the thermal equilibrium model yields the higher predicted performance.

(U) It is obvious from Figure 61 that the correlation of the 100 psia data with the thermal equilibrium model improves with the reduction in coolant flow rate. This suggests that the temperature reached by the coolant prior to expansion varies with the coolant flow rate and that the performance at 1000 psia will approach that predicted by the complete energy exchange model as coolant flow rates are reduced.

(U) The temperature of the coolant is influenced by its dissociation. The three reactions that occur are:

$$N_2O_4 \rightleftharpoons 2\ NO_2$$

$$2\ NO_2 \rightleftharpoons 2\ NO+O_2$$

$$2\ NO \longrightarrow N_2+O_2$$

The first two reactions occur very rapidly relative to the last reaction. The first two reactions are endothermic; the last reaction is exothermic. The NO temperature must be above 2500°R for its dissociation to occur. If the coolant is heated to 2500°R a constant enthalpy process during the exothermic reaction will produce a coolant temperature of approximately 5000°R.

IV, E, Cooled Chamber Performance (cont.)

(C) The thermal model was used in connection with the test specific impulses to evaluate the coolant temperatures. The resultant performance prediction as a function of the assumed amount of heat transferred to the coolant (expressed in terms of final coolant temperature) is plotted on Figure 62. From the figure it is seen that at 1000 psia the test I_{sp} of 185 sec occurred at a final coolant temperature of 1050°R and a final core temperature of 5630°R. In contrast, for the 100 psia case at a comparable flow ratio th test I_{sp} correlated with the point of coolant-core thermal equilibrium.

(U) Several conclusions can be drawn from Figure 62: (1) the temperature acquired by the coolant apparently is a function of the mass flow rate for a fixed nozzle size, (2) the temperature acquired by the coolant at a given flow rate ($\dot{w}_c/\dot{w}_t$) depends on thrust level and/or chamber pressure, and (3) the exothermic dissociation of NO to N_2 and O_2 apparently makes a significant contribution to the specific impulse contribution of the coolant.

2. ClF_3/MHF-3 Cooled Chamber Performance

(U) Tables 22 and 23 present a performance summary for the longer duration 32 L* 100 lb thrust Phase I and 25 L* 1000 lb thrust Phase II ClF_3 -cooled chamber tests. Since the coolant distribution during the 32 L* 1000 lb Phase I tests was irregular due to the presence of salts in the platelets and since the tests were very short, no performance evaluation was attempted. The 100 lb thrust 32 L* chamber data and the 1000 lb thrust 25 L* chamber data are plotted in Figure 63 which shows I_{sp} as a function of the coolant flow fraction. The performance prediction model used for the N_2O_4 - cooled chambers tests as discussed in Appendix II was applied to the ClF_3 - cooled chamber test data and the results are also shown in Figure 63.

(C) TABLE 22

ClF_3-COOLED 32 L* CHAMBER PERFORMANCE (100 LB THRUST) (U)

Test No.	Injector Mixture Ratio $(O/F)_i$	Theo. I_{sp} @ $(O/F)_i$ (sec)	Total Mixture Ratio $(O/F)_t$	Theo. I_{sp} @ $(O/F)_t$ (sec)	I_{sp}, Test (Vac) (sec)	% Theo. I_{sp} @ $(O/F)_t$	Coolant Flow Ratio $\dot{w}_c/\dot{w}_t$
1K-3D-							
104*	2.33	248.3	4.45	228.5	207.4	90.8	0.475
108*	2.34	248.3	3.86	239.2	190.1	79.5	0.312
110*	2.35	248.4	3.86	239.2	203.2	85.0	0.311
111*	2.38	248.4	3.79	240.1	198.5	82.6	0.293
112*	2.33	248.3	3.70	241.2	208.5	86.4	0.291
113	2.43	248.8	3.69	241.3	187.7	77.7	0.268
114	2.42	248.7	3.67	241.5	190.1	78.7	0.267

(C) TABLE 23

ClF_3-COOLED 25 L* CHAMBER PERFORMANCE (1000 LB THRUST) (U)

1K-5B-							
102	.835	228	1.84	249	158.0	63.4	34.8
105	2.66	253	4.43	230	167.9	73.0	32.6
106	2.65	253	4.43	230	166.8	72.5	32.6
109	2.69	253	4.26	234	174.2	74.4	29.8
110	2.62	253	4.13	236	176.7	74.8	29.4
111	2.70	253	4.04	238	174.0	73.0	26.4
112	2.70	253	4.02	238	175.7	73.8	26.2

*Water leak into chamber invalidates I_{sp} calculation.

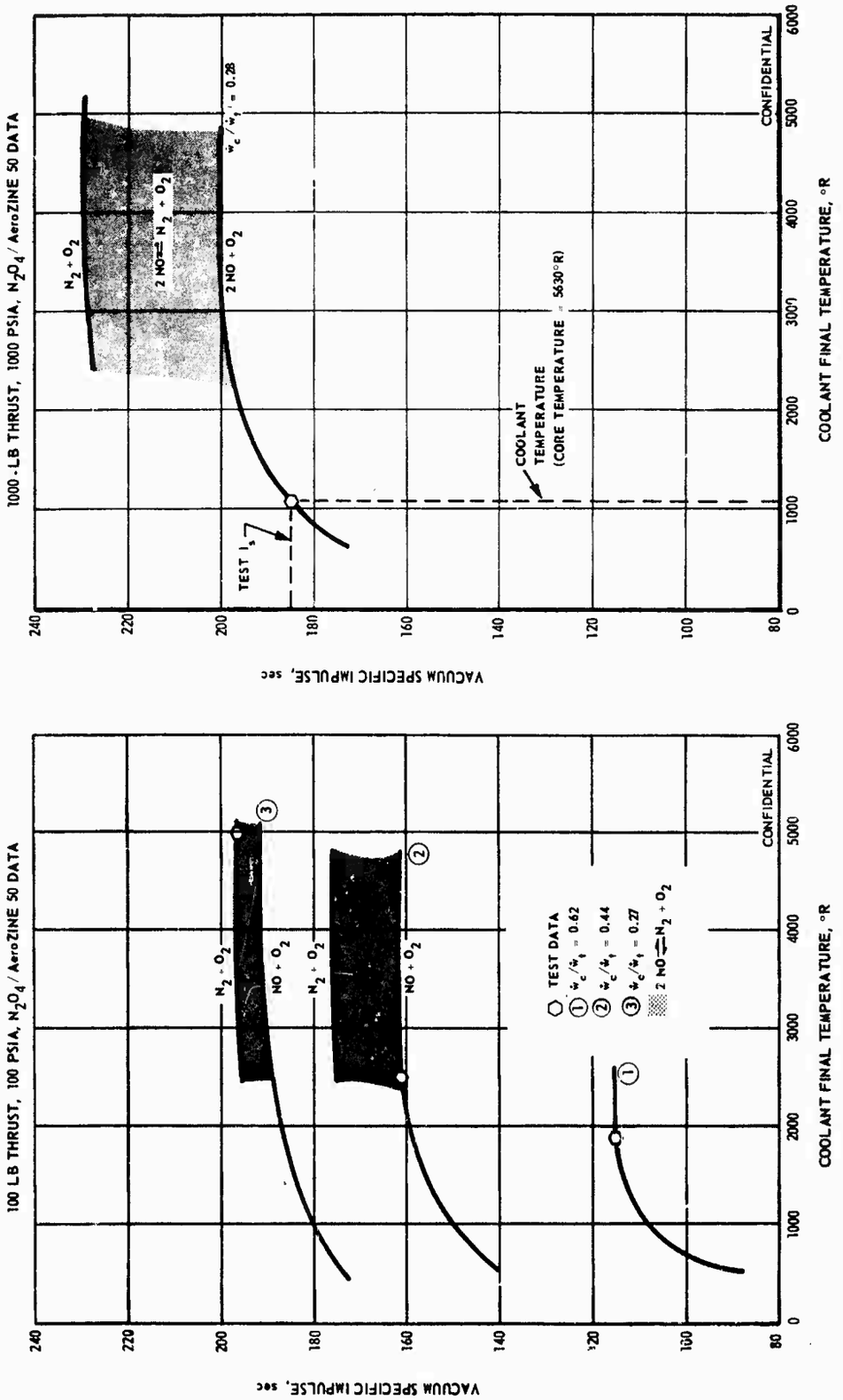

Figure 62. Effect of N_2O_4 Coolant Final Temperature on Performance (u)

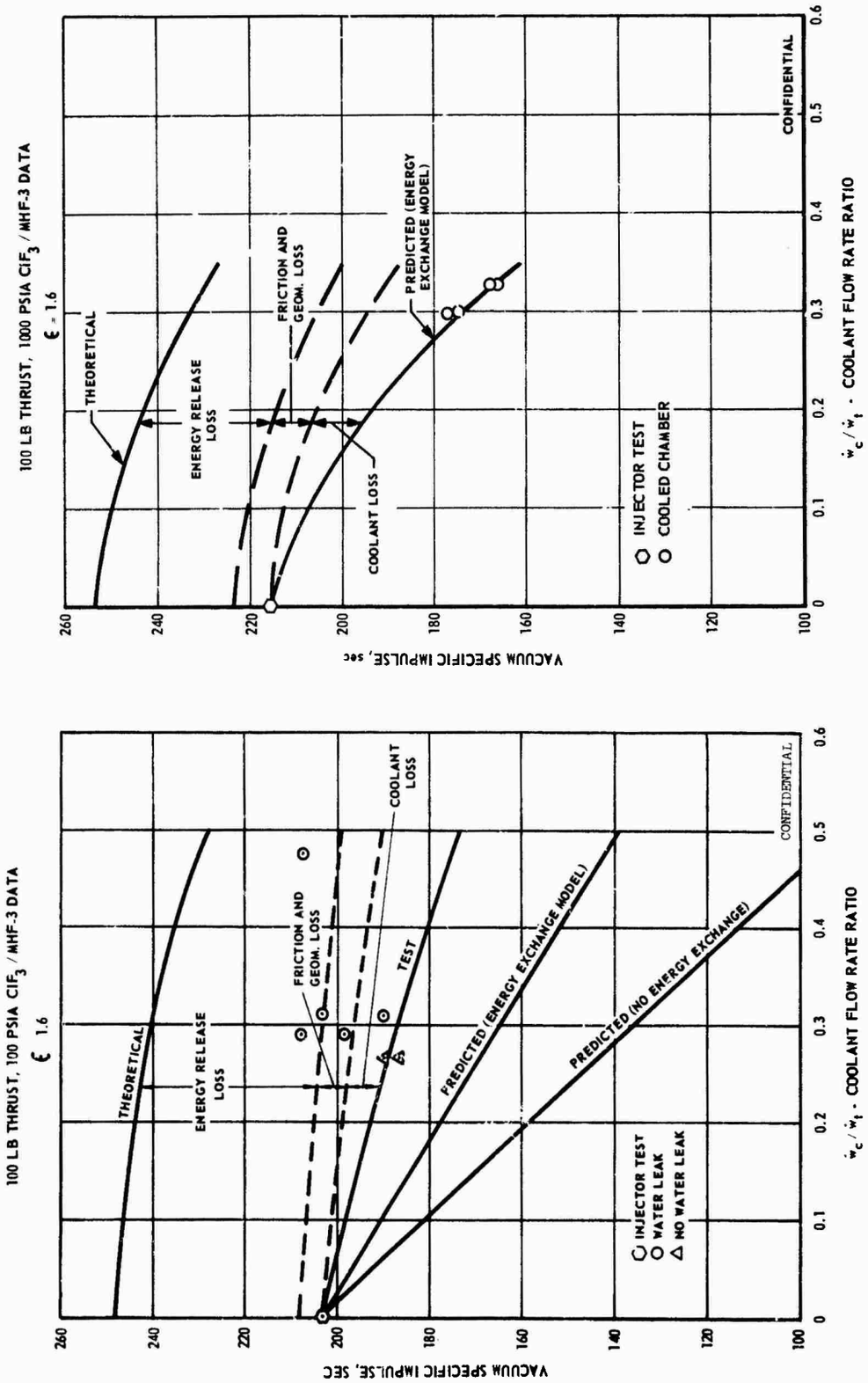

Figure 63. Effect of ClF_3 Coolant Flow Rate on Performance (u)

VI, E, Cooled Chamber Performance (cont.)

(U) As discussed in Section V,D,1,b a water leak occurred during some of the 100 lb thrust Phase I tests. Since the water leak into the chamber increased the flow rate by an unknown amount which could not be included in the I_{sp} calculations it resulted in a higher apparent I_{sp}. Data from test 1K-3D-104 were plotted in Figure 64 as a function of test duration to illustrate the effect of the water leak. The marked increase in performance about 35 seconds into the test is interpreted as an indication that the water leak became significant at that point. The coolant manifold was pressurized before and after the test; no water leakage into the chamber was observed before the test, but water was observed in the chamber at the end of the test.

(U) As can be seen in Figure 63 for the 100 lb thrust data the I_{sp} obtained on some of the tests is greater than that obtained with no coolant (the injector baseline performance tests). Water was leaking into the chamber at the conclusion of these tests. Two tests have been identified in Figure 63 and Table 22 as providing data unaffected by a water leak. They are tests 1K-3D-113 and -114. The water coolant circuit was pressurized before and after test 1K-3D-113 and no leakage of water into the chamber was observed. As shown in Figure 34 (Section V,D) the change in chamber Section I plenum pressure indicates that the water leak occurred about 20-25 seconds into test 1K-3D-114. Therefore, it was concluded that only tests -113 and -114 (prior to the water leak) provided valid performance data.

(U) There is a significant difference in the correlation of the 100 lb thrust and 1000 lb thrust data with the analytical model. As shown in Figure 63 on the basis of two tests with no water leak the 100 lb thrust experimental data are higher than the model predicts; the 1000 lb thrust experimental data correlate quite well with the model prediction. (The 1000 lb

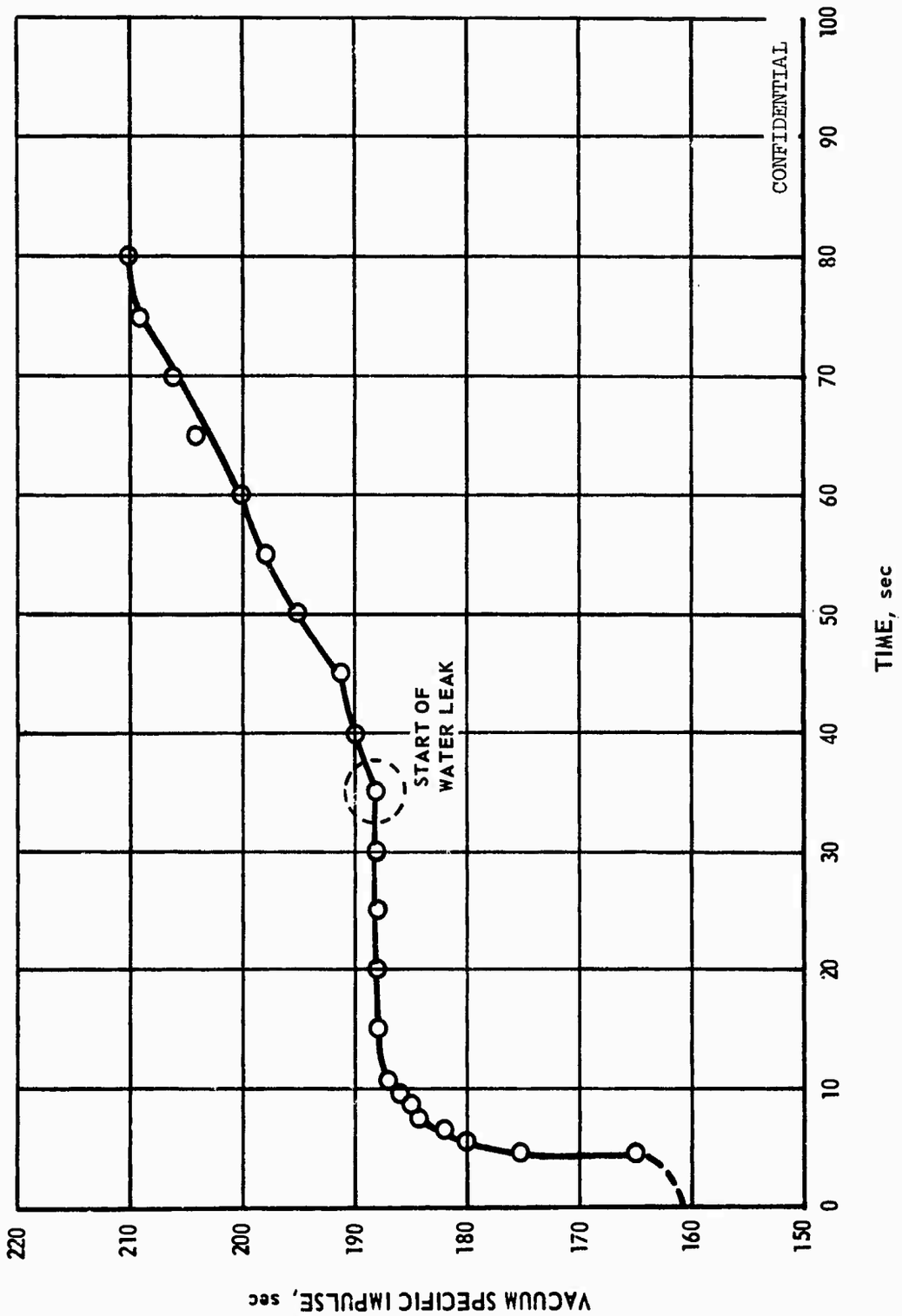

Figure 64. Effect of Chamber Water Leak on Performance (u)

VI, E, Cooled Chamber Performance (cont.)

thrust data from test 1KK-5B-112 was not included because the nozzle erosion makes it impossible to define the nozzle geometry.) There is a somewhat remote possibility that there was an unobserved water leak during test -113 which invalidates the results from tests -113 and -114. However, it is more likely that the difference results from combustion of some of the oxidizer coolant.

(U) The model assumes that there is no combustion between the core and the coolant. The N_2O_4-cooled chamber tests were made with injector mixture ratio that ranged from 1.95 to 2.2. Since stoichiometric* is approximately 2.2 there is very little chemical potential to cause combustion of the N_2O_4 coolant. Thus, the N_2O_4-cooled chamber data are consistent with this assumption in the model. The 100 lb thrust ClF_3-cooled chamber tests were made with an injector O/F that was 2.33 to 2.43; stoichiometric O/F is approximately 3.5*. Thus, there is considerable chemical potential for combustion of some of the coolant. For the 1000 lb thrust ClF_3-cooled chamber tests the injector mixture ratio was 2.6 to 2.7. Consequently less chemical potential was available between the coolant and the core, which may account for the agreement of the 1000 lb thrust data with the model.

(U) It is obvious from the analysis of the 1000 lb thrust data shown in Figure 63 that there are two significant factors that affect performance. The first is the cooling loss; the second is a mixture ratio loss. If there were no loss at all due to the unheated coolant there is still considerable loss due to operation at a high thrust chamber mixture ratio. Thus, it appears that considerable improvement in performance may result from operation of the cooled chambers at a lower injector mixture ratio.

*Stoichiometric is here defined as the O/F producing maximum enthalpy.

IV, E, Cooled Chamber Performance (cont.)

3. General Discussion

(U) The performance of the TRANSPIRE chambers can be improved by reduction of the coolant flow rate. Figure 65 shows the loss of performance due to the coolant for operation of the ClF_3- and N_2O_4-cooled chambers at 100 lb thrust and at 1000 lb thrust. The final test conditions and the design conditions are shown on this figure to summarize actual and potential performance. Only the ClF_3-cooled chamber at 100 lb thrust, 100 psia chamber pressure was operated with a coolant flow rate that was almost equal to the design value. The performance penalty for transpiration cooling chambers in the 100 to 1000 lb thrust range is predicted to be 8-9% ΔI_{sp}.

(U) The deviation of the 1000 psia N_2O_4 performance loss data from the rest of the data (Figure 65) is probably due to nozzle geometry differences between the cooled and ablative chambers. Discoloration, heat marks, and erosion on the aft end of the ablative and cooled chambers indicated that the exhaust plume attached to the aft end of the chambers during all 1000 psia testing, except for the 1000 psia N_2O_4 injector checkout tests. The silica buildup that occurred during these checkout tests formed a nozzle extension (see Figure 40) that precluded attachment. The performance degradation curve for N_2O_4 at 1000 psia (Figure 65) is probably higher than the rest of the data because the cooled chamber data includes nozzle losses (due to attachment) that did not occur during the injector checkout testing. TRANSPIRE testing on a company-sponsored program using ClF_3 at 1000 psia and a 7:1 water-cooled nozzle extension indicates that the attachment of the exhaust plume introduces a performance loss that is approximately 2 to 4% ΔI_{sp} at a coolant flow rate that is 30% of the total flow rate.

IV, E, Cooled Chamber Performance (cont.)

(U) Although the data used for the 100 psia ClF_3 performance loss determination were taken from tests in which no water leak into the chamber was detected there is a distinct possibility that a leak existed and was not detected. The additional unknown water mass would increase performance. Thus, the apparent low performance degradation for ClF_3 at 100 psia may be due to the more fuel rich mixture ratio conditions, but at the same time may be the result of a water leak.

(U) Because of the difference in nozzle geometries between the 1000 psia N_2O_4 ablative and cooled chambers, and because the 100 psia ClF_3 data could be affected by an undetected water leak, the 100 psia N_2O_4 and the 1000 psia ClF_3 performance data are considered to be the most reliable data.

(U) The performance loss that occurred when the ClF_3-cooled chamber was fired at 1000 psia with an injector O/F of 0.835 was estimated to be 11.5% ΔI_{sp}. The coolant flow rate was 35% of the total propellant flow rate. With the normal injector O/F (2.6 to 2.7) the performance loss at that coolant flow rate would be about doubled (see Figure 65). This substantial decrease in performance loss at low injector O/F plus the degradation that results because the high coolant flow rates produce high mixture ratios suggest that cooled chamber performance can be improved by operating with a lower (more fuel rich) injector mixture ratio. Testing on a company program with a 1:1 ClF_3-cooled 1000 psia TRANSPIRE chamber has shown that lower injector mixture ratios improve performance, but that this gain may be partially offset by an increased coolant flow required to offset increased wall temperatures. The test results are summarized in Table 24. C* was used as a measure of performance since attachment of the exhaust plume to area ratio 25 made I_{sp} difficult to evaluate.

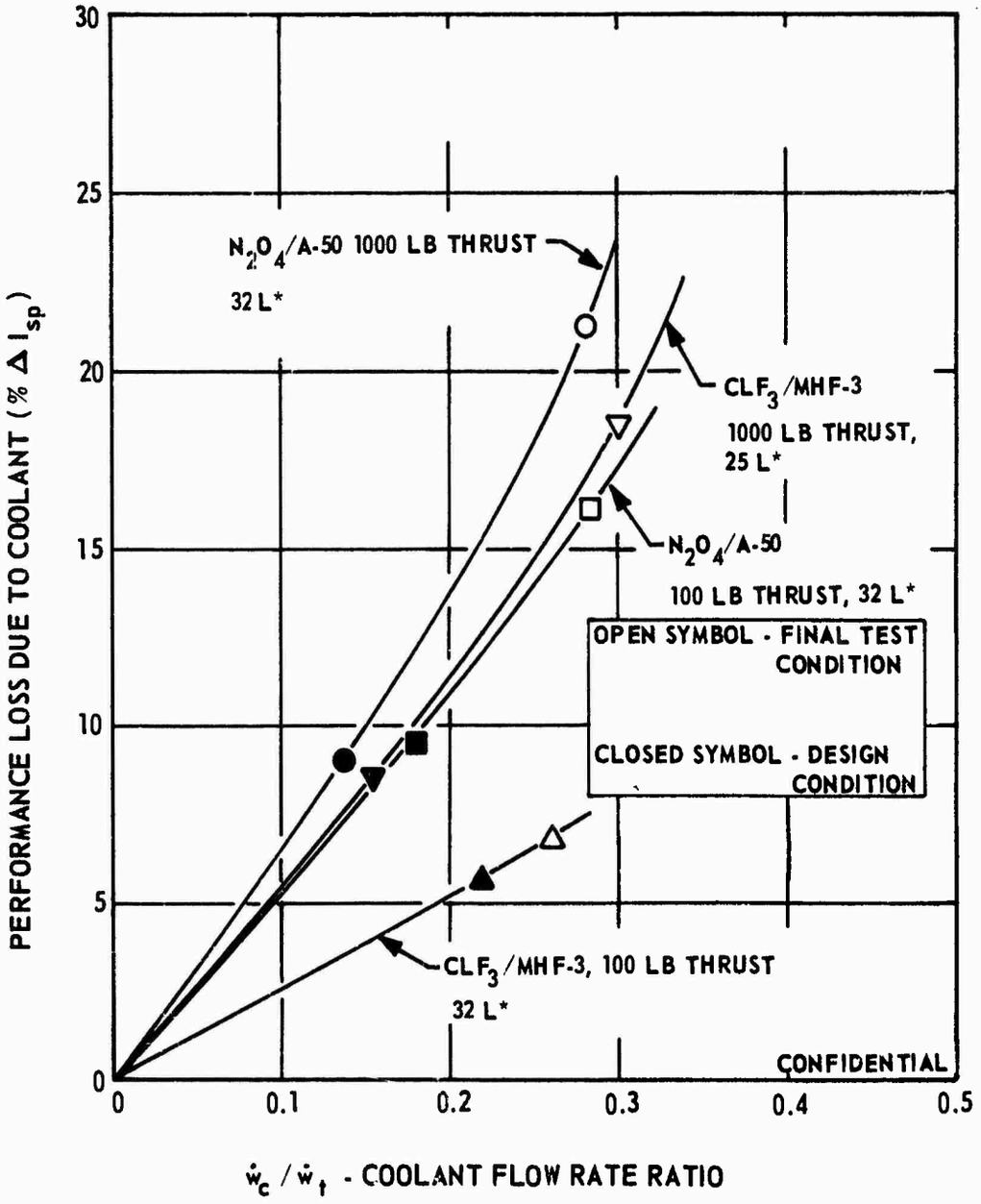

Figure 65. Performance Loss Due to Coolant (u)

IV, E, Cooled Chamber Performance (cont.)

(C) TABLE 24

EFFECT OF INJECTOR O/F ON PERFORMANCE (U)

Test No.	$\dot{w}_c/\dot{w}_t$	O/F Injector	O/F Chamber	ΔC^* (%)	Wall Temperatures (°F) TC 2-2	TC 3-4
1K-5C-102	0.268	2.71	4.07	13.8	1209	818
-103	0.267	2.72	4.07	14.2	1171	853
-104	0.263	2.55	3.82	13.4	1253	886
-105	0.256	2.285	3.41	11.5	1307	1017

(U) Figure 66 shows the performance loss that is predicted for high thrust TRANSPIRE chambers. The data on the figure is the 100 lb N_2O_4 and the 1000 ib thrust Phase II ClF_3 data. The curve in Figure 66 differs slightly from the 100 psia N_2O_4 and 1000 psia ClF_3 curves in Figure 65; the curves in Figure 65 are based on the model prediction of performance; the curve in Figure 66 is based on the data. Only a few data points are shown on Figure 66 for clarity. As the thrust level is increased the ratio of surface area to volume (propellant flow rate) decreases. Thus, the amount of coolant required at higher thrust levels increases in absolute value roughly in proportion to the surface area, but decreases in terms of the fraction of the total propellant flow rate. The cooled chamber data have been extrapolated to zero performance degradation at zero coolant flow in Figure 66 and the coolant flow requirements for 25 L* chambers at various thrust levels have been shown on the curve to indicate the performance loss that can be expected at the higher thrust levels.

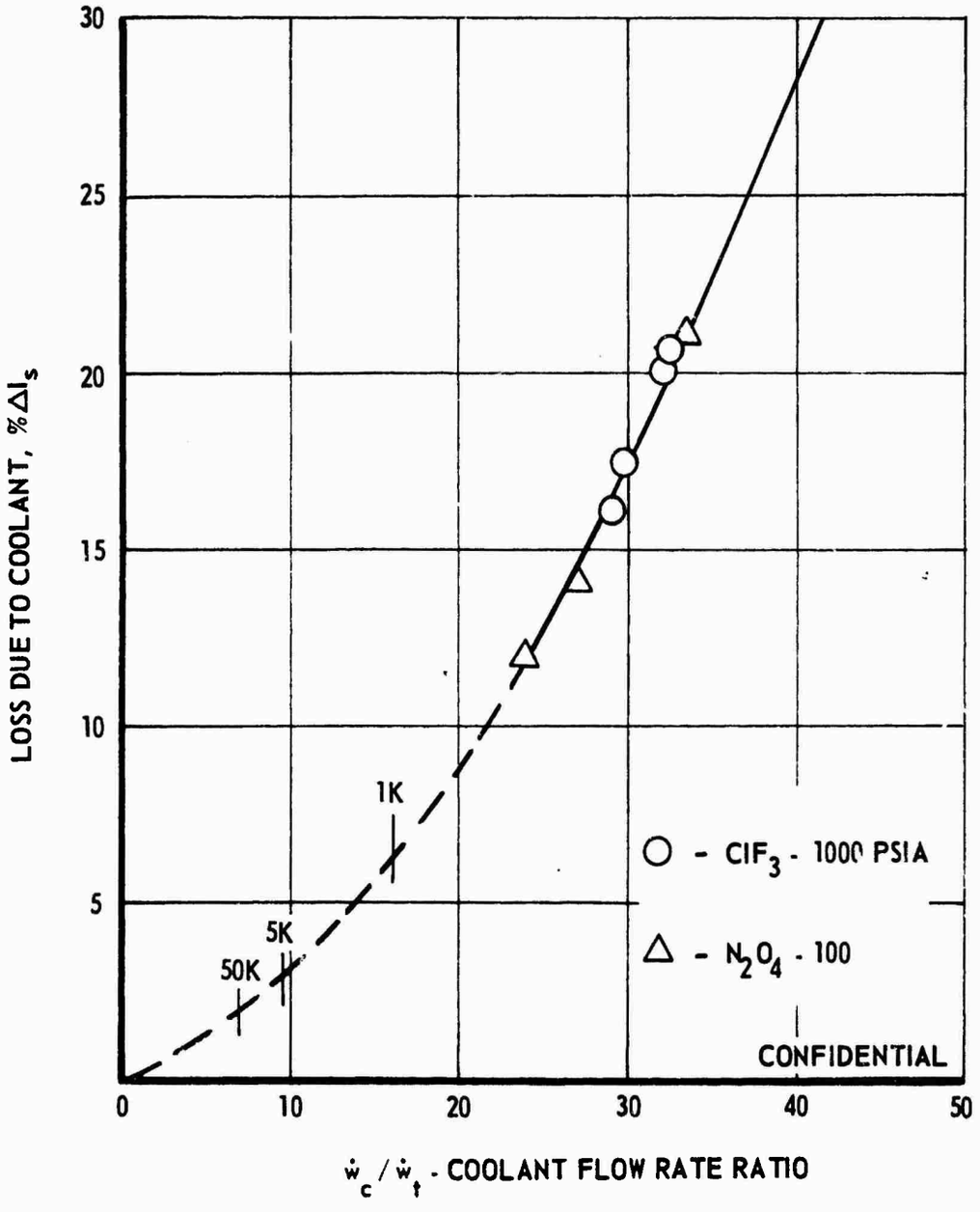

Figure 66. Performance Degradation Due to Coolant (u)

VII. SCALING

(U) This section discusses the applicability of the TRANSPIRE concept to a thrust chamber operating at 1000 psia and 5000 lb thrust. The correlation between anticipated and test results will be reviewed; recommended modifications will be discussed; the method of scaling will be exemplified.

A. CORRELATION BETWEEN TEST AND ANTICIPATED RESULTS

(U) The ClF_3-cooled nickel TRANSPIRE chamber was designed to operate with a 1200°F surface temperature. The N_2O_4-cooled stainless steel TRANSPIRE chamber was designed to operate at a 1500°F surface temperature. The coolant flow rates (nominal flow rates) that were predicted to produce these temperatures are given in Table 25 along with the actual steady state operating temperatures and flow rates. The coolant flow to each chamber section was not reduced to its minimum value.

(U) Injector streaking and surface roughness produced localized areas of abnormally high heat fluxes. In order to adequately cool these areas excessive coolant flow was required. As much as 80% of the chamber surface area was overcooled. In Section II of the N_2O_4- and ClF_3-cooled chambers (100 psia) and Section IV of the N_2O_4-cooled chamber (1000 psia) the heat streaks were not as pronounced. These chamber sections operated at temperatures below the design value with flow rates that were equal to (approximately) or less than nominal. The film cooling effect from overcooled upstream chamber sections probably influenced these results. However, it is apparent that: (1) in the absence of heat streaks the correlations between anticipated and actual test results was good and (2) the heat streaking must be mitigated if coolant flow rates are to be optimized.

(U) The correlation between the test data and the heat transfer and performance models is discussed in Section VI,D and Section VI,E. Graphical presentations are made in these sections of the data and the predicted results.

(C) TABLE 25

COOLED CHAMBER FINAL TEST CONDITIONS (U)

		100 psia				1000 psia			
Propellants	Section	$\dot{w}_c$ Coolant Flow Rate (lb/sec)	$\dot{w}_N$ Nominal Coolant Flow Rate (lb/sec)	$\frac{\dot{w}_c}{\dot{w}_N}$	Maximum Steady State Temperature (°F)	$\dot{w}_c$ Coolant Flow Rate (lb/sec)	$\dot{w}_N$ Nominal Coolant Flow Rate (lb/sec)	$\frac{\dot{w}_c}{\dot{w}_N}$	Maximum Steady State Temperature (°R)
N_2O_4/	I	0.0628	0.0353	1.78	1504	0.622	0.289	2.15	1650
AeroZINE 50	II	0.0216	0.0342	0.63	1200	0.560	0.280	2.00	1575
	III	0.0353	0.0077	4.59	1282	0.298	0.092	3.24	1500
	IV	0.0161	0.0050	3.22	400	0.093	0.078	1.19	1050
ClF_3/MHF-3	I	0.077	0.057	1.35	1136	0.519	0.216	2.4	1550
	II	0.032	0.055	0.58	954	0.702	0.466	1.50	961
	III	0.047	0.0125	3.76	655	0.275	0.173	1.59	925
	IV	0.015	0.0081	1.85	1003	---	---	---	---

VII, Scaling (cont.)

B. RECOMMENDED MODIFICATIONS

(U) For utilization of the TRANSPIRE concept in a 5000 lb thrust, 1000 psia application no changes are recommended to the basic design. The flow metering and hot spot prevention features worked as designed (see Section VI,C). The clocking feature not only effected substantial cost savings since the chamber was constructed with only seven platelet designs, but it provided the flexibility that permitted last minute design changes to be incorporated. For example, it permitted the flow to the instrumentation platelets to be set according to their thickness, which could not be measured until after fabrication of the platelets. The fabrication of metering platelets from sheet stock, the thickness of which can be controlled and measured, resulted in metering grooves that gave a predictable flow that was not dependent on the platelet fabrication process.

(U) Some minor changes are recommended. The inlet to the platelets should be redesigned to provide support for the thin metering platelet so that it cannot block the inlet (see Section VI,B). Improved instrumentation that will permit use of 0.010 inch instrumented platelets among 0.010 inch thick platelets in the critical throat area will improve data acquisition and interpretation and will simplify analysis, in addition to insuring that the instrumentation platelet is behaving exactly like its neighbors. The divider seal rings (see Section IV,C,3,a) should be constructed using a distribution type platelet so that they can be cooled by coolant flow on both sides and not rely on film cooling as is presently done. Two to three platelets upstream of each divider platelet were clocked to give maximum coolant flow to provide the film cooling for the divider. Because of film cooling carryover the thermocouples in the instrumentation platelets located approximately 0.050 to 0.10 inches downstream of the dividers consistently read low compared to the other thermocouple locations.

VII, B, Recommended Modifications (cont.)

(U) Other than elimination of injector streaking (which is a separate problem), the only major modification that is recommended is to the assembly procedure. The use of holes etched in the platelets in connection with index rods to align the platelets in final assembly was unsatisfactory. Because many of the index holes were oversized the fit of the rod in the index hole was not precise enough to return every platelet to the exact position it occupied during machining. Some platelets therefore were recessed on one side of the chamber and protruded from the wall on the opposite side. In Phase II the diameter of the index holes was enlarged by EDM while the entire stack was clamped in the machining fixture. This was done to insure that the holes in all the platelets were the same size and to ensure proper alignment of the holes. A tightly fitting index rod was fitted into the holes and then the chamber contour was machined. This method of mating the index rod to the holes improved the alignment, but because of tolerances perfect alignment was not obtained upon reassembly after cleaning. It is recommended that modular construction be used, and that once machined the modules should not be disassembled. The platelets should be cleaned, bonded together by welding or brazing, and the contour should be dry machined. The metal that is flowed into the coolant passages by the machining operation can be removed by electropolish. Instrumentation platelets can be located between modules.

VII, Scaling (cont.)

C. METHOD OF SCALING

(U) In going from the experimental conditions to new thrust levels not only the coolant flow requirements must be determined, but also the optimum platelet thickness, and the wall thickness required to prevent heat penetration to the flow metering channels. In determining the coolant flow required to maintain a given wall temperature the heats of reaction of the coolant and its film cooling effect must be considered.

(U) A simple formula for scaling that defines the critical controlling parameters can be developed from equation (13) of Appendix I:

$$\frac{T - T_{c,o}}{T_g - T_{c,o}} = \frac{e^{r_1(X-L)}}{1 + \frac{K_m r_1}{h_g}} \qquad (7)$$

Where $r_1 = -\frac{A}{2} + \sqrt{\frac{A^2}{4} + B}$

$A = h_L/GC_p t$

$B = h_L/K_m t$

C_p = Coolant heat capacity

G = Coolant mass velocity (based on depth of flow channel plus platelet thickness)

h_g = Gas-side heat transfer coefficient

h_L = Liquid side heat transfer coefficient

K_m = Platelet thermal conductivity

L = Distance from point of coolant inlet to hot gas surface

t = Platelet half thickness

T = Platelet temperature at X

$T_{c,o}$ = Coolant inlet temperature

T_g = Gas temperature

VII, C, Method of Scaling (cont.)

T_w = Surface temperature of wall (platelet)
X = Distance from point of coolant inlet

Solving for the temperature on the surface (X=L) and substituting for the terms r_1, A and B, this equation becomes:

$$\frac{T_w - T_{c,o}}{T_g - T_{c,o}} = \frac{1}{1 + \frac{K_m h_L}{h_g G C_p t}\left[\sqrt{\frac{1}{4} + \frac{G^2 C_p^2 t}{h_L K_m}} - \frac{1}{2}\right]} \qquad (8)$$

(U) Another form of this equation that is useful in scaling is:

$$\frac{T_g - T_w}{T_g - T_{c,o}} = \frac{1}{1 + \frac{h_g}{GC_p}\left[\frac{1}{2} + \sqrt{\frac{1}{4} + \frac{G^2 C_p^2 t}{h_L K_m}}\right]} \qquad (9)$$

If the recovery temperature at the wall is used for T_g no credit is taken for film cooling and the results become very conservative in high heat flux environments. The effect of chamber pressure, thrust, etc. are handled through the gas-side heat transfer coefficient.

(U) The analytical model described in Appendix I uses equation 13 of Appendix I to calculate the temperature distribution in the platelet. The temperature of the coolant as it exits from the platelet is then used in the film cooling calculation to determine the gas driving temperature. The model iterates this calculational procedure until the average boundary layer temperature across the end of the platelet equals the gas temperature used in equation 13.

VII, C, Method of Scaling (cont.)

(U) In the actual design of a chamber the wall temperature is specified and the computerized model solves for the coolant flow rate at specified axial stations. Thus the axial distribution of the coolant is determined. The temperature distribution in the platelet is also obtained and is used to select a wall thickness that insures that heat does not penetrate to the metering grooves. The coolant flow distribution and wall temperature profile are then used in the performance model to predict the performance loss due to cooling.

(U) This technique was applied to a TRANSPIRE chamber designed for operation at 5000 lb thrust, 1000 psia chamber pressure with ClF_3/MHF-3 as the propellants and ClF_3 as the coolant. A chamber L* of 34 was used which is the value of the L* of the Phase I chambers. With no heat streaking the coolant flow required to maintain a 1200°F wall temperature is 12.5% of the total propellant flow rate. The predicted coolant flow for the 1000 lb thrust, 1000 psia Phase I chamber is 19.5% and for the 100 lb thrust, 100 psia chamber is 22%. These calculations are conservative. A multiplier of 2.0 was used for the gas side heat transfer coefficient in the cylindrical section of the chamber and was decreased linearly with contraction ratio to a value of 1.0 in the throat. No allowance was made for film cooling carryover from upstream platelets.

REFERENCES

1. Liquid Hydrogen Rocket Motor Development - Second Bimonthly Progress Report, Ohio State University, 1948 (unclassified)

2. D. R. Bartz, "A Simple Equation for Rapid Estimationg of Rocket Nozzle Convective Heat Transfer Coefficients," Jet Propulsion , Jan. 1957, pp 49-51 (unclassified)

3. I. S. Donaldson, "On the Separation of a Supersonic Flow at a Sharp Corner," AIAA Journal, Vol. 5, No. 6 pp. 1086-1088 (unclassified)

4. R. S. Valentine, L. E. Dean, J. L. Pieper, "An Improved Method for Rocket Performance Prediction," J. Spacecraft and Rockets, Vol. 3, No. 9, Sept. 1960, pp 1409-1414 (unclassified)

APPENDIX I
HEAT TRANSFER MODEL

I. INTRODUCTION

(U) The cooling action of a TRANSPIRE cooled surface can be considered to be composed of two separate mechanisms. The first of these is what can be called internal cooling, or the transfer of heat between the platelets and coolant inside the wall itself. The second mechanism is film cooling, which is the suppression of heat flux to the wall as a result of the coolants being injected into the boundary layer after they leave the wall. These two mechanisms are coupled since the film cooling effect which is obtained depends upon the temperature of the coolant as it leaves the wall. Similarly, the heat flux into the wall and the temperature of the coolant as it leaves the surface depend upon the film cooling effectiveness.

(U) The approach which will be taken here is to derive separately the equations governing each of the two mechanisms. Once these equations are obtained the computational procedure which couples them will be outlined.

II. INTERNAL COOLING

(U) The thermal model for the internal cooling is shown in Figure 1. The wall is considered to be composed of platelets which are "2t" thick and having coolant channels between which are "D" deep. The coolant enters the channels at X=0 at a temperature $T_{c,o}$ and at a rate G per unit cooled wall surface area. At the end of the platelets, at X=L, the platelets are exposed to a hot gas at temperature T_g with a surface film coefficient h_g.

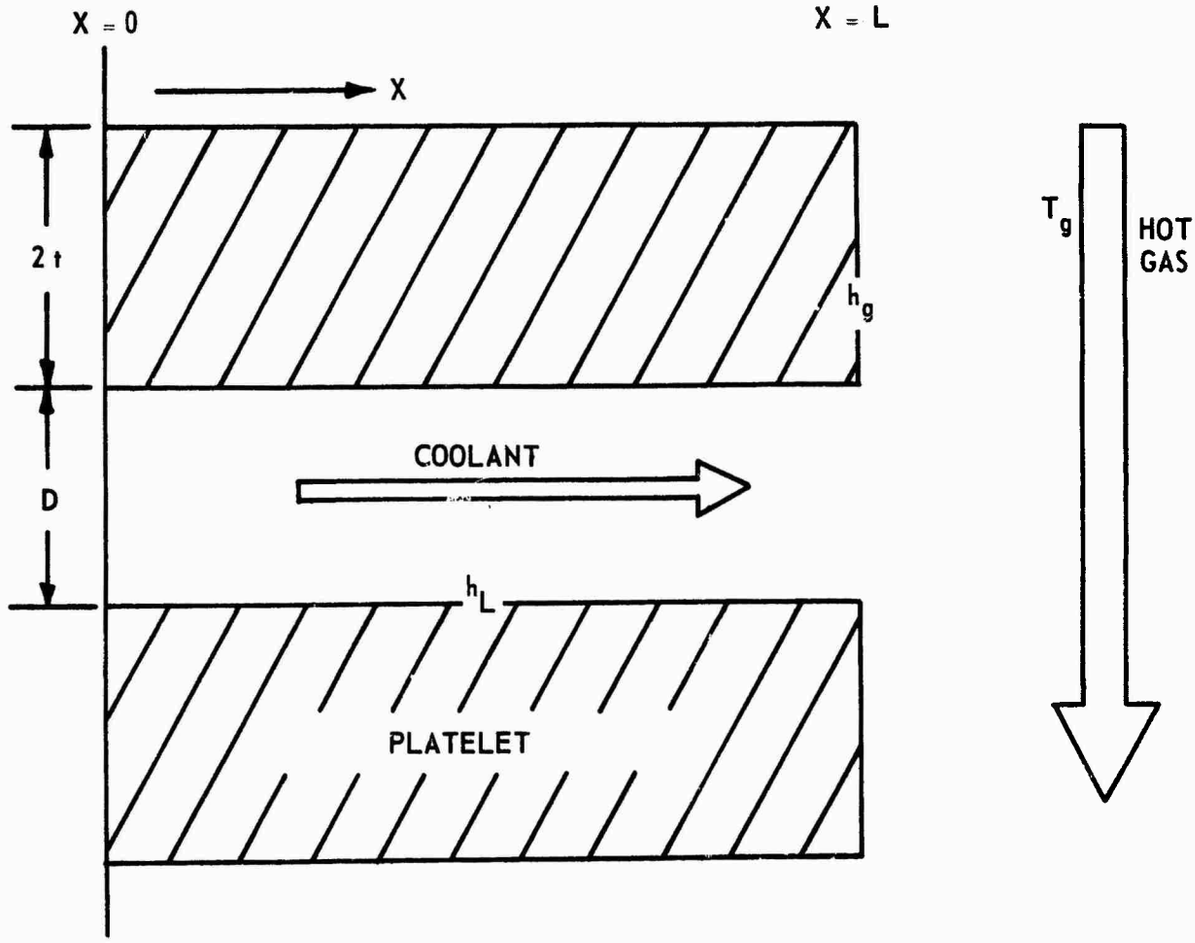

Figure 1

(U) It will be assumed that the heat conduction in the platelets is one-dimensional* and that the platelet material and coolant properties are not temperature dependent.

(U) The differential equation governing conduction in the platelet is:

$$K_m \, t \, \frac{d^2T}{dX^2} = h_L \, (T - T_c) \qquad (1)$$

where K_m = platelet conductivity
h_L = film coefficient between the platelet and coolant
T = platelet temperature at X
T_c = coolant temperature at X
t = platelet half thickness
X = distance from coolant inlet

(U) If X-direction conduction in the coolant is assumed to be negligible the differential equation describing the coolant temperature is:

$$G \, C_{p,c} \, t \, \frac{dT_c}{dX} = h_L \, (T - T_c) \qquad (2)$$

where $C_{p,c}$ = coolant specific heat
G = coolant weight flow rate per unit of cooled wall surface area

Combining equations (1) and (2)

$$\frac{d^3T}{dX^3} + A \, \frac{d^2T}{dX^2} - B \, \frac{dT}{dX} = 0 \qquad (3)$$

*Early in the program a two-dimensional numerical analysis of the platelet conduction showed that the one-dimensional approach is valid for thin platelets.

where $A = h_L/G\, C_{p,c}\, t$

$B = h_L/K_m\, t$

Using differential operator notation equation (3) can be written as:

$$(D^3 + AD^2 - BD)\, T = 0 \tag{3a}$$

The solution of equation (3a) is:

$$T = C_1 e^{r_1 X} + C_2 e^{r_2 X} + C_3 \tag{4}$$

$$r_1 = -A/2 + \frac{A^2}{4} + B \tag{5}$$

$$r_2 = -A/2 - \frac{A^2}{4} + B \tag{6}$$

(U) Three boundary conditions are required for the evaluation of the constants C_1, C_2, and C_3. At the platelet edge (X=L) the conduction into the platelet must equal the convective heat input from the hot gas stream.

$$\text{at } X=L,\ h_g (T_g - T) = K_m \frac{dT}{dX} \tag{7}$$

where h_g = surface (gas) film coefficient

T_g = hot gas temperature

(U) It will be assumed that the coolant inlet (or entrance to the thermal influence zone) is an adiabatic surface. This gives;

$$\text{at } X = 0,\ \frac{dT}{dX} = 0 \tag{8}$$

$$k_m t \frac{d^2T}{dX^2} = h_L (T - T_{c,o}) \tag{9}$$

where $T_{c,o}$ = coolant inlet temperature

(U) Evaluating C_1, C_2, and C_3 through the use of equations (7), (8), and (9), and rearranging produces

$$\frac{T - T_{c,o}}{T_g - T_{c,o}} = \frac{e^{r_1 X} - \left(\frac{r_1}{r_2}\right) e^{r_2 X}}{e^{r_1 L}\left[-\frac{r_1}{r_2} e^{(r_2 L)} + \frac{K_m}{h_g} r_1 \left(e^{r_1 L} - e^{r_2 L}\right)\right]} \tag{10}$$

where L = distance from coolant inlet to wall surface (platelet edge)

(U) It can be shown that for the range of values of interest

$$\left| e^{r_1 X} \right| >> \left| \frac{r_1}{r_2} e^{r_2 X} \right| \tag{11}$$

$$\left| e^{r_1 L} \right| >> \left| \frac{r_1}{r_2} e^{r_2 L} \right| \tag{12}$$

Employing equations (11) and (12) for simplifying equation (10) yields

$$\frac{T - T_{c,o}}{T_g - T_{c,o}} = \frac{e^{r_1 (X-L)}}{1 + \frac{K_m r_1}{h_g}} \tag{13}$$

(U) Equation (13) relates the temperatures existing at all points in the platelets to the properties of the coolant, the coolant flow rate, the platelet material properties and thickness, and the conditions at the hot gas boundary. This ation is the key equation used in the design and evaluation of the TRANSPIRE type platelets.

(U) The film coefficient "h_L" which exists between the coolant and the platelets can be evaluated using the expression for fully developed laminar flow between parallel plates.(1)

$$h_L = \frac{4\ K_c}{D} \tag{14}$$

where D = depth of coolant channel

K_c = coolant thermal conductivity

This value, when used in design, is on the conservative side since it is the minimum value which h_L can possibly have. Such things as entrance effects and phase changes can only act to increase h_L.

III. FILM COOLING

(U) The analysis of the film cooling effect achieved by the coolant after it leaves the wall will be somewhat different from the type of analysis used with the more conventional transpiration cooling systems. Normally in the analysis of transpiration cooling systems the assumption is made that the coolant is injected uniformly over the entire surface. This assumption will not be made in the present analysis. Rather, the analysis will treat the problem as one of highly refined multiple slot film cooling. There is a twofold reason for doing this. First, and most important, highly refined multiple slot film cooling is a more accurate description of the actual physical system

which the model is representing. The second reason for taking a multiple slot approach is that with the results of this approach it will be possible to account for the effect of platelet thickness on the film cooling effectiveness. Obviously, this cannot be done if the model assumes uniformly distributed coolant injection.

(U) The basic approach taken is similar to that of Stollery and El-Ehwany[2] except for some modifications to make the range of flows over which it is applicable somewhat broader. It is assumed that at each injection point the boundary layer begins to develop anew, and that the mass of gas in the boundary layer is composed of injected coolant plus enough entrained free-stream gas to give the total boundary layer gas flow. There is experimental justification for this approach. In work performed on film cooling with injection through a porous section[3] it was noted that the injected coolant appears to simply lift the existing boundary layer off the wall. Downstream of the point of injection the coolant and hot gas begin to mix, with the growth of the velocity profile in the coolant layer on the hot gas - coolant boundary not being too much unlike that of a turbulent boundary layer on a flat plate.

(U) The derivation will begin by assuming that the total mass flow rate in the boundary layer is composed of injected coolant plus enough entrained freestream gas to give the total boundary layer flow rate.

$$\dot{m}_{BL} = \dot{m}_c + \dot{m}_\infty \qquad \dot{m}_{BL} \geq \dot{m}_c$$

$\dot{m}_{BL}$ = boundary layer flow rate
$\dot{m}_c$ = coolant flow rate
$\dot{m}_\infty$ = flow rate of entrained freestream gases

The temperature of the boundary layer "T_{BL}" can be given by

$$T_{BL} = \frac{h_{BL}}{\dot{m}_{BL} C_{p,BL}} = \frac{(\dot{m}_{BL} - \dot{m}_c) C_{p,} T + \dot{m}_c T_c C_{p,c}}{(\dot{m}_{BL} - \dot{m}_c) C_{p,\infty} + \dot{m}_c C_{p,c}} \qquad (16)$$

$C_{p,\infty}$ = freestream specific heat
T_∞ = freestream total temperature
T_c = temperature of coolant as it leaves the wall
$C_{p,c}$ = coolant specific heat
$C_{p,BL}$ = boundary layer specific heat
h_{BL} = boundary layer film coefficient

The only unknown in eq. (16) is $\dot{m}_{BL}$. In general,

$$\dot{m}_{BL} = \int_0^\delta u dy \qquad (17)$$

δ = boundary layer thickness
u = local velocity
ρ = local density
y = normal distance from surface

(U) If it is assumed that similar velocity profiles exist in the boundary layer as it develops from the point of injection and that this profile is only a function of the freestream conditions then

$$u = u_\infty \left(\frac{y}{\delta}\right)^{1/n} \qquad (18)$$

n = a function of the freestream Reynolds number
u_∞ = freestream velocity

(U) Further assuming that a uniform density exists across the boundary layer and that this is equal to the freestream density " " (a reasonably good assumption in both the chamber and throat).

$$\rho = \rho_\infty \tag{19}$$

$$\dot{m}_{BL} = \int_0^\delta c_\infty \mu_\infty \left(\frac{y}{\delta}\right)^{1/n} dy = \frac{n}{n+1} \rho_\infty u_\infty \delta \tag{20}$$

(U) It can be shown that for a developing boundary layer the boundary layer thickness can be expressed

$$\delta = Z^{\frac{n+1}{n+3}} \left[\frac{n \quad (C_n)}{(n+2)(n+3)} \right]^{\frac{2n}{n+1}} \left(\frac{\rho_\infty \mu_\infty}{\mu_\infty} \right)^{\frac{2}{n+1}} \Bigg]^{-\frac{n+1}{n+3}} \tag{21}$$

Z = distance over which the boundary layer has been developing

C_n = a function of n, values of which are given on Page 507 of Ref. (4).

μ_∞ = free stream viscosity

Combining equation (20) and (21)

$$\dot{m}_{BL} = \left[\frac{n}{n+1} \right] \left[\frac{n \quad (C_n)}{(n+2)(n+3)} \right]^{\frac{2n}{n+1}} \Bigg]^{-\frac{n+1}{n+3}} (\rho_\infty u_\infty)^{\frac{2}{n+3}} Z^{\frac{n+1}{n+3}} \tag{22}$$

Let: $R_Z = \alpha \left(\dot{m}_{BL}/\dot{m}_c\right)$ (23)

(U) Based on the data presented by Stollery and El-Ehwany the value of " " should be somewhere between .80 and .85, for the conditions encountered with the TRANSPIRE designs. This constant compensates to a certain extent for some of the assumptions made earlier, particularly as regards the temperature distribution across the boundary layer.

(U) The effective local boundary layer temperature can now be obtained by combining equations (16), (22), and (23).

$$T_{BL} = T_c \text{ for } 0 < \frac{\dot{m}_{BL}}{\dot{m}_c} < 1.0 \tag{24}$$

$$T_{BL} = \frac{(R_Z - 1)\,\dfrac{C_{p,\infty}}{C_{p,c}}\,T_{o,\infty} + T_c}{(R_Z - 1)\,\dfrac{C_{p,\infty}}{C_{p,c}} + 1}, \quad \frac{\dot{m}_{BL}}{\dot{m}_c} > 1.0 \tag{25}$$

where $T_{o,\infty}$ = freestream stagnation temperature

$$R_Z = \frac{0.82}{\dot{m}_c}\left(\frac{n}{n+1}\right)^{\frac{2n}{n+1}}\left(\frac{n}{(n+2)(n+3)}\right)^{-\frac{n+1}{n+3}}(C_n)^{\frac{2}{n+3}}(\mu_\infty)^{\frac{n+1}{n+3}}(\rho_\infty u_\infty)^{\frac{n+1}{n+3}} Z \tag{26}$$

(U) In order to combine the film cooling equations with the internal cooling equations, to calculate the cooling operation of the TRANSPIRE wall, it is necessary that several additional operations be performed. The gas temperature "T_g" in equation (13), and the boundary layer temperature "T_{BL}" in equations (24) and (25) are in essence the same quantity. These two temperatures are not strictly equivalent, however, since T_g refers to an average driving temperature existing over the end of the platelet while T_{BL} is a local temperature which varies in the direction of stream flow. The relationship between these two temperatures is given by

$$T_g = \frac{\int_{D}^{D+2t} T_{BL}\, dZ}{2t} \tag{27}$$

It should also be noted that the flow rates G of eq. (13) and $\dot{m}_c$ of eq. (24) and (26) are not the same. The relationship between them is

$$\dot{m}_c = \frac{G\ (2t+D)}{\pi d} \tag{28}$$

where d = local chamber diameter

(U) The general calculational procedure in the use of these equations is to first select a platelet thickness, material, coolant flow channel depth, and design surface temperature. A coolant flow rate G and coolant temperature as it leaves the wall ($T_{c,L}$) are assumed. With these values and the use of equations (24), (25), (27), and (28), a value of T_g is found. With this T_g (the platelet surface temperature T_L and the use of equation (13) and equation (29)) the originally assumed coolant temperature $T_{c,L}$ can be checked by

$$(T_{c,L} - T_{c,L})\ G\ C_{p,c} = h_g\ (T_g - T_L) \tag{29}$$

where $T_{c,L}$ = coolant temperature as it leaves wall
T_L = platelet surface temperature

If the assumed and calculated values of $T_{c,L}$ are considerably different a new value of $T_{c,L}$ should be assumed and the calculation procedure repeated. If the assumed and calculated values are very nearly equal the platelet surface temperature T_L is checked to see how it compares with the desired design value. If it is either too high or too low the coolant flow rate is increased or decreased and the procedure repeated. If the calculated surface temperature is about equal to the desired value the design is finished at this point.

(U) There is a comment which should be made relative to the evaluation of equations (25) and (27). As they now stand they tacitly assume that once the coolant in the boundary layer has traveled the thickness of one platelet, it is lost to the cooling system and no more cooling benefit is derived from it. This lack of film cooling carryover from one platelet to the next can be compensated for by assuming that the freestream gas feeding the boundary layer is composed of the boundary layer coming off the preceding platelets.

(U) The entire design procedure given above has been programmed on a digital computer. Film cooling carryover from the two platelets upstream of the one being analyzed has also been included.

IV. PLATELET HYDRAULIC EQUATIONS

(U) The coolant flow in the platelet flow control channels is laminar. The pressure drop - flow relationship employed for these channels is the equation for fully developed laminar flow in rectangular passages.

$$Q = \frac{aD^3}{16\mu}\left(\frac{\Delta P}{\Delta L}\right)\left(\frac{4}{3} - 0.836\,\frac{D}{a}\right) \qquad (30)$$

Q = volumetric flow rate

a = channel width

D = channel depth

μ = coolant viscosity

$\frac{\Delta P}{\Delta L}$ = pressure gradient in the channel

(U) The validity of this equation for these small passages has been proven in numerous flow tests of both the test units used in this program and other programs.

(U) Entrance and exit losses although generally very small are also taken into consideration.

REFERENCES APPENDIX I

1. W. M. Rohsenow, and H. Choi, Heat Mass and Momentum Transfer, Prentice-Hall, Inc., 1961, p. 141, Unclassified.

2. J. A. Stollery, A. A.M. El Ehwany, "A Note on the Use of a Boundary-Layer Model for Correlating Film Cooling Data," Int. J. Heat and Mass Transfer, Vol. 8, pp 55-65, 1965, Unclassified.

3. R. J. Goldstein, G. Shavit, T. S. Chen, "Film Cooling Effectiveness With Injection Through a Porous Section," J. Heat Transfer, Trans. ASME, Series C, August 1965, Unclassified.

4. H. Schlicting, Boundary Layer Theory, McGraw-Hill Book Company, Inc., 1960, Unclassified.

APPENDIX II
PERFORMANCE MODEL

I. INTRODUCTION

(U) To design a transpiration cooled chamber to meet specific performance requirements, a means of predicting I_{sp} must be available. The following presents a first step toward the development of a performance prediction method for transpiration cooled thrust chambers. In the development of the model, a prime objective was simplicity to facilitate its use as an easily applied tool. Therefore, some limiting assumptions were proposed which will require revision in future model developments.

II. MODEL DESCRIPTION

A. NOMENCLATURE

A	=	Area
A_c	=	Coolant exit area, $in.^2$
A_e	=	Exit area, $in.^2$
A_t	=	Throat area, $in.^2$
$C_{p,C}$	=	Specific heat of core, Btu/lb °F
$C_{p,c}$	=	Specific heat of coolant, Btu/lb °F
f_w	=	Isentropic flow function $\frac{\dot{w}}{P_c}\frac{T_o R}{A}$
H	=	Enthalpy, Btu/lb
I_{sp}	=	Vacuum specific impulse, sec
$I_{sp,C}$	=	I_{sp} of core, sec
$I_{sp,c}$	=	I_{sp} of coolant sec
M	=	Mach number
$(O/F)_i$	=	Injector oxidizer to fuel mixture ratio
$(O/F)_t$	=	Total oxidizer to fuel mixture ratio
P_e	=	Nozzle exit pressure, psia

P_c = Chamber pressure, psia

P_{c1} = Coolant stagnation pressure, psia

R = Gas constant, ft/°R

T_{C1} = Core flame temperature reduced from theoretical by energy release loss, °R

T_{C2} = Core flame temperature reduced by energy release loss and energy transfer to the coolant, °R

T_{c1} = Coolant entrance temperature, °R

T_{c2} = Coolant final stagnation temperature, °R

$\dot{w}_C$ = Core flowrate, lb/sec

$\dot{w}_c$ = Oxidizer coolant flowrate, lb/sec

$\dot{w}_t$ = Total flowrate $\dot{w}_c + \dot{w}_C$, lb/sec

B. ASSUMPTIONS

(U) 1. There is no combustion between the coolant and the combusting core. This assumption was chosen (1) because of inherent analysis simplicity (2) treating each stream tube component separately without chemical interaction has met with success for other applications and (3) for the N_2O_4 data, which accounted for the majority of the Phase I data, the assumption of no combustion was considered valid because of the lack of chemical reaction potential between the injector core and coolant (core O/F of 2.0 vs stoichiometric O/F of 2.2).

(U) 2. Coolant stagnation pressure is the same as the chamber or nozzle static pressure at the point of coolant entrance.

(U) 3. Coolant final stagnation temperature is the same regardless of entrance point.

(U) 4. The energy required to heat the coolant to its stagnation temperature is obtained from the core, and the core chamber enthalpy is reduced by the amount.

(U) 5. The friction loss factor is applied to the theoretical I_{sp} at the overall O/F.

(U) 6. The geometry loss factor is applied to the maximum potential I_{sp} of the stream tube summation.

(U) 7. The recombination loss factor is applied to the core only at its mixture ratio.

C. APPLICATION OF MODEL

(U) The model assumes that no combustion occurs between core and coolant, and that the enthalpy gain of the coolant is equal to the chamber enthalpy loss of the core:

$$\dot{w}_c \int_{T_{c1}}^{T_{c2}} C_{p,c}\, dT_c = \dot{w}_C \int_{T_{C1}}^{T_{C2}} C_{p,C}\, dT_C$$

(U) The above energy balance requires a method of calculating the final coolant temperature (T_{c2}), which presented the most difficulty in the model application. For the present study, the assumption was imposed that all of the coolant existed in thermal equilibrium with the core during the nozzle expansion process. (i.e., $T_{c2} = T_{C2}$). Therefore, the above energy balance may be solved for final temperature, which is the reduced temperature of the core and the stagnation temperature of the coolant. The core I_{sp} may be evaluated at this reduced temperature from the AGC chemical composition program 166 data. The coolant is expanded isentropically from its stagnation conditions at each section to the exit pressure, and the corresponding ΔH noted. It may be shown that the vacuum $I_{sp,c}$ for this process is expressed by:

$$I_{sp,cc} = \sqrt{\frac{2J\Delta H}{g}} + \frac{A_c}{A_e}\,\frac{P_e A_e}{\dot{w}_t}$$

The ratio A_c/A_e may be solved by assuming a uniform exit pressure, and iterating for the core and coolant area summation that equals the exit area. AGC chemical composition data (Program 166) is used for the core and the isentropic flow function (f_w) is used for the coolant in the iteration processes. The total I_{sp} of the engine may then be calculated by summing the component I_{sp}'s as follows:

$$I_{sp} = \left[\frac{\dot{w}_C}{\dot{w}_t} \times (I_{sp,C})\right]_{T_{C2}} + \sum\left[\frac{\dot{w}_c}{\dot{w}_t}\sqrt{\frac{2J\Delta H}{g}} + \frac{A_c}{A_e}\cdot\frac{P_e A_e}{\dot{w}_t}\right]$$

D. EXAMPLE CALCULATION WITH MODEL

(C) Given: Parameters from N_2O_4 cooled

Test No. 171

Injector O/F = 2.1 $\quad T_{C1} = (\eta_{er}) \times$ (Adiab. flame temp)

P_c = 100 psia $\quad$ = 97% x 5633 = 5470°R

$\dot{w}_c/\dot{w}_t$ = .257

$\dot{w}_C/\dot{w}_t$ = .743

$\dot{w}_c$ Sect I = .0546 lb/sec

$\dot{w}_c$ Sect II = .0276 lb/sec

$\dot{w}_c$ Sect III = .0380 lb/sec

$\dot{w}_c$ Sect IV = .044 lb/sec

$\dot{w}_t$ = .638 lb/sec

A_e/A_t = 1.6

Want: Predicted I_{sp}

Solution:

(C) Solve heat balance for reduced temperature $T_2 = T_{c2} = T_{C2}$ at coolant-core thermal equilibrium

$$\frac{\dot{w}_c}{\dot{w}_t}(H_{T2} - H_{537})_c = \frac{\dot{w}_c}{\dot{w}_t}\int_{537}^{T_2} C_{p,C}\,dT = \frac{\dot{w}_C}{\dot{w}_t}\int_{5470}^{T_2} C_{p,C}\,dT = \frac{\dot{w}_C}{\dot{w}_t}(H_{5470} - H_{T2})_C$$

Assume T_2 = 5000R

.257(1340) = 345 = .743 $(H_{5470} - H_{T2})$ = .743(464)

Core T_2 = 5035R for the 464 Btu/lb H of core

5000 = 5035, say $T_c = T_C$ = 5020R

Energy balance is satisfied with core-coolant thermal equilibrium

x $I_{sp,C}$ = 225.0 sec (theoretical @ 5020R)

Recombination loss = .2% x 225 = .45 sec

$\frac{\dot{w}_C}{\dot{w}_t} x\ I_{sp,C}$ = (.743)(225.0 - .45) = 167 sec

Coolant I_{sp}:

(C) Section I & II: P_{c1} = 100 psia, T_c = 5020R, P_e = 23 psia

$(H_{P_{c1}, T_c} - H_{P_e c})$ = 390 Btu/lb (isentropic expansion from P_{c1}, T_c to P_e)

$$I_{sp} = \frac{A_c}{A_e} \times \frac{P_e A_e}{\dot{w}_t} = \sqrt{\frac{2J390}{g}} \left(\frac{\dot{w}_c}{\dot{w}_t}\right)_{I,II} = 17.6 \text{ sec}$$

(C) Section III: $P_{c1} = 82$ psia $T_c = 5020$R, $P_e = 23$ psia
$\Delta H = 360$ Btu/lb

$$I_{sp} = \frac{A_c}{A_e} \cdot \frac{P_e A_e}{\dot{w}_t} = \left(\frac{\dot{w}_c}{\dot{w}_t}\right)_{III} \sqrt{\frac{2J360}{g}} = 7.8 \text{ sec}$$

(C) Section IV: $P_{c1} = 30$ psia, $T_c = 5020$R, $P_e = 23$ psia
$\Delta H = 10$ Btu/lb (isentropic expansion from P_{c1}, T_c to P_e)

$$I_{sp} = \frac{A_c}{A_e} \cdot \frac{P_e A_e}{\dot{w}_t} = \left(\frac{\dot{w}_c}{\dot{w}_t}\right)_{IV} \sqrt{\frac{2J10}{g}} = 0.7 \text{ sec}$$

$$\frac{A_c}{A_e} \cdot \frac{P_e A_e}{\dot{w}_t} = 11.3 \text{ sec (assuming uniform exit pressure)}$$

(C) $$\text{MAX } I_{sp} = \frac{\dot{w}_C}{\dot{w}_t} \times I_{sp,C} + \sum \frac{\dot{w}_c}{\dot{w}_t} \sqrt{\frac{2J\Delta H}{g}} + \frac{A_c}{A_e} \cdot \frac{P_e A_e}{\dot{w}_t}$$

$$= 167.0 + 17.6 + 7.8 + 0.7 + 11.3 = 204.4 \text{ sec}$$

Frict. loss = .7% x 225 sec		= 1.6 sec
Geom loss	= 1.9% x 204.4 sec	= 3.9 sec
	Σ nozzle losses	5.5 sec

Predicted I_{sp} = 204.4 - 5.5	= 198.9 sec
Test I_{sp}	= 205.6 sec
Error	= 6.7 sec
% Error	= 3.06%

APPENDIX III

DATA

LIST OF TABLES

Section	Title	Table
I	N_2O_4 - 100 psia Chamber Pressure	
	Test Conditions (U)	1
	Pressure Drops (U)	2
	Steady State Temperatures (U)	3
	Injector Flow Rates and Mixture Ratios (U)	4
II	N_2O_4 - 1000 psia Chamber Pressure	
	Test Conditions (U)	5
	Pressure Drops (U)	6
	Steady State Temperatures (U)	7
	Injector Flow Rates and Mixture Ratios (U)	8
III	ClF_3 - 100 psia Chamber Pressure	
	Test Conditions (U)	9
	Pressure Drops (U)	10
	Steady State Temperatures (U)	11
	Injector Flow Rates and Mixture Ratios (U)	12
IV	ClF_3 - 1000 psia Chamber Pressure (Phase I)	
	Test Conditions (U)	13
	Pressure Drops (U)	14
	Steady State Temperatures (U)	15
	Injector Flow Rates and Mixture Ratios (U)	16
V	ClF_3 - 1000 psia Chamber Pressure (Phase II)	
	Test Conditions (U)	17
	Pressure Drops (U)	18
	Steady State Temperatures (U)	19
	Injector Flow Rates and Mixture Ratios (U)	20

SECTION I

DATA FROM N_2O_4 TESTS AT 100 PSIA CHAMBER PRESSURE

(C) TABLE 1

TEST CONDITIONS (U)

Test No.	Thrust (lb)	Chamber Pressure (psia)	Flow Rate* Coolant (lb/sec)	Injector Oxidizer Flow Rate (lb/sec)	Injector Fuel Flow Rate (lb/sec)	Total Propellant Flow Rate (lb/sec)	Overall Mixture Ratio
1K-3C-							
104	134	133	0.816	0.327	0.164	1.31	6.97
106	116	124	0.701	0.326	0.164	1.19	6.26
109	121	128	0.552	0.326	0.164	1.04	5.35
110	111	111	0.487	0.325	0.164	0.976	4.95
111	106	113	0.438	0.322	0.165	0.925	4.61
113	123	121	0.388	0.326	0.164	0.877	4.38
121	126	121	0.341	0.327	0.163	0.831	4.10
122	126	121	0.342	0.325	0.165	0.832	4.04
123	126	121	0.339	0.325	0.164	0.828	4.05
129	117	118	0.325	0.323	0.153	0.801	4.23
143	110	111	0.235	0.326	0.149	0.710	3.76
144	111	111	0.235	0.327	0.150	0.711	3.74
145	112	111	0.233	0.326	0.149	0.709	3.76
146	**	78	0.232	0.324	0.155	0.711	3.59
148	110	111	0.213	0.324	0.150	0.687	3.58
151	112	111	0.211	0.325	0.152	0.688	3.53
152	112	110	0.211	0.324	0.151	0.686	3.54
154	119	113	0.211	0.324	0.148	0.683	3.61
159	114	111	0.181	0.324	0.152	0.657	3.32
162	111	111	0.173	0.324	0.151	0.648	3.29
165	114	110	0.173	0.324	0.149	0.646	3.34
166	109	110	0.173	0.326	0.151	0.650	3.30
168	107	110	0.167	0.324	0.153	0.643	3.23
171	112	110	0.164	0.324	0.150	0.638	3.25
172	108	110	0.165	0.325	0.150	0.640	3.27
174	109	112	0.160	0.324	0.155	0.639	3.12
177	108	110	0.157	0.325	0.150	0.633	3.22
181	107	111	0.158	0.326	0.152	0.636	3.18
185	108	110	0.178	0.325	0.152	0.655	3.31
189	110	108	0.153	0.325	0.149	0.627	3.21
190	104	105	0.154	0.325	0.152	0.631	3.15
192	101	108	0.152	0.325	0.148	0.625	3.22
193	103	109	0.152	0.324	0.149	0.625	3.19

*Venturi flow rates
**No steady state

(C) TABLE 2

PRESSURE DROPS (U)

Test No.	Chamber Pressure (psia)	Chamber Plenum Pressure (psia)				Platelet Pressure Drop (psid)			
		Sect.I	Sect.II	Sect.III	Sect.IV	Sect.I	Sect.II	Sect.III	Sect.IV
1K-3C-									
104	133	253	249	327	529	125	116	226	486
106	124	215	242	315	531	91	118	220	490
109	128	193	215	325	545	64	87	227	504
110	111	177	172	302	552	66	60	216	515
111	113	154	173	301	556	41	59	214	519
113	121	168	163	317	561	47	43	225	521
121	121	161	164	314	561	40	43	221	522
122	122	159	161	316	562	38	39	223	523
123	121	159	162	314	560	37	41	221	520
129	118	149	156	318	559	30	38	228	520
143	111	136	134	245	571	25	23	160	535
144	111	136	134	247	567	24	23	162	531
145	111	136	134	250	564	25	23	165	528
146	78	71	70	245	572	-	-	165	546
148	111	130	130	256	569	19	19	171	532
151	111	128	127	259	558	17	17	174	521
152	110	127	127	260	557	17	17	175	521
154	113	129	130	264	558	17	17	178	521
159	111	129	124	212	565	17	12	127	529
162	111	129	123	198	562	18	12	113	526
165	110	129	123	198	562	18	12	114	526
166	110	129	122	199	565	19	12	115	529
168	110	128	120	201	558	18	10	117	522
171	110	128	119	200	558	18	9	116	522
172	110	128	119	201	561	18	9	117	525
174	112	130	119	202	558	18	7	117	522
177	110	128	117	194	561	18	7	110	525
181	111	130	119	197	563	20	8	113	527
185	118	133	119	192	399	23	9	107	363
189	108	129	115	192	255	21	7	110	219
190	105	127	113	192	255	22	8	111	221
192	108	130	114	198	257	21	6	115	222
193	109	130	115	197	249	21	6	114	214

(C) TABLE 3

STEADY STATE TEMPERATURES (U)

Test No.	$\dot{w}_{c,I}$ Sect. I Coolant Flow Rate (lb/sec)	$\dot{w}_{c,I}/\dot{w}_N$ Sect. I	Duration (sec)	Temperatures (°F) Section I					
				TC 9-1	TC 9-2	TC 9-3	TC 9-4	TC 8-1	TC 8-2
1K-3C-									
104	0.371	10.51	10.6				109	100	121
106	0.258	7.32	1.9		89		110	121	123
109	0.187	5.40	1.9		943		114	125	120
110	0.187	5.40	1.4	96			101	129	111
111	0.138	3.91	1.4	116			111	160	119
113	0.139	3.94	10.7	105			115	130	134
121	0.112	3.18	30.4	140	140			138	148
122	0.112	3.18	30.6		142	163		140	
123	0.111	3.15	60.3		143			137	
129	0.096	2.72	2.0	120	126			236	130
143	0.070	1.98	10.7	130	142			147	812
144	0.070	1.98	30.9		143	658		142	
145	0.070	1.98	60.2	140	145			146	862
146	0.062	1.76	1.4	193	248			294	294
148	0.055	1.56	10.6	178	154			182	1008
151	0.054	1.53	10.7			760	492	975	
152	0.054	1.53	30.7			190		398	1342
154	0.055	1.56	60.4	626	533	1010		770	1494
159	0.055	1.56	31.8	525		882	767	1221	
162	0.055	1.56	30.7	457		872		773	1100
165	0.055	1.56	30.6			868			1255
166	0.055	1.56	30.9			884			1323
168	0.055	1.56	10.5	210		700		156	702
171	0.055	1.56	30.7	336		824		162	1136
172	0.055	1.56	31.0		186				1212
174	0.055	1.56	10.4	363		737		320	875
177	0.055	1.56	30.9	397	894			587	1350
181	0.055	1.56	31.0		175				1320
185	0.062	1.76	10.8	227		574		149	843
189	0.062	1.76	30.8	377		834		164	1095
190	0.062	1.76	30.5						
192	0.062	1.76	400.6	280		927		153	1511
193	0.062	1.76	401.3						

(C) TABLE 3 (cont.)

STEADY STATE TEMPERATURES (U)

Test No.	$\dot{w}_{c,II}$ Sect. II Coolant Flow Rate (lb/sec)	$\dot{w}_{c,II}/\dot{w}_N$ Sect. II	Temperatures (°F) Section II							
			TC 7-1	TC 7-2	TC 7-3	TC 7-4	TC 4-1	TC 4-5	TC 4-7	TC 4-8
1K-3C-										
104	0.324	9.47		113		111	128		113	
106	0.323	9.45		124		115	131		128	
109	0.242	7.08	128		122	137			134	
110	0.176	5.15	118			107	132		129	
111	0.176	5.15	119			116	132		133	
113	0.124	3.63	136			124	142		143	
121	0.105	3.07	133		140	148	147		146	
122	0.105	3.07	134				145			141
123	0.104	3.04	133					144		141
129	0.105	3.07	235			132	141	144	143	
143	0.063	1.84	143			150	141	191	253	
144	0.063	1.84	133		138			162		233
145	0.063	1.84	137					167		
146	0.055	1.61	244			356	127	292	155	
148	0.051	1.49	449			508	161	727	520	
151	0.050	1.46	300		415					703
152	0.050	1.46	147					641	581	650
154	0.050	1.46	154			377	217	686	578	
159	0.038	1.11	260			496	278	829	836	
162	0.035	1.02	294			535	315	874	870	
165	0.035	1.02				566		873	837	
166	0.035	1.02	151		480	536		852	862	
171	0.027	0.79	245			702	555	962	1007	
172	0.027	0.79			488		693	840		
174	0.023	0.67	674			809		1083	1043	
177	0.023	0.67	394			763	661	1047	1082	
181	0.023	0.67	157		468			1079		
185	0.021	0.61				169	260	976	947	
189	0.021	0.61	122			156	625	933	976	
190	0.021	0.61				829				
192	0.021	0.61				153	593	1121		
193	0.021	0.61			764			1196		

(C) TABLE 3 (cont.)

STEADY STATE TEMPERATURES (U)

Test No.	Temperatures (°F) Section II						
	TC 5-1	TC 5-2	TC 5-3	TC 5-4	TC 5-5	TC 5-7	TC 5-8
1K-3C-							
104			111			108	
106			118			114	
109			126			114	
110			119			113	
111			122			113	
113			133			128	
121			138				
122	109		139				
123	114	130	141	129	114	137	120
129			146			129	
143			145			139	
144			140				
145	117	130	139	126	120		127
146			342			258	
148			334			172	
151			253				
152	148	160	180	139	149		158
154			224			193	
159			554			546	
162			619			561	
165			568			551	
166	318	491	596	345	294	592	428
168			703			526	
171			761			844	
172	366	519		361	459		699
174			941			902	
177			851			965	
181	636	816		693	600		869
185			952			802	
189			851			806	
190							
192		879	983			1089	
193				755	766		1021

(C) TABLE 3 (cont.)

STEADY STATE TEMPERATURES (U)

Test No.	$\dot{W}_{c,III}$ Sect. III Coolant Flow Rate (lb/sec)	$\dot{W}_{c,III}/\dot{W}_N$ Sect. III	Temperatures (°F) Section III			
			TC 3-1	TC 3-2	TC 3-3	TC 3-4
1K-3C-						
104	0.079	10.02		114		126
106	0.078	10.01		121		125
109	0.079	10.02		122		125
110	0.080	10.04		122		122
111	0.080	10.04		119		
113	0.080	10.04	138	121		
121	0.080	10.04	144	129		
122	0.080	10.04		127	128	
123	0.079	10.02	130			
129	0.080	10.04	143	131		
143	0.055	7.15	173	166		
144	0.055	7.15		155		
145	0.055	7.15		157	135	
146	0.070	9.10	157	141		
148	0.062	8.05	268	198		
151	0.062	8.05		166		
152	0.062	8.05		159	136	
154	0.062	8.05	193			
159	0.043	5.58		269		
162	0.038	4.94		592		
165	0.038	4.94	789	567	180	
166	0.038	4.94		577		
168	0.038	4.94		554		
171	0.038	4.94		596		
172	0.038	4.94	296		387	
174	0.038	4.94		727		
177	0.035	4.55		754		
181	0.035	4.55	1021		594	
185	0.035	4.55		732		
189	0.035	4.55		679		
190	0.035	4.55				
192	0.035	4.55				
193	0.035	4.55				

(C) TABLE 3 (cont.)

STEADY STATE TEMPERATURES (U)

Test No.	Temperatures (°F) Section III							
	TC 2-1	TC 2-2	TC 2-3	TC 2-4	TC 2-5	TC 2-6	TC 2-7	TC 2-8
1K-3C-								
104			123				97	
106			129				114	
109			137				129	
110			124				121	
111			129				124	
113			142					
121		139	168					
122	100		171	131	97	125		110
123			217					
129		147	198					
143		202	332					
144			368	181	106	149		124
145			333					
146		151	183					
148		213	307					
151			244	159	104	151		
152			231					
154		175	238					
159		350	831			176		
162		478	1085			198		
165	129	433	1022	311	133			211
166								
168		482	1144		212			
171		511	1158			244		
172			898	242	151			239
174		497	873			270		
177		478	1125			281		
181	159		1213	456	162			289
185		608	1301			264		
189		579	1246			267		
190								
192		525	1267			262		
193		151	1241	461	173			312

(C) TABLE 3 (cont.)

STEADY STATE TEMPERATURES (U)

Test No.	$\dot{w}_{c,IV}$ Sect. IV Coolant Flow Rates (lb/sec)	$\dot{w}_{c,IV}/\dot{w}_N$ Sect. IV	Temperatures (°F) Section IV TC 1-1	TC 1-2
1K-3C-				
104	0.043	8.6	109	110
106	0.043	8.6	107	106
109	0.040	8.0	128	108
110	0.044	8.8	105	102
111	0.045	9.0	108	102
113	0.046	9.2	120	108
121	0.046	9.2		112
122	0.046	9.2		112
123	0.046	9.2		109
129	0.045	9.0		112
143	0.046	9.2		199
144	0.046	9.2		205
145	0.046	9.2		201
146	0.046	9.2		101
148	0.046	9.2		141
151	0.045	9.0		152
152	0.045	9.0		156
154	0.045	9.0		165
159	0.046	9.2		205
162	0.046	9.2		274
165	0.046	9.2		
166	0.046	9.2		
168	0.045	9.0		208
171	0.045	9.0		222
172	0.046	9.2		
174	0.045	9.0		210
177	0.046	9.2		289
181	0.046	9.2		
185	0.030	6.0		377
189	0.016	3.2		370
190	0.016	3.2		297
192	0.016	3.2		
193	0.016	3.2		

(C) TABLE 4

INJECTOR FLOW RATES AND MIXTURE RATIOS (U)

Test No.	Pressure at Ox Venturi (psia)	Pressure at Fuel Venturi (psia)	(Potter Meter) Ox Flow Rate (lb/sec)	(Potter Meter) Fuel Flow Rate (lb/sec)	(Venturi) Ox Flow Rate (lb/sec)	(Venturi) Fuel Flow Rate (lb/sec)	(Venturi) Total Injector Flow Rate (lb/sec)	Mixture Ratio (Injector Venturis)
1K-3C-								
104	551	332	0.314	0.161	0.327	0.164	0.491	1.99
106	546	331	-	0.165	0.326	0.164	0.490	1.99
109	551	331	0.315	0.165	0.326	0.164	0.490	1.99
110	555	332	0.313	0.165	0.325	0.164	0.489	1.98
111	557	336	0.315	0.165	0.322	0.165	0.487	1.95
113	556	328	0.315	0.162	0.326	0.163	0.489	2.00
121	556	328	0.316	0.163	0.327	0.163	0.490	2.00
122	558	338	0.316	0.163	0.325	0.165	0.490	1.97
123	556	332	0.313	0.163	0.325	0.164	0.489	1.98
129	553	288	0.312	0.154	0.323	0.153	0.476	2.11
143	560	274	0.316	0.150	0.326	0.149	0.475	2.19
144	559	277	0.316	0.150	0.327	0.150	0.477	2.18
145	557	275	0.315	0.150	0.326	0.149	0.475	2.19
146	563	294	0.315	0.152	0.324	0.155	0.479	2.09
148	562	280	0.314	0.151	0.324	0.150	0.474	2.16
----	559	285	0.292	0.151	0.325	0.152	0.477	2.14
152	557	282	0.306	0.150	0.324	0.151	0.475	2.15
154	556	272	0.314	0.149	0.324	0.148	0.472	2.19
159	560	284	0.317	0.152	0.324	0.152	0.476	2.13
162	556	282	0.316	0.152	0.324	0.151	0.475	2.15
165	556	274	0.317	0.150	0.324	0.149	0.473	2.17
166	559	281	0.314	0.151	0.326	0.151	0.477	2.16
168	556	286	0.316	0.152	0.324	0.152	0.476	2.13
171	555	279	0.317	0.151	0.324	0.150	0.474	2.16
172	559	278	0.319	0.151	0.325	0.150	0.475	2.17
174	555	294	0.316	0.155	0.324	0.155	0.479	2.09
177	557	279	0.316	0.151	0.325	0.150	0.475	2.17
181	559	284	0.318	0.152	0.326	0.152	0.478	2.15
185	556	286	0.312	0.153	0.325	0.152	0.477	2.14
189	557	274	0.314	0.149	0.325	0.149	0.474	2.18
190	558	285	-	-	0.325	0.152	0.477	2.14
192	556	270	0.318	0.148	0.325	0.148	0.473	2.20
193	555	274	0.315	0.149	0.324	0.149	0.473	2.17

SECTION II

DATA FROM N_2O_4 TESTS AT
1000 PSIA CHAMBER PRESSURE

(C) TABLE 5

TEST CONDITIONS (U)

Test No.	Thrust (lb)	Chamber Pressure (psia)	Flow Rate* Coolant (lb/sec)	Injector Oxidizer Flow Rate (lb/sec)	Injector Fuel Flow Rate (lb/sec)	Total Propellant Flow Rate (lb/sec)	Overall Mixture Ratio
1K-3C-							
198	915	958	1.45	2.52	1.29	5.26	3.07
205	917	935	1.48	2.40	1.20	5.08	3.23
207	907	926	1.47	2.51	1.22	5.20	3.26
210	941	943	1.57	2.52	1.22	5.21	3.26
211	937	942	1.47	2.53	1.22	5.22	3.27
212	936	939	1.47	2.52	1.22	5.21	3.27
213	933	945	1.47	2.52	1.21	5.21	3.28
---	943	946	1.47	2.52	1.22	5.22	3.27
215	948	944	1.47	2.53	1.22	5.22	3.29
216	955	942	1.47	2.52	1.22	5.22	3.27
218	944	948	1.48	2.52	1.22	5.22	3.28
219	906	925	1.48	2.54	1.15	5.16	3.50
220	950	963	1.48	2.53	1.26	5.26	3.19

(C) TABLE 6

PRESSURE DROPS (U)

Test No.	Chamber Pressure (psia)	Chamber Plenum Pressure (psia)				Platelet Pressure Drop (psid)			
		Sect. I	Sect. II	Sect. III	Sect. IV	Sect. I	Sect. II	Sect. III	Sect. IV
1K-3C-									
198	958	1198	1157	1691	1589	240	199	859	1277
205	935	1206	1259	1732	1673	271	325	1017	1369
207	926	1187	1301	1731	1688	261	375	1022	1386
210	943	1199	1218	1809	1719	257	275	1088	1411
211	942	1189	1223	1818	1708	246	281	1097	1401
212	939	1181	1248	1817	1728	242	309	1098	1412
213	945	1190	1227	1852	1745	245	281	1129	1437
214	946	1195	1246	1873	1773	249	300	1149	1466
215	944	1190	1292	1877	1814	246	347	1155	1506
216	942	1194	1254	1901	1758	252	312	1181	1450
218	948	1191	1230	1883	1742	243	282	1157	1432
219	925	1177	1218	1876	1769	252	293	1169	1467
220	963	1215	1261	1895	1776	252	297	1159	1462

(C) TABLE 7

STEADY STATE TEMPERATURES (U)

Test No.	$\dot{w}_{c,I}$ Sect. I Coolant Flow Rate (lb/sec)	$\dot{w}_{c,I}/\dot{w}_N$ Sect. I	Duration (sec)	Temperatures (°F) Section I TC 9-1	TC 9-2	TC 9-3	TC 8-1	TC 8-2
1K-3C-								
198	0.599	2.07	0.51	372	249	391	324	430
205	0.599	2.07	5.37	-	1189	987	867	406
207	0.595	2.06	5.0	-	-	879	-	-
210	0.594	2.06	32.6	1183	1442	1148	390	878
211	0.595	2.06	15.5	1032	1373	1056	399	1058
212	0.595	2.06	29.1	787	286	1172	399	1012
213	0.594	2.06	21.7	1004	1356	837	419	1044
214	0.596	2.06	23.7	1212	1448	854	405	990
215	0.596	2.06	54.9	1318	1569	965	407	1001
216	0.596	2.06	102.8	1477	1649	1137	399	1158
218	0.597	2.07	101.3	986	306	1172	416	923
219	0.598	2.07	31.3	797	291	1297	345	914
220	0.597	2.07	31.0	1035	318	1258	425	942

Test No.	$\dot{w}_{c,II}$ Sect. II Coolant Flow Rate (lb/sec)	$\dot{w}_{c,II}/\dot{w}_N$ Sect. II	Temperature (°F) Section II										
			TC 7-3	TC 7-4	TC 5-1	TC 5-2	TC 5-3	TC 5-4	TC 5-6	TC 5-7	TC 5-8	TC 4-1	TC 4-7
1K-3C-													
198	0.521	1.86	253	378	-	244	307	-	-	441		973	860
205	0.521	1.86	349	458	-	298	325	-	-	794		1319	1337
207	0.518	1.85	175	616	188	300	-	252	-	-	269	1425	-
210	0.518	1.85	362	420	-	320	327	-	-	384		1402	1152
211	0.518	1.85	348	429	-	325	345	-	-	384		1448	1133
212	0.518	1.85	354	407	-	337	348	-	-	366		1644	1210
213	0.518	1.85	377	516	-	323	340	-	-	396		1462	1235
214	0.520	1.86	387	560	-	325	345	-	-	402		1445	1321
215	0.520	1.86	377	567	-	341	316	-	-	391		1563	1450
216	0.520	1.86	-	416	-	347	308	-	244	371		-	1106
218	0.521	1.86	-	504	-	343	342	-	-	246	399	-	1126
219	0.521	1.86	-	439	-	309	331	-	-	242	381	-	1109
220	0.521	1.86	-	688	-	346	334	-	-	252	406	-	1167

Test No.	$\dot{w}_{c,III}$ Sect. III Coolant Flow Rate (lb/sec)	$\dot{w}_{c,III}/\dot{w}_N$ Sect. III	Temperature (°F) Section III						
			TC 2-1	TC 2-2	TC 2-4	TC 2-5	TC 2-6	TC 2-8	TC 3-3
1K-3C-									
198	0.244	2.66	-	712	-	-	454	-	445
205	0.273	2.97	-	807	-	-	624	-	873
207	0.272	2.96	292	-	999	340	655	416	1034
210	0.272	2.96	-	815	-	-	584	-	862
211	0.272	2.96	-	809	-	-	555	-	938
212	0.272	2.96	-	838	-	-	603	-	961
213	0.272	2.96	-	766	-	-	571	-	963
214	0.273	2.97	-	760	-	-	656	-	994
215	0.273	2.97	-	783	-	-	734	-	1072
216	0.273	2.97	-	731	-	-	578	-	1084
218	0.273	2.97	-	724	-	-	689	461	1021
219	0.273	2.97	-	554	-	-	630	521	910
220	0.273	2.97	-	638	-	-	679	528	1104

Test No.	$\dot{w}_{c,IV}$ Sect. IV Coolant Flow Rate (lb/sec)	$\dot{w}_{c,IV}/\dot{w}_N$ Sect. IV	Temperature (°F) Section IV
			TC 1-2
1-K-3C-			
198	0.0857	1.10	745
205	0.0857	1.10	1089
207	0.0855	1.10	-
210	0.0855	1.10	1018
211	0.0855	1.10	1031
212	0.0855	1.10	1056
213	0.0853	1.09	981
214	0.0856	1.10	1009
215	0.0856	1.10	973
216	0.0856	1.10	1066
218	0.0856	1.10	-
219	0.0858	1.10	-
220	0.0856	1.10	-

(C) TABLE 8

INJECTOR FLOW RATES AND MIXTURE RATIOS (U)

Test No.	Pressure at Ox. Venturi (psia)	Pressure at Fuel Venturi (psia)	(Potter Meter) Ox. Flow Rate (lb/sec)	(Potter Meter) Fuel Flow Rate (lb/sec)	(Venturi) Ox. Flow Rate (lb/sec)	(Venturi) Fuel Flow Rate (in/sec)	(Venturi) Total Injector Flow Rate (lb/sec)	Mixture Ratio (Injector Venturis)
1K-3C-								
198	2239	1441	2.53	1.24	2.52	1.29	3.81	1.95
205	2039	1245	2.46	1.19	2.40	1.20	3.60	2.00
207	2228	1286	2.45	1.18	2.51	1.22	3.73	2.06
210	2235	1288	3.48	1.18	2.51	1.22	3.74	2.06
211	2244	1288	2.48	1.18	2.53	1.22	3.75	2.07
212	2239	1285	2.46	1.18	2.52	1.220	3.74	2.07
213	2223	1271	2.41	1.18	2.52	1.21	3.74	2.08
214	2228	1288	2.47	1.19	2.52	1.22	3.75	2.06
215	2230	1274	2.48	1.18	2.53	1.226	3.74	2.08
216	2230	1289	2.48	1.19	2.52	1.22	3.75	2.06
218	2223	1278	2.48	1.18	2.52	1.22	3.74	2.07
219	2229	1127	2.50	1.11	2.54	1.15	3.68	2.21
220	2222	1354	2.49	1.22	2.53	1.26	3.79	2.01

SECTION III

DATA FROM ClF_3 TESTS AT 100 PSIA CHAMBER PRESSURE

(C) TABLE 9

TEST CONDITIONS (U)

Test No.	Thrust (lb)	Chamber Pressure (psia)	Coolant Flow Rate (lb/sec)	Injector Oxidizer Flow Rate (lb/sec)	Injector Fuel Flow Rate (lb/sec)	Total Propellant Flow Rate (lb/sec)	Overall Mixture Ratio
1K-3D-104	112	121	0.208	0.329	0.141	0.768	4.45
108	113	118	0.215	0.333	0.142	0.690	3.86
110	122	118	0.213	0.331	0.141	0.685	3.86
111	115	116	0.197	0.334	0.140	0.671	3.79
112	121	118	0.194	0.331	0.142	0.667	3.70
113	102	111	0.171	0.331	0.136	0.638	3.69
114	103	112	0.171	0.332	0.137	0.640	3.67

(C) TABLE 10

PRESSURE DROPS (U)

Test No.	Chamber Pressure (psia)	Chamber Plenum Pressure (psia)				Platelet Pressure Drop (psid)			
		Sect. I	Sect. II	Sect. III	Sect. IV	Sect. I	Sect. II	Sect. III	Sect. IV
1K-3D-104	121	156	156	243	230	34	35	150	190
108	118	146	144	225	182	27	26	134	143
110	118	144	143	224	180	26	25	134	141
111	116	149	139	220	25	33	22	131	-
112	118	149	139	219	27	31	21	128	-
113	111	147	122	199	107	35	11	114	70
114	112	148	123	196	138	37	11	111	101

(C) TABLE 11

STEADY STATE TEMPERATURES (U)

Test No.	$\dot{w}_{c,I}$ Sect. I Coolant Flow Rate (lb/sec)	$\dot{w}_{c,I}/\dot{w}_N$ Sect. I	Duration (sec)	Temperatures (°F) Section I TC 9-1	TC 9-2	TC 9-4	TC 8-1	TC 8-2
1K-3D-104	0.113	1.98	11.0		580	150	135	125
108	0.078	1.37	11.4		1040	702	384	145
110	0.077	1.35	21.2	1073	1126	1026		
111	0.077	1.35	10.9		901	906	362	
112	0.076	1.33	27.9		1045	1104	430	
113	0.077	1.35	17.5		823	1062	372	1041
114	0.077	1.35	78.0		844	1136	368	1092

Test No.	$\dot{w}_{c,II}$ Sect. II Coolant Flow Rate (lb/sec)	$\dot{w}_{c,II}/\dot{w}_N$ Sect. II	Temperatures (°F) Section II TC 5-2	TC 5-3	TC 5-6	TC 5-7	TC 4-1	TC 4-2	TC 4-3	TC 4-4	TC 4-6	TC 4-8
1K-3D-104	0.103	1.86		116		128	148	144		143		138
108	0.075	1.36		256		131	554	519		606		156
110	0.074	1.34	283		71			556	611		349	
111	0.058	1.05	696	335		553	612	576	664	723		
112	0.057	1.03	618	399		528	676	633	716	785		
113	0.032	0.58		633		690	727	763	799	865		
114	0.032	0.58		631		743	758	807	863	954		

(C) TABLE II (cont.)

STEADY STATE TEMPERATURES (U)

Test No.	$\dot{w}_{c,III}$ Sect III Coolant Flow Rate (lb/sec)	$\dot{w}_{c,III}/\dot{w}_N$ Sect III	Temperatures (°F) Section III							
			TC 3-1	TC 3-2	TC 3-3	TC 3-4	TC 2-2	TC 2-3	TC 2-6	TC 2-7
1K-3D-104	0.057	4.56		122	111			171		119
108	0.047	3.76		364	116			541		175
110	0.047	3.76	349			116	493	552	169	214
111	0.047	3.76			201			649	464	539
112	0.046	3.68			246			655	443	506
113	0.047	3.76			462			583	451	509
114	01047	3.76			563			563	464	528

Test No.	$\dot{w}_{c,IV}$ Sect. IV Coolant Flow Rate (lb/sec)	$\dot{w}_{c,IV}/\dot{w}_N$ Sect. IV	Temperatures (°F) Section IV	
			TC 1-1	TC 1-2
1K-3D-104	0.025	3.09	209	119
108	0.015	1.85	523	318
110	0.015	1.85	523	
111	0.015	1.85	981	359
112	0.015	1.85	1003	355
113	0.015	1.85	716	744
114	0.015	1.85	571	683

(C) TABLE 12

INJECTOR FLOW RATES AND MIXTURE RATIOS (U)

Test No.	Pressure at Ox. Venturi (psia)	Pressure at Fuel Venturi (psia)	(Potter Meter) Ox. Flow Rate (lb/sec)	(Potter Meter) Fuel Flow Rate (lb/sec)	(Venturi) Ox. Flow Rate (lb/sec)	(Venturi) Fuel Flow Rate (lb/sec)	(Venturi) Total Injector Flow Rate (lb/sec)	Mixture Ratio (Injector Venturis)
1K-3D-								
104	391	395	0.313	0.131	0.329	0.141	0.470	2.33
108	398	399	0.331	0.132	0.333	0.142	0.472	2.34
110	395	396	0.324	0.133	0.331	0.141	0.472	2.35
111	401	391	0.333	0.132	0.334	0.140	0.474	2.38
112	393	397	0.127	0.132	0.331	0.142	0.473	2.33
113	394	367	0.329	0.128	0.331	0.136	0.467	2.43
114	397	373	0.333	0.130	0.332	0.137	0.469	2.42

SECTION IV

DATA FROM ClF_3 TESTS AT
1000 PSIA CHAMBER PRESSURE

(C) TABLE 13

TEST CONDITIONS (U)

Test No.	Thrust (lb)	Chamber Pressure (psia)	Coolant Flow Rate (lb/sec)	Injector Oxidizer Flow Rate (lb/sec)	Injector Fuel Flow Rate (lb/sec)	Total Propellant Flow Rate (lb/sec)	Thrust Chamber Mixture Ratio
1K-3D-							
115	873	993	2.09	2.55	1.08	5.58	4.06
116	890	1023	1.99	2.51	1.06	5.43	4.02
117	873	1027	2.14	2.29	1.07	5.53	4.04
118	892	1074	2.19	2.36	1.12	5.66	4.08

(C) TABLE 14

PRESSURE DROPS (U)

Test No.	Chamber Pressure (psia)	Chamber Plenum Pressure (psia)				Platelet Pressure Drop (psid)			
		Sect. I	Sect. II	Sect. III	Sect. IV	Sect. I	Sect. II	Sect. III	Sect. IV
1K-3D-									
115	993	1415	1393	1662	1625	422	400	942	1293
116	1023	1449	1354	1609	1562	426	331	868	1219
117	1027	1732	1546	1897	1531	705	508	1154	1187
118	1074	1775	1584	1944	1535	701	510	1165	1175

(C) TABLE 15

STEADY STATE TEMPERATURES (U)

Test No.	$\dot{W}_{c,I}$ Sect. I Coolant Flow Rate (lb/sec)	$W_{c,I}/W_N$ Sect. I	Duration (sec)	Temperatures (°F) Section I TC 9-2	TC 8-1
1K-3D-					
116	0.837	1.74	1.35	400	320
117	0.898	1.87	2.29	340	320
118	0.922	1.92	2.44	275	310

Test No.	$\dot{W}_{c,II}$ Sect. II Coolant Flow Rate (lb/sec)	$W_{c,II}/W_N$ Sect. II	Temperatures (°F) Section II TC 4-1	TC 4-2	TC 4-4	TC 4-6	TC 5-3
1K-3D-							
116	0.763	1.63	920	620	620	800	290
117	0.820	1.76	615	600	540	940	--
118	0.841	1.81	600	600	495	190	--

Test No.	$\dot{W}_{c,III}$ Sect. III Coolant Flow Rate (lb/sec)	$W_{c,III}/W_N$ Sect. III	Temperatures (°F) Section III TC 2-3	TC 2-7
1K-3D-				
116	0.310	2.95	530	910
117	0.333	3.17	530	960
118	0.341	3.25	530	795

Test No.	$\dot{W}_{c,IV}$ Sect. IV Coolant Flow Rate (lb/sec)	$W_{c,IV}/W_N$ Sect. IV	Temperatures (°F) Section IV TC 1-1	TC 1-2
1K-3D-				
116	0.07	1.04	892	1052
117	0.076	1.11	749	1077
118	0.078	1.14	733	943

(C) TABLE 16

INJECTOR FLOW RATES AND MIXTURE RATIOS (U)

Test No.	Pressure at Ox. Venturi (psia)	Pressure at Fuel Venturi (psia)	(Potter Meter) Ox. Flow Rate (lb/sec)	(Potter Meter) Fuel Flow Rate (lb/sec)	(Venturi) Ox. Flow Rate (lb/sec)	(Venturi) Fuel Flow Rate (in/sec)	(Venturi) Total Injector Flow Rate (lb/sec)	Mixture Ratio (Injector Venturis)
1K-3D-								
115	2232	1968	2.55	1.08	2.62	1.09	3.71	2.40
116	2235	1888	2.51	1.06	2.62	1.07	3.69	2.45
117	2163	1956	2.29	1.07	2.59	1.09	3.68	2.38
118	2309	1978	2.36	1.12	2.67	1.10	3.77	2.43

SECTION V

DATA FROM PHASE II ClF_3
TESTS AT 1000 PSIA CHAMBER PRESSURE

(C) TABLE 17

TEST CONDITIONS (U)

Test No.	Thrust (lb)	Chamber Pressure (psia)	Coolant Flow Rate (lb/sec)	Injector Oxidizer Flow Rate (lb/sec)	Injector Fuel Flow Rate (lb/sec)	Total Propellant Flow Rate (lb/sec)	Thrust Chamber Mixture Ratio
1K-5B-102	845	918	1.902	1.58	1.90	5.38	1.84
106	942	985	1.880	2.82	1.06	5.76	4.43
109	950	964 (1)	1.661	2.84	1.06	5.56	4.27
110	943	958 (1)	1.598	2.77	1.06	5.43	4.11
111	910	953	1.412	2.86	1.06	5.33	4.03
112	920	955	1.407	2.88	1.07	5.36	4.02

(1) P_c tap plugged. Chamber pressure calculated from injector pressures, propellant flow rates and injector Kw values for fuel and oxidizer determined from test -106.

(C) TABLE 18

PRESSURE DROPS (U)

Test No.	Chamber Pressure (psia)	Chamber Plenum Pressure (psia)			Platelet Pressure Drop (psid)		
		Sect. I	Sect. II	Sect. III	Sect. I	Sect. II	Sect. III
1K-5B-101	(2)	292	367	956	227	289	772
102		288	363	930	224	286	751
106		277	348	895	236	300	782
109		268	259	828	335	226	755
110		266	260	814	228	224	730
111		313	205	604	276	176	560
112		346	210	635	302	173	565

(2) Data taken during coolant lead time before firing. Chamber pressure is atmospheric pressure.

(C) TABLE 19

STEADY STATE TEMPERATURES (U)

Test No.	$\dot{w}_{c,\,I}$ Sect. I Coolant Flow Rate (lb/sec)	$\dot{w}_{c,\,I}/\dot{w}_N$ Sect. I	Duration (sec)	Temperature (°F) Section I TC 7-1	TC 7-2	TC 6-2
1K-5B-102	0.550	2.55	0.75	296	--	
106	0.550	2.55	2.43	1143	248	224
110	0.519	2.40	8.86	1596	275	233
112	0.545	2.52	1.04	--	--	225

Test No.	$\dot{w}_{c,\,II}$ Sect. II Coolant Flow Rate (lb/sec)	$\dot{w}_{c,\,II}/\dot{w}_N$ Sect. II	Temperatures (°F Section II TC 5-2	TC 5-1	TC 4-4	TC 4-3	TC 3-4	TC 3-3	TC 3-2	TC 3-1
1K-5B-102	0.92B	1.99	--	192	--	133	--	--	--	330
106	0.913	1.96	250	290	320	288	568	541	663	528
110	0.702	1.51	290	341	395	356	789	767	961	716
112	0.587	1.26	325	328	--	385	747	699	879	699

Test No.	$\dot{w}_{c,\ I}$ Sect. III Coolant Flow Rate (lb/sec)	$\dot{w}_{c,\ III}/\dot{w}_N$ Sect. II	Temperatures (°F) Section III			
			TC 1-1	TC 1-2	TC 1-3	TC 2-1
1K-5B-102	0.424	2.45	592	403	--	349
106	0.417	2.41	638	--	438	460
110	0.377	2.18	656	--	520	493
112	0.275	1.59	925	--	--	768

(C) TABLE 20

INJECTOR FLOW RATES AND MIXTURE RATIOS (U)

Test No.	Pressure at Ox. Venturi (psia)	Pressure at Fuel Venturi (psia)	(Potter Meter) Ox. Flow Rate (lb/sec)	(Potter Meter) Fuel Flow Rate (lb/sec)	(Venturi) Ox. Flow Rate (lb/sec)	(Venturi) Fuel Flow Rate (lb/sec)	(Venturi) Total Injector Flow Rate (lb/sec)	Mixture Ratio (Injector Venturis)
1K-5B-102	2150	1942	--	--	1.58	1.90	3.48	0.84
106	2124	1986	2.60	0.98	2.82	1.06	3.88	2.66
110	2066	1989	2.55	0.98	2.77	1.06	3.83	2.60
112	2215	2000	2.65	0.99	2.88	1.07	3.95	2.70

UNCLASSIFIED

Unclassified
Security Classification

DOCUMENT CONTROL DATA · R&D
(Security classification of title, body of abstract and indexing annotation must be entered when the overall report is classified)

1. ORIGINATING ACTIVITY (Corporate author) Aerojet-General Corporation Liquid Rocket Operations Sacramento, California 95809	2a. REPORT SECURITY CLASSIFICATION Confidential 2b. GROUP 4

3. REPORT TITLE

Demonstration of an Advanced Transpiration-Cooled Thrust Chamber (U)

4. DESCRIPTIVE NOTES (Type of report and inclusive dates)

Final Report

5. AUTHOR(S) (Last name, first name, initial)

Blubaugh, A. L. Zisk, E. J.

6. REPORT DATE	7a. TOTAL NO OF PAGES	7b. NO OF REFS
October 1967	255	eight

8a. CONTRACT OR GRANT NO.	9a. ORIGINATOR'S REPORT NUMBER(S)
AF 04(611)-10922 b. PROJECT NO. c. Project 3058 Task 305803 d.	AFRPL-TR-67-198 9b. OTHER REPORT NO(S) (Any other numbers that may be assigned this report)

10. AVAILABILITY/LIMITATION NOTICES IN ADDITION TO SECURITY REQUIREMENTS WHICH MUST BE MET, THIS DOCUMENT IS SUBJECT TO SPECIAL EXPORT CONTROLS, AND EACH TRANSMITTAL TO FOREIGN GOVERNMENTS OR FOREIGN NATIONALS MAY BE MADE ONLY WITH PRIOR APPROVAL OF AFRPL (RPPR/STINFO), EDWARDS, CALIFORNIA, 93523

11. SUPPLEMENTARY NOTES	12. SPONSORING MILITARY ACTIVITY
	Air Force Rocket Propulsion Lab. Edwards, California

13. ABSTRACT AN ADVANCED TRANSPIRATION-COOLED THRUST CHAMBER CONCEPT HAS BEEN TESTED EXTENSIVELY WITH BOTH N_2O_4 AND ClF_3 AS COOLANTS. THIS CONCEPT UTILIZES STACKED ULTRA-THIN (0.001 TO 0.020 IN.) PLATELETS TO FORM A POROUS COMBUSTION CHAMBER WALL. EACH PLATELET CONTAINS PRECISE FLOW CONTROL CHANNELS WHICH METER THE COOLANT FLOW TO THE COOLED SURFACE AND PREVENT THE FORMATION AND GROWTH OF LOCAL HOT SPOTS. TO DEMONSTRATE FEASIBILITY OF THE CONCEPT, TWO COMPLETELY TRANSPIRATION COOLED CHAMBERS WERE FABRICATED AND TESTED. A TOTAL OF 121 TESTS WERE MADE WITH THE N_2O_4-COOLED CHAMBER (STAINLESS STEEL) FOR A CUMULATIVE FIRING DURATION OF 3076.7 SECONDS. NINETY-SIX TESTS WERE MADE AT THE 100 LB THRUST LEVEL AND 25 TESTS AT THE 1000 LB THRUST LEVEL. THE CUMULATIVE FIRING DURATION FOR THE ClF_3-COOLED CHAMBER (NICKEL) WAS 219.2 SECONDS. THIRTEEN TESTS WERE MADE AT THE 100 LB THRUST LEVEL AND 16 TESTS WERE MADE AT THE 1000 LB THRUST LEVEL. THERMAL DATA OBTAINED DURING THESE TESTS INDICATE THAT, ASIDE FROM INJECTOR STREAKING EFFECTS, THE TRANSPIRE SYSTEM OPERATED AS DESIGNED.

DD FORM 1473

Unclassified
Security Classification

UNCLASSIFIED

UNCLASSIFIED

Security Classification

14. KEY WORDS	LINK A		LINK B		LINK C	
	ROLE	WT	ROLE	WT	ROLE	WT
TRANSPIRATION COOLING						
FILM COOLING						
N_2O_4/AEROZINE 50						
CLF_3/MHF-3						
OXIDIZER COOLING						
TRANSPIRE						

INSTRUCTIONS

1. **ORIGINATING ACTIVITY:** Enter the name and address of the contractor, subcontractor, grantee, Department of Defense activity or other organization *(corporate author)* issuing the report.

2a. **REPORT SECURITY CLASSIFICATION:** Enter the overall security classification of the report. Indicate whether "Restricted Data" is included. Marking is to be in accordance with appropriate security regulations.

2b. **GROUP:** Automatic downgrading is specified in DoD Directive 5200.10 and Armed Forces Industrial Manual. Enter the group number. Also, when applicable, show that optional markings have been used for Group 3 and Group 4 as authorized.

3. **REPORT TITLE:** Enter the complete report title in all capital letters. Titles in all cases should be unclassified. If a meaningful title cannot be selected without classification, show title classification in all capitals in parenthesis immediately following the title.

4. **DESCRIPTIVE NOTES:** If appropriate, enter the type of report, e.g., interim, progress, summary, annual, or final. Give the inclusive dates when a specific reporting period is covered.

5. **AUTHOR(S):** Enter the name(s) of author(s) as shown on or in the report. Enter last name, first name, middle initial. If military, show rank and branch of service. The name of the principal author is an absolute minimum requirement.

6. **REPORT DATE:** Enter the date of the report as day, month, year; or month, year. If more than one date appears on the report, use date of publication.

7a. **TOTAL NUMBER OF PAGES:** The total page count should follow normal pagination procedures, i.e., enter the number of pages containing information.

7b. **NUMBER OF REFERENCES:** Enter the total number of references cited in the report.

8a. **CONTRACT OR GRANT NUMBER:** If appropriate, enter the applicable number of the contract or grant under which the report was written.

8b, 8c, & 8d. **PROJECT NUMBER:** Enter the appropriate military department identification, such as project number, subproject number, system numbers, task number, etc.

9a. **ORIGINATOR'S REPORT NUMBER(S):** Enter the official report number by which the document will be identified and controlled by the originating activity. This number must be unique to this report.

9b. **OTHER REPORT NUMBER(S):** If the report has been assigned any other report numbers *(either by the originator or by the sponsor)*, also enter this number(s).

10. **AVAILABILITY/LIMITATION NOTICES:** Enter any limitations on further dissemination of the report, other than those imposed by security classification, using standard statements such as:

(1) "Qualified requesters may obtain copies of this report from DDC."

(2) "Foreign announcement and dissemination of this report by DDC is not authorized."

(3) "U. S. Government agencies may obtain copies of this report directly from DDC. Other qualified DDC users shall request through

_____."

(4) "U. S. military agencies may obtain copies of this report directly from DDC. Other qualified users shall request through

_____."

(5) "All distribution of this report is controlled. Qualified DDC users shall request through

_____."

If the report has been furnished to the Office of Technical Services, Department of Commerce, for sale to the public, indicate this fact and enter the price, if known.

11. **SUPPLEMENTARY NOTES:** Use for additional explanatory notes.

12. **SPONSORING MILITARY ACTIVITY:** Enter the name of the departmental project office or laboratory sponsoring *(paying for)* the research and development. Include address.

13 **ABSTRACT:** Enter an abstract giving a brief and factual summary of the document indicative of the report, even though it may also appear elsewhere in the body of the technical report. If additional space is required, a continuation sheet shall be attached.

It is highly desirable that the abstract of classified reports be unclassified. Each paragraph of the abstract shall end with an indication of the military security classification of the information in the paragraph, represented as *(TS) (S) (C)* or *(U)*.

There is no limitation on the length of the abstract. However, the suggested length is from 150 to 225 words.

14. **KEY WORDS:** Key words are technically meaningful terms or short phrases that characterize a report and may be used as index entries for cataloging the report. Key words must be selected so that no security classification is required. Identifiers, such as equipment model designation, trade name, military project code name, geographic location, may be used as key words but will be followed by an indication of technical context. The assignment of links, rules, and weights is optional.

Security Classification

SUPPLEMENTARY

INFORMATION

AEROJET-GENERAL CORPORATION
POST OFFICE BOX 15847 • SACRAMENTO, CALIFORNIA 95813

PROPULSION DIVISION

9601:0900

24 February 1969

To: Recipient of Technical Report AFRPL-TR-67-198 Entitled, "Demonstration of an Advanced Transpiration-Cooled Thrust Chamber" (u)

Gentlemen:

The above final report was forwarded to you on or about 31 October 1967 in accordance with the distribution list supplied under cognizant Government contract.

The United States Patent Office recently imposed a Secrecy Order upon a patent application having to do with the Transpire concept. The above referenced technical report consequently is subject to the patent secrecy order.

By terms of the Secrecy Order you are prohibited from disclosing or publishing the subject matter of this invention or any information relating thereto, in any way to any person not previously cognizant of the invention except by first obtaining written consent of the Commissioner of Patents. The secrecy Order has been modified by a Permit which permits disclosure under certain conditions to Government employees, their designees, or persons employed by or working with Aerojet whose duties involve development, manufacture, or use of the subject matter of this patent application, by or for the U. S. Government, provided such persons are also advised of the Secrecy Order.

Enclosed is a copy of a United States Patent Office Secrecy Order Notice. A copy of this notice should be affixed to the cover page of any publication or technical data in your possession which relates to the subject patent application. Also, you should notify any persons to whom you have given information relating to the subject patent application that the Secrecy Order has been issued and provide them with a copy of the Patent

Office Secrecy Order Notice. Although there are no express handling provisions provided with regard to material under a Patent Office Secrecy Order, we ask that you safeguard it in the same manner as information classified "confidential." If you are not equipped to provide such safeguards, please return the publication to us, double-wrapped similar to classified material.

Your cooperation in fulfilling the obligation imposed by the Secrecy Order is essential. The law, 35 USC 186, provides criminal penalties for violation of a Secrecy Order up to a $10,000 fine or imprisonment for not more than two years, or both.

Very truly yours,

W. G. Dallas, Manager
Thrust Chambers
Engineering Contracts
Liquid Rocket Operations

Enclosure:
(1) Secrecy Order Notice

Technical Report AFRPL-TR-67-198 Entitled, "Demonstration of an Advanced Transpiration-Cooled Thrust Chamber" (u)

United States Patent Office Secrecy Order

NOTICE

The Aerojet-General Corporation has filed patent applications in the U. S. Patent Office to cover inventions disclosed in this publication, and the Commissioner of Patents has issued a secrecy order thereon.

Compliance with the provisions of this secrecy order requires that those who receive a disclosure of the secret subject matter be informed of the existence of the secrecy order and of the penalties for the violation thereof.

The recipient of this report is accordingly advised that this publication includes information which is now under a secrecy order. It is requested that he notify all persons who will have access to this material of the secrecy order.

Each secrecy order provides that any person who has received a disclosure of the subject matter covered by the secrecy order is

> "in nowise to publish or disclose the invention or any material information with respect thereto, including hitherto unpublished details of the subject matter of said application, in any way to any person not cognizant of the invention prior to the date of the order, including any employee of the principals, but to keep the same secret except by written permission first obtained of the Commissioner of Patents."

Although the original secrecy order forbids disclosure of the material to persons not cognizant of the invention prior to the date of the order, a supplemental permit attached to each order does permit such disclosure to:

> "(a) Any officer or employee of any department, independent agency, or bureau of the Government of the United States.
>
> "(b) Any person designated specifically by the head of any department, independent agency or bureau of the Government of the United States, or by his duly authorized subordinate, as a proper individual to receive the disclosure of the above indicated application for use in the prosecution of the war.
>
> "The principals under the secrecy are further authorized to disclose the subject matter of this application to the minimum necessary number of persons of known loyalty and discretion, employed by or working with the principals or their licensees and whose duties involve cooperation in the development, manufacture or use of the subject matter by or for the Government of the United States, provided such persons are advised of the issuance of the secrecy order."

No other disclosures are authorized, without written permission from the Commissioner of Patents. Public Law No. 239, 77th Congress, provides that whoever shall "willfully publish or disclose or authorize or cause to be published or disclosed such invention, or any material information with respect thereto," which is under a secrecy order, "shall, upon conviction, be fined not more than $10,000 or imprisoned for not more than two years or both." In addition, Public Law No. 700, 76th Congress, provides that the invention in a patent may be held abandoned, if it be established that there has been a disclosure in violation of the secrecy order.

It must be understood that the requirements of the secrecy order of the Commissioner of Patents are in addition to the usual security regulations which are in force with respect to activities of the Aerojet-General Corporation. The usual security regulations must still be observed notwithstanding anything set forth in the secrecy order of the Commissioner of Patents.